



ESCOLA DE DOUTORAMENTO  
INTERNACIONAL DA USC

Damián  
Insua Costa

Tese de doutoramento

A CLIMATOLOGY OF  
WESTERN MEDITERRANEAN  
PRECIPITATION EXTREMES  
FOCUSING ON THE STUDY OF  
MOISTURE ORIGIN

Santiago de Compostela, 2021







TESE DE DOUTORAMENTO

**A CLIMATOLOGY OF WESTERN  
MEDITERRANEAN PRECIPITATION  
EXTREMES FOCUSING ON THE  
STUDY OF MOISTURE ORIGIN**

Damián Insua Costa

ESCOLA DE DOUTORAMENTO INTERNACIONAL DA UNIVERSIDADE DE SANTIAGO DE COMPOSTELA  
PROGRAMA DE DOUTORAMENTO EN ENERXÍAS RENOVABLES E SUSTENTABILIDADE  
ENERXÉTICA



SANTIAGO DE COMPOSTELA

ANO 2021



D./Dna. **Damián Insua Costa**

Título da tese: **A climatology of western Mediterranean precipitation extremes focusing on the study of moisture origin**

Presento a miña tese, seguindo o procedemento axeitado ao Regulamento, e declaro que:

- 1) A tese abarca os resultados da elaboración do meu traballo.
- 2) De ser o caso, na tese faise referencia ás colaboracións que tivo este traballo.
- 3) Confirmo que a tese non incorre en ningún tipo de plaxio doutros autores nin de traballos presentados por min para a obtención doutros títulos.
- 4) A tese é a versión definitiva presentada para a súa defensa e coincide a versión impresa coa presentada en formato electrónico

E comprométome a presentar o Compromiso Documental de Supervisión no caso de que o orixinal non estea na Escola.

En **Santiago de Compostela, 30 de decembro de 2021.**

**Sinatura electrónica**



## AUTORIZACIÓN DO DIRECTOR / TITOR DA TESE

**A climatology of western Mediterranean precipitation  
extremes focusing on the study of moisture origin**

D./Dna. Gonzalo Miguez Macho

D./Dna. María del Carmen Llasat Botija

INFORMA/N:

Que a presente tese, correspóndese co traballo realizado por D/Dna. Damián Insua Costa, baixo a miña dirección/titorización, e autorizo a súa presentación, considerando que reúne os requisitos esixidos no Regulamento de Estudos de Doutoramento da USC, e que como director desta non incorre nas causas de abstención establecidas na Lei 40/2015.

De acordo co indicado no Regulamento de Estudos de Doutoramento, declara tamén que a presente tese de doutoramento é idónea para ser defendida en base á modalidade de Monográfica con reprodución de publicacións, nos que a participación do/a doutorando/a foi decisiva para a súa elaboración e as publicacións se axustan ao Plan de Investigación.

En Santiago de Compostela, 30 de decembro de 2021



# Agradecementos e dedicatoria

A miña nai Begoña, muller brava. Partiríase a cara por Ángel, Jairo e Damián onde e cando fixese falla. Pelexou para que os seus fillos estudaran, e ao final conseguíuno. A meu pai Ángel, mecánico de profesión pero labrego de corazón. Coma toda a xente do campo, ten sempre un ollo posto na terra e outro no ceo. Recordo cando, sendo eu un neno, me ensinou que as folerpas de neve se podían distinguir na base da nube, moito antes de que chegaran ao chan. Non estaría a escribir estas palabras se non fose por eles dous.

A Oliva, a miña compañeira inseparable. Aguantou con paciencia todas as miñas ansias e preocupacións cada vez que voltaba da facultade. O seu amor e agarimo déronme o alento que precisaba para chegar ata aquí.

A Gonzalo, o meu director. Remato a tese pensando que tiven a sorte de ter un xefe co que sempre me entendín e do que aprendín ata o último día. A Carmen, a miña outra directora. Acolleume con cariño xa durante os meus tempos de estudante en Barcelona e deume sempre o seu valioso consello cando o precisei. Non podo máis que sentirme orgulloso de ter sido o voso estudante.

Aos meus queridísimos irmáns, Ángel e Jairo. A moitos outros membros da familia. A todos os meus amigos, tanto do grupo de investigación como de fóra do grupo. Durante todos estes anos espero ter sabido transmitirvos o aprecio que sinto por cada un de vós. E se non o souben facer, espero poder facelo nos anos que, de seguro, nos quedan por vivir xuntos.

Tamén a algúns que xa non están pero que sempre me acompañaron.

A todos, grazas.



En Santiago de Compostela, a 21 de decembro de 2021





# Contents

<b>Summary</b>	<b>15</b>
<b>Resumen</b>	<b>19</b>
<b>Resumo</b>	<b>23</b>
<b>Resumo estendido</b>	<b>27</b>
<b>1 General Introduction</b>	<b>33</b>
1.1 Motivation, objectives and thesis outline . . . . .	33
1.1.1 Motivation . . . . .	33
1.1.2 Objectives . . . . .	34
1.1.3 Thesis outline . . . . .	34
1.2 Physical processes associated with extreme rainfall . . . . .	35
1.2.1 Atmospheric moisture content . . . . .	35
1.2.2 Updraft intensity . . . . .	36
1.3 The western Mediterranean region . . . . .	39
1.4 Moisture transport and tracking . . . . .	43
1.5 Numerical simulation of the atmosphere . . . . .	45
<b>2 Extreme precipitation events in the western Mediterranean region</b>	<b>47</b>
2.1 Introduction . . . . .	47
2.2 Data . . . . .	49
2.2.1 Precipitation datasets . . . . .	49
2.2.2 Flooding data . . . . .	50
2.2.3 ERA5 reanalysis . . . . .	51
2.3 Methodology . . . . .	51
2.3.1 Setting a threshold for extreme day detection . . . . .	51
2.3.2 Classifying extreme days by weather type . . . . .	53
2.3.3 Ranking events by magnitude . . . . .	54
2.4 Results . . . . .	54
2.4.1 Spatial distribution of extreme rains . . . . .	54
2.4.2 Magnitude of events . . . . .	56
2.4.3 Weather types causing extreme precipitation . . . . .	57
2.4.4 Temporal distribution of extreme rains . . . . .	59
2.4.5 Final dataset and examples . . . . .	60
2.5 Summary and conclusions . . . . .	63



APPENDIX . . . . .	65
<b>3 Implementation and validation of a moisture tracking tool in an atmospheric model</b>	<b>67</b>
3.1 Introduction . . . . .	67
3.2 Implementation of the moisture tagging capability . . . . .	68
3.2.1 General formulation . . . . .	68
3.2.2 Moisture tracer tendencies formulation . . . . .	69
3.3 Moisture tracer validation . . . . .	73
3.3.1 Experimental setup . . . . .	73
3.3.2 Methodology . . . . .	73
3.3.3 Validation results . . . . .	77
3.4 Application example: lake evaporation as moisture source in the Great Lakes snowstorm of 2014 . . . . .	80
3.4.1 Experimental design . . . . .	81
3.4.2 Results . . . . .	82
3.5 Summary and conclusions . . . . .	85
<b>4 Case study: the catastrophic flooding episodes of the autumn of 1982 in Spain</b>	<b>87</b>
4.1 Introduction . . . . .	87
4.2 Methods . . . . .	89
4.2.1 Experimental design . . . . .	89
4.2.2 Model configuration and data used . . . . .	90
4.3 The October event . . . . .	90
4.3.1 Synoptic situation and precipitation . . . . .	90
4.3.2 Moisture origin . . . . .	92
4.3.3 Precipitation origin . . . . .	93
4.4 The November event . . . . .	96
4.4.1 Synoptic situation and precipitation . . . . .	96
4.4.2 Moisture origin . . . . .	97
4.4.3 Precipitation origin . . . . .	99
4.5 Summary and conclusions . . . . .	101
<b>5 Climatology of moisture sources in western Mediterranean extreme precipitation events</b>	<b>103</b>
5.1 Introduction . . . . .	103
5.2 Methods . . . . .	104
5.2.1 Extreme precipitation events studied . . . . .	104
5.2.2 Moisture source configuration . . . . .	104
5.2.3 Simulation set-up . . . . .	105
5.2.4 ENSO correlations . . . . .	106
5.3 Results . . . . .	106
5.3.1 Moisture always comes from multiple sources . . . . .	106
5.3.2 Intra-annual variability of moisture sources . . . . .	108
5.3.3 Remote contributions prevail in the most intense cases . . . . .	108
5.3.4 Moisture sources and weather types . . . . .	109
5.3.5 High efficiency of Mediterranean water vapour . . . . .	111

---

5.3.6	Tropical-extratropical interactions . . . . .	112
5.3.7	Correlation between moisture contributions and ENSO . . . . .	113
5.4	Summary and conclusions . . . . .	114
	APPENDIX . . . . .	115
<b>6</b>	<b>General Conclusions</b>	<b>121</b>
	<b>List of Figures</b>	<b>125</b>
	<b>List of Tables</b>	<b>131</b>
	<b>List of publications</b>	<b>133</b>
	<b>Appendix: Copyright Permissions</b>	<b>135</b>
	<b>Bibliography</b>	<b>139</b>





# Summary

The torrential rains that frequently affect the western Mediterranean region have been extensively studied by researchers because of the catastrophic impacts they cause, but nevertheless, the origin of these extreme rainfall events in terms of humidity remains unclear. Despite previous studies suggesting that the contribution of moisture from remote sources plays a key role, the idea that the large amounts of water recorded in these events originate from the mild Mediterranean Sea waters remains strongly rooted in society and even in some academic circles. The fact that these previous studies have focused on specific case studies and/or specific regions, often employing qualitative techniques for the study of moisture sources, has probably prevented the drawing of general conclusions and the establishment of a clear model of the sources feeding Mediterranean precipitation extremes.

The main objective of this thesis is to study a large number of cases with a wide spatial and temporal coverage in order to draw more robust conclusions and to definitively clarify the origin of the moisture that fuels these potentially catastrophic events. In order to achieve this final objective, extensive preliminary work is necessary, organized around different sub-objectives. For example, we first had to develop a state-of-the-art moisture tracking tool, as well as detect and characterise the main extreme precipitation events that have affected the western Mediterranean since 1980. This preliminary work, in fact, constitutes the major part of the thesis (Chapters 2, 3 and 4) and has led to the publication of several papers. A brief summary of the different chapters of the thesis is presented below, highlighting the main results and conclusions.

**Chapter 1** briefly introduces some basic concepts for the development of the thesis, such as the physical mechanisms governing extreme rainfall or the different methods for moisture tracking. It also presents the study region, the western Mediterranean, and its main geographical and climatic characteristics.

**Chapter 2** contains a compilation of western Mediterranean extreme precipitation events for the period 1980-2015. First, the events are detected from a high-resolution gridded precipitation database using a combination of a statistical threshold and a constant threshold. Subsequently, they are ranked by magnitude and grouped by weather type. This characterisation of the events also allows us to extract detailed information on their spatial and temporal distribution. Finally, a database with all the information obtained is created and made available to other researchers through an article published in a high impact journal [1]. For the study of moisture sources, this chapter is crucial even though it does not directly address this issue, since it is necessary beforehand to select the events to be analysed.

**Chapter 3** presents the main tool of this thesis, an online Eulerian technique for moisture source tracking coupled to the Weather Research and Forecasting (WRF) atmospheric model. This technique had been used previously but had not been tested. A complete revision of the model code was necessary, which resulted in a significant increase in the accuracy of the tool.

The mathematical formalism behind the technique as well as its validation was presented in an article [2], which also includes a case study as an example. In particular, to show the versatility of the tracking tool, the contribution of the Great Lakes to a snowstorm was quantified. The results showed that more than 50% of the snowfall recorded in the most affected areas came from lake evaporation, demonstrating their decisive role. For the study of moisture sources in the Mediterranean, the most important conclusion of this chapter is that the tool used is able to provide very accurate figures for the contribution of the sources (with errors of less than 1%). This is a drastic improvement over previous studies, most of which provide qualitative rather than quantitative analysis and/or use tracking tools with unknown accuracy.

**Chapter 4** is the first to deal directly with the problem of moisture sources fuelling extreme rainfall in the Mediterranean. The atmospheric moisture tracking tool presented in the previous chapter is applied to two case studies; the catastrophic flood events of autumn 1982 that particularly affected Spain, one in October and the other in November. This study, which gave rise to another article [3], serves as a first step for the application of the methodology to a much larger number of events (Chapter 5). The results showed that in both the October and November events the contribution of remote sources, including the North Atlantic and tropical and subtropical sources, was crucial. The latter contributed more than 30% in the October event and more than 50% in the November case. The contribution of the Mediterranean Sea was very high in the October event but still less than 50%, while in the case of November it acted as a secondary source, moderately enhancing precipitation (contribution less than 20%). This chapter therefore reinforces the conclusions of previous studies and also our starting hypothesis, by showing the determinant role of distant sources.

**Chapter 5** is the most important chapter of the thesis as it finally responds to the main objective set at the beginning, i.e. to establish a clear model of the moisture sources involved in these western Mediterranean extreme precipitation events by analysing a large number of cases. Based on the experience acquired in the study of the 1982 cases (Chapter 4), an experiment is designed in which 160 events are simulated with the moisture tracking model (Chapter 3). These are selected from the database of extreme precipitation events previously created (Chapter 2). Specifically, the 160 cases with the highest magnitude are selected. The configuration of the simulations is improved by extending the simulation domain, allowing for the evaluation of even the most distant sources such as the Pacific Ocean or the Southern Hemisphere. The results show that the average contribution from the Mediterranean Sea is 35% and is rarely dominant (contribution above 50%). The contribution of the Atlantic Ocean, including the North Atlantic and tropical Atlantic, is practically the same as that of the Mediterranean (25% North Atlantic, 10% tropical Atlantic). The contribution of all remote sources is however higher than the local ones (Mediterranean Sea plus nearby land) by 10%. This dominance of remote sources is marginally more pronounced for the most extreme cases. Our experiment also shows that the contribution of the Mediterranean in terms of precipitation is higher (by 7%) than in terms of precipitable water, just the opposite than in the case of the Atlantic. Finally, the role of tropical sources, which together contribute 17.3% of extreme precipitation on average, is highlighted. Tropical moisture intrusions into the Mediterranean usually occur via Africa through tropical plumes, although we show that part of the moisture transported through Africa actually originates from other sources such as the tropical Atlantic. If tropical moisture is added to that from other extremely distant sources, such as the North Pacific, we find that up to a quarter of the total Mediterranean extreme rainfall could originate thousands of kilometres away. Generally the contribution of these extremely distant sources is small on its own, but

together they can play a very important role as a rainfall enhancer.

**Chapter 6** summarises the main conclusions of the thesis in a question-and-answer format.





# Resumen

Las frecuentes lluvias extremas que afectan a la región del Mediterráneo Occidental han sido ampliamente estudiadas por los investigadores debido a los impactos catastróficos que causan, pero, sin embargo, el origen de estos eventos de lluvia extrema en términos de humedad sigue sin ser del todo claro. A pesar de que estudios previos sugieren que la contribución de fuentes remotas juega un papel clave, la idea de que las grandes cantidades de agua registradas en estos eventos se originan en las aguas templadas del Mar Mediterráneo permanece fuertemente arraigada en la sociedad e incluso en algunos círculos académicos. El hecho de que estos estudios previos se hayan centrado en casos de estudio concretos y/o regiones concretas, a menudo usando técnicas cuantitativas para el estudio de las fuentes de humedad, ha evitado el establecimiento de conclusiones generales y de un modelo claro de las fuentes que alimentan los extremos pluviométricos mediterráneos.

El principal objetivo de esta tesis es estudiar un alto número de casos con una amplia cobertura espacial y temporal para así poder obtener conclusiones robustas y aclarar definitivamente el origen de la humedad en estos eventos potencialmente catastróficos. Para alcanzar este objetivo último, ha sido necesario un extenso trabajo preliminar, organizado en diferentes subobjetivos. Por ejemplo, primeramente, tuvimos que poner a punto una herramienta para el rastreo de humedad de última generación, así como detectar y caracterizar los principales eventos de lluvia extrema que afectaron el Mediterráneo Occidental desde el año 1980. Este trabajo preliminar, de hecho, constituye la mayor parte de esta tesis (Capítulos 2, 3 y 4) y ha dado lugar a la publicación de varios artículos. A continuación, se presenta un breve resumen de los diferentes capítulos de la tesis, destacando los principales resultados y conclusiones.

El **Capítulo 1** introduce brevemente algunos conceptos básicos necesarios para el desarrollo de la tesis, como por ejemplo los mecanismos físicos que gobiernan la lluvia extrema o los diferentes métodos para el rastreo de humedad. También presenta la región de estudio, el Mediterráneo Occidental, y sus principales características geográficas y climáticas.

El **Capítulo 2** contiene una recopilación de eventos de precipitación extrema en el Mediterráneo Occidental para el período 1980-2015. Primero, los eventos fueron detectados a partir de una base de datos de precipitación en rejilla de alta resolución usando la combinación de un umbral estadístico con uno constante. Posteriormente, estos fueron ordenados por magnitud y agrupados por tipos de tiempo. Esta caracterización de los eventos también nos permitió obtener información detallada de su distribución espacial y temporal. Finalmente, se creó una base de datos con toda la información obtenida, la cual fue puesta a disposición de otros investigadores a través de un artículo publicado en una revista de alto impacto [1]. Para el estudio de fuentes de humedad este capítulo es crucial, aunque no trata directamente este tema, ya que es necesario seleccionar de antemano los eventos a analizar.

El **Capítulo 3** presenta la principal herramienta de esta tesis, una técnica euleriana en

línea para el rastreo de fuentes de humedad acoplada al modelo atmosférico Weather Research and Forecasting (WRF). Esta técnica ya había sido utilizada previamente pero no había sido testada. Fue necesaria una revisión completa del código del modelo, lo cual resultó en un incremento significativo en la precisión de la herramienta. El formalismo matemático detrás de la técnica, así como su validación fueron presentados en un artículo [2], el cual también incluye un caso de estudio como ejemplo. En particular, para mostrar la versatilidad de la herramienta de rastreo, se cuantificó la contribución de los Grandes Lagos a una tormenta de nieve. Los resultados mostraron que más del 50% de la nieve registrada en las áreas más afectadas procedía de la evaporación sobre los lagos, demostrando así su papel decisivo. Para el estudio de fuentes de humedad en el Mediterráneo, la conclusión más importante de este capítulo es que la herramienta es capaz de aportar cifras muy precisas para la contribución de las fuentes (con errores inferiores al 1%). Esto representa una mejora drástica sobre estudios anteriores, la mayoría de los cuales proporcionan un análisis cualitativo en lugar de cuantitativo y/o usan técnicas de rastreo de precisión desconocida.

El **Capítulo 4** es el primero en tratar directamente con el problema de las fuentes de humedad que alimentan la lluvia extrema en el Mediterráneo. La técnica de rastreo de humedad atmosférica presentada en el capítulo previo es aplicada a dos casos de estudio; los catastróficos episodios de inundaciones del otoño de 1982 que afectaron especialmente a España, uno en octubre y otro en noviembre. Este estudio, que dio lugar a la publicación de otro artículo [3], sirve como un primer paso para la aplicación de la metodología a un número mucho mayor de eventos (Capítulo 5). Los resultados mostraron que tanto en el evento de octubre como en el de noviembre la contribución de fuentes remotas, incluyendo el Atlántico norte y las fuentes tropicales y subtropicales, fue crucial. Estas últimas contribuyeron con más del 30% en el evento de octubre y más el 50% en el caso de noviembre. La contribución del Mediterráneo fue muy alta en el evento de octubre, pero aun así inferior al 50%, mientras que en el caso de noviembre actuó como una fuente secundaria, intensificando moderadamente las lluvias (contribución menor al 20%). Este capítulo refuerza polo lo tanto las conclusiones de estudios anteriores y también nuestra hipótesis inicial, al mostrar claramente el papel determinante de las fuentes distantes.

El **Capítulo 5** es el más importante de la tesis ya que finalmente responde al objetivo principal marcado al principio, es decir, analizando un alto número de eventos, establecer un modelo claro de las fuentes de humedad involucradas en los eventos de lluvia extrema del Mediterráneo Occidental. Basándonos en la experiencia adquirida en el estudio de los casos de 1982 (Capítulo 4), se diseñó un experimento en el cual se simularon 160 eventos con la herramienta de rastreo de humedad (Capítulo 3). Estos fueron seleccionados de la base de datos de episodios de lluvia extrema previamente creada (Capítulo 2). Específicamente, se seleccionaron los 160 casos de mayor magnitud. La configuración de las simulaciones se mejoró al extender el dominio de simulación, con lo cual se pudo evaluar hasta las fuentes más distantes como el océano Pacífico o el hemisferio sur. Los resultados muestran que la contribución media del Mar Mediterráneo es del 35% y raramente es dominante (contribución por encima del 50%). La contribución del océano Atlántico, incluyendo el Atlántico norte y el Atlántico tropical, es prácticamente la misma que la del Mediterráneo (25% Atlántico Norte y 10% Atlántico tropical). La contribución de todas las fuentes remotas es sin embargo superior en un 10% a la contribución de las locales (compuestas por el Mar Mediterráneo y las tierras locales). El dominio de las fuentes remotas es ligeramente más pronunciado para los casos más extremos. Nuestro experimento también demuestra que la contribución del Mediterráneo en términos de

precipitación es más alta (en un 7%) que en términos de agua precipitable, justo al revés que para el caso del Atlántico. Finalmente, se profundizó en el papel de las fuentes tropicales, las cuales contribuyen un promedio del 17.3% en conjunto. Las intrusiones de humedad tropical en el Mediterráneo ocurren usualmente a través de África por medio de plumas tropicales, aunque nosotros mostramos que parte de la humedad transportada a través de África se origina en otras fuentes como el Atlántico tropical. Si a la humedad tropical le añadimos la de otras fuentes extremadamente distantes, como el Pacífico norte, encontramos que hasta un cuarto del total de la lluvia extrema mediterránea podría tener su origen a miles de kilómetros. Generalmente la contribución de estas fuentes extremadamente distantes es pequeña por separado, pero juntas pueden jugar un papel importante como potenciadoras de la precipitación.

El **Capítulo 6** resume las principales cuestiones de la tesis en un formato pregunta y respuesta.



# Resumo

As frecuentes chuvias extremas que afectan á rexión do Mediterráneo Occidental foron amplamente estudadas polos investigadores debido aos impactos catastróficos que causan, pero, sen embargo, a orixe destes eventos de chuva extrema en termos de humidade segue sen ser totalmente clara. A pesar de que estudos previos suxiren que a contribución de fontes remotas xoga un papel clave, a idea de que as grandes cantidades de auga rexistradas nestes eventos se orixinan nas augas mornas do Mar Mediterráneo permanece fortemente arraigada na sociedade e incluso nalgúns círculos académicos. O feito de que estes estudos previos se centrasen en casos de estudo concretos e/ou rexións concretas, a miúdo usando técnicas cuantitativas para o estudo das fontes de humidade, evitou o establecemento de conclusións xerais e dun modelo claro das fontes que alimentas os extremos pluviométricos mediterráneos.

O principal obxectivo desta tese é estudar un alto número de casos cunha ampla cobertura espacial e temporal para así poder obter conclusión máis robustas e aclarar definitivamente a orixe da humidade nestes eventos potencialmente catastróficos. Para alcanzar este obxectivo último, necesitouse un extenso traballo preliminar, organizado en diferentes subobxectivos. Por exemplo, primeiramente, tivemos que por a punto unha ferramenta de rastrexo de humidade de última xeración, así como detectar e caracterizar os principais eventos de chuva extrema que afectaron o Mediterráneo Occidental dende o ano 1980. Este traballo preliminar, de feito, constitúe a maior parte desta tese (Capítulos 2, 3 e 4) e dou lugar á publicación de varios artigos. A continuación, preséntase un breve resumo dos diferentes capítulos da tese, desatacando os principais resultados e conclusión.

O **Capítulo 1** introduce brevemente algún conceptos básicos necesarios para o desenvolvemento da tese, como por exemplo os mecanismos físicos que gobernan a chuva extrema ou os diferentes métodos para o rastrexo de humidade. Tamén presenta a nosa rexión de estudo, o Mediterráneo Occidental, e as súas principais características xeográficas e climáticas.

O **Capítulo 2** contén unha recompilación de eventos de precipitación extrema no Mediterráneo Occidental para o período 1980-2015. Primeiro, os eventos foron detectados a partir dunha base de datos de precipitación extrema en reixa de alta resolución empregando a combinación dun limiar estatístico cun constante. Posteriormente, estes foron ordenados por magnitude e agrupados por tipos de tempo. Esta caracterización dos eventos tamén nos permitiu obter información detallada da súa distribución espacial e temporal. Finalmente, creouse unha base de datos con toda a información obtida, a cal foi posta a disposición doutros investigadores a través dun artigo publicado nunha revista de alto impacto [1]. Para o estudo de fontes de humidade este capítulo é crucial, aínda que non trata directamente este tema, xa que é necesario seleccionar de antemán os eventos a analizar.

O **Capítulo 3** presenta a ferramenta principal desta tese, unha técnica euleriana en liña para o rastrexo de fontes de humidade axustada ao modelo atmosférico Weather Research and Forecasting (WFR). Esta técnica xa fora empregada previamente pero non se testara.

Foi necesaria unha revisión completa do código do modelo, o cal resultou nun incremento significativo da precisión da ferramenta. O formalismo matemático detrás da técnica, así como a súa validación foron presentados nun artigo [2], o cal tamén inclúe un caso de estudo como exemplo. En particular, para mostrar a versatilidade da ferramenta de rastrexo, cuantificouse a contribución dos Grandes Lagos a unha tormenta de neve. Os resultados mostraron que máis do 50% da neve rexistrada nas áreas máis afectadas proviña da evaporación dos lagos, demostrando así o seu papel decisivo. Para o estudo de fontes de humidade no Mediterráneo, a conclusión máis importante deste capítulo é que a ferramenta é capaz de aportar cifras moi precisas para a contribución das fontes (con erros inferiores ao 1%). Isto representa unha mellora drástica sobre estudos anteriores, a maioría dos cales proporcionan unha análise cualitativa en lugar de cuantitativa e/ou usan técnicas de rastrexo de precisión descoñecida.

O **Capítulo 4** é o primeiro en tratar directamente co problema das fontes de humidade que alimentan a chuvia extrema no Mediterráneo. A técnica de rastrexo de humidade atmosférica presentada no capítulo anterior aplícase a dous casos de estudo; os catastróficos episodios de inundacións do outono de 1982 que afectaron especialmente a España, un en outubro e outro en novembro. Este estudo, que deu lugar á publicación doutro artigo [3], serve como primeiro paso para a aplicación da metodoloxía a un número moito maior de eventos (Capítulo 5). Os resultados mostraron que tanto no evento de outubro como no de novembro a contribución de fontes remotas, incluíndo o Atlántico norte e as fontes tropicais e subtropicais, foron cruciais. Estas últimas contribuíron con máis do 30% no evento de outubro e máis do 50% no caso de novembro. A contribución do Mediterráneo foi moi alta no evento de outubro, pero aínda así inferior ao 50%, mentres que no caso de novembro actuou como unha fonte secundaria, intensificando moderadamente as chuvias (contribución menor ó 20%). Este capítulo reforza polo tanto as conclusións de estudos anteriores e tamén a nosa hipótese inicial, ao mostrar claramente o papel determinante das fontes distantes.

O **Capítulo 5** é o máis importante da tese xa que finalmente responde ao obxectivo principal marcado ao principio, é dicir, analizando un alto número de eventos, establecer un modelo claro das fontes de humidade involucradas nos eventos de chuvia extrema do Mediterráneo Occidental. Baseándonos na experiencia adquirida no estudo dos casos de 1982 (Capítulo 4), deseñouse un experimento no cal se simularon 160 eventos coa ferramenta de rastrexo de humidade (Capítulo 3). Estes foron seleccionados da base de datos de episodios de chuvia extrema previamente creada (Capítulo 2). Especificamente, seleccionáronse os 160 casos de maior magnitude. A configuración das simulacións mellorouse ao estender o dominio de simulación, co cal púidose avaliar ata as fontes máis distantes coma o océano Pacífico ou o hemisferio sur. Os resultados mostran que a contribución media do Mar Mediterráneo é do 35% e raramente é dominante (contribución por enriba do 50%). A contribución do océano Atlántico, incluíndo o Atlántico norte e o Atlántico tropical, é practicamente a mesa que a do Mediterráneo (25% Atlántico Norte e 10% Atlántico tropical). A contribución de todas as fontes remotas é sen embargo superior nun 10% á contribución das locais (compostas polo Mar Mediterráneo e as terras locais). O dominio das fontes remotas é lixeiramente máis pronunciado para os casos máis extremos. O noso experimento tamén demostra que a contribución do Mediterráneo en termos de precipitación é máis alta (nun 7%) que en termos de auga precipitable, xusto ao revés que para o caso do Atlántico. Finalmente, afondouse no papel das fontes tropicais, as cales contribuíron unha media do 17.3% en conxunto. As intrusionés de humidade tropical no Mediterráneo ocorren usualmente a través de África por medio de plumas tropicais, aínda que nós mostramos que parte da humidade transportada a través de África orixínase noutras

fontes como o Atlántico tropical. Se á humidade tropical engadimos a de outras fontes extremadamente distantes, coma o Pacífico norte, atopamos que ata un cuarto do total da chuvia extrema mediterránea podería ter a súa orixe a miles de quilómetros. Xeralmente a contribución destas fontes extremadamente distantes é pequena por separado, pero xuntas poden xogar un papel importante como potenciadoras da precipitación.

O **Capítulo 6** resume as principais conclusión da tese nun formato pregunta e resposta.





# Resumo estendido

A idea detrás desta tese xurdiu no ano 2016 cando estaba estudando o máster de meteoroloxía na Universidade de Barcelona. No ano anterior fixera o meu traballo de fin de grao no Grupo de Física Non Lineal (GFNL) da Universidade de Santiago de Compostela, no cal se estaba a levar a cabo un proxecto sobre ríos atmosféricos e sobre a orixe da humidade que transportan. Por outra banda, durante o meu ano como estudante de meteoroloxía en Barcelona tiven a oportunidade de coñecer e aprender dos investigadores do grupo GAMA (Grupo de Análisis de situaciones Meteorológicas Adversas), dedicado ao estudo das chuvias extremas e inundacións na rexión mediterránea. A metade de curso, cando tiven que decidir o tema do meu traballo de fin de máster, foi case inmediato pensar en combinar as potencialidades de ambos grupos; a experiencia do GFNL no estudo de fontes de humidade coa experiencia de GAMA no estudo de fenómenos extremos. Finalmente, o meu traballo de fin de máster consistiu en analizar os dous eventos de inundacións catastróficas que afectaron a España en 1982 dende o punto de vista da orixe da humidade. Algún tempo despois, este traballo acabaría dando lugar a un dos artigos que compoñen esta tese.

O estudo de fontes de humidade no Mediterráneo xa fora tratado por outros investigadores anteriormente. Polo tanto, a priori esta non representaba unha liña de investigación rompedora. Sen embargo, cando estaba a facer o meu traballo de fin de máster decatámonos que, a pesar dos estudos previos, había aínda moitas cuestións sen resolver e o debate a cerca de onde viña a auga que alimentaba os extremos de precipitación mediterráneos aínda non estaba cerrado. A razón principal era que os autores anteriores tendían a centrarse no estudo duns poucos casos. Só uns poucos académicos estudaran un conxunto importante de eventos, pero concentrados en áreas concretas, coma o sueste de Francia, por exemplo. Este feito facía imposible extraer conclusións xerais, senón máis ben conclusións concretas para casos concretos ou zonas concretas. Ademais, o tipo de ferramenta de rastrexo de humidade que estaba operativa no GFNL, coñecida como trazadores de vapor de auga (WVTs, polas súas siglas en inglés) e a cal é considerada actualmente como a máis precisa para cuantificar a procedencia das chuvias, case non se aplicara nunca para o estudo de eventos extremos e moito menos no Mediterráneo. Polo tanto consideramos que se aplicabamos esta ferramenta a un número significativo de casos que cubriran unha boa parte da rexión mediterránea, poderíamos facer unha contribución importante e cerrar definitivamente o debate sobre este asunto. Deste razoamento xurdiu a motivación para esta tese, que comezou en outubro de 2016.

A parte da motivación científica, había tamén unha motivación social para contestar a principal cuestión exposta na tese. Esta motivación tiña a súa orixe na crenza fortemente arraigada nalgúns sectores de que os eventos de chuvias torrenciais no Mediterráneo son sempre alimentados polas supostamente altas cantidades de vapor de auga proporcionadas polas mornas augas do Mar Mediterráneo. Esta crenza é palpable cada vez que ocorre un evento de inundacións catastrófico, xa que os medios tenden a explicar estes eventos, aparte

doutras razóns, en termos dun fluxo cálido e húmido de orixe mediterránea. A nosa experiencia previa, así como algúns estudos anteriores, indicaban que esta explicación non era correcta, ou, polo menos, non totalmente adecuada. Por exemplo, os resultados que obtivéramos para as inundacións de 1982 durante o meu traballo de fin de máster mostráronnos que a contribución do Mediterráneo en termos de humidade, aínda que importante, non era dominante. Un dos principais obxectivos da tese era por tanto obter unha cifra robusta para a contribución do Mar Mediterráneo e, se a nosa hipótese inicial era acertada, contribuír a desmitificar a explicación tradicional destes episodios.

O comezo da tese consistiu na posta a punto dos WVTs que estaban xa en uso naquel momento no GFNL. Esta ferramenta xa mostrara un gran potencial para o estudo de fontes de humidade pero non se validara, polo que os resultados que aportaba, aínda que razoables, podían ser cuestionables. Por este motivo, os primeiros meses de traballo consistiron en validar a ferramenta de rastrexo. Ademais, fíxose unha revisión profunda do código Fortran no que a ferramenta estaba programada, o que deu lugar a unha mellora moi significativa na súa precisión. En realidade, o código correspondente aos WVTs estaba embebido nun código moito máis extenso, xa que este tipo de ferramentas axústanse a un modelo atmosférico, no noso caso o Weather Research and Forecasting (WRF, polas súas siglas en inglés). O traballo consistiu polo tanto en revisar as partes do código do modelo nas que os WVTs estaban embebidos. Por razóns obvias, rematamos por empregar o nome WRF-WVTs para referirnos ao modelo coa técnica de rastrexo de humidade incorporada. Despois deste traballo preliminar de melloras, diferentes experimentos co modelo mostraban que tiña unha alta precisión. Neste momento decidimos publicar un artigo para presentar a formulación matemática detrás da nosa ferramenta e para presentar o traballo de validación que se fixera. Este artigo incluía tamén un caso de estudo como exemplo. Para mostrar a versatilidade do modelo WRF-WVTs, escollemos para analizar un evento de neve extrema, a nevada por efecto lago de novembro de 2014, que afectou á zona dos Grandes Lagos de Norteamérica. A continuación móstrase o resumo deste artigo, que se corresponde co Capítulo 3 desta tese.

- Unha nova ferramenta de marcado de humidade, coñecida usualmente como método dos trazadores de vapor de auga (WVTs, polas súas siglas en inglés) ou método euleriano en liña, implementouse no modelo meteorolóxico rexional Weather Research and Forecasting (WRF, polas súas siglas en inglés), habilitándoo para estudos precisos de fontes de humidade atmosférica e das traxectorias seguidas por esta. Aquí presentamos o método e a súa formulación, xunto con detalles da súa implementación no WRF. Realizamos unha validación profunda cunha simulación dun mes de duración sobre Norte América a 20 km de resolución rastrexando todas as fontes posibles: bordes laterais, superficies continentais, marítimas e lagos, así como a humidade presente inicialmente. Estimamos os erros como as cantidades de humidade ou precipitación que non poden ser asignadas a ningunha das fontes. Os resultados da validación indican que o método exhibe unha alta precisión, con erros considerablemente inferiores ao 1% durante o período de simulación completo, tanto para a precipitación como para a auga precipitable. Aplicamos o método á tormenta de neve por efecto lago de novembro de 2014, que afectou á zona norteamericana dos Grandes Lagos, co obxectivo de cuantificar a contribución da evaporación sobre os lagos ás enormes acumulacións de neve observada durante o evento. Realizamos simulacións nun dominio aniñado a 5 km de resolución coa técnica de rastrexo demostrando que arredor do 30-50% da precipitación nas rexións inmediateamente a sotavento tiñan a súa orixe na humidade evaporada sobre os Grandes

Lagos. Esta contribución aumentaba ata o 50-60% do total da neve nas zonas máis afectadas, o que suxire que os fluxos de evaporación sobre os lagos tiveron un papel fundamental á hora de producir as acumulacións de neve máis extremas do episodios, as cales resultaron nos maiores impactos socioeconómicos.

Despois da posta a punto da ferramenta de rastrexo de humidade, decidimos continuar co traballo que comezara durante o meu máster. Melloramos a configuración do experimento, incluíndo unha importante mellora na selección das fontes de humidade a rastrexar e tamén no xeito no que se cuantificaban as fraccións de precipitación procedentes das distintas fontes. A análise dos datos en xeral e a representación dos resultados en particular foron tamén melloradas. Como se comentou antes, os casos analizados foron os eventos de inundacións do outono de 1982. Estes dous episodios causaron un enorme impacto en España a distintos niveis. Primeiramente debido ao coste en vidas e propiedades, pero tamén debido á súa repercusión social e mediática. Como exemplo, estes marcaron un antes e un despois dentro do antigo Instituto Nacional de Meteoroloxía (hoxe Axencia Estatal de Meteoroloxía), xa que, despois da catástrofe, as técnicas de predición foron melloradas e ampliadas, así como o sistema de avisos meteorolóxicos. Algúns investigadores xa analizaran o papel do transporte de humidade para estes episodios, pero a orixe da humidade aínda non se cuantificara. Despois de varias simulacións, confirmouse que a contribución do Mediterráneo por si soa estaba lonxe de poder explicar as grandes cantidades de precipitación rexistradas. Finalmente, os resultados encontrados foron presentados nun artigo, o cal compón o Capítulo 4 desta tese e cuxo resumo móstrase a continuación.

- As inundacións e inundacións repentinas son frecuentes no sur de Europa como resultado de fortes precipitacións que habitualmente descargan máis de 200 mm en menos de 24 horas. Aínda que as condicións meteorolóxicas favorables para estas situacións foron amplamente estudadas, existe aínda unha cuestión pendente: que fontes de humidade poderían explicar tanta precipitación? Para contestar a esta pregunta, o modelo atmosférico rexional Weather Research and Forecasting (WRF, polas súas siglas en inglés) con unha técnica de marcado de humidade recentemente implementada foi empregado para analizar as fontes de humidade en dous eventos de inundacións catastróficas ocorridos no outono de 1982 (un en outubro e outro en novembro) na zona do Mediterráneo Occidental, a cal vese afectada regularmente por este tipo de episodios de tempo adverso. O procedemento consiste en seleccionar de antemán rexións fonte potenciais para o evento extremo en consideración, e despois realizar simulacións usando a técnica de marcado para cuantificar a contribución relativa de cada unha das fontes seleccionadas á precipitación. Para estes eventos estudamos a influencia de catro posibles fontes: (1) evaporación sobre o Mar Mediterráneo Occidental; (2) evaporación sobre o Mar Mediterráneo Central; (3) evaporación sobre o Atlántico Norte; e (4) advección dende o Atlántico tropical e subtropical e dende África. Os resultados mostran que estas catro fontes de humidade explican a maioría da precipitación acumulada, sendo o aporte tropical e subtropical o máis relevante en ambos casos. No evento de outubro, a evaporación no Mediterráneo Occidental e Central e tamén no Atlántico norte tiveron unha importante contribución. Sen embargo, no episodios de Novembro a humidade tropical e subtropical foi responsable de máis da metade da chuvia acumulada, mentres que a evaporación sobre o Mediterráneo Occidental e o Atlántico Norte xogaron un papel secundario e a contribución do Mediterráneo Central foi case despreziable. Polo

tanto, as fontes remotas foron cruciais: no evento de outubro xogaron un papel similar ás fontes locais, mentres que no caso de novembro foron claramente dominantes. En ambos episodios, o transporte de humidade a longa distancia dende os trópicos e subtropicos tivo lugar en capas medias da troposfera, a través de plumas de humidade ben definidas con porcións de mestura máximas en niveis medios.

Tendo só analizados dous casos, tiñamos o mesmo problema que os estudos anteriores, isto é, non podíamos extraer conclusións xerais. Polo tanto, necesitábamos simular un gran número de casos que afectasen non só a España, senón tamén a outras zonas do Mediterráneo. A primeira opción considerada foi empregar unha base de datos de inundacións. Sen embargo, este procedemento tiña varias desvantaxes, relacionadas co feito de que as inundacións non só dependen de factores atmosféricos, senón tamén de outros como a topografía ou o uso do solo. Por este motivo, un evento altamente catastrófico podería ser, en termos de precipitación, menos importante que un evento con poucos danos debido á pouca vulnerabilidade das zonas afectadas por este. Isto era de gran importancia para nós porque unha das cuestións que estabamos tratando de resolver era se os casos máis extremos se caracterizaban por un maior aporte (relativo) de humidade dende zonas tropicais. Polo tanto, os eventos non podían ser detectados e ordenados en base ao seu impacto, senón que tiña que ser en base á chuvia rexistrada. Por outra banda, había algúns estudos que se centraban en detectar eventos de chuvia extrema a partir de medidas directas realizadas con pluviómetros, pero estes normalmente centrábanse en países concretos. En consecuencia finalmente decidimos realizar a nosa propia detección e caracterización dos eventos a ser simulados. Debido á dificultade de obter datos de precipitación de alta densidade para o Mediterráneo completo, decidimos centrarnos no sector occidental, incluíndo Italia, Andorra e as costas mediterráneas de España e Francia. Os eventos foron detectados no período 1980-2015 e posteriormente ordenados por magnitude e agrupados por tipo de tempo. Esta detallada análise nun período de 36 anos foi empregada para construír unha climatoloxía de eventos extremos na rexión do Mediterráneo Occidental. Dita climatoloxía foi presentada noutro artigo, correspondente ao Capítulo 2 desta tese, o cal se resume no seguinte parágrafo.

- A rexión do Mediterráneo Occidental sofre frecuentemente os efectos devastadores das inundacións, causadas por enormes acumulacións de chuvia que algunhas veces recordan aos valores producidos por sistemas tropicais. A pesar da relevancia climática e social deste tipo de episodios, hai algunhas cuestións fundamentais que aínda hoxe son difíciles de contestar, por exemplo: onde se rexistran máis casos dentro da rexión? Ou, cales foron os episodios máis potencialmente perigosos? Neste estudo identificamos, e posteriormente reunimos e unificamos información de todos os eventos diarios ocorridos entre 1980 e 2015. Usando a base de datos de precipitación en reixa de alta resolución MESCAN, os eventos son detectados e, para cada caso, a data e as zonas afectadas son gardadas. Posteriormente, os eventos son ordenados de acordo á súa magnitude e clasificados por tipos de tempo. Ademais, úsanse as bases de datos de inundacións FLOODHYMEX e EM-DAT para comprobar se os eventos de chuvia provocaron inundacións. Toda esta información rexístrase nunha base de datos de acceso aberto para o público. Os resultados mostran que o maior número de eventos por ano rexístrase na rexión francesa de Languedoc-Rosellón e na Comunidade Valenciana. Os casos de maior magnitude, que maiormente están asociados a inundacións, presentan unha marcada estacionalidade, ao ocorrer arredor dun 80% deles nos meses de setembro,

outubro e novembro. Finalmente, mostramos que só catro tipos de tempo están presentes na maioría dos días con chuvias perigosas no Mediterráneo Occidental. A situación meteorolóxica máis perigosa caracterízase por unha zona de baixas presións en todos os niveis troposféricos no Atlántico Oriental, formando un patrón de bloqueo cunha dorsal anticiclónica que tende a estenderse dende o Mediterráneo Central ata Europa Central. Arredor do 40% dos casos máis extraordinarios están asociados con esta configuración. Como exemplo, o famoso episodio de Piemonte (Italia) do ano 1994, entre os 10 primeiros máis intensos, foi causado por un patrón atmosférico deste tipo.

Unha vez feita a detección, posta a punto a ferramenta de rastrexo de humidade e tendo xa experiencia na súa aplicación no Mediterráneo, dispuxémonos a simular un alto número de eventos. A configuración do experimento foi mellorada con respecto á empregada para os episodios catastróficos de 1982. A principal modificación afectou á elección do dominio de simulación e á elección das fontes de humidade. Decidimos estender o dominio para que cubriese case por completo o hemisferio sur, de tal forma que puidésemos rastrexar ata as fontes máis remotas, coma o Océano Pacífico. Ao usar un dominio tan grande, xunto co feito de que tiñamos que comezar as simulacións un mes antes do inicio do evento para dar tempo suficiente a que a humidade se evaporase, aumentou moito o coste computacional do experimento. Aínda así fomos capaces de simular 160 casos no tempo dispoñible.

Os resultados obtidos confirmaron a nosa hipótese inicial xa que a fracción de precipitación con orixe mediterránea é do 35% de media, e raramente excede o 50%. Isto é obviamente unha contribución importante, pero lonxe do papel dominante que moitas veces se lle supón a esta fonte. Tamén encontramos que o Océano Atlántico, incluíndo o Atlántico norte e o Atlántico tropical, tivo unha contribución moi similar á do Mar Mediterráneo. Finalmente, encontrouse que as fontes extremadamente distante, como as tropicais, aínda que xeralmente teñan contribucións pequenas por separado, xuntas xogan un papel crucial como potenciadoras da precipitación. Os resultados mostraron que en algúns casos, unha parte significativa da chuvia rexistrada orixinábase en fontes tan distantes como o hemisferio sur ou o Pacífico tropical. Ademais, fíxose un estudo detallado da variación na contribución das diferentes fontes en función da época do ano e dos tipos de tempo. Todos estes resultados foron incluídos nun artigo final que xa foi revisado e aceptado e será publicado proximamente. O resumo deste artigo, correspondente ao Capítulo 5, preséntase a continuación.

- A rexión do Mediterráneo foi declarada como un punto quente no contexto do cambio climático debido, entre outras razóns, ao previsible incremento nas chuvias extremas que frecuentemente afectan esta zona densamente poboada. Sen embargo, segue sen ser de todo certo ata que punto estas chuvias torrenciais están conectadas con outras rexións fora do Mediterráneo. Aquí simulamos 160 eventos de precipitación extrema cun modelo atmosférico habilitado para un rastrexo de humidade de última xeración e demostramos que o transporte de humidade a gran escala é un factor máis importante que a evaporación sobre as fontes locais. Encontramos que a fracción de precipitación media con orixe no Mediterráneo é só do 35%, mentres que o 10% ven da evapotranspiración sobre terras próximas (en Europa continental) e un 25% orixínase no Atlántico norte. O restante 30% procede de varias fontes máis distante, en ocasións tan remotas como o Pacífico tropical ou o hemisferio sur, indicando conexións directas con múltiples zonas do planeta e unha redistribución global de enerxía. Os nosos resultados apuntan cara a importancia

de enfocar estes eventos extremos dende unha perspectiva máis global e menos rexional, especialmente cando intentan atribuírse ao cambio climático.

Polo tanto, a mensaxe última desta tese é que a contribución do Mar Mediterráneo a estes eventos extremos é incuestionablemente moi relevante, pero se queremos comprendelos completamente non podemos empregar un enfoque puramente rexional, xa que as fontes remotas e moi remotas son tamén moi importantes á hora de explicalos. A principal implicación desta conclusión é que cando investigamos estes eventos de chuva extrema mediterráneos no contexto do cambio climático, non só debe prestarse atención as alteracións locais en curso froito deste fenómeno, como o incremento na temperatura das augas do Mar Mediterráneo observado nos últimos anos, senón tamén a outras posibles alteracións en rexións máis afastadas.



# Chapter 1

## General Introduction

High inter-annual or intra-annual variability in the precipitation regime is a recurrent climate feature of much of the most populated regions of our planet. This high variability is directly connected with the incidence of extreme hydro-meteorological events, such as torrential rainfall or droughts [4] and consequently, flood damages or water shortages are issues to which most countries are subject. More specifically, floods, mainly caused by heavy rain [5], impact more people than any other type of natural hazard in the world, and for this reason, extreme precipitation resulting in inundation has been thoroughly studied with the main objective of reducing the high economic and human costs caused by this type of catastrophic episodes. However, prospects for the future in this respect are not encouraging; the Clausius-Clapeyron equation establishes a quasi-exponential increase in humidity with temperature, of about 7% per degree Celsius, which implies that global warming inevitably leads to more available water vapour in the atmosphere, increasing the odds of heavy rainfall [6, 7, 8]. As a consequence, since 2000, flood-related disasters have already increased by 134% compared with the previous two decades (State of the Global Climate 2021: WMO Provisional report, [https://library.wmo.int/index.php?lvl=notice\\_display&id=21982#.YdV\\_kmjMI2x](https://library.wmo.int/index.php?lvl=notice_display&id=21982#.YdV_kmjMI2x)).

### 1.1 Motivation, objectives and thesis outline

#### 1.1.1 Motivation

The western Mediterranean region (WMR) frequently suffers from the adverse effects of floods, associated with the development of strong convective situations giving rise to relatively short but intense periods of rain. In some specific cases, up to 800 mm of rainfall [9] and near 1,000 deaths [10, 11] have been recorded in a single day. Extreme rainfall and flooding are not only essential elements of climate in the WMR, but also key social features due to the enormous impact they cause [12, 13, 14]. Flood episodes such as the case of Tous (Spain) in October 1982 or Piedmont (Italy) in November 1994 have been analysed by researchers [e.g. 15, 16] and are still remembered by the population and the media because they claimed the lives of more than 100 people [10]. Moreover, studies show that, in some parts of this region, heavy daily rainfall and flooding occurrence have increased in recent years [17, 18, 13, 19] and will continue to do so in the coming decades [e.g. 20, 21, 22, 23] coinciding with the expected trend in the global precipitation regime to become more extreme. Therefore, prevention and research in the field of extreme rains and floods in the Mediterranean must continue to advance in bringing together

efforts from different countries and disciplines, as it is currently the case within the HYMEX international program [24, 25].

Extreme precipitation events (EPEs) have traditionally been explained in the WMR, dynamic and geographical factors aside, as being a consequence of the potential instability and water vapour content associated with the high heat and evaporation fluxes from the Mediterranean Sea, which in late summer can reach temperatures of 30°C. However, different studies have suggested that other ocean basins, especially the Atlantic, may contribute significant amounts of moisture to the high precipitation values recorded during these episodes [26, 27, 28, 29, 30, 31, 32, 33, 34, 3]. In addition, while factors such as strong instability or the presence of a Mediterranean low in the vicinity are commonly associated with EPEs [35, 36], the concurrence of these weather features does not ensure the development of extreme precipitation. For example, in autumn, and also in other seasons, the presence of Mediterranean cyclones is certainly much more frequent than the occurrence of catastrophic flooding episodes. Thus, an important question arises: could a very humid flow associated with large-scale circulations outside the Mediterranean be a discriminating factor among many similar local situations in which only one produces an EPE? Or, in other words, is the moisture supply of EPEs in the Mediterranean dominated by local-scale mechanisms or is it more connected to processes in other parts of the planet than previously thought? The main objective of this thesis is to expand and improve on previous knowledge on the origin of the moisture feeding Mediterranean rainfall extremes in order to give a definitive answer to this question.

### **1.1.2 Objectives**

The primary objective of the thesis is to quantify the contribution of local and remote sources to Mediterranean EPEs. To achieve this general goal, there are a number of sub-objectives, several of which related to necessary preliminary work : (1) To obtain a database of EPEs for the western Mediterranean in the period 1980-2015 using an impact-related threshold and high-resolution precipitation data, (2) To rank events by magnitude and group them by weather type, (3) To tune an online Eulerian tool for moisture tracking (see Section 1.4) and validate it, and (4) To test this tool checking its applicability to the study of moisture origin in the Mediterranean region. Once these previous sub-objectives have been achieved, those related to the main objective of the thesis are directly addressed: (5) To set up an experiment that allows to analyse all sources, from local to the most remote ones such as the Pacific Ocean, (6) To select a high number of EPEs from the previously created database , (7) To simulate these events with the moisture tracking tool, (8) From the simulations, quantify the contribution to precipitation of each source for all events, (9) To group the sources into local and remote to clarify which of these play a more relevant role on average, (10) To analyse how the variability of source contribution depends on the intensity of the event and the atmospheric pattern, (11) To compare contributions in terms of precipitation and precipitable water, and (12) To assess in detail the contribution of tropical sources and in general of very distant sources.

### **1.1.3 Thesis outline**

The results obtained throughout the thesis will be shown in Chapters 2,3,4 and 5, which summarise the work carried out within the OPERMO (*Origen de la precipitación extrema en la región del Mediterráneo Occidental*) project, funded by the Spanish Ministry of Economy,



Industry and Competitiveness (CGL2017-89859-R) to achieve the objectives posed above. The events to be studied are defined in Chapter 2, where a compilation of the main EPEs over a 36-year period and their characterisation (objectives 1 and 2) are carried out. In Chapter 3 we present and validate the moisture tracking technique used in this thesis (objective 3). Once the events to be studied have been detected and analyzed, and the tracking tool has been configured, we apply it to quantify the fraction of precipitation coming from the different sources. Chapter 4 shows an analysis of the origin of the moisture for 2 infamous flood events in the autumn of 1982 (objective 4). Finally, based on the experience gained from employing our tool in these two cases, we designed a much more ambitious experiment in which we track moisture in more than one hundred cases. Therefore, Chapter 5, which presents the results of these experiments, is perhaps the most important, as it finally addresses most of the objectives set for this thesis (objectives 5-12).

In the rest of the present chapter we introduce some basic concepts: we present the main physical mechanisms governing extreme precipitation; we define our study region, the western Mediterranean, and its main geographical and climatic characteristics; we briefly describe the different existing moisture tracking techniques, both coupled to atmospheric models (online) and uncoupled (offline); and we conclude by presenting the basics of atmospheric modelling. This general introduction will be brief, as the chapters that follow also each have their own introductory section.

## 1.2 Physical processes associated with extreme rainfall

For clouds to form, water vapour evaporating at the surface must be lifted to higher atmospheric layers by an updraft. In the updraft, the air expands progressively and thus cools down. When the dew point is reached, the water vapour condenses and some of this cloud water may eventually precipitate back to the surface. For heavy precipitation to occur, the vertical moisture flux must be strong, i.e. both the amounts of water vapour and the intensity of the updraft must be high. This will cause the moisture input into the cloud to be strong so that the outflow, i.e. precipitation, can also be strong. Following this reasoning, the precipitation rate ( $R$ ) can be defined as [37]:

$$R = P_e w q \quad (1.1)$$

Where  $w$  is the vertical wind speed,  $q$  the mixing ratio of the rising air (mass of water/mass of dry air) and  $P_e$  the precipitation efficiency, i.e. the ratio of the mass of water falling as precipitation to the mass of water entering the cloud. Unless efficiency is very low, which will generally only occur in environments with very low relative humidity, high values of  $w$  and  $q$  will ensure high precipitation rates, thus heavy rainfall. These two key variables in the genesis of extreme rainfall will be discussed separately below.

### 1.2.1 Atmospheric moisture content

In Eq 1.1 the flux ( $wq$ ) is evaluated at the entrance of the cloud. However, to estimate the total moisture content in the atmospheric column, it is more usual to vertically integrate the mixing ratio ( $q$ ) as follows:

$$TPW = \frac{1}{g} \int_{p_0}^{p_t} q \cdot dp \quad (1.2)$$

Where  $TPW$  is the total precipitable water, which measures the mass of water per square metre that is instantaneously available for precipitation. In Eq 1.2  $p$  refers to pressure,  $g$  to gravity acceleration and the integration limits range from the surface ( $p_0$ ) to the last pressure level available for calculation ( $p_t$ ). High  $TPW$  values certainly ensure that the updraft, if any, will transport high water vapour amounts. There are two possible ways to achieve high  $TPW$  values: high local evapotranspiration rates or strong horizontal moisture transport. Evaporation can be parametrised over the ocean as [38]:

$$E = c_e U dq = c_e U (q_s(SST) - q_a) \quad (1.3)$$

Where  $c_e$  is the turbulent exchange coefficient,  $U$  is the near-surface wind speed,  $q_s$  is the saturation specific humidity at sea surface temperature ( $SST$ ) and  $q_a$  is the specific humidity of the air above the water body. Broadly speaking,  $E$  will be greater the higher the water temperature, the stronger the wind and the lower the water vapour content of the air. On land, however, water availability is limited and Eq. 1.3 is no longer valid. The most common formula for calculating terrestrial evapotranspiration is the Penman-Monteith equation, which requires additional variables such as incoming radiation or stomatal resistance. On a global scale, it is estimated that 85% of evaporation occurs over the oceans. However, most of the evaporated water returns to the ocean and only a small part, about 10%, precipitates over the continents. Two-thirds of this 10% is eventually recycled and only one-third runs off back into the sea (Fig. 1.1).

On the other hand, moisture transport is usually assessed by vertically integrating the horizontal moisture flux:

$$IVT = \sqrt{\left(\frac{1}{g} \int_{p_0}^{p_t} q \cdot u \cdot dp\right)^2 + \left(\frac{1}{g} \int_{p_0}^{p_t} q \cdot v \cdot dp\right)^2} \quad (1.4)$$

Where  $IVT$  stands for integrated water vapour transport and (u,v) refers to the zonal and meridional wind components, respectively. Since Eq 1.4 is wind dependent, high  $IVT$  values need not only high moisture values but also strong winds. For this reason, maximum  $IVT$  is usually reached in low-level jets, which in turn are usually the core of atmospheric rivers [39]. It is known that the Mediterranean region can be affected by both Atlantic [3] and (newly defined) Mediterranean [40] atmospheric rivers but the origin of the moisture transported by them remains uncertain.

Precisely the main objective of this thesis is to quantify which of these two processes (evaporation over local sources or transport from remote regions) plays a more relevant role in feeding Mediterranean precipitation extremes. Our research is therefore framed within the study of the atmospheric branch of the hydrological cycle (Fig. 1.1).

## 1.2.2 Updraft intensity

There are four main air lifting mechanisms: (1) convection, (2) large-scale lifting, (3) orographic forcing and (4) low-level convergence. The most intense updrafts are associated with convection, while the other three cause updrafts of more moderate intensity and generally

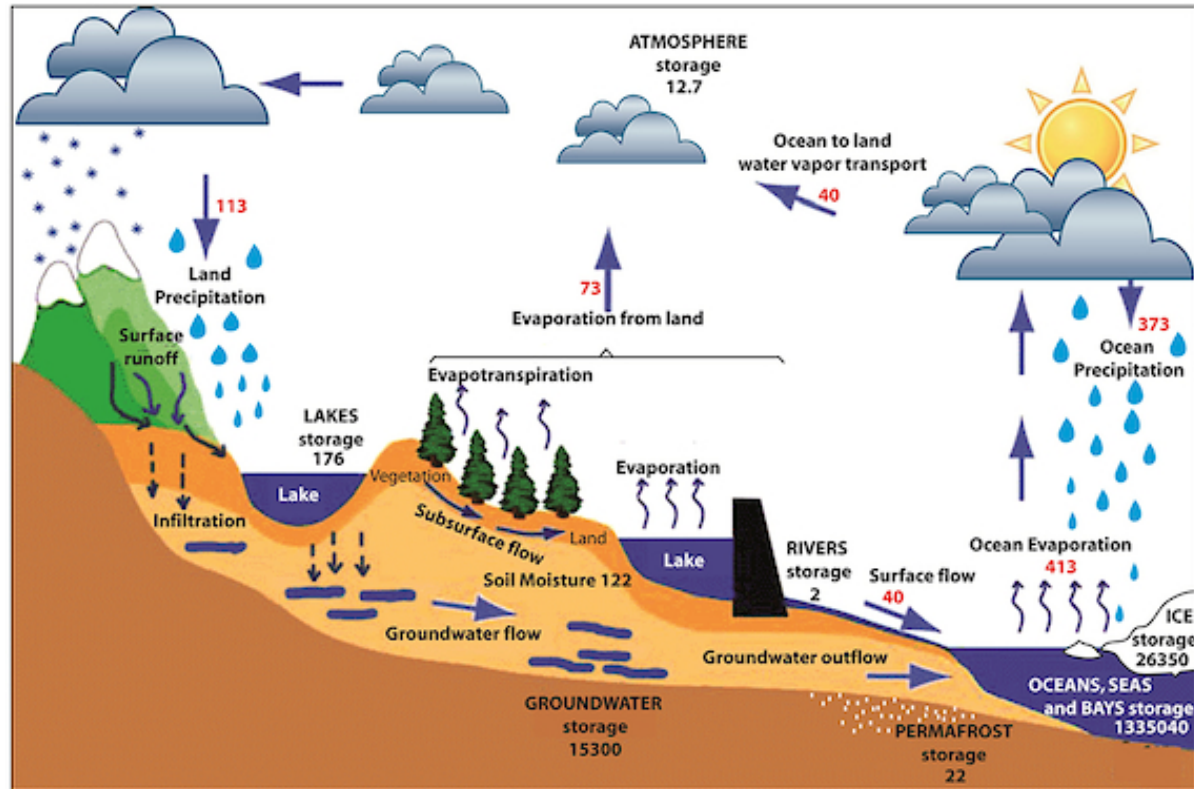


Figure 1.1: Storage (black numbers) and transport (red numbers) of water within the hydrological cycle (adapted with permission of John Wiley and Sons from ref. [38]).

result in stratiform precipitation. However, (1) would often not be possible without (2), (3) and (4) as these usually act as triggers and/or enhancers of convection.

Convection is closely related to buoyancy ( $b$ ), which can be defined on the basis of Archimedes' principle:

$$b = g \left( \frac{T_p - T_e}{T_e} \right) \quad (1.5)$$

Meaning that an air parcel will be positively buoyant when it has a higher temperature ( $T_p$ ) than its environment ( $T_e$ ). Convection therefore refers to the rising motions caused by a positive buoyancy force. Buoyancy serves in turn to introduce the concept of thermal instability. Instability is said to exist when an air parcel becomes positively buoyant when subjected to an infinitesimal vertical (upward) displacement. This means that under unstable conditions, any small disturbance will be enough to trigger convection. Thermal instability is a function of the lapse rate, i.e. of the temperature variation with height. In a humid atmosphere, conditional instability is said to exist when the environmental lapse rate ( $\Gamma_E$ ) is higher than the saturated adiabatic lapse rate ( $\Gamma_S$ ), which measures the temperature variation with height of an adiabatically rising parcel of saturated air. Mathematically [41]:

$$-\frac{dT}{dz} > \frac{g}{c_p} \left( \frac{1 + Lq_*/RT}{1 + \beta Lq_*/c_p} \right) \quad (1.6)$$

Where the left-hand term refers to  $\Gamma_E$  and the right-hand term to  $\Gamma_S$ , which is derived

from the first law of thermodynamics. In this equation  $T$  is air temperature,  $z$  height,  $g$  gravity acceleration,  $c_p$  specific heat at constant pressure,  $L$  latent heat of condensation,  $q_*$  saturation specific humidity and  $R$  and  $\beta$  are constants. The term "conditional instability" refers to the fact that it is conditional on the air being saturated. If  $\Gamma_E$  were high enough to exceed the dry adiabatic lapse rate ( $\Gamma_D = g/c_p$ ) instability would appear even if saturation is not reached and would therefore be called "absolute".

Instability can be measured using different indices, of which *CAPE* (convective available potential energy) is perhaps the most widely used. It is estimated vertically integrating buoyancy (Eq 1.5) as follows:

$$CAPE = \int_{LFC}^{EL} b \, dz = g \int_{LFC}^{EL} \left( \frac{T_p - T_e}{T_e} \right) dz \quad (1.7)$$

Where *LFC* is the level of free convection and *EL* the equilibrium level. The *CAPE* index represents the maximum amount of kinetic energy per unit mass that an air parcel could acquire by freely ascending from *NCL* to *NE*. Therefore, the maximum updraft velocity can be estimated directly from the *CAPE*:

$$w_{max} = \sqrt{2(CAPE)} \quad (1.8)$$

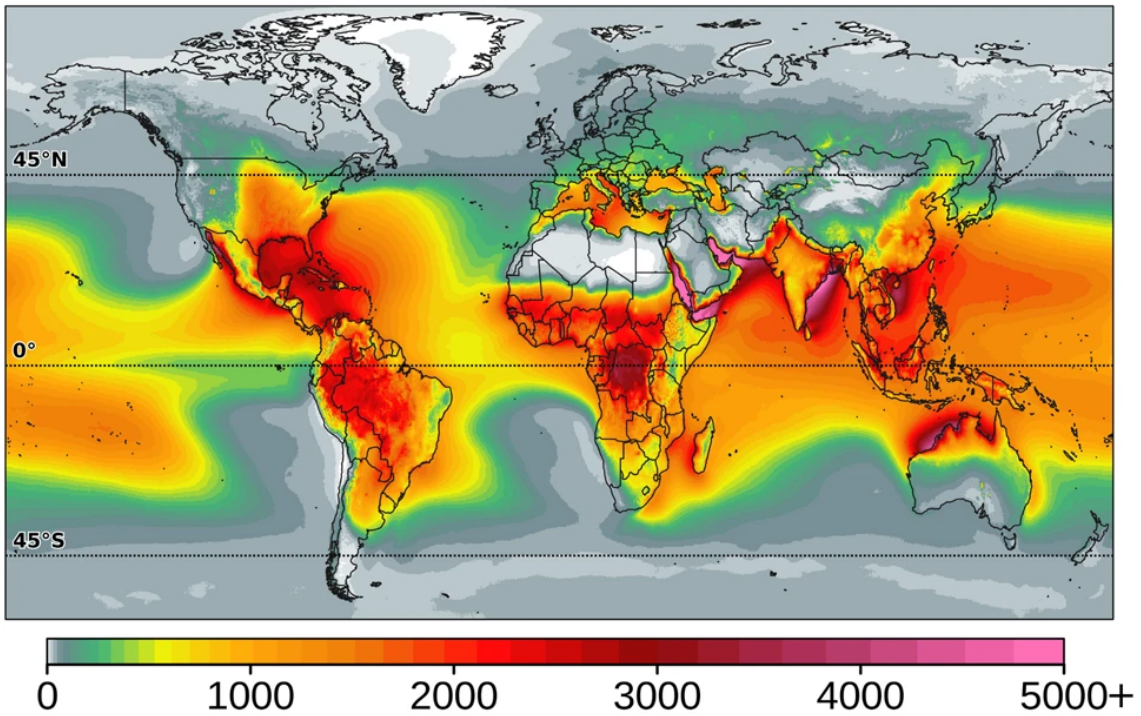


Figure 1.2: Climatology (annual mean) of the 95<sup>th</sup> percentile of the *CAPE* over the period 1979-2019. Data are from the ERA5 reanalysis [42] (adapted with permission of Springer Nature from ref. [43]).

For low *CAPE* values, convection may occur but it is usually shallow. Deep convection generally arises for *CAPE* values higher than  $1000 \text{ J} \cdot \text{kg}^{-1}$ . More specifically, *CAPE* values between 1000 and  $2500 \text{ J} \cdot \text{kg}^{-1}$  indicate a risk of moderate convection, values between 2500 and  $4000 \text{ J} \cdot \text{kg}^{-1}$  are adequate to support strong convection and values above  $4000 \text{ J} \cdot \text{kg}^{-1}$  can



lead to extreme convection [44]. Under such unstable conditions, highly organised thunderstorm systems, such as mesoscale convective complexes, quasi-linear convective systems or supercells may develop (if other atmospheric factors are also adequate). The areas bordering the Mediterranean Sea are characterised by high *CAPE* values (Fig. 1.2) and many of the catastrophic EPEs that occur there are associated with these highly severe thunderstorm systems [e.g. 45, 46, 47, 48, 49, 50, 51]. As we said at the beginning of this section, convection needs, in addition to high instability, a triggering mechanism. High *CAPE* values do not ensure the development of thunderstorms if that mechanism is not able to overcome inhibition, that is, to bring an air parcel to the level of free convection (*LFC*) in which its temperature would be higher than that of its surroundings. Large-scale lifting, described by the quasi-geostrophic omega equation [see 52], is one of the most important triggers and usually appears at the leading edge of upper-level troughs as a consequence of the cyclonic vorticity advection, and hence divergence, that occurs in that area. Orographic lift is another of the most frequent triggering mechanisms and results from the horizontal airflow blocking produced by mountains. Low-level convergence, another typical trigger, is by definition associated with an ageostrophic airflow, which may be due to different reasons, such as an orographic deflection of the flow or an interaction between two air masses with different density and temperature (fronts). Moreover, all these mechanisms can strengthen updrafts, not just trigger them.

Finally, we note that humidity in Eq 1.1 plays a doubly important role because the updraft velocity ( $w$ ) will also be dependent on the mixing ratio ( $q$ ). This is because the temperature of a rising air parcel, and thus its buoyancy, is increased by the release of latent heat from condensation. In other words, more moisture means more latent heat and therefore a higher buoyancy force.

### 1.3 The western Mediterranean region

From the beginning of the thesis we aimed to broaden the study region with respect to previous research on the origin of the moisture fuelling EPEs in the Mediterranean, which focused on specific areas, such as northwestern Italy [32] or southeastern France [30]. For this purpose, we have considered the entire western Mediterranean with the exception of the African part. The selected region of study is shown in Fig. 1.3, in which each coloured area indicates a different sub-region. Our research will focus on the zones of Spain, France and Italy surrounding the western sector of the Mediterranean Basin. Hereafter, the term WMR refers to the combination of these regions.

To select the region of study we use the Nomenclature of Territorial Units for Statistics or NUTS (by its French acronym), a standard for the classification of the territory used by the European Union. This standard subdivides the EU Member States into three categories (NUTS1, NUTS2 and NUTS3) according to socio-economic criteria. Table 1.1 shows for each sub-region the names of the different NUTS encompassed, along with additional information, such as total area. Note that Andorra is not included in the table because it is not a EU Member State, but it is part of Region 2.

The grouping of these territories into different sub-regions is based on a climatological criterion relying on our previous experience, the distribution of the relief and large scale atmospheric flow exposure. For example, some areas within Region 1 will generally be affected by heavy rainfall when the wind is from the east, while Region 2 will be more favoured by south-easterly flows and Region 3 by southerly winds (see fourth column in Table 1.1). The

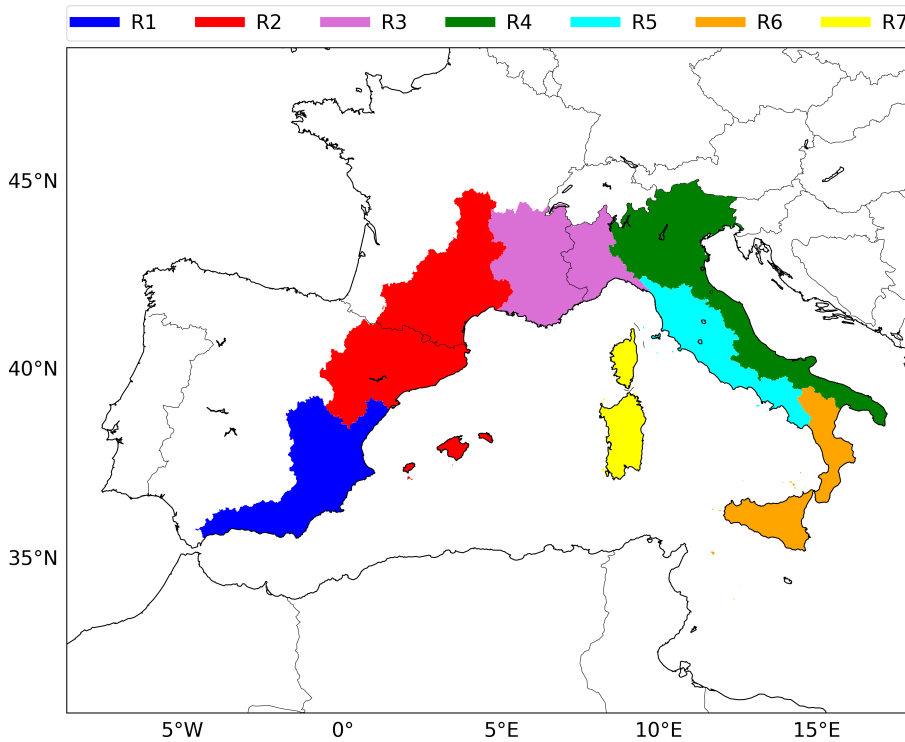


Figure 1.3: Region of study. Each colour represents a different sub-region.

selection of a climatological instead of a political criterion explains why some regions are formed by territories from different countries.

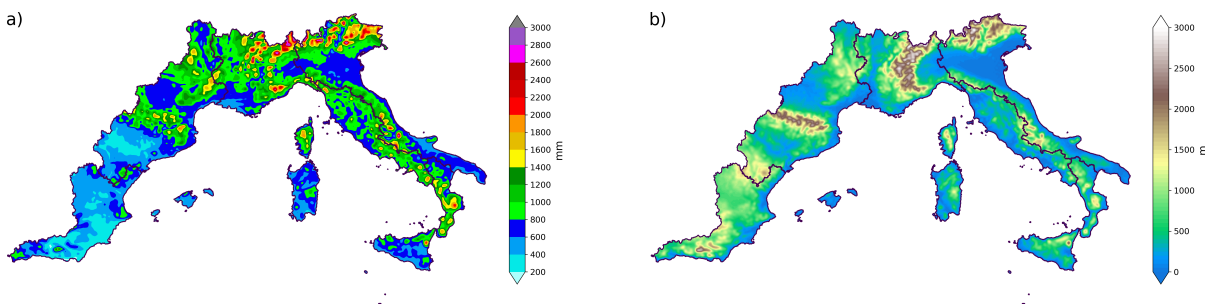


Figure 1.4: Annual mean precipitation for the climatological period 1980-2015 (a) and topography (b) of the western Mediterranean region. Data are from the MESCAN analysis [53].

In Fig. 1.4b we show a key geographical feature of the WMR: its abrupt orography with multiple mountain systems, among which the Pyrenees (Region 2) and the Alps (Region 3 and 4) stand out. All the sub-regions present a pronouncedly rough terrain, with elevations from sea level to mountains well above 2000 meters. This abrupt relief has direct consequences on the climatology. For example, the average annual precipitation (Fig. 1.4a) is strongly linked to the topography, with the highest values (more than 2000 mm per year) being found in the highest mountains of the Alps and Apennines (Region 3 and 4). The Spanish sector is clearly the driest, mainly Region 1, where annual rainfall is below 400 mm over a large area. This type of orography and its proximity to the sea also partly explains the high occurrence of EPEs in

Table 1.1: Information from the seven regions considered in the study. For each region (rows) we show in columns (from left to right): name of the different sub-regions (NUTS) encompassed, total area (in thousand of  $km^2$ ) and the main orientation of the coastline.

	NUTS2	NUTS3	Area ( $10^3 km^2$ )	Wind exposure
Region 1	Valencian Community Region of Murcia	Cuenca Albacete Almería Granada Málaga	95	East
Region 2	Balearic Islands Catalonia Aragon Languedoc-Roussillon Midi-Pyrénées Auvergne	–	184	Southeast
Region 3	Provence-Alpes-Côte d’Azur Rhône-Alpes Liguria Piedmont Aosta Valley	–	109	South
Region 4	South Tyrol Trentino Lombardy Friuli Venezia Giulia Veneto Emilia-Romagna Marche Abruzzo Molise Apulia	–	130	Northeast
Region 5	Tuscany Umbria Lazio Campania	–	62	Southwest
Region 6	Basilicata Calabria Sicily	–	51	Southeast
Region 7	Corsica Sardinia	–	33	–

this area, as it is often the surrounding mountains that trigger and intensify convection [e.g. 16, 54, 55]. The precipitation distribution in the WMR is bimodal, with a maximum in spring and a maximum in autumn (Fig. 1.5). There is, however, considerable variability within the region. For example, in the alpine areas (Regions 3 and 4) rainfall accumulations during the summer months are very significant, while in Calabria (Region 6) the maximum monthly precipitation

occurs in winter.

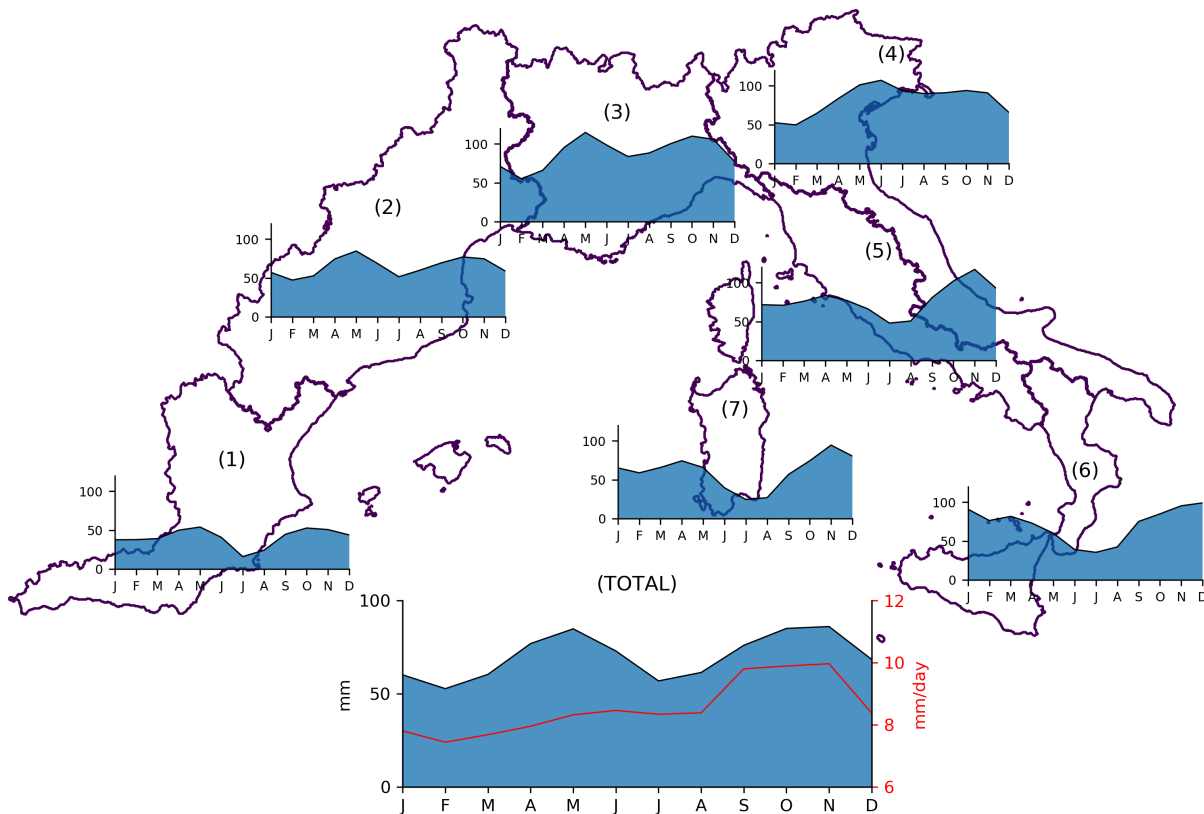


Figure 1.5: Monthly distribution of precipitation for the seven sub-regions and for the entire region (TOTAL). The red line indicates the average daily precipitation on wet days. Data are from the MESCAN analysis [53] and monthly averages are calculated in the period 1980-2015.

The spring and autumn rainfall peaks have different characteristics. Spring precipitation is typically associated with afternoon convection over land and, for this reason, tends to be more prominent inland than on the coast [56]. Autumn precipitation is concentrated on fewer days (see red line in Fig. 1.5), which means that it is more intense on average. In fact, as we will see in Chapter 2, most EPEs in the WMR, as well as major floods [12], occur in this season.

The fact that extreme rainfall tends to be concentrated in autumn is partly explained by the annual cycle of sea surface and air temperature (Fig. 1.6). During the warmer months, i.e. from April to August, the sea surface temperature is very similar to the air temperature, so that the lapse rate is reduced and consequently the thermal instability over the sea is inhibited. In winter the vertical thermal gradient is much greater, but the low temperatures limit the moisture holding capacity of the air. This results in low precipitable water values (Fig. 1.6), which also reduce potential instability and the likelihood of heavy rainfall. In autumn, however, temperatures still remain above 20 degrees Celsius, thus with high mean precipitable water values, while the sea-air temperature contrast is already high. From a thermodynamic point of view, this makes it the most favourable season for torrential rains. Obviously, atmospheric dynamics, and not only thermodynamics, play also a crucial role. The southward displacement of the jet stream at the end of the summer favours the appearance of Atlantic or Mediterranean lows or cut-off lows [COLs; e.g. 57, 58] during autumn, which in turn can favour dynamic forcings (convergence and divergence) and the organisation of a persistent low-level warm and moist flow. In fact, some



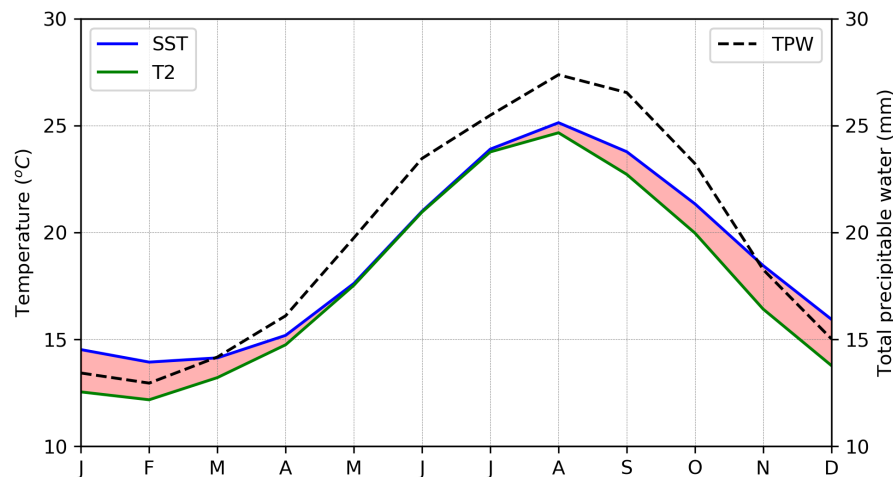


Figure 1.6: Monthly mean of sea surface temperature (blue), 2 meters air temperature (green) and total precipitable water (black) over the western Mediterranean basin. The red shading marks the sea-air temperature difference. Data are from the ERA5 reanalysis [42] and monthly averages are calculated in the period 1980-2015.

studies indicate that in more than 80% of WMR heavy rain cases there is a cyclone located nearby [59, 60]. In the next chapter we will show the main weather types leading to EPEs in the WMR, which are indeed characterised by a cyclone in the vicinity of the Mediterranean Sea. For a detailed review of the most frequent atmospheric conditions resulting in Mediterranean EPEs see also Llasat [55] and Dayan et al. [61].

## 1.4 Moisture transport and tracking

The study of the moisture sources feeding rainfall goes back decades, but the tools we have for this purpose have greatly improved in recent years. Precipitation origin is difficult to assess using observations, so the most widespread methods are based on the use of numerical moisture tracking models. The four main types are: analytical models, offline Eulerian models, Lagrangian models and online Eulerian models [38]. All of them have increasingly better representation of the physical processes affecting atmospheric moisture, assimilate more observations and run at higher resolutions. Consequently, we have an increasingly better understanding of the atmospheric branch of the hydrological cycle.

Analytical models, derived from the conservation equation of atmospheric water mass [62], have been widely used in calculations of the recycling ratio, which quantifies the contribution of local evapotranspiration to precipitation [63, 64, 65, 66]. A great advantage of these methods is their simplicity and low computational cost, at the expense, however, of strong assumptions, such as that water vapour of all origins is well mixed in the column [67], that limit their applicability. For this reason, analytical models can only provide a first order estimation of the recycling ratio. In more recent years, these models have been refined, and some of the former initial assumptions have been relaxed. Some newer analytical models can quantify the contribution of remote moisture sources to local precipitation, while improving recycling ratio calculations [68]. Nevertheless, most models still assume that moisture of all origins is well-mixed in the atmospheric column, notwithstanding some attempts to relax the hypothesis

[69], and this can significantly compromise their results [70].

Offline Eulerian methods, the so-called 2-D moisture tracking models [71, 72, 73], are an alternative to traditional analytical models especially useful for calculations of continental moisture recycling ratios on a global scale (Fig. 1.7). This method uses vertically integrated variables for calculations, and hence still assumes the well-mixed atmosphere hypothesis, which leads to errors particularly in regions of significant vertical shear [74]. However, in recent years this hypothesis has been relaxed by adding an additional vertical level to some offline Eulerian models (i.e., moving from a single column to two layers), which has considerably improved the results provided by this method [75].

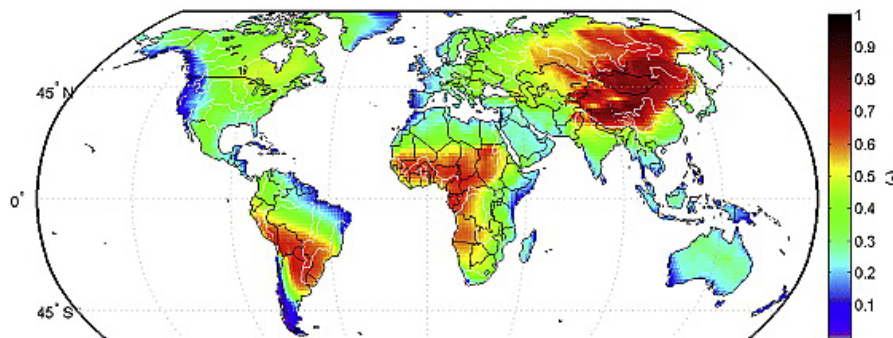


Figure 1.7: Continental precipitation recycling estimated from an offline Eulerian model. It is estimated that, on average, 40% of precipitation on land comes from terrestrial evapotranspiration (adapted with permission of John Wiley and Sons from ref. [72]).

Lagrangian models, based on the spatio-temporal tracking of individual fluid particles (Fig. 1.8), are possibly the most extended method to study sources and sinks of moisture. There are currently two main classes of Lagrangian models: the method of quasi-isentropic back-trajectories [76] and the method of dispersion of Lagrangian particles [77]. Lagrangian models have been extensively used in climatic studies of atmospheric water vapour sources [e.g. 78, 79] and in the diagnosis of the origin of moisture in EPEs [e.g. 80, 81]. Among the advantages of the method are computational efficiency, that source regions to analyze do not need to be selected a priori, since particles can be traced back in time, and furthermore, that when using reanalysis data for calculations, they effectively introduce an observational constraint. Lagrangian models include, nevertheless, some simplifications in their formulation that can result in serious biases. For example, the method of dispersion of Lagrangian particles does not allow for a clear separation between evaporation (E) and precipitation (P), in addition to neglecting liquid water and ice, which results in an overestimation of both E and P. For its part, the method of quasi-isentropic back-trajectories does not have this limitation, since evaporation and precipitable water content are needed for calculations; however, the well-mixed atmosphere hypotheses is still invoked, since water from surface evaporation is assumed to contribute uniformly throughout the column; and moreover, phase changes along the path of the parcels are not considered.

Online Eulerian methods, generally known as water vapour tracers (WVTs) are based on coupling a moisture tagging technique with a global or regional climate model. This strategy enables WVTs to fully consider all physical processes affecting atmospheric moisture, such as advection, molecular and turbulent diffusion, convection and cloud microphysics, thereby

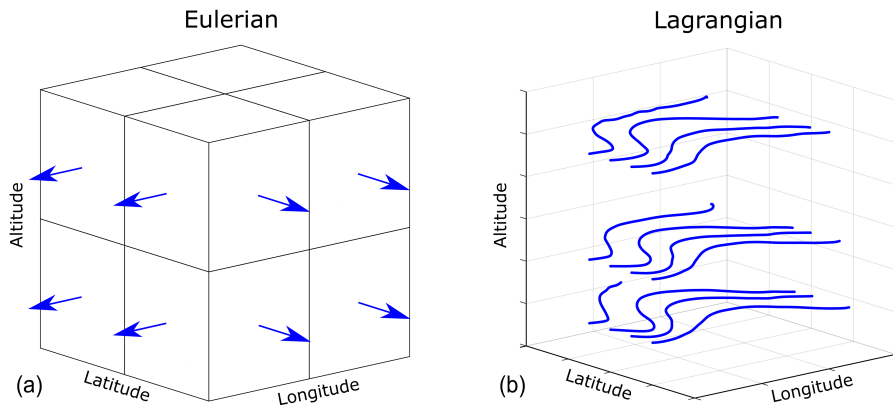


Figure 1.8: Schematic representation of the difference between Lagrangian and Eulerian moisture tracking models. The Eulerian approach is grid-based while the Lagrangian is trajectory-based (adapted with permission of Copernicus Publications from ref. [82]).

avoiding errors associated with offline methods. For this reason, this is presently regarded as the most accurate technique for the study of atmospheric moisture sources for precipitation. It has, nevertheless, some shortcomings, mainly related to the fact that it implies running an atmospheric model and relying on results from the simulation, since the method cannot be applied a posteriori, i.e., based for example on atmospheric analyses. Biases in WVTs are therefore not so much linked to the strategy itself, but to the model where they are coupled; hence the method provides sound results only if the atmospheric model simulation is realistic. In addition, the associated computational cost is much higher than in any of the other methodologies mentioned above. This technique will be the one used in this thesis, so it will be analyzed in depth in Chapter 3. Since WVTs are coupled to climate models, in the following subsection we will make a brief introduction to atmospheric modelling.

## 1.5 Numerical simulation of the atmosphere

The origin of atmospheric modelling dates back to the early 20th century when Abbe [83] and Bjerknes [84] proposed that the equations governing the behaviour of the atmosphere could be used to predict the future state of atmospheric variables from present values. In the 1920s, Richardson attempts, unsuccessfully, to make the first weather prediction [85]. Since then, progress in the field of atmospheric modelling has continued, and it has become one of the most advanced and impactful scientific disciplines [86]. Atmospheric modelling is essentially a mathematical problem which consists in solving a set of differential equations, the so-called primitive equations:

$$\left\{ \begin{array}{l} (1) \quad \frac{d\mathbf{v}}{dt} = -\frac{1}{\rho}\nabla p - 2\boldsymbol{\Omega} \times \mathbf{v} + \mathbf{g} + \nu\nabla^2\mathbf{v} \\ (2) \quad \frac{1}{\rho}\frac{d\rho}{dt} + \nabla \cdot \mathbf{v} = 0 \\ (3) \quad c_v\frac{dT}{dt} + p\frac{d\alpha}{dt} = J \\ (4) \quad p = \rho R_d T \end{array} \right. \quad (1.9)$$

Where (1) is the Navier–Stokes equation (conservation of momentum), (2) is the continuity equation (conservation of mass), (3) is the thermodynamic energy equation (conservation of

energy) and 4 is the ideal gas equation. This system, however, does not have an analytical solution so it has to be solved using numerical methods. These can be divided into finite difference and spectral methods. The finite difference method consists of approximating derivatives by differences while the spectral methods approximate the spatial variations of dependent variables in terms of finite series of orthogonal functions [52]. Broadly speaking, regional models (solving equations for a part of the planet) use finite differences while global models (solving equations for the whole planet) use also spectral methods. In this thesis, the moisture tracking technique employed is coupled to a regional atmospheric model and therefore, the method to solve the equations will be finite differences.

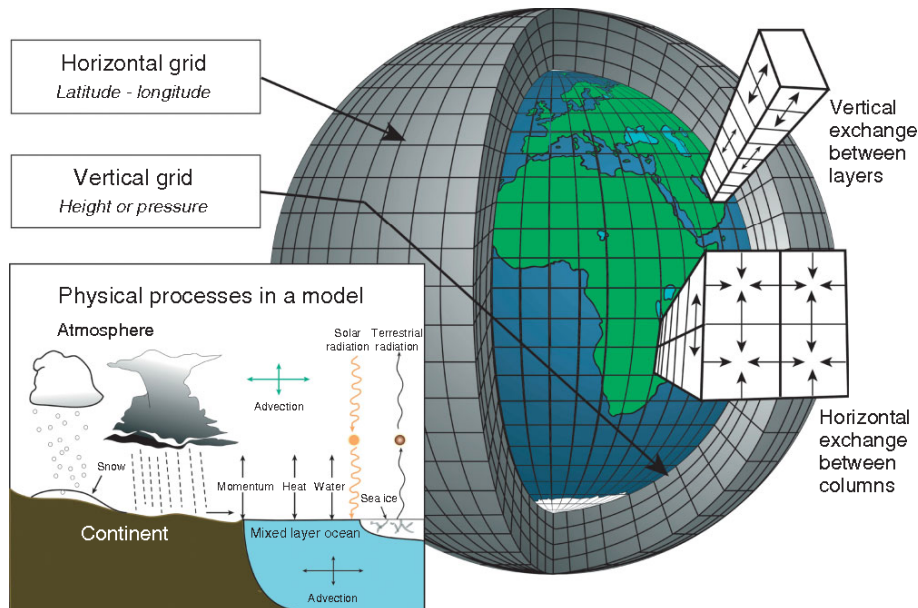


Figure 1.9: Schematic representation of the space discretisation used by the finite difference method (adapted with permission of John Wiley and Sons from ref. [87]).

The fact that the equations must be solved by numerical methods implies a discretisation of space and time. Today, global models run with a discretised space (grid) in steps of 10 to 100 km while regional models can run from 100 m to 10 km or so. This discretisation has the immediate consequence that processes smaller in scale (subgrid) than the model resolution are not explicitly solved when integrating the primitive equations. Therefore, these unresolved processes have to be parameterised, i.e. they have to be represented using the resolved variables. Such processes are for example cloud microphysics, convection or turbulence. In Section 3.2.2 we will see how the effects of these subgrid-scale processes on atmospheric humidity are parameterised.

Solving Eq 1.9 on scales of a few kilometres or less requires enormous computational power and data storage. For this reason, numerical models are often run on supercomputers. In this thesis we use the Finisterrae II supercomputer (from the Galician Supercomputing Center), which has 320 compute nodes, 7712 cores, 44544 GB of memory and 750000 GB of high-performance storage.

# Chapter 2

## Extreme precipitation events in the western Mediterranean region

\* The results from this chapter have already been published as D. Insua-Costa<sup>1</sup>, M. Lemus-Cánovas<sup>2</sup>, G. Miguez-Macho<sup>1</sup>, and M. C. Llasat<sup>3</sup>, “Climatology and ranking of hazardous precipitation events in the western Mediterranean area”, *Atmospheric Research*, vol. 255, p. 105521, 2021.

<sup>1</sup> CRETUS, Non-linear Physics Group, Universidade de Santiago de Compostela, Galicia, Spain

<sup>2</sup> Climatology Group, Department of Geography, Universitat de Barcelona, Catalonia, Spain

<sup>3</sup> Departament of Applied Physics, Universitat de Barcelona, Barcelona, Spain

### 2.1 Introduction

Despite all previous research efforts, there are, however, some apparently simple but very important questions about western Mediterranean precipitation extremes that have so far not yet been answered, such as: where do more EPEs occur? How many are registered annually? Or, which ones were the most extreme? The main objective of this chapter is to obtain a comprehensive characterization of all precipitation events that had the potential to cause significant damage occurred throughout the entire WMR from 1980 to 2015, thereby providing answer, among others, to the questions posed above.

Detecting the potentially catastrophic precipitation episodes that have affected the WMR would require a very high density of precipitation data, given their very high spatial variability. However, rain gauges are often too far apart from each other and even where the rain gauge density is sufficient, the data is frequently not open access; therefore, the task is hampered by the unavailability of observations in many areas within the region. Early studies in the United States evidenced the same observational constraint. Brooks and Stensrud [88] presented a climatology of heavy rains on short timescales and, in spite of the high station density used, found that their results presented important deficiencies since many of the events were not correctly detected by the observational network.

In the WMR, however, the studies conducted on extreme and heavy precipitation are solely based on rain gauge data. Romero et al. [89] built a daily heavy rainfall database from 1964 to 1993 in the Spanish Mediterranean region using data from 410 weather stations. They



considered as extreme those days in which daily rainfall exceeded 100 mm and confirmed that many of the events took place in the surroundings of the Sierra de Aitana (Alicante) during autumn. More recently, Ramos et al. [90] created a ranking of extreme daily precipitation events in the Iberian Peninsula, including the Spanish Mediterranean area. They used the IB02 precipitation database [91, 92], derived from data collected by more than 2800 rain gauges spread throughout Iberia. Using a pluviometric threshold based on normalized precipitation anomalies, they found, for example, that the major episode affecting this region between 1950 and 2008 was that of November 1982. In Italy, Brunetti et al. [93] employed precipitation data from 75 observation stations and detected a total of 87 EPEs in the period 1951-2001. For the definition of extreme event, they considered a threshold based on the average annual precipitation recorded by each station. In France, Ricard et al. [94] elaborated a heavy precipitation event database using more than 1200 rain gauges located in the southern part of the country. They worked with a constant threshold of 150 mm for identifying days with extreme rainfall and found 305 episodes in the period 1967-2006. Jansa et al. (2001), in the context of the MEDEX project [36], analysed a wider region, covering much of the WMR from 1991 to 1996. In this case they applied a threshold of 60 mm/24 h for the whole region, except in Algeria where the threshold was of 30 mm/24 h.

In summary, all the aforementioned earlier studies provide valuable information but are limited by the exclusive use of in situ precipitation measurements. Furthermore, they all analyse different sub-regions within the WMR and the methods employed to detect heavy or extreme precipitation episodes vary widely from study to study, which evidences that defining extreme or heavy event is a controversial point, since each researcher usually imposes one criterium of his or her own. In addition, these studies use precipitation thresholds that are not necessarily related to impacts; thus, they cannot provide a general analysis within the WMR of events with the potential to cause damage.

Indeed, whether or not introducing impacts into the definition of extreme events is a hotly debated topic today [e.g. 95]. In the literature, extreme precipitation generally refers to precipitation that exceeds a statistical threshold, for example a percentile, and the term heavy precipitation is usually reserved for rainfall that exceeds a constant threshold, for example 100 mm. However, neither extreme nor heavy precipitation are necessarily extreme in terms of impacts [96]; thus, a specific strategy is required to identify hazardous events. From now on, when referring to the precipitation events studied in this thesis, we will generally keep the term "extreme" as it is the most widespread in the literature, however, we must keep in mind that we do not use this term only in the statistical sense, but also in the sense of potential impacts.

Although defining a threshold associated with impacts can be tremendously complex, a very recent study [97] shows that the combination of a fixed precipitation threshold with a statistical one (in their case, a percentile) provides the highest correlation with economic losses, and we will use a similar strategy to identify the events to consider in our case. Additionally, we will use flood databases to verify that the selected events were indeed mostly conducive to damages.

Our precise goals are to obtain a detailed picture of the spatial and temporal distribution of EPEs in the western Mediterranean, a ranking of events according to their magnitude and a classification by weather type assigning a characteristic atmospheric pattern to each. Our analysis of the atmospheric conditions that usually generate hazardous rainfall situations in the WMR will be more concise and have a more general scope than in previous studies, which most often only focus on a small part of the region, obtaining a large number of potential patterns

[e.g. 98, 99, 100, 101, 102, 103] that make it difficult to establish a simple and clear overview of the synoptic configurations that affect the region as a whole.

All the resulting information from our study has been compressed in a single database. Thus, the main novelties of such database, and in general of this research, are: (1) it includes events from the entire WMR and for a long period (36 years), (2) the information it provides goes beyond the spatiotemporal location of the episodes, since it also contains additional data such as the magnitude or the associated weather type, (3) it is based on a gridded high-resolution precipitation dataset, built not only from rain gauge measurements and, therefore, avoiding in part the observational deficiency that affects other studies and (4) the events in the database are detected using an impact related threshold. The generated EPEs database has been made freely accessible to other authors.

The chapter is structured as follows: Section 2.2 and 2.3 describes, respectively, the data and the methodology used. In these sections we show, for example, the high-resolution precipitation database used and the selected method to detect the events. Section 2.4 discusses the results, where we present the EPEs database and the climatology created. Finally, Section 2.5 contains a summary and conclusions of the work.

## 2.2 Data

### 2.2.1 Precipitation datasets

For the detection of EPEs, we use the MESCAN precipitation analysis system [53], which has been recently developed within the European Reanalysis and Observations for Monitoring (EURO4M) project. It comes from the merger of two previous surface analyses (hence its name): MESan [104] and CANari [105]. MESCAN is based on a model background field adjusted with observations. The background data is a reanalysis generated from the HIRLAM model and downscaled from 22 to 5.5 km. Rain gauge measurements are from a high-density observational network covering the whole of Europe. Thus, it provides accurate daily gridded rainfall data from 1961 to 2015, which are especially useful for climatological purposes.

The two main advantages of MESCAN are: (1) it includes our entire region (the WMR) and period (1980-2015) of interest, so we do not have to mix data from different precipitation datasets, often incompatible because of their dissimilar characteristics and (2) by using a high-resolution reanalysis as background field, it provides a good precipitation estimate compared with other methods that only use rain gauge data, especially in places where there are no direct measurements. Therefore, it is very appropriate for capturing heavy precipitation events. Its main drawbacks are: (1) its temporal resolution is only one day, so it is not suitable for detecting very short duration events and (2) assimilated rain gauge observations are inhomogeneously distributed, which could result in diminished event detection numbers in some parts of the region, not because of climatological factors but because of a lower observational density.

In order to evaluate the impact of deficiency (2) above on detection skill, we compare the results obtained from MESCAN with those from two other precipitation databases, the SPREAD [106] and the APGD [107] gridded datasets, both constructed using a very dense observational network and at the same spatial resolution of 5 km, which is similar to that of MESCAN (5.5 km), thus making them especially appropriated for the validation of the latter. SPREAD covers Spain and APGD the entire Alpine region, areas where the observational

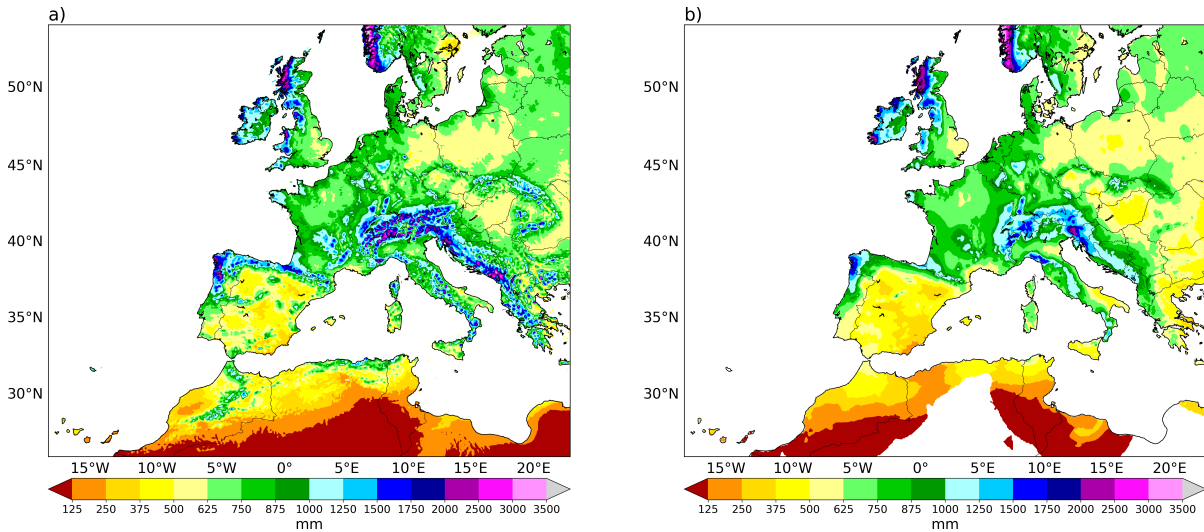


Figure 2.1: Annual mean precipitation on land from MESCAN (a) and from E-OBS (b) for the climatological period 1980-2015.

density of MESCAN is lower than, for example, in France. Results show (see Fig. 2.10 in the Appendix to this chapter) that despite the reduced number of ingested observations in MESCAN in these areas, EPEs are still well captured, since the number of detections is in good agreement with that obtained with SPREAD and APGD. Therefore, we conclude that this drawback does not significantly affect the results obtained in this study.

Figure 2.1a shows the average annual precipitation over Europe and northern Africa from MESCAN. Its high resolution (5.5 km) is very evident in how it adequately reproduces the strong orographic dependence of precipitation. Figure 2.1b shows the same field but from E-OBS v20.0e [108], one of the most widely used gridded precipitation datasets. Although both are generally similar in terms of magnitude, the spatial distribution of precipitation in E-OBS is less realistic than in MESCAN. For example, E-OBS is not able to properly represent the orographic enhancement of precipitation in the different mountain systems of the region, a deficiency mainly due to the exclusive use of interpolated observations to build the gridded database. In summary, we argue that, for our purpose, MESCAN is much more suitable than other datasets.

## 2.2.2 Flooding data

We use flooding occurrence data from the FLOODHYMEX [13, 109] and EM-DAT (<http://www.emdat.be/>) datasets to further characterize the detected events in our EPEs database. Additionally, we employ flooding information in these datasets to validate our EPEs detections. As floods (including urban floods, flash-floods and surface water floods) in the Mediterranean region are mainly rainfall-related, flood data can be crossed with EPEs identified from MESCAN precipitation data to ensure that detections are indeed correct.

The FLOODHYMEX database was developed in the framework of the HYMEX project, hence its name. It contains information about the date, place, physical features of the hazard (precipitation, discharge, etc) and impacts of all the catastrophic or large floods recorded in a selected region of the Mediterranean for a given period. They are identified as catastrophic in



basis of the methodology usually applied to classify flood events according to their impact [110, 19]; that is, it provides information about integrated flood risk, not flood hazard (as it would be the case if using discharge data alone). FLOODHYMEX was created with the ambition of becoming a common database of damage producing floods in the Mediterranean region, based on a rigorous analysis of daily information and using the same criteria to characterise all the events and regions [109]. FLOODHYMEX includes floods in Spain (Catalonia, Valencian Community and the Balearic Islands), France (Languedoc-Roussillon, Midi-Pyrenees, Provence-Alpes-Côte d’Azur), Italy (Calabria) and Greece. The database currently covers the 35-year period from 1981 to 2015. In total, FLOODHYMEX contains information on 171 flood events, which can have a duration of one or more days and affect one or several regions. The latest public version can be found at [http://mistrals.sedoo.fr/?editDatsId=1150&datsId=1150&project\\_name=MISTRALS&q=floodhymex](http://mistrals.sedoo.fr/?editDatsId=1150&datsId=1150&project_name=MISTRALS&q=floodhymex).

The main advantage of FLOODHYMEX is the highly detailed information it provides. Its main disadvantage is that it does not fully cover our region of interest and study period. For this reason, we use an additional flood dataset, EM-DAT (Emergency Events Database), which employs more restrictive criteria than FLOODHYMEX, thereby including less cases, but it is global, so it covers the whole Mediterranean region and for a long period (from 1900 onwards). FLOODHYMEX will be our reference flood database, but in areas or periods not covered by it, the information will be completed with EM-DAT.

### 2.2.3 ERA5 reanalysis

ERA5 [42] is the most recent (5th generation) global atmospheric reanalysis of the European Centre for Medium-Range Weather Forecasts (ECMWF), providing hourly data from 1979 to near-real time. ERA5 stands out for its high resolution (31 km in horizontal and 137 vertical levels), as well as for the vast amount of historical assimilated observations, and it represents a major improvement over its predecessor, the ERA-Interim reanalysis. We use ERA5 to classify EPEs according to the associated weather types. The variables used here for such classification are geopotential at 500 hPa, sea level pressure and precipitation, which have been obtained for the entire study period (1980-2015) every 6 hours.

## 2.3 Methodology

### 2.3.1 Setting a threshold for extreme day detection

In this work the threshold is based on normalized daily precipitation anomalies, a method recently used by Ramos et al. [90] to detect and rank EPEs in the Iberian Peninsula. For a given MESCAN grid point  $(i, j)$ , the normalized departure from the climatology ( $N_{ij}$ ) of a daily precipitation amount  $P_{ij}$  is:



$$N_{ij} = \frac{P_{ij} - \overline{P_{ij}}}{\sigma_{ij}} \quad (2.1)$$

Where  $\overline{P_{ij}}$  is the mean daily precipitation and  $\sigma_{ij}$  is the standard deviation (std) from this daily mean. We introduce three novelties with regard to the methodology used by Ramos et al. [90]: (1) we don’t use a running mean to calculate the mean daily precipitation and std, (2) we

consider all days in the calculation of the daily mean and std, not only wet days and (3) we impose a minimum value in the threshold. The main reason to avoid a running mean is that we wanted a static threshold that could be applied indistinctly to every day of the year. In addition, we take into account dry days in the calculations because it is essential to properly characterize the precipitation variability and because some previous studies have shown that the widely used approach of discarding dry days [e.g. 111] can sometimes lead to misleading results.

Including dry days, results in our daily mean and std taking lower values, and for this reason, we detect a daily precipitation event when at least in one MESCAN grid cell the precipitation anomaly reaches ten standard deviations, i.e.,  $N_{ij} > 10$ , instead of the  $N_{ij} > 2$  used in Ramos et al. [90]. Therefore, if we keep in mind Eq. (2.1), our threshold ( $T_{ij}$ ) could be written as:

$$T_{ij} = \overline{P_{ij}} + 10\sigma_{ij} \quad (2.2)$$

And the condition to detect an event in a grid point ( $i, j$ ) will be  $P_{ij} > T_{ij}$ . Since daily means tend to be small (especially when considering also dry days), the previous equation is dominated by  $\sqrt{\sum P_{ij}^2}$ ; therefore, the wettest places, and especially those with frequent large daily precipitation records, will have a more demanding threshold, which makes sense because they are likely the best adapted to high precipitation amounts.

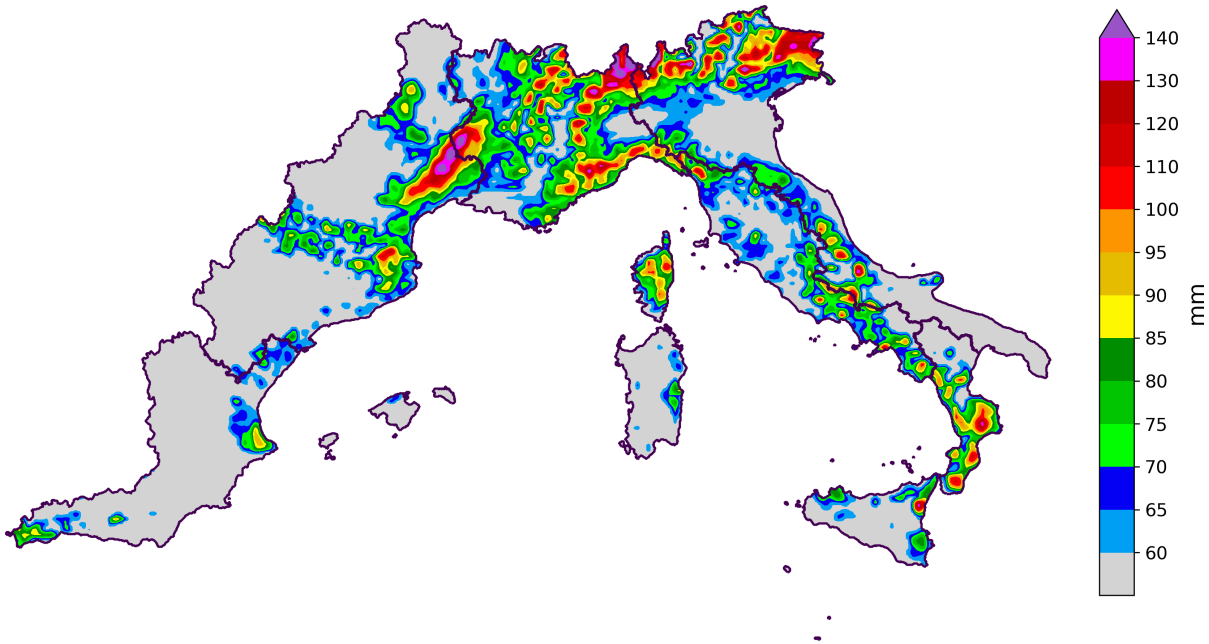


Figure 2.2: Threshold (mm) used to detect potentially catastrophic daily rainfall. Grey indicates 60 mm.

Nevertheless, this statistical threshold can take too low values in some places of our region, of around 30 mm, especially in semi-desert areas of Spain. From the perspective of impacts, a relatively small rain amount could cause damage, for example, due to the presence of a soil with low infiltration capacity; however, in the WMR, large rainfall accumulations are usually needed to wreak havoc. Thus, we impose a minimum value in the threshold, which we set at 60 mm according to the criteria used in the MEDEX project [36]. Since we are working with a gridded rainfall database, the threshold is applied at each grid cell, i.e. to the value representing

the spatially averaged rainfall in a region of  $5.5\text{km}^2$  (the resolution of MESCAN), thus a value of 60 mm certainly translates into higher local (sub-grid) values.

In summary, in this study we use a combination of a statistical precipitation threshold with a fixed one, given that the minimum value can also be regarded as a constant threshold. This is the same approach used in Liu et al. [97] to set an impact-related threshold. Figure 2.2 shows the combined threshold, which we ultimately use for the detection of potentially catastrophic precipitation events. It ranges from 60 mm, i.e. the minimum value, to more than 140 mm in some mountainous areas, which indicates that our threshold adapts to the climatic characteristic of each location. For example, in the Alps, daily rainfall of about 100 mm is relatively frequent due to the orographic enhancement of precipitation; thus, the threshold is more demanding there, so that only days with higher than normal rainfall are considered. The number of days in which this threshold is exceeded in at least one point in the region's grid across the 36-year period analysed is 1991.

### 2.3.2 Classifying extreme days by weather type

In this study the methodology used to classify EPEs by weather types is based on a principal component analysis (PCA) approach, a widely used methodology to this end [112, 113, 114, 115]. We apply a PCA to a temporal mode (T-mode) matrix of 500 hPa geopotential height, mean sea level pressure and daily precipitation, all of them obtained from ERA5 reanalysis data for consistency. Thus, in the T-mode matrix, the variables (columns) are the 1991 extreme days identified, and the observation (rows) are the grid points from the ERA5 geographical area used ( $30^{\circ}\text{-}50^{\circ}\text{N}$ ,  $15^{\circ}\text{W-}23^{\circ}\text{E}$ ). For a given EPE, the values of sea level pressure and 500 hPa geopotential are taken at the time of maximum precipitation of the day, which is determined from 6-hourly ERA5 precipitation, so that if the maximum rainfall is recorded from 18 to 00:00 UTC, the considered fields correspond to 18:00 UTC. This strategy responds to the rapidly evolving nature of many of the weather systems resulting in EPEs, whereby daily means of the meteorological variables may not represent properly the conditions leading to the observed high rainfall accumulations.

After applying the PCA to the previously standardized original data matrix, new variables are obtained, the principal components (PC), which are linear combinations of the original variables. The method employed to determine the number of components to retain is the well-known Scree Test [116], based on the amount of explained variance by each PC. These PCs are subsequently rotated by means of a varimax rotation, in order to obtain the maximum variance explained for each PC [117]. From the rotated PCs we obtained the loadings, the correlation matrix, which indicates the degree of correlation of all considered days with each PC. In this sense, the assignment of each day to each PC is based on the maximum correlation value. Day 1 is assigned to the PC with the highest correlation, and so on. This methodology allows classing each of the events into a unique weather type, even when their correlation with all PCs is low. To account for this lack of representativeness in some cases, the days whose correlation with all PCs is  $< 0.4$ , are assigned as undefined. The R package `synoptReg` [118] is used to develop such classification. After applying this method, each day with potentially catastrophic rainfall will be associated with a (single) weather type.

### 2.3.3 Ranking events by magnitude

Once all the daily events in our period of interest have been identified, we order them according to their magnitude, obtaining a ranking in which the events at the top are the most hazardous, potentially causing high damage. Following the recommendations of the World Meteorological Organization, the magnitude in a grid point  $i,j$  will be defined as the difference between the accumulated rainfall ( $P_{ij}$ ) and the established threshold for that point ( $T_{ij}$ ):

$$m_{ij} = P_{ij} - T_{ij} \quad (2.3)$$

And the overall magnitude of the event will be:

$$M = \bar{m}A \quad (2.4)$$

Where  $\bar{m}$  is the spatial average of the local magnitudes and  $A$  is the fraction of the total continental area of the WMR affected by the episode, i.e. the area where the threshold (Fig. 2.2) is exceeded. In summary, for an event to be of high magnitude, it must affect a large region or, if not, very intensely affect a smaller region. If the event produces highly above-threshold precipitation over a large region, an extraordinary magnitude is assured.

## 2.4 Results

### 2.4.1 Spatial distribution of extreme rains

For each MESCAN grid cell, the number of days on which the corresponding threshold (Fig. 2.2) is exceeded during the period 1980-2015, i.e., the total number of days with extreme rainfall, is shown in Fig. 2.3.

An important conclusion can be drawn immediately from Fig. 2.3: EPEs are concentrated in only a small part of the WMR, organized in coastal strips with two main extensions inland. The coastline from Murcia (Spain) to Genoa (Italy) across Regions 1, 2 and 3, is the most affected. The other coastal stretches impacted are the Ionian coasts of Calabria and Sicily (Region 6) and the Tyrrhenian coasts of the islands of Corsica and Sardinia (Region 7). In France extreme rainfall extends inland along the south eastern sector of the French Massif Central as well as up the Rhone Valley. For its part, in Italy, the potentially catastrophic precipitation is extended towards the western Alps from the heavily impacted shores of Liguria. We note that the largest number of episodes are not recorded in the highest zones. In the Alps, the most affected area is the mountain slope rising west from the Po Valley. This does not mean that in these high elevation locations rainfall has to be necessarily less, but that the same rain accumulation might not be statistically extreme there. In any case, the orography plays a major role, since it is fundamental in producing precipitation enhancement in the high mountains, but also in lower areas at their foot. In addition, there are also other small affected zones spread irregularly throughout the region, such as the coast around Malaga (Spain, Region 1) or Naples (Italy, Region 5).

Among regions as a whole, 1, 2 and 3 are the most affected, whereas 4 and 5 are the least. The areas surrounding the Gulf of Lion (Region 2) and the coastal strip of the Valencian Community (Region 1) are the most exposed to extreme rains in the entire region. Here we find the absolute maximum value of potentially catastrophic rain days, with around 30 from 1980 to

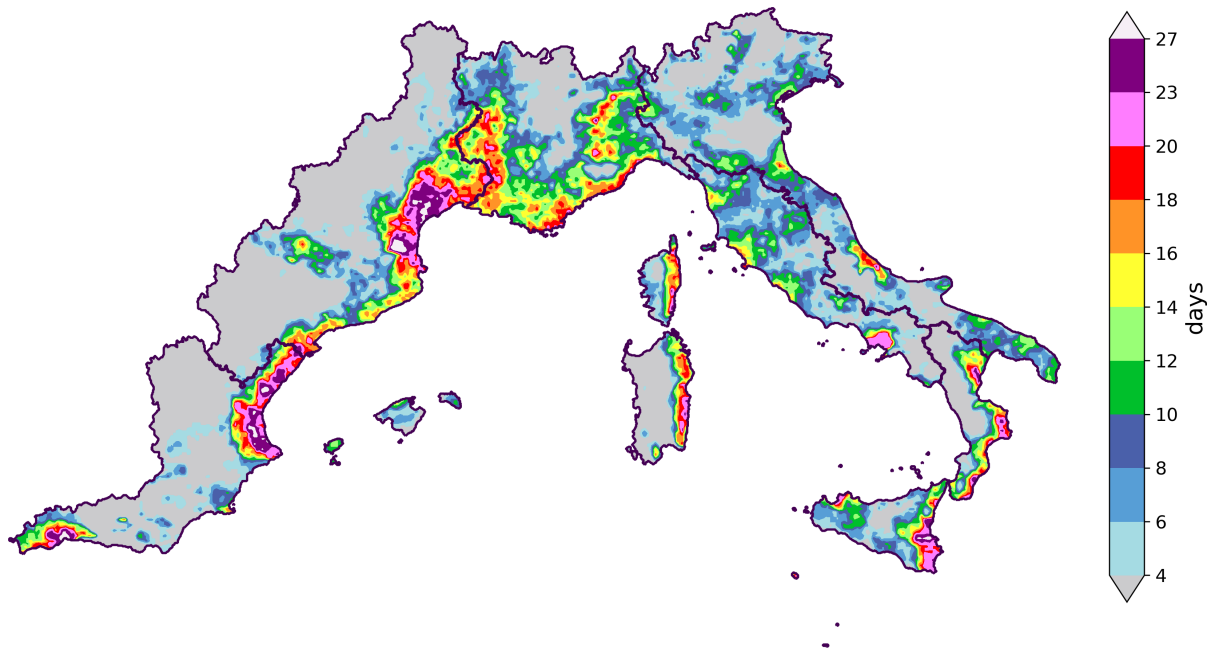


Figure 2.3: Spatial distribution of extreme precipitation in the western Mediterranean region: total number of potentially catastrophic rain days from 1980 to 2015. Grey indicates 0 to 3 days.

2015, almost one per year. The rest of the frequently affected territories, including the Liguria and Piedmont regions or the east coast of Corsica, Sardinia, Calabria and Sicily, have similar values, greater than 15 days over a vast area, with peaks of more than 20 days especially in Region 6.

From Fig. 2.3 we can also infer that within the WMR the main factor for the occurrence of extreme rains is the proximity to the coast. This is a key point in relation to flood risk, because most of the region's population is settled in coastal areas. Some of the region's major cities are thus heavily exposed to torrential rains. The southern or eastern orientation of the coastline also appears to be a crucial factor, suggesting that southerly or easterly flows at low levels are often associated with stronger thermal or dynamic instability situations. In the WMR, warm and moist air advection is almost assured when the wind blows from these directions, which favours the accumulation of large amounts of rain. This is why the Western Mediterranean Oscillation [WeMO; 119] is a good predictor of heavy rainfall in this area [120], since its negative phase is univocally associated with these southerly or easterly wind components [121]. As stated above, orography also plays a very important role. As evidence, note that maximum values in Fig. 2.3 generally appear as peaks located very close to the sea, but slightly inland, which means that small slopes near the most affected coastal stretches can substantially enhance heavy rainfall.

Finally, we note that, since we are working with daily rainfall data, this climatology does not include most very short duration episodes, such as a case of 30 mm in 1 hour associated with strong afternoon convection. These brief episodes, although may cause some local damage, are not usually associated with major disasters. There are, however, some cases, where a local storm discharges vast amounts of water onto a very vulnerable site, potentially causing devastating flash floods. Inevitably, such episodes will not be adequately captured by MESCAN because of their local nature. In addition, since they affect very small areas, their magnitude cannot be

classified as exceptional in terms of generated rainfall from the broader perspective of the entire western Mediterranean region. They can, nevertheless, be exceptional from the point of view of impacts, but these are subject to other factors that have nothing to do with precipitation. Had we considered these episodes of very reduced temporal and spatial scale, the values shown in Fig. 2.3 would have increased substantially.

## 2.4.2 Magnitude of events

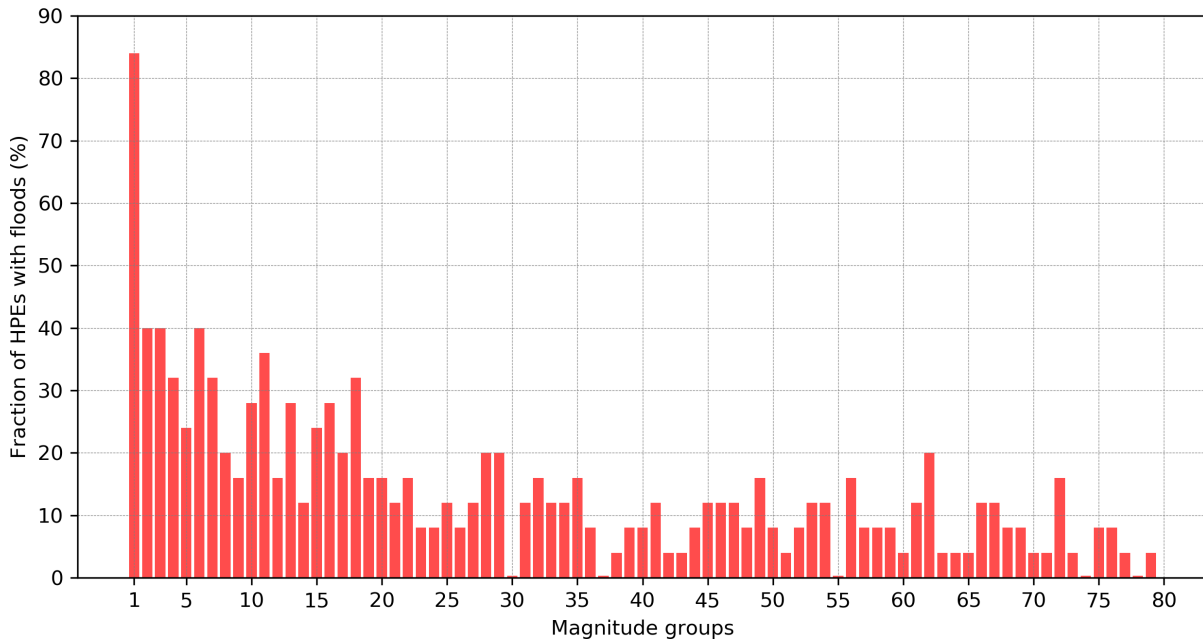


Figure 2.4: Relationship between the magnitude of events and flood occurrence. Each magnitude bin is made of 25 events. The magnitude of the bins decreases in the x-axis from left to right, so that bin 1 is composed of the 25 most extreme cases. The fraction of EPEs with floods indicates (in percent) how many of the events in each bin caused severe flooding.

Here we group events according to their magnitude in bins of 25 and calculate within each bin the fraction of cases that appear also in FLOODHYMEX and/or EM-DAT. Results are depicted in Fig. 2.4. If the assignment of magnitude were correct, the more extreme the events in the bin are, the greater the number of flood occurrences. Figure 2.4 shows that more than 80% of the most extreme cases (bin 1) are associated with flooding and that in general this percentage is reduced by lowering the magnitude, which suggests that the used method works. Note that the used flooding datasets generally contain only severe floods, so these percentages could be higher if we had also considered minor flooding episodes. Table 2.1 shows these 25 extraordinary cases ranked by magnitude. The specific numerical values obtained by applying Eq. (2.4) are not shown because they lack physical sense; they are only used to order the events. 21 out of the 25 episodes led to flooding, which is an indication of their severity, and indeed most of the events in this table are easily recognizable by the impact they caused. Some examples are the catastrophic floods produced in the Gard event of September 2002 [in 9th position; 122] or in the more recent Genoa event of November 2011 [in 5th position 123]. A particularly remarkable case is that of November 1982, first in our ranking, which caused devastating floods in



Andorra, Spain and France [124], as Ramos et al. [90], using other data and methods, also found this event to be the most extreme since at least 1950 in the Iberian Peninsula. This demonstrates its exceptionality in climatological terms.

In some cases, a bin of events of lesser magnitude may be associated with a greater number of floods. It should always be borne in mind that flooding and its effects do not only depend on the meteorological variables, but are also subject to other factors, such as land use or population density, which could increase vulnerability, thus risk. Care should also be taken in interpreting the position of events in the ranking. The magnitude of the events is obviously subject to an uncertainty derived from the possible inaccuracies in the amounts of rainfall provided by MESCAN.

### 2.4.3 Weather types causing extreme precipitation

We classify all identified events into four groups according to the maximum correlation with one of the four principal components considered and then we obtain average maps for each of these groups of days. Figure 2.5 shows these average maps, which represent the most recurrent atmospheric patterns in the WMR when potentially catastrophic rainfall occurs, as combined they explain 77% of the total variance. A greater number of principal components would have explained a higher fraction of the variance; however, we think that working with a reduced number of weather types is much more practical and enlightening. As stated above, here weather types are based on two classic atmospheric variables; sea level pressure and 500 hPa geopotential height, represented in Fig. 2.5 by black contours and colour shades respectively. In addition, we have introduced daily precipitation in the weather type classification, so that we can also identify the areas most exposed to rainfall, marked with a magenta contour in Fig. 2.5.

These four predominant atmospheric patterns are well recognizable and agree well with the spatial distribution of the frequency of extreme rains shown in Fig. 2.3. Weather type 1 (Fig. 2.5a) is characterized by a low-pressure area in the Atlantic, both at low and high levels. In this case, an upper-level ridge could emerge from the Mediterranean toward Central Europe generating a block pattern. Usually a secondary low pressure system forms off the coast of the Spanish Levant as a result of topographic troughing to the lee of the Iberian Peninsula, which helps to organize a warm and moist flow at low levels. Under this situation, the northern sector of the WMR, especially south-eastern France and north-western Italy, is usually the most impacted because it is very exposed to south-southeasterly winds. Weather type 2 (Fig. 2.5b) is marked by a Mediterranean cyclogenesis: a low-pressure system develops at the leading edge of a trough digging south into the Mediterranean Sea. The abrupt topography of the surrounding region is crucial in the generation of a low-level precursor for this type of cyclogenesis. The alpine orographic effect makes the low center most frequently appear in the Gulf of Genoa (Genoa Low), as reflected in Fig. 2.5b. The heavy rainfall generated by this type of cyclone especially affects the Alps and the areas by the Ligurian Sea, although intense precipitation could also occur in other parts of Italy, such as on the coasts of the Tuscany and Lazio regions. Weather type 3 (Fig. 2.5c) is well known in Spain: an upper level cut-off low, originated from an Atlantic trough, is situated in the vicinity of the Iberian Peninsula. Simultaneously, an extensive low-pressure zone at lower levels emerges from North Africa giving rise to an intense easterly flow along the Levant coast. Torrential rains usually appear in this Spanish coastal region when this synoptic pattern is present. The French region of Languedoc-Roussillon could also be

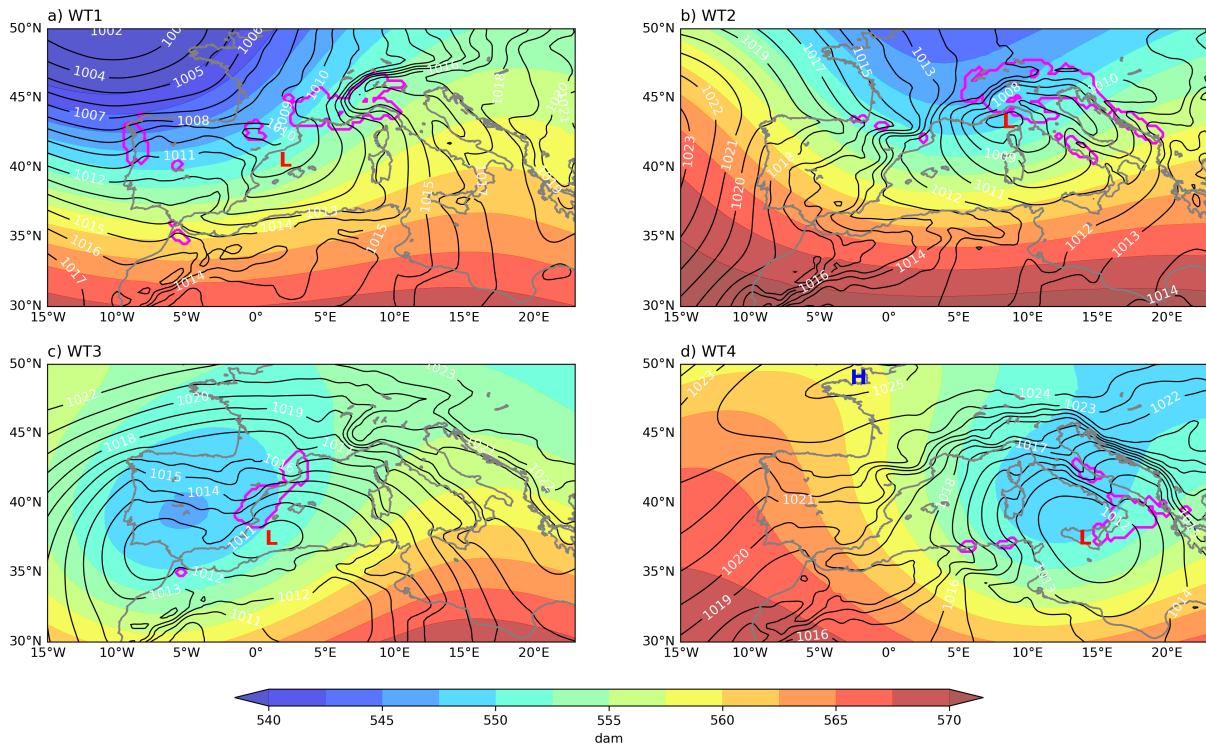


Figure 2.5: Mean sea level pressure (black contours, hPa), geopotential height (colours, dam) and daily precipitation (magenta contour, amounts above 10 mm) of the four most frequent atmospheric patterns associated with extreme precipitation in the western Mediterranean region, referred to as weather type 1 (a), 2 (b), 3 (c) and 4 (d).

affected by this weather type, especially its southern part. Finally, Weather type 4 (Fig. 2.5d) is especially hazardous for southern Italy. An upper level trough dives south from Central Europe with its axis tilted to the west and, at the surface, a low-pressure system develops and moves northward from Africa, just like for type 3, but in this case located further east. Calabria and Sicily are the most affected in this case because they are positioned at the leading edge of the trough, where the strongest dynamic forcings tend to occur. The south-eastern coast of these territories is particularly exposed because it receives directly the warm and humid winds from the Ionian Sea. In addition, some areas facing the Adriatic Sea, such as the Abruzzo region, may also record heavy rains under this situation.

But, which of these four meteorological situations is the most frequent? The answer to this question is found in Fig. 2.6a, showing the percentage of events associated with each atmospheric pattern. The weather type causing most episodes is number 2, with 31.1%, followed by 1, 4 and 3, in this order. Almost 5% of the episodes are undefined cases, not associated with any of the four atmospheric patterns considered. Since the detected episodes have been ordered according to their magnitude, we can also analyse the synoptic configurations leading to the most extraordinary events. Figure 2.6b is identical to Fig. 2.6a but, instead of taking into account all identified events, we now consider only the 100 cases with the greatest magnitude. 40% of the most severe cases are produced by weather type 1, so it is perhaps the most hazardous pattern. Type 2, although frequently causing EPEs, appears to have a low potential to produce extraordinary events, being responsible for around 15% of those. In contrast, weather type 3, despite being the least frequent, shows a greater capacity to produce



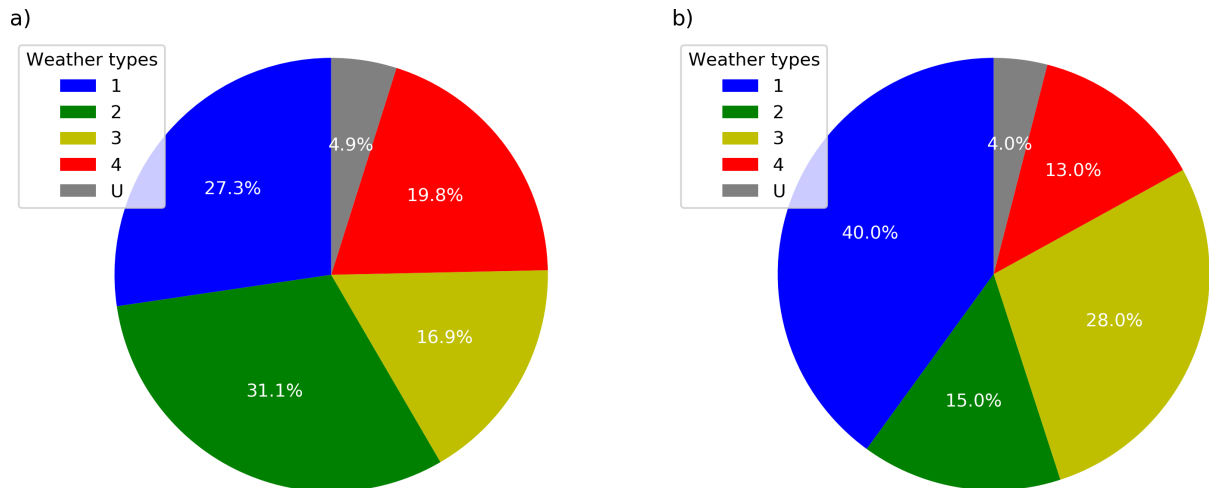


Figure 2.6: Fraction of events (in %) associated with weather type 1 (blue), 2 (green), 3 (yellow) and 4 (red), for total episodes (a) and for the top 100 cases in the magnitude ranking (b). Gray indicates the fraction of undefined (U) events, not associated with any of the four types considered.

exceptional cases, with a share of more than 25%. Conversely, type 4 is quite frequent, but it is the pattern associated with the least number of exceptional cases, only 13%. About 4% of the most extraordinary episodes have an undefined pattern, different from 1, 2, 3 and 4.

Different causes could explain why some weather types generate more extraordinary cases than others, which is a subject that is beyond the scope of this study. But one of the reasons that seems more evident from observing Fig. 2.5 is that the effective area exposed to maritime winds during a type 1 or 3 atmospheric pattern is greater than when there is a type 2 or 4. In addition, for weather types 1 and 3, the presence of an emerging blocking high to the east is also common, which could cause these situations to be more persistent.

#### 2.4.4 Temporal distribution of extreme rains

Figure 2.7a shows a bar diagram with the average percentage of total annual events occurring monthly, indicating with different colours for each bar, the fractions corresponding to each of the four recurrent weather types discussed previously. Most episodes take place in autumn [confirming previous knowledge, e.g. 125, 13], with almost half of all those registered each year concentrated in this season. The incidence of EPEs in either September, October or November is close to 15% of the annual total, with December and January being also relatively prone to extreme rainfall. In contrast, during the rest of the year from February to August, only about 5% of events per month occur. Contributions to winter months are more usual in the eastern part of the WMR, that is to say, Italy and, specifically, the South of Italy. As an example, in Region 6 more than 25% of total cases occur in December and January (not shown).

In general, weather type 1 is predominant for the cases occurring in the months with most events (September, October, November and December). However, for most of the warm season, from May to August, other atmospheric patterns cause more events, especially type 2. This is largely due to the Azores subtropical high moving poleward and displacing Atlantic low-pressure systems further north during summer, therefore preventing them from directly affecting the WMR. For this same reason, during the warmest months (July and August) there

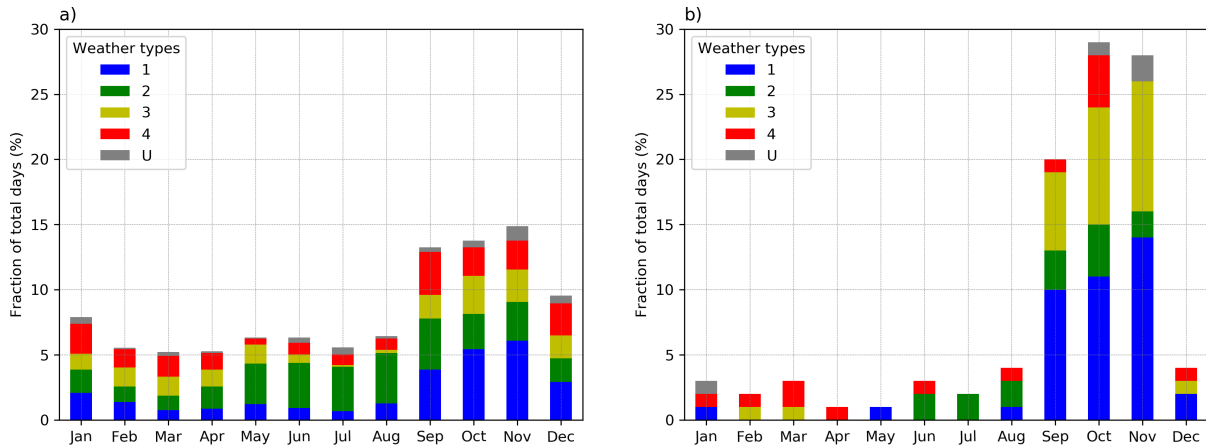


Figure 2.7: Temporal distribution of potentially catastrophic rainfall in the western Mediterranean region, for total episodes (a) and for the 100 most extreme cases (b). Bars indicate the percentage of events (on average) that occur each month. Gray indicates the fraction of undefined (U) events, not associated with any of the four types considered.

are almost no events associated with weather type 3. In the first part of the year, from January to April, the four types cause practically the same number of cases.

Finally, if we only consider the most severe cases, the top 100 episodes in our magnitude ranking, the seasonality is much more pronounced (Fig. 2.7b), that is to say, practically all the extraordinary episodes take place in the autumn months. During September, October and November in conjunction, more than 75% of all yearly episodes are recorded. This indicates that cases occurring during the rest of the year are usually minor episodes. Some of these minor cases could occasionally cause major damage if the rains are concentrated in a vulnerable place, but only very rarely will there be events that severely affect a vast region. The extraordinary autumn events are mainly caused by weather type 1, with type 3 being also very relevant, which is congruent with results in Fig. 2.6b.

## 2.4.5 Final dataset and examples

To conclude, we collect all the presented information into a file in CSV (comma-separated values) format, which is available for download at <https://www.sciencedirect.com/science/article/pii/S0169809521000739?via%3Dihub>. The file contains data from the 1991 daily episodes detected. Information in the EPEs database is organized in columns and each row corresponds to a single event. As an example, Table 2.1 shows the data for the first 25 events. Because in the database the episodes are positioned according to their magnitude (first column), these are the 25 most extraordinary cases recorded in the whole period. Columns 2 and 3 in Table 2.1 show, respectively, each episode's date and affected regions. If an event affects more than one region, they will be linked by a hyphen (e.g. "R1-R2", if the event affects Regions 1 and 2). Column 4 shows the weather type associated with each daily event and column 5 indicates whether or not there was flooding according to FLOODHYMEX and EM-DAT data. In addition, four additional columns can be found in the CSV file, showing, for each episode, the total area affected and gridded precipitation characteristics (maximum, mean and standard deviation).

Finally, we show four representative examples of EPEs occurred in the 1980s in different

Table 2.1: The first 25 episodes in the EPEs database, i.e., the 25 episodes with the highest magnitude (those in the first bin of Fig. 2.4). For each episode (rows) we show in columns (from left to right): the position in the ranking, dates, the affected regions, the associated weather type and whether or not there was flooding, according to FLOODHYMEX and EM-DAT data.

Number ranking	Date	Regions	Weather type	Floods
1	1982-11-07	R1-R2-R3	1	YES
2	1999-11-12	R2-R7	3	YES
3	2003-12-01	R2-R3	1	YES
4	1993-09-23	R2-R3-R4-R5-R7	2	YES
5	2011-11-05	R2-R3-R6-R7	1	YES
6	1994-11-05	R3-R4-R5-R7	1	YES
7	2000-10-23	R1-R2	3	YES
8	1993-09-22	R2-R3	2	YES
9	2002-09-08	R2-R3	1	YES
10	1992-09-26	R1-R2	1	YES
11	1987-11-04	R1	3	YES
12	1989-09-04	R1-R2	3	YES
13	1982-02-16	R2	3	YES
14	1994-01-06	R2-R3	1	NO
15	2000-10-14	R3-R5-R7	U	YES
16	2014-11-04	R3-R4	2	YES
17	2010-06-15	R3	2	YES
18	2006-01-30	R2-R6-R7	U	NO
19	1996-11-12	R2-R3	3	NO
20	1982-10-20	R1	3	YES
21	2010-10-10	R2-R6-R7	3	YES
22	2003-12-03	R2	3	YES
23	1997-09-30	R1	3	YES
24	2009-09-28	R1	3	NO
25	1996-09-11	R1-R2	3	YES

areas of the WMR and in different months, one case for each of the four weather types described before, all of which caused severe flooding (please, find them in the top 100 of our ranking). Figure 2.8 depicts sea level pressure and 500 hPa geopotential height (from ERA5) at 12:00 UTC for the day of the event and Figure 2.9 total accumulated precipitation (from MESCAN) for the four daily episodes. The first of these corresponds to the case of 7 November 1982, which is the first episode in our ranking. The synoptic situation that produced the event (Fig. 2.8a) clearly corresponds to weather type 1, with a deep cyclone over the Atlantic, blocked by an anticyclonic ridge to the east. The persistent southerly winds, which transported large amounts of moisture from the Atlantic [3], left the most notable precipitation records (Fig. 2.9a) in the Pyrenees and in the south-eastern sector of the French Massif Central (Region 2). The weather type 2 example occurred during 23 August 1984. Heavy rainfall was caused by a low-pressure system generated on the leading edge of a pronounced trough entering the Mediterranean from the northwest. Therefore, although the surface low formed slightly to the west of the Gulf

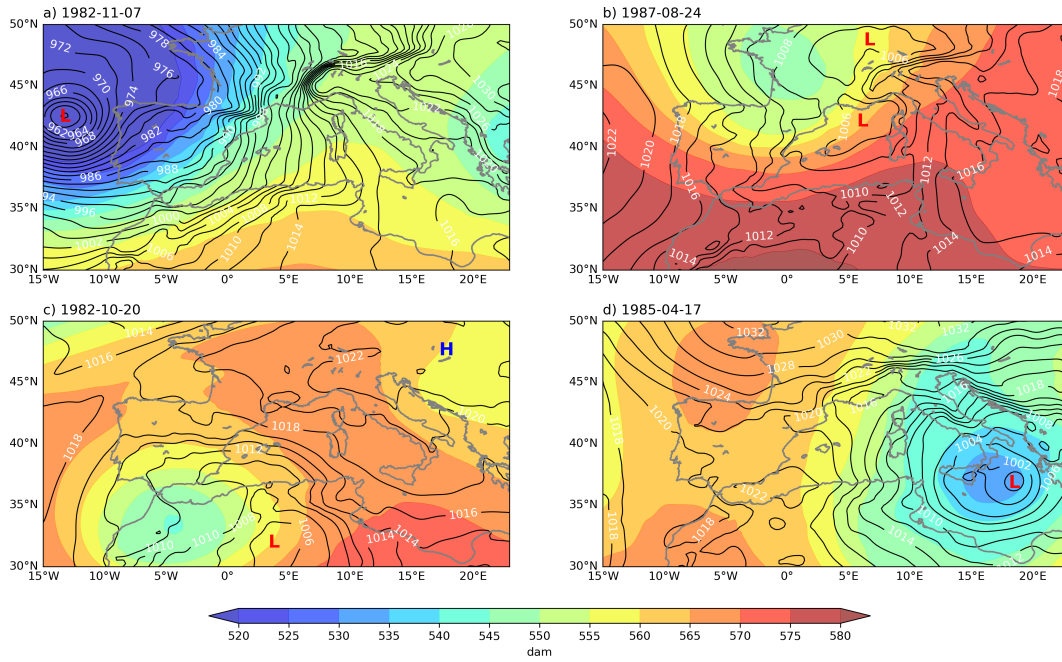


Figure 2.8: Mean sea level pressure (contours, hPa) and 500hPa geopotential height (colours, dam) for the example episodes of weather type 1 (a), 2 (b), 3 (c) and 4 (d). The fields are shown at 12:00 UTC on the day of the events.

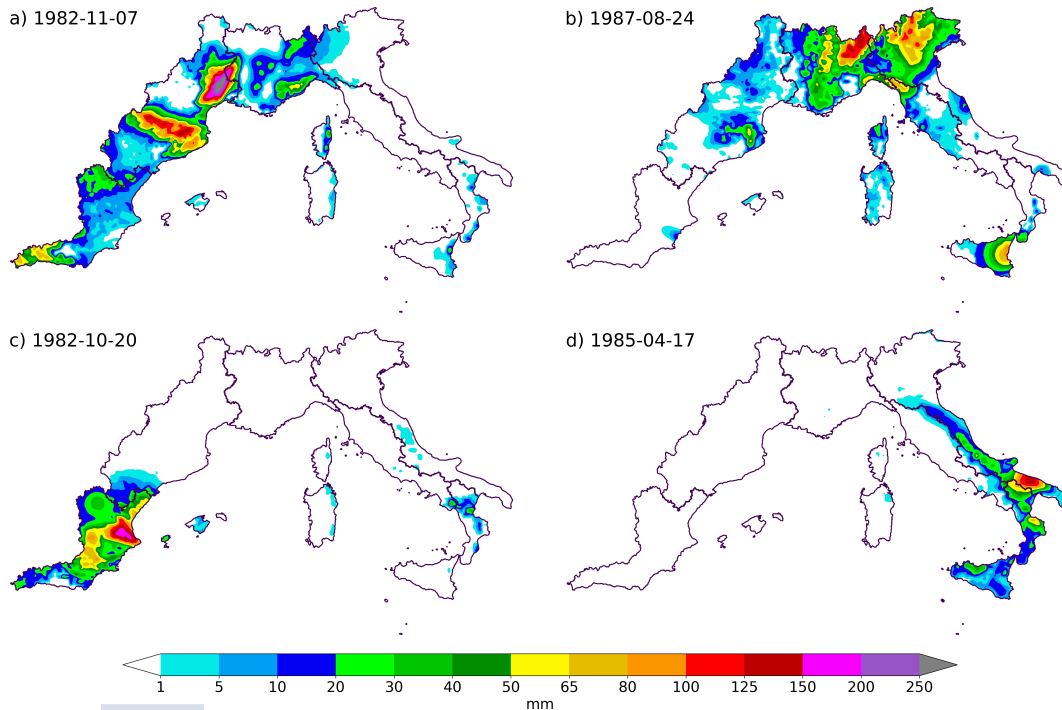


Figure 2.9: Accumulated precipitation during the example episodes of Fig. 2.8.

of Genoa in this case (Fig. 2.8b), it corresponds to a weather type 2. This episode especially affected Regions 3 and 4, causing catastrophic floods in northern Italy, although heavy rainfall also impacted Region 6 (Fig. 2.9b) and floods extended to Belgium and Spain. In Fig. 2.8c and

2.9c we show the meteorological configuration leading to the infamous flooding case of Tous (Spain), which is an example of weather type 3. The excessive rains recorded during 20 October 1982 in the Valencian Community (Fig. 2.9c) were in this case caused by a low pressure system over northern Africa, with a characteristic cut-off low aloft and intense south-easterly winds at lower levels (Fig. 2.8c). The fourth and last example took place on 17 April 1987 and was associated with low pressures in the east part of the WMR (Fig. 2.8d), clearly coinciding with weather type 4. In this case, heavy rains and floods affected southern Italy (Fig. 2.9d), where the low pressures were centred. All of these events are clear examples of the four most common atmospheric patterns found, although in other cases the match between synoptic configuration and weather type is not so apparent. It is obvious that only four weather types cannot perfectly describe all situations and that there are events that do not exactly fit into any of them, especially summer cases, when the synoptic scale forcings are generally less important.

## 2.5 Summary and conclusions

The main objective of this work was to build a database, condensing and unifying the information on all EPEs occurring in the western Mediterranean region from 1980 to 2015. The events' detection was based on the MESCAN precipitation analysis system, a daily gridded high-resolution (5.5 km) dataset constructed from a combination of a downscaled reanalysis and interpolated rain gauge measurements. The procedure consisted in defining extreme precipitation days by means of a spatially variable precipitation threshold. This threshold was constructed from the combination of a fixed threshold of 60 mm with a statistical one, based on the normalized daily precipitation anomaly. The procedure, which is similar to that in Liu et al. [97] for defining an impact-related threshold, ensures that, for every point, precipitation on the detected dates is extreme as well as a truly high amount. Subsequently, we classified the detected potentially catastrophic days according to the atmospheric pattern present by using a principal component analysis approach. Finally, we ranked events by magnitude, which was defined using the excess rainfall above the threshold, as well as the total area affected. In order to validate the used methodology, we crossed our list of identified extreme days with the FLOODHYMEX and EM-DAT flooding databases.

We summarize our main findings in the following ten conclusions:

1. The total number of extreme rainfall days detected across the entire western Mediterranean in the 36-year period 1980-2015 is 1991. For each individual sub-region, this means that there are between 5 and 15 days per year, confirming the high frequency of occurrence of these type of episodes in the area.
2. In the western Mediterranean, most EPEs are concentrated in just three distinct coastal areas: the entire coastal stretch from Murcia (Spain) to Genoa (Italy), the east coast of Corsica and Sardinia and the Ionian coast of Calabria and Sicily.
3. Extreme rain episodes extend inland mainly through the Rhone Valley, as well as along the south east sectors of the French Massif Central and the Alps mountainous systems. The remaining events are unevenly distributed in different parts of the region.
4. In addition to the proximity to the coast, the orientation of the latter is also crucial; in coastal areas facing south or east, frequent torrential rains are almost assured. In some

places, this results in a well-defined border between recurrently affected and unaffected zones, such as in the Spanish Levant.

5. Population density in the region is highest in coastal areas, precisely where potentially catastrophic precipitation is more frequent, which increases significantly flood risk. In particular, populations in the Valencian Community and in the Languedoc-Roussillon region are the ones exposed to a greater number of EPEs. In these coastal territories we found peaks of 30 events, almost 1 per year.
6. The most favourable months for the development of dangerous rainfall situations are September, October and November, in which 40% of the cases recorded each year are concentrated (almost 15% in each of them).
7. Major episodes (of greater magnitude) present a strict seasonality; the vast majority, more than 75%, are concentrated in the three autumn months (SON). From December to September EPEs can occur, but the atmosphere does not show a high potential to produce extraordinary amounts of rain. Therefore, episodes taking place in winter, spring or summer are generally less severe, although they can occasionally cause significant damage if their associated heavy rains are concentrated in a vulnerable location.
8. The synoptic scale configurations leading to extreme rainfall in the western Mediterranean are recurrent: only four weather types explain most of the daily episodes.
9. The synoptic configuration most frequently producing extraordinary (high magnitude) events is the following: a low-pressure system vertically extended to all tropospheric levels in the eastern Atlantic, forming a block pattern with an anticyclonic ridge located further east. This atmospheric pattern causes more than 40% of the major episodes.
10. A block pattern such as the one described in the previous paragraph was the precursor of fatal episodes at the top of our ranking such as Piedmont 1994 or Gard 2002, demonstrating the potential of this atmospheric configuration for producing catastrophic damage.

In summary, our results shed light on different aspects of potentially catastrophic rains in the western Mediterranean. All information generated has been made public and available to other researchers, with the main objective of further expanding and improving the current knowledge on these catastrophic weather events. In future work we will adapt episode detection for the using of the new European CERRA reanalysis (in process; <https://climate.copernicus.eu/copernicus-regional-reanalysis-europe-cerra>), which will replace MESCAN introducing major improvements. The CERRA system will provide precipitation data in near-real time, allowing us to update the extreme rainfall database with that same frequency.





## APPENDIX

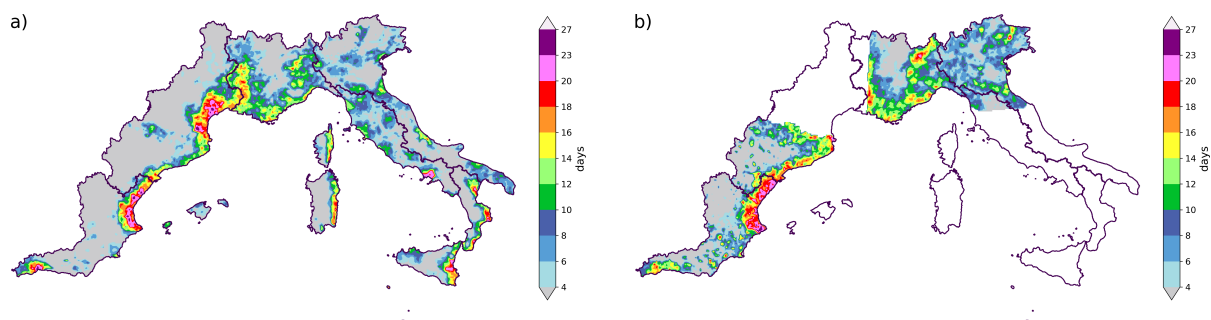


Figure 2.10: Total number of hazardous rain days from 1980 to 2008 according to MESCAN (a) and SPREAD combined with APGD (b).





# Chapter 3

## Implementation and validation of a moisture tracking tool in an atmospheric model

\* The results from this chapter have already been published as D. Insua-Costa<sup>1</sup> and G. Miguez-Macho<sup>1</sup>, “A new moisture tagging capability in the Weather Research and Forecasting model: Formulation, validation and application to the 2014 Great Lake-effect snowstorm”, *Earth System Dynamics*, vol. 9, no. 1, pp. 167–185, 2018.

<sup>1</sup> CRETUS, Non-linear Physics Group, Universidade de Santiago de Compostela, Galicia, Spain

### 3.1 Introduction

Water vapour tracers were introduced in general circulation models in the early studies of Koster et al. [126] and Joussaume et al. [127]. There were successive later implementations in different global models [128, 129, 130, 131, 132, 74, 133], all of them proving very useful in climatic studies of precipitation moisture sources. WVTs in global models allow for investigations at the planetary scale, covering all existing moisture source regions. However, given the coarse resolution common to most of these models, some processes such as surface hydrology or water vapour transport in complex topography areas, are subject to sizeable biases, which compromise conclusions drawn from the WVTs method. WVTs in regional climate models, which employ a much finer resolution and significantly improve the representation of small-scale features of the hydrology cycle, are perhaps the best alternative for diagnosing precipitation moisture sources in events of reduced temporal and spatial scales, such as EPEs. They can also be useful in climatic studies at the regional scale. The first implementation of the moisture tagging capability in a regional atmospheric model was in the climate high-resolution model (CHRM) by Sodemann et al. [134], and more have followed since in different models [135, 136, 33, 137].

Although the different implementations of WVTs in global or regional models have in common the theoretical approach, they can, nevertheless, be somewhat different in practice. These differences are not only due to the model or parameterizations used, but also to the considerations and simplifications that authors assume in their own implementations, which can

Table 3.1: The different WVTs implementations (including the present): reference, name of the models in which the WVTs tool has been implemented and scale of these models.

Reference of the implementation	Model name	Model scale
Joussaume et al. (1986)	LMD	Global
Koster et al. (1986)	NASA/GISS	Global
Numaguti (1999)	CCSR-NIES	Global
Werner et al. (2001)	ECHAM4	Global
Bosilovich and Schubert (2002)	GEOS-3	Global
Noone and Simmonds (2002)	MUGCM	Global
Bosilovich et al. (2003)	FVGCM	Global
Sodemann et al. (2009)	CHRM	Regional
Goessling and Reick (2013)	ECHAM6	Global
Knoche and Kunstmann (2013)	MM5	Regional
Miguez-Macho et al. (2013)	WRF 3.4.1	Regional
Winschall et al. (2014)	COSMO	Regional
Arnault et al. (2016)	WRF 3.5.1	Regional
Singh et al. (2016)	CAM5	Global
Insua-Costa and Miguez-Macho (2018)	WRF 3.8.1	Regional

potentially lead to significant inaccuracies. It is therefore fundamental to validate the method's precision before it can be reliably applied in practical cases.

This chapter presents a new moisture tagging tool recently added to the Weather Research and Forecasting (WRF V3.8.1) regional meteorological model (WRF-WVTs hereafter). Even though a preliminary version of the tool has already been tested in an older version of the model [136, 138, 139], we discuss here the formulation and implementation details of the method, and perform a thorough validation, thus avoiding the reliability uncertainty from which many other implementations of the kind suffer. The study is structured as follows: Section 3.2 describes the formulation and implementation into WRF of the WVTs method. Section 3.3 contains the validation strategy and results. Section 3.4 shows results from an example application, and finally Section 3.5 includes a summary and conclusions of the work.

## 3.2 Implementation of the moisture tagging capability

### 3.2.1 General formulation

The basis of the moisture tagging technique is to replicate for moisture tracers the prognostic equation for total moisture:

$$\frac{\partial q_n}{\partial t} = -\vec{v} \cdot \nabla q_n + v_q \cdot \nabla^2 q_n + \left( \frac{\partial q_n}{\partial t} \right)_{PBL} + \left( \frac{\partial q_n}{\partial t} \right)_{microphysics} + \left( \frac{\partial q_n}{\partial t} \right)_{convection} \quad (3.1)$$

where  $q_n$  refers to the different moisture species considered, namely water vapour, cloud water, rain water, snow, ice and graupel. The first two terms on the right hand side in Eq. (3.1) represent the tendencies due to advection and molecular diffusion, respectively, and the others

correspond to tendencies resulting from parameterized turbulent transport (Planetary Boundary Layer, PBL scheme), microphysics and convection. The latter three terms account for subgrid physical processes affecting atmospheric moisture, such as phase changes and precipitation, or redistribution by convection and turbulent diffusion.

To replicate Eq. (3.1), six new variables  $tq_n$  are created corresponding to the tracers of the different moisture species: tvapour, tcloud, train, tsnow, tice, tgraupel. The general form of the prognostic equation for WVTs is totally analogous to Eq. (3.1), just replacing  $q_n$  by  $tq_n$ . The Eulerian form of this equation and the fact that it is solved simultaneously with Eq. (3.1), are the reasons for the method to be classified as “online” Eulerian. One could think that since the prognostic equations for WVTs and total moisture have the same form, it would suffice with repeating the calculations performed for total moisture species for the tracer species, and just change initial or boundary conditions. However, this is not the case, since the behavior of the tagged moisture is not independent from that of total moisture. In other words, the tagged moisture does not evolve as if it was completely on its own. A very simple example of this is saturation conditions and phase changes, which would hardly occur if only tagged moisture were considered. When an air parcel saturates, it does so in regards to its total moisture content, independently of whether its tracer moisture content is high or low. Similarly, since it is total moisture that determines the thermodynamical setting for turbulence and convection, primary and derived variables in the basis of the parameterizations of those processes, such as virtual temperature, dew point, profile instability, convective available potential energy (CAPE), level of free convection, eddy diffusivity, and many more, must be computed using total moisture, even when calculations are performed for tagged moisture tendencies. Therefore, the prognostic equations for tracer moisture must be solved coupled to the governing equations of the model, i.e. “online”, although tracer variables do not appear elsewhere and hence do not have an effect in the model’s dynamics in any way.

Thus, for the implementation of WVTs into WRF, three fundamental parameterizations of the model such as the turbulence (PBL) scheme, microphysics and convection, must be modified for calculating the associated tracer moisture tendencies, as discussed above. Conversely, advection and diffusion routines can be simply called for tracers in the same way as for total moisture or any other scalar, since in these processes tracer moisture can indeed be treated independently from total moisture. We note that it is important to use an advection numerical scheme that is positive definite, conserves mass and minimizes numerical diffusion, in order to limit numerical errors in WVTs calculations. Both total moisture and tagged moisture must use the same scheme. All other components of the model remain unchanged, since they do not affect moisture dynamics directly.

### 3.2.2 Moisture tracer tendencies formulation

Of the several scheme options available, we have altered for moisture tagging the Yonsei University [YSU; 140] PBL scheme, the WRF-Single-Moment 6-class [WSM6; 141] microphysics scheme and the Kain-Fritsch [142] convective parameterization. These schemes have been selected because they are some of the most commonly used and show a reliable performance in numerous situations.

#### Boundary layer parametrization

The equation of turbulent diffusion for moisture [140]:

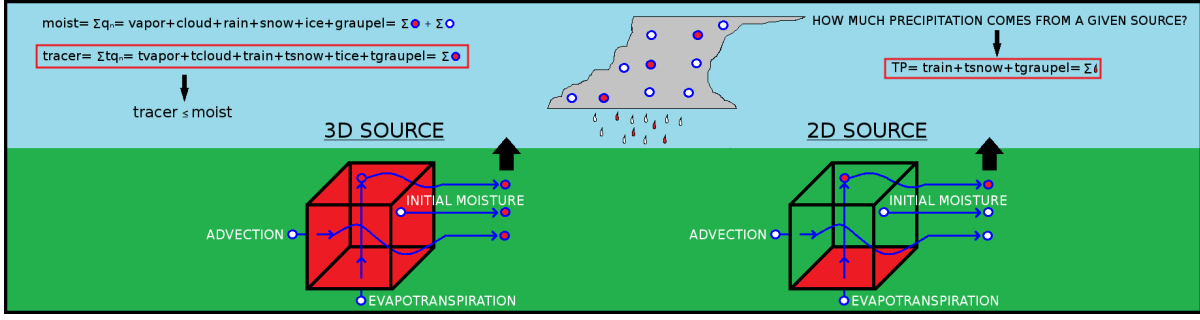


Figure 3.1: Sketch representing the fundamentals of the moisture tracers method, including the tagging of 3D and 2D moisture sources.

$$\left(\frac{\partial q_n}{\partial t}\right)_{PBL} = \frac{\partial}{\partial z} \left[ K_q \left( \frac{\partial q_n}{\partial z} - \gamma_q \right) - \overline{(w'q'_n)}_h \left( \frac{z}{h} \right)^3 \right] \quad (3.2)$$

is solved in this parameterization for  $q_n$  = water vapour, cloud water and ice, with boundary conditions:

$$\begin{cases} \eta = 1 \implies K_q \left( \frac{\partial q_n}{\partial z} \right) = -\frac{Q_E}{\rho_{air}} \\ \eta = \eta_{end} \implies K_q \left( \frac{\partial q_n}{\partial z} \right) = 0 \end{cases} \quad (3.3)$$

where  $Q_E$  represents the water vapour flux at the surface.

To compute turbulent diffusion for tracer species, we replicate Eq. (3.2), keeping the same eddy diffusivity coefficients  $K_q$ , turbulent vertical velocity  $w'$  and boundary layer height  $h$  as in the total moisture calculation:

$$\left(\frac{\partial tq_n}{\partial t}\right)_{PBL} = \frac{\partial}{\partial z} \left[ K_q \left( \frac{\partial tq_n}{\partial z} - \gamma_{tq} \right) - \overline{(w'tq'_n)}_h \left( \frac{z}{h} \right)^3 \right] \quad (3.4)$$

Boundary conditions are analogous to Eq. (3.3):

$$\begin{cases} \eta = 1 \implies K_q \left( \frac{\partial tq_n}{\partial z} \right) = -\frac{TQ_E}{\rho_{air}} \\ \eta = \eta_{end} \implies K_q \left( \frac{\partial tq_n}{\partial z} \right) = 0 \end{cases} \quad (3.5)$$

considering that now  $TQ_E$  is the tracer water vapour flux at the surface, which, when upward, is equal to that of total water vapour in the areas that are selected for tagging, and zero in the rest.

### Microphysics parameterization

The tendencies computed in the WSM6 microphysics parameterization account for grid scale precipitation and for the different phase changes among the several species considered (water vapour, cloud water, rain water, ice, snow and graupel):

$$\left(\frac{\partial q_n}{\partial t}\right)_{microphysics} = \sum_x \frac{\partial Q_{q_x \rightarrow q_n}}{\partial t} - \sum_x \frac{\partial Q_{q_n \rightarrow q_x}}{\partial t} - \frac{q_n}{\rho_{air}} \frac{\partial}{\partial z} (\rho_{air} \cdot V_{q_n}) \quad (3.6)$$

where  $Q_{q_x \rightarrow q_n}$  and  $Q_{q_n \rightarrow q_x}$  refer to the amount of moisture species  $q_x$  transformed via phase change into moisture species  $q_n$  and viceversa, respectively [141]. The last term on the right hand side of Eq. (3.6) represents the tendency due to hydrometeor  $q_n$  fallout, with an associated mass-weighted mean terminal velocity  $V_{q_n}$ . In the latter case,  $q_n$  refers only to rain water, snow, ice or graupel.

We consider that phase changes among the different tracer species occur in amounts proportional to their total moisture counterparts:

$$TQ_{tq_x \rightarrow tq_n} = \frac{tq_x}{q_x} \cdot Q_{q_x \rightarrow q_n} \quad TQ_{tq_n \rightarrow tq_x} = \frac{tq_n}{q_n} \cdot Q_{q_n \rightarrow q_x} \quad (3.7)$$

where the proportionality coefficients in Eq. (3.7) correspond to the tracer fraction in the species undergoing the change ( $tq_x/q_x$  when  $tq_x$  changes phase, and  $tq_n/q_n$  when  $tq_n$  does).

Bearing the latter consideration in mind, we replicate Eq. (3.6) to calculate moisture tracers' tendencies:

$$\left( \frac{\partial tq_n}{\partial t} \right)_{microphysics} = \sum_x \frac{\partial TQ_{tq_x \rightarrow tq_n}}{\partial t} - \sum_x \frac{\partial TQ_{tq_n \rightarrow tq_x}}{\partial t} - \frac{tq_n}{\rho_{air}} \frac{\partial}{\partial z} (\rho_{air} \cdot V_{q_n}) \quad (3.8)$$

Sedimentation processes yielding precipitation rates are computed in this WSM6 parameterization with a forward semi-Lagrangian advection scheme with mass conservation and positive definition [143], from which total accumulated grid-scale rain, snow and graupel are obtained. Applying the same strategy, we obtain the corresponding precipitation amounts for tracers. The ratio of tracer rain, snow and graupel to their total counterparts provides information about the contribution of the selected moisture sources to precipitation.

### Convective parameterization

Following the formalism in Bechtold et al. [144], the effect of convection in moisture can be generally described as:

$$\left( \frac{\partial q_n}{\partial t} \right)_{convection} = \frac{1}{\rho_{air} \cdot A} \left[ \frac{\partial}{\partial z} (M^u + M^d) q_n - (\epsilon^u + \epsilon^d) q_n + \delta^u q_n^u + \delta^d q_n^d \right] + S_{q_n} \quad (3.9)$$

where  $A$  is the grid cell area,  $M^u$  and  $M^d$  are the mass fluxes in updraft and downdraft,  $\epsilon^u - \epsilon^d$  and  $\delta^u - \delta^d$  represent mass exchanges between cloud and environment in the updraft and downdraft due to entrainment and detrainment processes, respectively;  $q_n^u$  and  $q_n^d$  refer to the moisture amounts present in updraft and downdraft, and finally  $S_{q_n}$  corresponds to sources and sinks of moisture species  $q_n$  in the convective cloud, linked to phase changes and precipitation. The Kain-Fritsch parameterization considers up to five moisture species ( $q_n$  of water vapour, cloud water, rain water, snow and ice), but not all are equally treated, and simplified forms of Eq. (3.9) are used for some of them [145, 146, 142].

Similarly to the previously discussed parameterizations, we replicate the general equation for convective moisture tendencies (Eq. 3.9) for the case of tracers:

$$\left( \frac{\partial tq_n}{\partial t} \right)_{convection} = \frac{1}{\rho_{air} \cdot A} \left[ \frac{\partial}{\partial z} (M^u + M^d) tq_n - (\epsilon^u + \epsilon^d) tq_n + \delta^u tq_n^u + \delta^d tq_n^d \right] + S_{tq_n} \quad (3.10)$$

where the proportionality assumption of Eq. (3.7) is applied again to calculate amounts in tracer phase changes.

In the Kain-Fritsch parameterization, a large fraction of the liquid water or ice that forms in the updraft is converted to precipitation [146], which can evaporate or sublimate on the way to the ground, resulting finally in total accumulated cumulus precipitation. The replication of these processes for tracers yields cumulus tracer precipitation. As in the case of the microphysics scheme, the ratio of tracer to total precipitation quantifies the existing contribution from the selected moisture sources.

### Tracers initialization and boundary conditions

Tracer initial and lateral boundary conditions are usually set to zero, even though this does not always have to be the case, as we show when we perform the validation of the method in Section 3.3 and in the nested simulation discussed in Section 3.4. Lower boundary conditions depend largely on the moisture source to analyze. The implementation that we present here of the WVTs method allows for the tracking of moisture from two and three-dimensional sources (Fig. 3.1).

#### a. 2D source

Working with a two dimensional source commonly refers to tagging surface evapotranspiration fluxes ( $Q_E$ ) from a certain region or interest  $A_{2D}$ . The flux of tracer water vapour at the surface  $TQ_E$  can be written as:

$$\begin{cases} Q_E(x, y, t) > 0 \implies TQ_E(x, y, t) = Q_E(x, y, t) & \forall (x, y, t) \in A_{2D} \\ Q_E(x, y, t) < 0 \implies TQ_E(x, y, t) = \frac{tvapour(x, y, \eta=1, t)}{vapour(x, y, \eta=1, t)} \cdot Q_E(x, y, t) & \forall (x, y, t) \end{cases} \quad (3.11)$$

Negative fluxes indicate dew (or frost) deposition, and in this case, we use again the proportionality assumption for phase changes, as elsewhere in the atmosphere (Eq. 3.7). The tracer deposition flux is simply the total deposition flux times the tracer fraction in the water vapour of the first atmospheric level. The resulting flux  $TQ_E$  is used in Eq. (3.5) as lower boundary condition for moisture turbulent diffusion in the PBL parameterization.

#### b. 3D source

Any three dimensional volume  $V_{3D}$  can be set as a 3D source for moisture tagging. This can refer to the entire atmosphere over a region of interest, or to only a part of it (for example the stratosphere). Setting the lateral boundaries plus the adjacent relaxation zone as 3D wall-like source regions is also the most convenient strategy for tagging incoming moisture fluxes from the exterior of the regional model domain.

To turn any given set of model domain points  $V_{3D}$  into a 3D source for moisture tracers, we simply impose:

$$tq_n(x, y, \eta, t) = q_n(x, y, \eta, t) \quad \forall (x, y, \eta, t) \in V_{3D} \quad (3.12)$$





### 3.3 Moisture tracer validation

#### 3.3.1 Experimental setup

The validation simulation for the newly implemented moisture tagging tool is performed with the WRF model version 3.8.1 [147], for the duration of one month (November 2014) and with a domain D1 of 20km horizontal resolution and 35 vertical levels (Fig. 3.2). Initial and boundary conditions, updated every six hours, were obtained from the National Centers for Environmental Prediction (NCEP) Final (FNL) Operational Model Global Tropospheric Analyses, available at  $1^\circ$  resolution [148]. In addition to the YSU PBL, WSM6 microphysics and Kain-Fritsch convective parameterizations that we adapted to calculate the corresponding tracer tendencies (as described in Section 3.2), in the simulations, we also use the Noah Land Surface Model [Noah LSM; 149] and the Rapid Radiative Transfer Model [RRTM; 150] and Dudhia [151] schemes for long and shortwave radiation, respectively. Moisture and tracer advection are calculated with the 5th order Weighted Essentially Non-Oscillatory [WENO; 152] scheme with positive definite limiter. Spectral nudging of waves longer than around 1000 km is activated to avoid distortion of the large scale circulation within the regional model domain due to the interaction between the model's solution and the lateral boundary conditions [153].

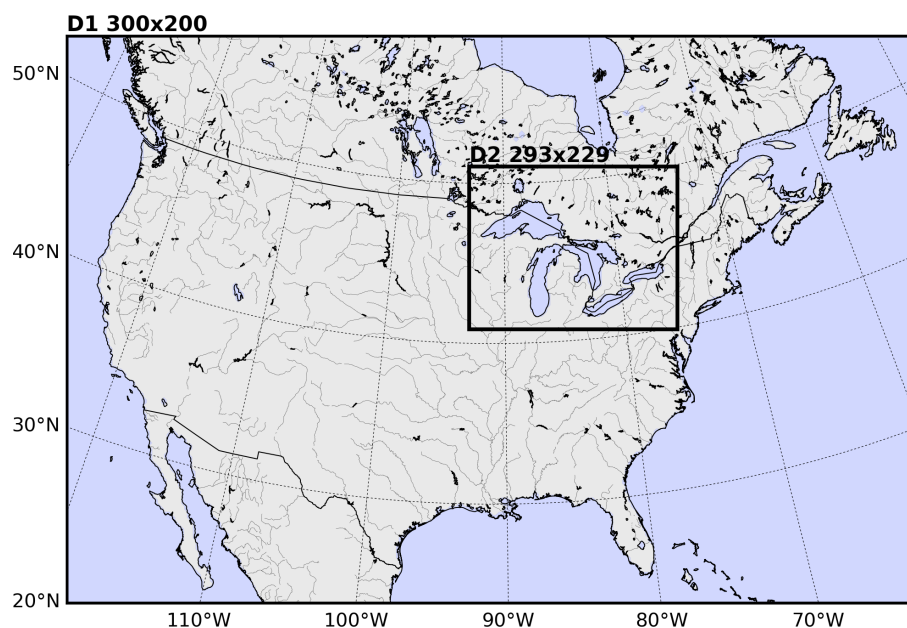


Figure 3.2: Simulation domains for the validation (D1) and example application experiments (D2).

#### 3.3.2 Methodology

The methodology followed to validate WVTs is analogous to that used previously by Bosilovich and Schubert [130] and Sodemann et al. [134], and it is based on tagging moisture from all possible sources, so that if the method were exact, the difference between tracer and total moisture should be zero. In other words, let  $S_n$  (with  $n = 1, 2, 3, \dots$ ) be a set of moisture sources covering all possible atmospheric moisture sources,  $tq_{S_n}$  the total moisture (the sum of

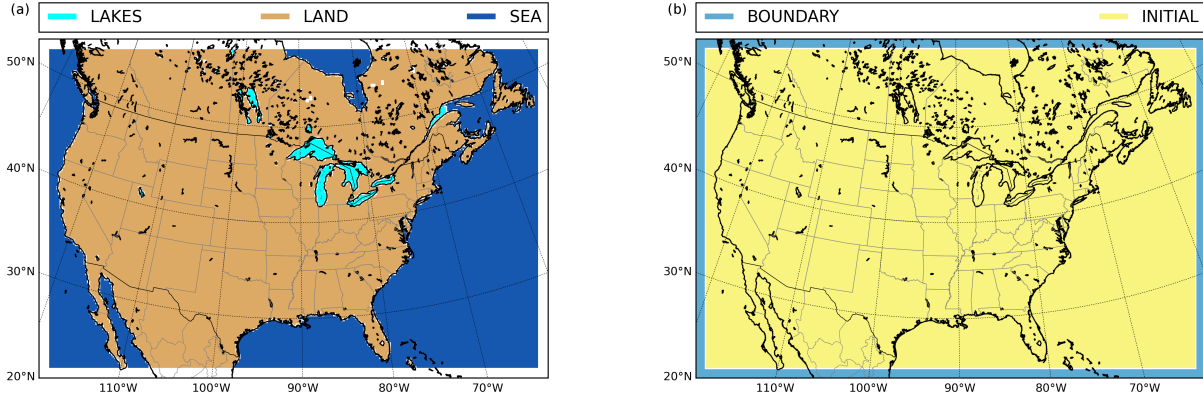


Figure 3.3: Moisture sources considered for validation calculations: two-dimensional (a) and three-dimensional (b).

all moisture species) from each source  $S_n$ , and  $q$  the total moisture, then the absolute error ( $\varepsilon_a$ ) of the method can be written as:

$$\varepsilon_{a,q}(x, y, \eta, t) = \sum_n tq_{S_n}(x, y, \eta, t) - q(x, y, \eta, t) \quad (3.13)$$

or in terms of precipitable water, integrating Eq. (3.13) in the vertical yields:

$$\varepsilon_{a,TPW}(x, y, t) = \sum_n TTPW_{S_n}(x, y, t) - TPW(x, y, t) \quad (3.14)$$

where  $TTPW_{S_n}$  refers to the total precipitable water coming from source  $S_n$  and  $TPW$  is the total precipitable water simulated by the model. Similarly, for precipitation:

$$\varepsilon_{a,TP}(x, y, t) = \sum_n TP_{S_n}(x, y, t) - P(x, y, t) \quad (3.15)$$

where  $TP_{S_n}$  corresponds to the precipitation from source  $S_n$  and  $P$  is the total precipitation produced by the model. Equation (3.15) can also be applied to any particular type of precipitation, such as rain, snow or graupel, individually.

Here, we have divided the possible moisture sources into five ( $S_1, \dots, S_5$ ), three of them two-dimensional (Fig. 3.3a) and two three-dimensional (Fig. 3.3b). The two-dimensional source regions cover all evaporative sources within the domain, namely sea, land and lakes, whereas the three-dimensional sources tag incoming moisture from the lateral boundaries and the moisture contained in the full atmospheric volume of the domain at initial time. For the latter purpose, the three-dimensional source “INITIAL” (Fig. 3.3b) is activated only at the first time step of the simulation. The “BOUNDARY” source (Fig. 3.3b) is a wall-like volume encompassing the relaxation zone where lateral boundary conditions are applied, along the domain’s outer edges. To prevent moisture from evaporative or initial condition sources to be counted twice, this boundary volume becomes a sink for tracers of these other origins, that is, tagged moisture species from other sources are set to zero when they enter BOUNDARY. All possible atmospheric moisture sources are covered by the aforementioned five, and therefore Eq. (3.13), (3.14) and (3.15) should be fulfilled at all times with zero error if the method were perfectly accurate.

To provide insights on the temporal evolution of the error, we follow the statistical treatment



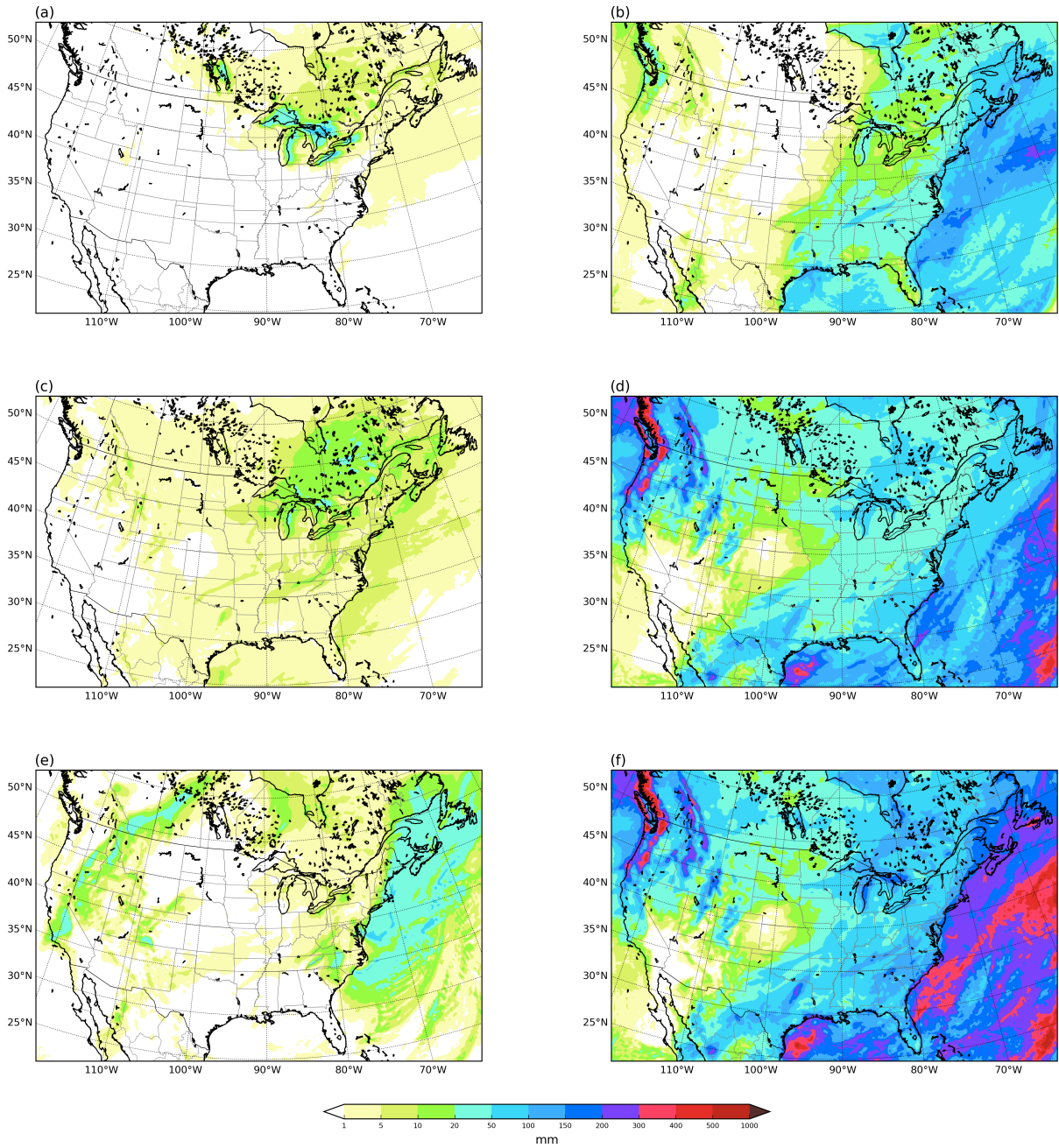


Figure 3.4: Total monthly accumulated tracer precipitation (*mm*): from lake evaporation (a), sea evaporation (b), land evapotranspiration (c), lateral boundary advection (d), initial moisture (e) and sum of all contributions (f).

of Bosilovich and Schubert [130], based on the calculation of the mean (ME) and standard deviation (SD) of the error at each point in time, that can be written as (following the notation used previously):

$$\begin{cases} ME = \frac{1}{N} \sum_{i=1}^N \epsilon_{a\alpha}^i \\ SD = \sqrt{\frac{\sum_{i=1}^N (\epsilon_{a\alpha}^i - ME)^2}{N}} \end{cases} \quad (3.16)$$

where  $N$  is the number of grid cells in the domain and  $\alpha$  can correspond to  $TP$  (total tracer precipitation or rain, snow or graupel separately) or  $TTPW$  (tracer total precipitable water).

An alternative statistical treatment, which is very visual and can be used as a second test of the reliability of the method, is that of Sodemann et al. [134], based on computing the relative contribution of each moisture source to total precipitable water, total precipitation or to each type of precipitation (rain, snow or graupel) separately. The calculation returns the relative error of the mean values of those variables at each instant in time. For example, let  $\bar{P}$  the mean total precipitation, then the contribution (in %) of each source  $S_n$  is:

$$F_{TP_{S_n}} = 100 \cdot \frac{\overline{TP}_{S_n}}{\bar{P}} \quad (3.17)$$

where  $\overline{TP}_{S_n}$  represents the mean total precipitation from source  $S_n$ . Then, if the method were perfectly accurate, the sum of all contributions ( $\sum_n F_{TP_{S_n}}$ ) should equal 100%. The degree of deviation of this sum with respect to the latter value yields the relative error ( $\epsilon_r$ ) of the mean tracer precipitation:

$$\epsilon_{r_{\overline{TP}}} = \sum_n 100 \cdot \frac{\overline{TP}_{S_n}}{\bar{P}} - 100 = 100 \cdot \frac{\sum_n \overline{TP}_{S_n} - \bar{P}}{\bar{P}} \quad (3.18)$$

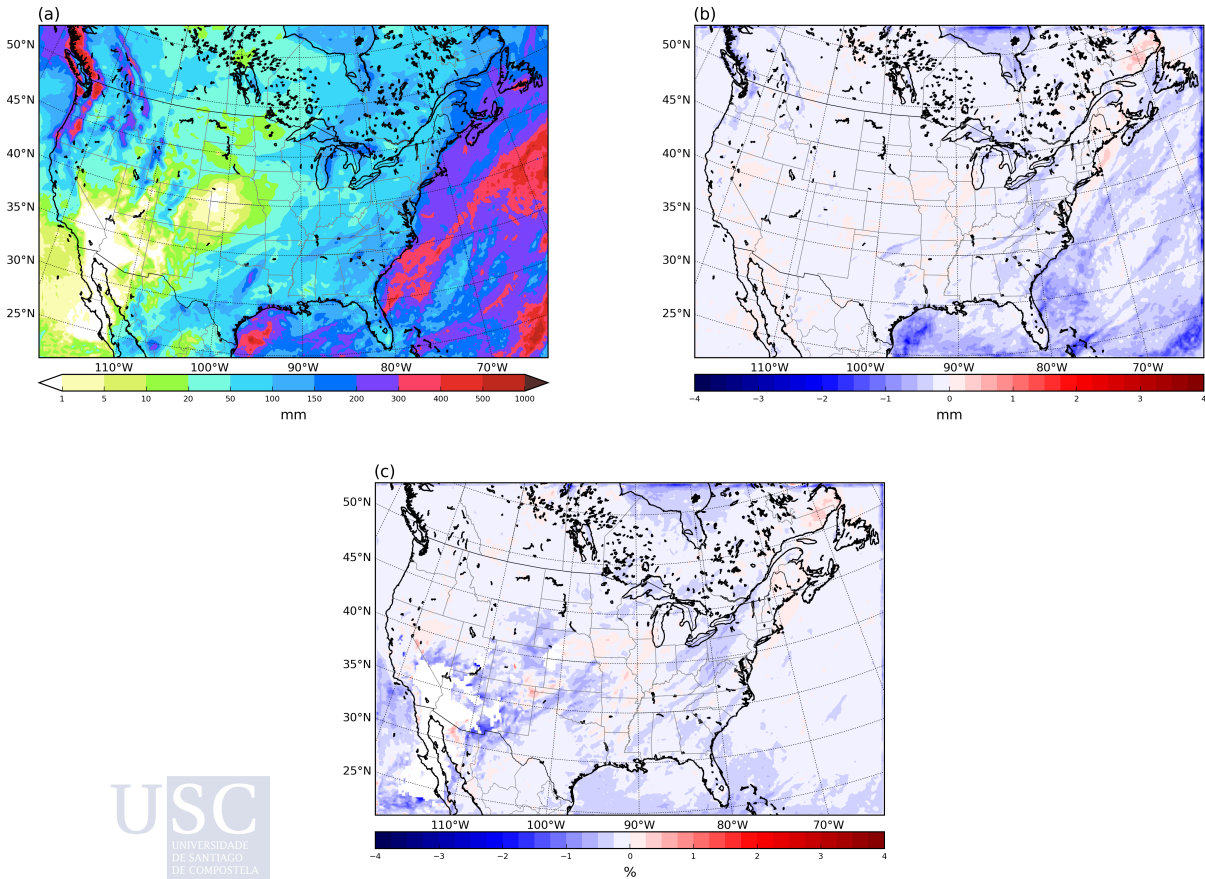


Figure 3.5: Total monthly accumulated model precipitation ( $mm$ ) (a), tracer precipitation absolute error ( $mm$ ) (b) and tracer precipitation relative error (%) in areas where precipitation exceeds 1 mm (c).

The above equation can be applied not only to total precipitation, but also to any particular type of precipitation or to total precipitable water. Finally, we note that the concept of relative error of the mean variables should not be confused with the mean relative error, which would be expressed, following the notation used in the equation above, as:

$$\overline{\varepsilon_{rTP}} = \frac{1}{N} \sum_{i=1}^N \left( 100 \cdot \frac{\sum_n TP_{S_n} - P}{P} \right)_i \quad (3.19)$$

This last variable will also be used during the validation treatment shown below.

### 3.3.3 Validation results

As mentioned earlier, the validation experiment is a monthly long simulation for November 2014 over North America. Figure 3.4 shows the results obtained in this simulation for total precipitation from each of the five analyzed sources ( $TP_{S1}$ ,  $TP_{S2}$ , ...) depicted in Fig. 3.3, and the total sum of precipitation from all sources ( $\sum_n TP_{S_n}$ ). The relaxation zone along the boundaries is excluded in these figures. The largest contribution to total precipitation is from external advection into the domain, and in the eastern half of it, also from sea evaporation. Lake evaporation is locally important around the Great Lakes and in Canada, where most smaller lakes in the grid are located. Evapotranspiration over land is not very relevant in the month of November, and neither is its contribution to precipitation. Moisture present at initial time precipitates significantly only toward the eastern boundary of the domain, in the downwind direction of the dominant westerly flow.

According to Eq. (3.15), for the absolute error to be zero at each point, the result in Fig. 3.4f should exactly match the total precipitation calculated by the model, shown in Fig. 3.5a. The values of this error (i.e the differences between the results of Fig. 3.4f and Fig. 3.5a) are depicted in Fig. 3.5b. The maximum deviations between the sum of the precipitation coming from the five considered sources and the total precipitation calculated by the model, occur over the sea, near the domain's edges, and hover around -3 mm. These values correspond to very low relative errors (Fig. 3.5c), since the cumulative precipitation in these areas during the month of November is very high, often exceeding 300 mm. In most regions, however, the absolute error is clearly less than 1 mm, close to zero for the most part and thus very small, even in the relative sense. Neglecting cells where the total monthly precipitation is less than 1mm to avoid arithmetical problems, the area-averaged value of the relative error (Eq. 3.19) is -0.17%, with a standard deviation of 0.20%. The maximum relative error found at any point is only -3.73% in areas of the US desert southwest with low accumulated precipitation during the simulated month of November.

Figure 3.6 shows at 3h intervals, the mean error (ME) and standard deviation (SD) for the three precipitation types, rain (Fig. 3.6a), snow (Fig. 3.6c) and graupel (Fig. 3.6e), throughout the monthly period of simulation. Values of the mean error are very close to zero at all times, with small standard deviations of about 0.05 mm/day for rain, 0.01 mm/day for snow and 0.005 mm/day for graupel, indicating that the compensations between positive and negative errors are not very relevant. As expected, the error is larger for the domain-wide most abundant precipitation types (rain and snow, in this order) and smaller for the most residual type of precipitation (graupel). Bosilovich and Schubert [130] found mean errors very close to zero for precipitation, as in our case, but comparatively much larger standard deviations of about 0.2 mm/day ( $\sim 5\%$ ). In addition, Fig. 3.6 shows the relative contribution of each

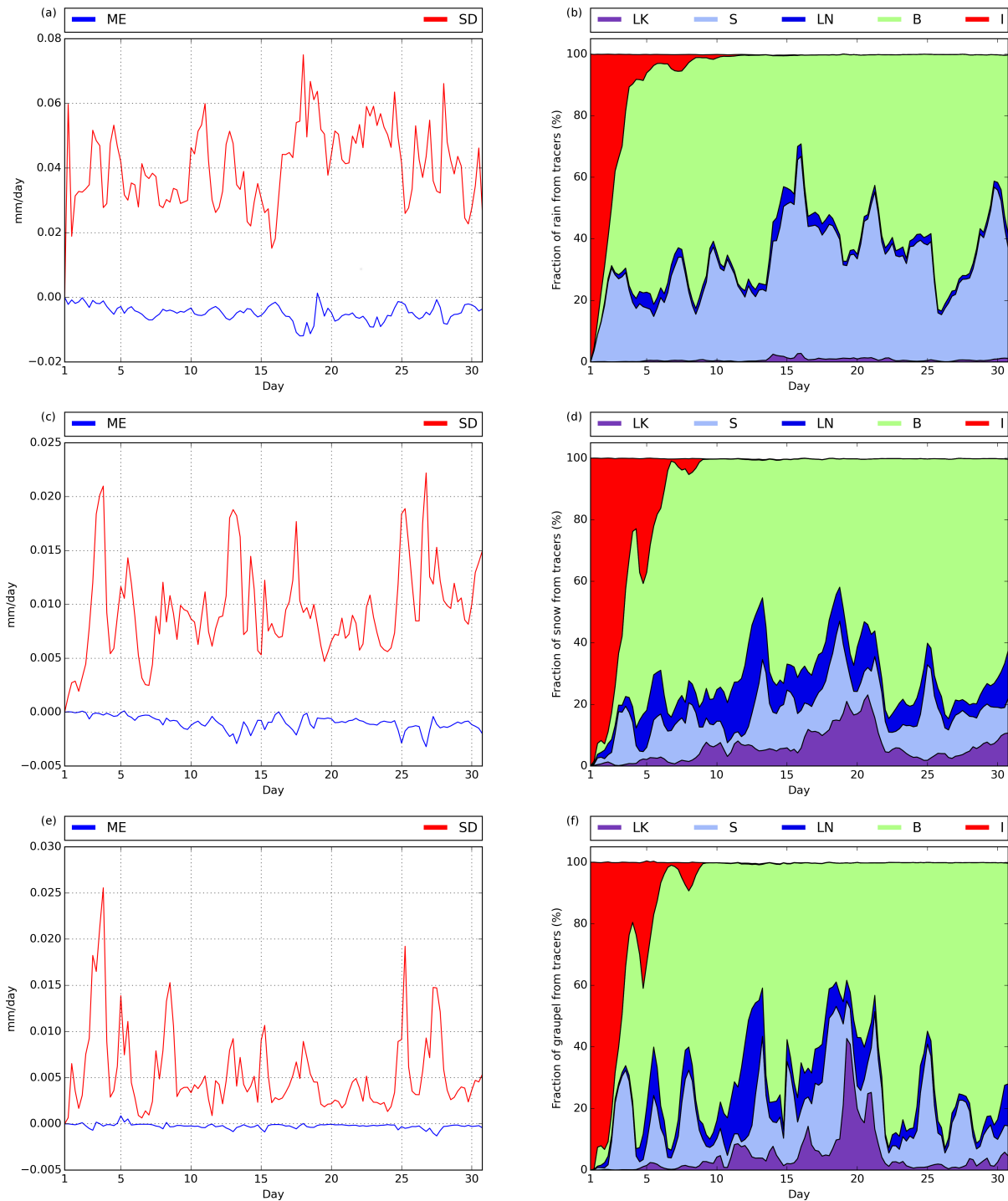


Figure 3.6: Mean error (blue) and standard deviation (red) (*mm*) for 3h accumulated tracer rain (a), tracer snow (c) and tracer graupel (e). Relative contribution of each moisture source [lake evaporation (LK, purple), sea evaporation (S, light blue), land evapotranspiration (LN, dark blue), lateral boundary advection (B, green), initial moisture (I, red)] to 3h accumulated rain (b), snow (d) and graupel (f).

considered moisture source to area averaged rain (Fig. 3.6b), snow (Fig. 3.6d) and graupel (Fig. 3.6f). Moisture initially present in the domain’s atmospheric columns only contributes to



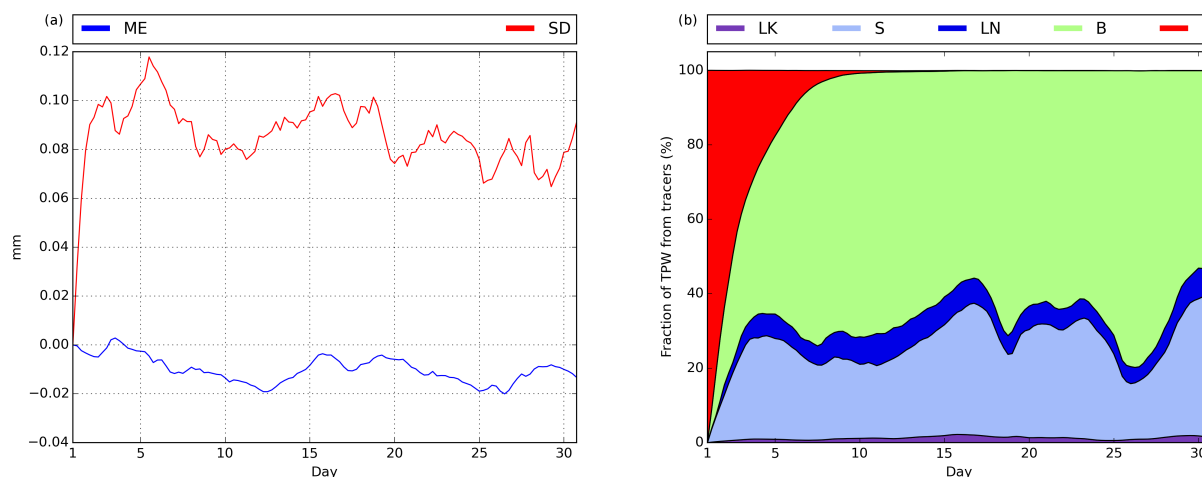


Figure 3.7: Same as Fig. 3.6 but for total precipitable water (TPW) (*mm*).

any precipitation type during approximately the first week of simulation. Rain is roughly about 40% of sea evaporation origin, and 60% from moisture influxes from the lateral boundaries, with this values oscillating throughout the month. In comparison with rain, snow and graupel have a stronger contribution from external moisture advection, and also from land evapotranspiration and lake evaporation, and much less fraction of sea evaporation input. As these figures are cumulative diagrams, the upper line (which separates the white zone from the color zone), indicates the combined contribution of all sources to precipitation. The deviation of this line from 100% represents the relative error of mean domain precipitation (Eq. 3.18), which, as it is apparent, is very small for all three precipitation types and at all times. Further discussion will follow later in this section.

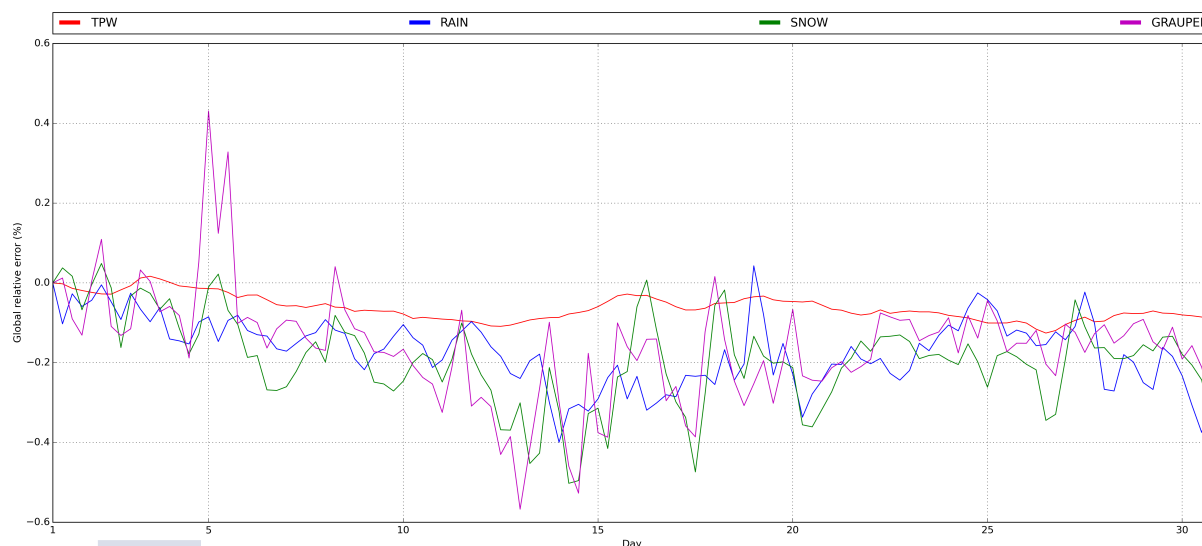


Figure 3.8: Relative error for mean domain tracer total precipitable water (TPW, red), 3h accumulated tracer rain (blue), tracer snow (green), and tracer graupel (purple).

Validation results in terms of total precipitable water are presented in the diagrams of Fig. 3.7, which are similar to those in Fig. 3.6 for precipitation. In this case, the mean error (Fig. 3.7a) takes values around -0.01 mm, whereas the standard deviation is about 0.1 mm,

which are very small numbers. To contextualize these results, we refer again to Bosilovich and Schubert [130], who show a mean error around  $-0.5$  mm ( $\sim 2\%$ ) and standard deviation of about  $0.5$  mm.

Finally, Fig. 3.8 shows in more detail the time evolution of the relative error of mean domain precipitation of all three types, as well as of mean domain TPW. This corresponds to the deviation from 100% in the cumulative values in figures Fig. 3.6b, d, f and Fig. 3.7b, as discussed previously. Numbers are similar for the three precipitation types and do not exceed  $\pm 0.4\%$ . On average, about  $0.2\%$  of precipitation is not associated with any of the five considered moisture sources; i.e., the mean domain relative error is around  $-0.2\%$ . For TPW, errors are even smaller. In this case, the deviation of the sum of contributions from all sources from 100%, is roughly  $-0.1\%$  (Fig. 3.8), which means that only  $0.1\%$  of TPW is not traceable. Sodemann et al. [134] found, at first, errors that were around  $10\%$  for TPW, and later this value was improved to  $1-2\%$  [154]. Finally, we note that during the simulation period (one month) there is no increasing trend in these errors, which attests the method's stability.

Both the small absolute and relative values of the analyzed error measures in this section, together with the lack of trends in the errors, demonstrate the high accuracy and soundness of the method. Finally, with regard to the causes of these inaccuracies, most likely, they are largely caused by numerical errors derived from the very large moisture tracer gradients that occur in some regions of the domain, for example, in the separation region between the BOUNDARY source (Fig. 3.3b) and the interior of the domain. These sharp transitions can induce small errors in the advection scheme and also stronger numerical diffusion than for full moisture. In addition, other errors, such as rounding errors or small inaccuracies in the water budget, contribute secondarily.

### **3.4 Application example: lake evaporation as moisture source in the Great Lakes snowstorm of 2014**

Heavy snowstorms are common meteorological phenomena in the North American Great Lakes region during autumn and winter months, usually associated with the intrusion of a cold and dry polar air mass over the warmer lake waters [e.g. 155, 156, 157, 158, 159]. The resulting large water-atmosphere temperature contrast increases heat and moisture fluxes from the lakes, destabilizing the planetary boundary layer [e.g. 160, 161] and leading to an activation and/or intensification of precipitation downwind. In some occasions snow bands formed during these events produce huge snow accumulations, with high socioeconomic impacts [e.g. 162, 163, 164].

It is well established that heat and moisture fluxes from the lakes are fundamental in the development of these episodes, since they cease to occur once open waters freeze over. Given the low moisture content of polar air masses, it is also likely that without evaporative fluxes from the lakes, large accumulations of snow would not be possible. It is still not clear, however, what the actual input of lake water to snowfall is in these events. Studies about the contribution of evaporated moisture from the Great Lakes to precipitation in lake-effect snowstorms are scarce, based on the analysis of the isotopic composition of precipitation (the so-called physical moisture tracers) and do not correspond to particular extreme events but to climatic periods [165, 166]. The WRF-WVTs tool that we present here can contribute to clarify this question, and, as an application example, in this section, we quantify the role of the Great Lakes as

moisture sources in the famous case of the November 2014 severe lake-effect snowstorm, the so-called “Snowvember” by local residents, which affected especially New York state (mainly cities bordering lakes Erie and Ontario and, in particular, the Buffalo area) between 17 and 21 November, causing at least 13 fatalities, widespread food and gas shortages due to blocked roads and, in general, many other traffic problems and material losses derived from the storm [167].

### 3.4.1 Experimental design

The example application experiment is run for 4.5 days (17:00-00:00 to 21:00-12:00UTC November) in a D2 domain nested within the validation simulation and encompassing the Great Lakes region with a horizontal resolution of 5km and the same 35 vertical levels as the parent domain D1 (Fig. 3.2). Tracer moisture from the parent domain can feed the nested domain through its lateral boundaries, which are not set to zero. The simulation serves also as an example of the versatility of the tagging tool. The physics settings in this experiment are identical to those in the validation simulation, except for spectral nudging and the convective parameterization, which are turned off.

Figure 3.9 shows the general synoptic situation for the selected case, in terms of surface pressure and 850hPa temperature (Fig. 3.9a) along with 500hPa geopotential height and temperature (Fig. 3.9b), both at 12:00UTC on 18 November 2014. The situation is that which is typically associated with Great Lake-effect snowstorms: a deep trough with low temperatures aloft over the region, causing intense west-northwest winds at lower levels across the Great Lakes and very cold air advection. The lakes were mostly ice free at this time, with temperatures between 0 and 8°C, the warmest in Lake Erie (Fig. 3.10b), contrasting markedly with the below -15°C values at 850hPa. The topography of the area is also shown in Fig. 3.10, with the highest terrain east of Lake Erie.

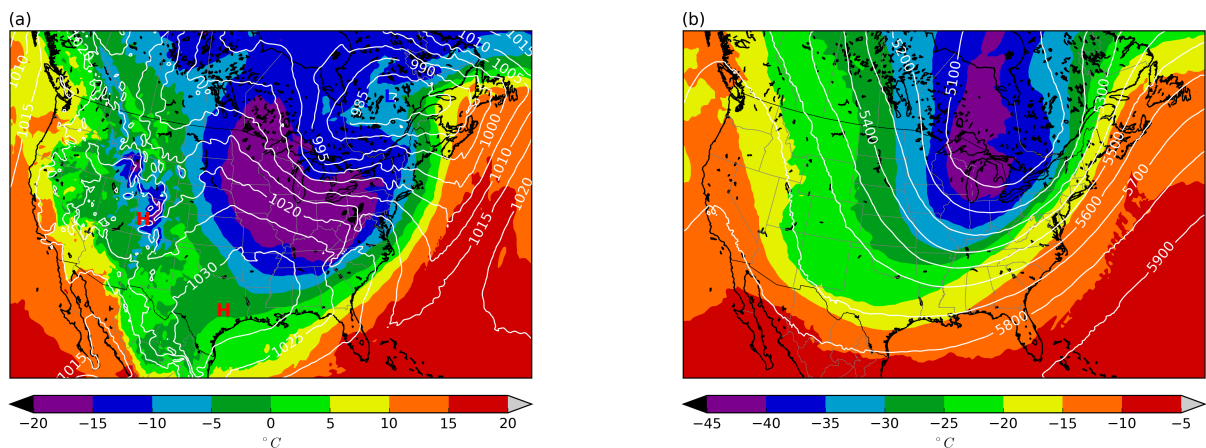


Figure 3.9: Synoptic situation on 18 November 2014 at 12:00 UTC. Mean sea level pressure (contours,  $hPa$ ) and 850hPa temperature (shades,  $^{\circ}C$ ) (a). Geopotential height (contours,  $m$ ) and 500 hPa temperature (shades,  $^{\circ}C$ ) (b).

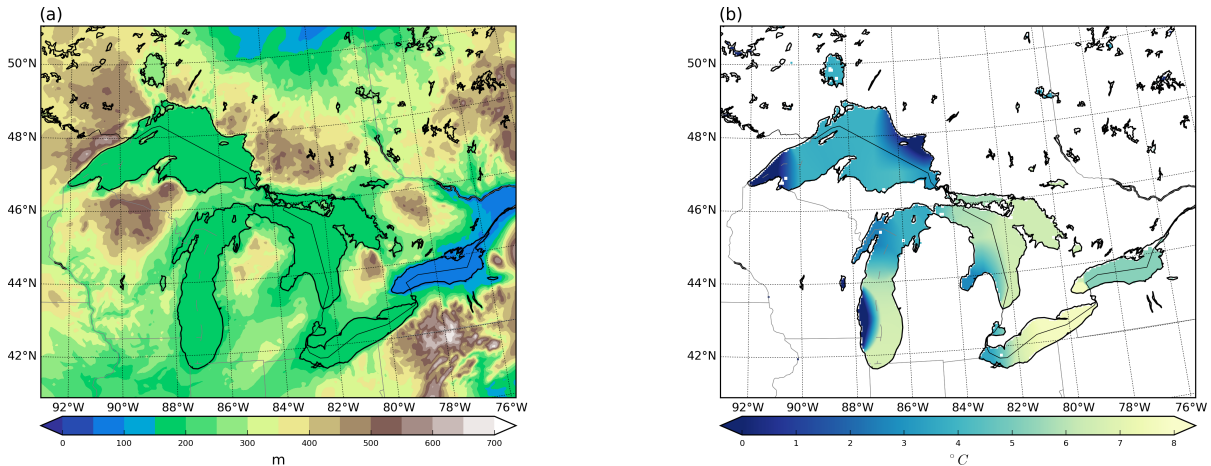


Figure 3.10: Topography of the nested domain ( $m$ ) (a) and lake surface temperature of the Great Lakes ( $^{\circ}C$ ) (b) on 18 November 2014 at 12:00 UTC.

### 3.4.2 Results

#### Precipitable water

Figure 3.11 shows the daily evolution, from 17 to 20 November 2014, of the precipitable water originating from evaporation in the lakes and the 10m wind at 12:00 UTC. Paired panels depict the percentage of total precipitable water that those amounts represent, together with 850hPa temperature. At 12:00 UTC on 17 November, a short wave trough was pushing past the region. Winds ahead of the associated front were still from the south over lakes Erie and Ontario, with moderately low temperatures above  $-6^{\circ}C$  at 850hPa; however, behind the trough, a very cold air mass was already in place over lakes Superior, Michigan and Huron, where winds had already veered and were at this time from the west-northwest direction. The enhancement of evaporation from the lakes is already apparent at this time, with precipitable water plumes from lakes Superior and Huron with values around 2-3mm, which represent a contribution of 20-30% of the total. After frontal passage, the next day, winds increase in intensity and change direction to the west-northwest, and the cold air settles in with temperatures around  $-16^{\circ}C$  at 850hPa. The arrival of the cold and dry air mass, together with the wind intensity rise, augment evaporation fluxes from the surface of the lakes, so that the precipitable water with this origin practically doubles with respect to the previous day, increasing the lake moisture contribution to about 30-60% of the total. The highest values are attained in plumes aligned with the main wind direction that originate from open waters and extend leeward of the lakes. The cold air stays in place for the next days and lake water evaporation values remain high; however, the direction of the moisture plumes from this source vary as wind changes due to the approach of another short wave trough, turning more toward the north as the flow becomes southerly on 19 November and again westward of the lakes when winds turn in this direction on 20 November. In the areas where the 850hPa temperatures remain below about  $-15^{\circ}C$  during the short wave passage, plumes of moisture from the lakes still develop, with an input of lake moisture above 30% of total content.



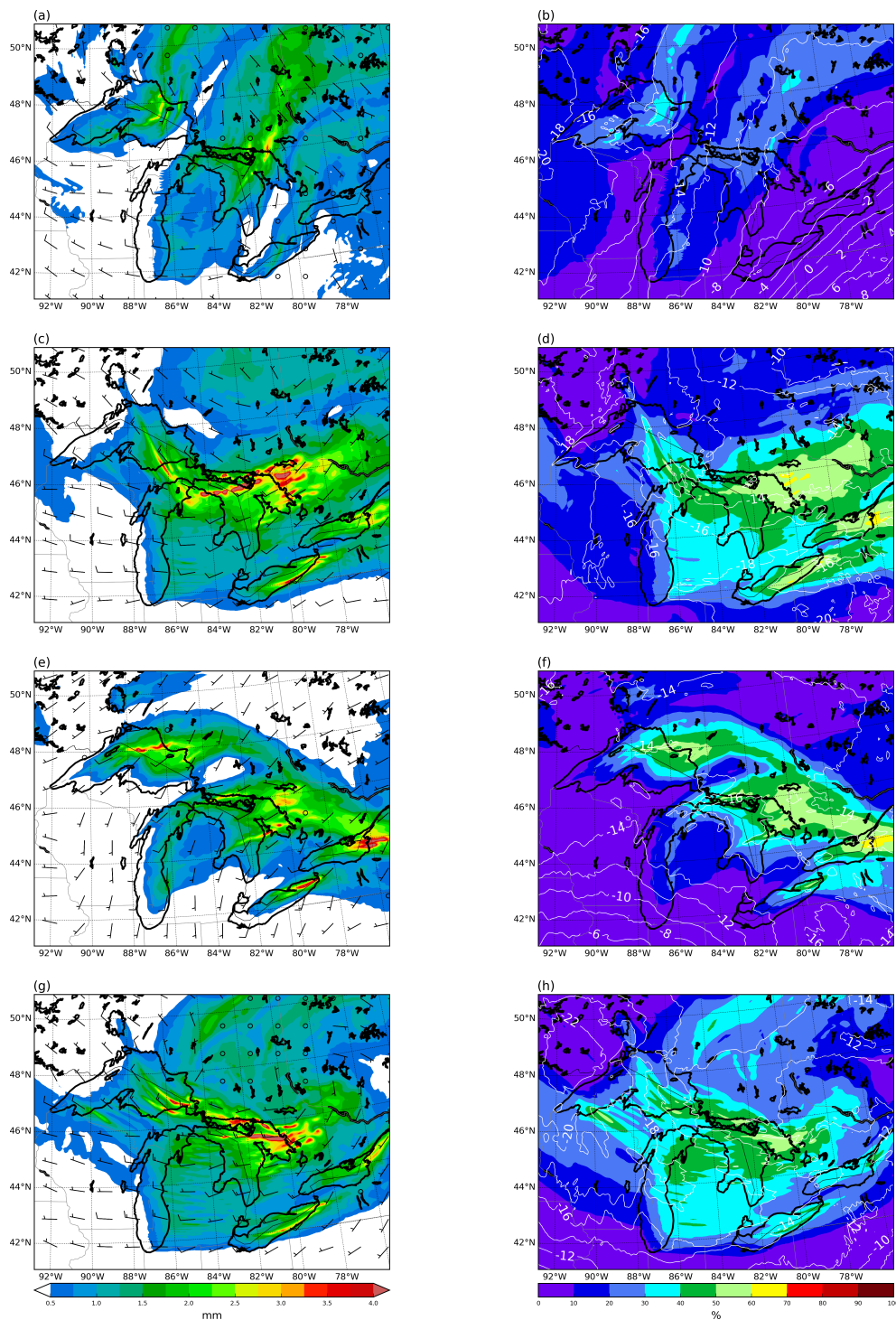


Figure 3.11: Total precipitable water (*mm*) originating from lake evaporation on 17 (a), 18 (c), 19 (e) and 20 (g) November 2014 at 12:00 UTC and their percentage contribution to total precipitable water for the same times (b, d, f, h). Wind barbs show 10m winds and contours 850hPa temperature ( $^{\circ}\text{C}$ ).

### Precipitation

The previous results suggest that the lakes' contribution to atmospheric moisture in the region is very significant for this event, and we assess next whether this is also the case for

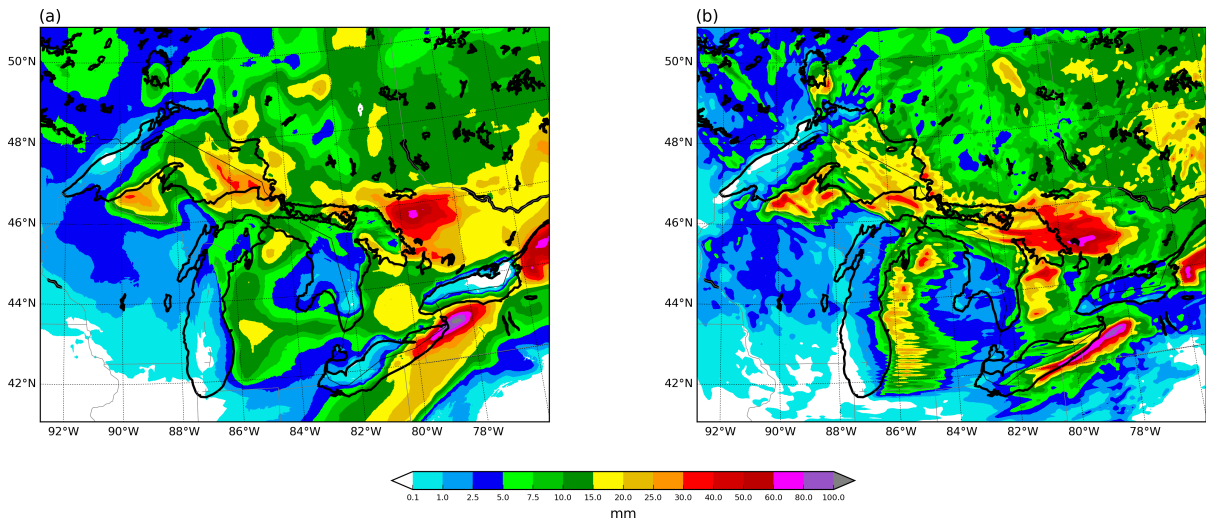


Figure 3.12: Observed (a) and simulated (b) accumulated snow water equivalent (*mm*) from 17 November at 06:00 UTC to 21 November at 06:00 UTC.

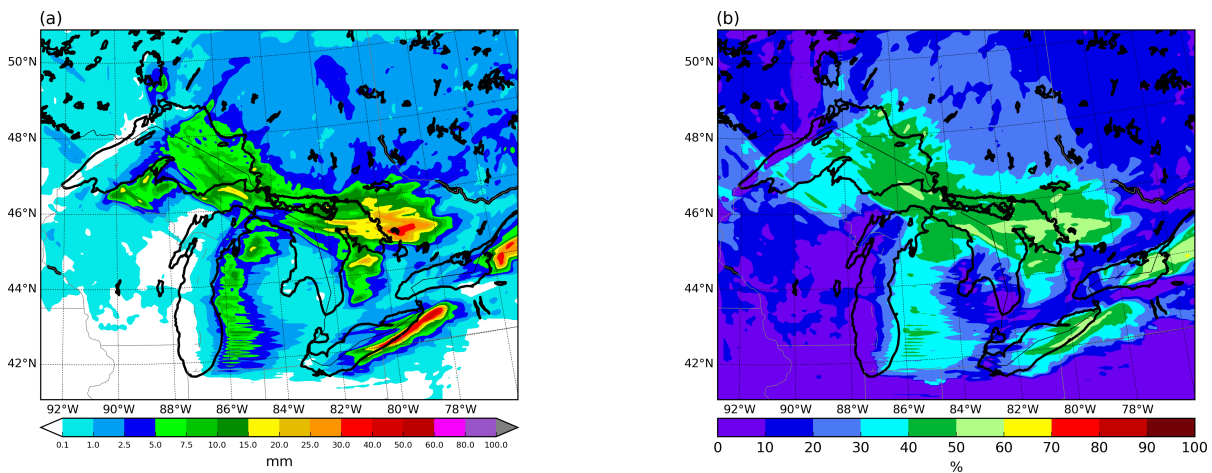


Figure 3.13: Simulated accumulated tracer snow water equivalent (i.e., coming from the lakes' evaporation) (*mm*) (a) and its percentage contribution to total simulated accumulated snow water equivalent (b) from 17 November at 06:00 UTC to 21 November at 06:00 UTC.

precipitation. Observed snowfall totals for the period between 17 November at 06:00UTC and 21 November at 06:00UTC (Fig. 3.12a, from NOAA's National Snow Analyses data; Carroll et al. [168]) were very high, with peak values close to 100mm in the Buffalo, NY, area, to the lee of Lake Erie, and with other pockets of over 60mm of snow water equivalent accumulations on the leeward shores of lakes Huron and Ontario, where orographic lifting from the existing hills further enhances precipitation. Figure 3.12b shows model results for the same period, which are in very good agreement with the observations, in amounts and distribution. This is particularly true for the aforementioned areas of highest snowfall totals.

The part of precipitation originating from lake evaporation during the same 4-day period is shown in Fig. 3.13, in terms of absolute (Fig. 3.13a) and relative (Fig. 3.13b) values to total accumulations. The role of the lakes as moisture sources is very relevant. In general, in all regions immediately downwind of the Great Lakes, water vapour with this origin accounts for

more than 30% of precipitation. The areas where the contribution of lake water vapour fluxes to precipitation is largest coincide with the locations of maximum snowfall totals, to the lee of lakes Huron, Erie and Ontario. Here, more than 50% of the snow water equivalent has its source in lake evaporation, which attests to the fundamental role of lake moisture in producing the observed localized extreme accumulations during these events. In regions further from the lakes, the pattern of total precipitation and that of precipitation originating from lake evaporation lose correlation.

### 3.5 Summary and conclusions

We presented here a new moisture tagging tool, coupled to the WRF model v3.8.1, for the analysis of precipitation sources and atmospheric humidity pathways in general. The technique is framed within the online Eulerian methods usually known as WVTs. We first detailed the method's formulation and its implementation into WRF, which required the modification of the turbulent, microphysics and cumulus parameterizations for the calculation of the associated tracer tendencies. We then assessed the method's precision with a validation strategy consisting in tagging moisture from all possible sources and evaluating the difference between the sum of all these contributions and total moisture results, in terms of precipitable water and precipitation. We identified the method's error with these deviations. The sources considered were incoming fluxes from the model grid's lateral boundaries, the moisture initially present in the entire atmospheric volume of the domain and surface evaporation. We further divided evaporative sources into three, namely ocean, land and lakes, which made the validation somewhat more challenging. We performed a 1-month long (November 2014) continental-scale (North America), 20km resolution model simulation for this purpose and found that the deviations of area-averaged variables are consistently about -0.1% for precipitable water and -0.2% for 3h accumulated rain, snow or graupel. This means that there is a small amount of precipitable water and precipitation that the method cannot link to any source. There is no noticeable increasing trend in these errors during the month-long period of simulation. The mean relative error and the standard deviation for the monthly accumulated precipitation is -0.17 and 0.2%, respectively, about the same as for the 3h values throughout the same period. These results demonstrate the robustness of our WRF-WVTs implementation as a sound and highly accurate tool to track atmospheric moisture pathways.

Finally, as an example application of the moisture tagging technique, we simulated the Great Lake-effect snowstorm of 2014, aiming at quantifying the contribution of evaporative fluxes from the lakes to total precipitable water and especially to snowfall amounts in this event. We employed for this purpose a nested grid within the validation domain, covering the Great Lakes region at 5km resolution and simulated the 4-day period from 17 November at 06:00UTC to 21 November at 06:00UTC. Results show the activation of the lake effect upon arrival of a cold and dry arctic air mass over the area, with the formation of total precipitable water plumes originating from the lakes and extending tens and even hundreds of kilometers in the downwind direction. As expected, the model shows how the lake effect intensifies with colder and stronger west or northwesterly surface winds and tapers off with warmer and weaker southerly airflows. The contribution of lake-evaporated moisture to total precipitable water within the plumes is generally above 30% across the area downwind of the lakes when temperatures at 850hPa are below around  $-15^{\circ}\text{C}$ , and exceeds 60% in plumes to the lee of lakes Huron, Ontario and Erie when conditions are most favorable for lake effect on 18 November.

The model simulation reproduces faithfully observed snowfall accumulations during the 4-day period, with maximum amounts of close to 100mm of snow water equivalent in the Buffalo, NY, area, to the lee of Lake Erie and other pockets with values above 60mm on the leeward shores of lakes Huron and Ontario. It is in these locations of highest impact where the contribution of lake evaporation to precipitation is largest, between 50 and 60% of the total. In general, for all regions immediately downwind of the lakes, the input of lake moisture to precipitation is about 30-50% and diminishes gradually at further distances.

These results highlight the important contribution of evaporative moisture fluxes from the lake surfaces in the genesis of precipitation during Great Lake-effect snowstorms. They also suggest that this input is fundamental in producing the most extreme accumulations, with the highest socioeconomic impacts, in the Buffalo, NY, area and other locations to the lee of the lakes, especially Erie, Ontario and Huron. To draw a more robust general conclusion, an in-depth investigation with a sufficient number of cases and further diagnostics would be needed; however, this is beyond the scope of the present thesis and a matter of future work, since our intent here is to simply illustrate with a practical example the possibilities of WRF-WVTs as a powerful tool for moisture tracking.

# Chapter 4

## Case study: the catastrophic flooding episodes of the autumn of 1982 in Spain

\* The results from this chapter have already been published as D. Insua-Costa<sup>1</sup>, G. Miguez-Macho<sup>1</sup>, and C. Llasat<sup>2</sup>, “Local and remote moisture sources for extreme precipitation: A study of the two catastrophic 1982 western Mediterranean episodes”, *Hydrology and Earth System Sciences*, vol. 23, no. 9, pp. 3885–3900, 2019.

<sup>1</sup> CRETUS, Non-linear Physics Group, Universidade de Santiago de Compostela, Galicia, Spain

<sup>2</sup> Departament of Applied Physics, Universitat de Barcelona, Barcelona, Spain

### 4.1 Introduction

Several authors have attempted in the past to answer the key question of this thesis, posed earlier in the General Introduction section: where does the moisture that fuels Mediterranean precipitation extremes come from? Reale et al. [27], employing the quasi-isentropic water vapour back-trajectory method [76], showed that moisture transported by three (westward moving) Atlantic tropical systems and their extra-tropical remnants contributed significantly to the series of floods that affected the north-western and north-central Mediterranean in September and October of 1998. Turato et al. [28] with the same tool demonstrated that remote moisture sources, mainly the Atlantic Ocean, were crucial in the October 2000 Piedmont flood, and concluded that the contribution of evaporated moisture in the Mediterranean was lower than presumed, at around 20% of the total. Duffourg and Ducrocq [30] studied the moisture origin and pathways in ten EPEs that took place during the autumn of years 2008 and 2009 in the French Mediterranean region. They also used a water vapour back-trajectory technique, in this case coupled to the Meso-NH atmospheric model (i.e., on-line), concluding that when anticyclonic conditions are dominant during the 3 or 4 days prior to the EPE, the contribution of the moisture from the Mediterranean Sea is clearly dominant, whereas when cyclonic conditions prevail, remote moisture sources have a major role. Pinto et al. [32], combining a qualitative with a backward trajectory analysis, studied a large number of events (classified in six clusters) occurred in northwestern Italy between 1938 and 2002, and found that the North Atlantic is a relevant moisture source for precipitation, particularly important in the extraordinary cases. More recently, Krichak et al. [34] applied a similar method for more than 50 intense cool season



EPEs recorded in different parts of the Mediterranean region from 1962 to 2007. Their results highlighted the outstanding role played by tropical moisture reaching the Mediterranean from the Atlantic Ocean and the Arabian Sea. All these studies agree on the importance of the moisture contribution from remote sources, thus supporting the hypothesis that a very large moisture supply from regions outside the Mediterranean is often a key factor in these types of episodes. However, practically all of them were carried out with Lagrangian models, which do not allow for accurate quantitative analysis in specific case studies [77], but rather a qualitative analysis based on the trajectory of the Lagrangian air parcels. Thus, for example, although Krichak et al. [34] study 50 events, they do not provide figures for the contribution of any of the moisture sources analysed. Some of these studies attempt to quantify the contributions in terms of variation in moisture content along the trajectories [e.g. 30]. However, this procedure is highly subject to inaccuracies, since air parcels can gain or lose moisture by processes such as convergence or divergence, which have nothing to do with a surface input of moisture from the sources.

In this chapter we present an example of the application of water vapour tracers for the study of moisture origin in Mediterranean EPEs. It is precisely the application of this moisture tracking technique that represents the main novelty of this chapter, since this tool has only been applied to Mediterranean EPEs by Winschall et al. [31]. These authors analyzed the origin of moisture feeding the extreme precipitations in Piedmont in November 2002, and found that the three main sources were land evapotranspiration, evaporation from the Mediterranean and North Atlantic moisture. This chapter is therefore an introduction to the study of Mediterranean precipitation extremes with WVTs and acts as a preamble to Chapter 5, in which this high-precision tracking tool will be applied to the study of a much larger number of EPEs.

Precisely, we will apply the method to two infamous EPEs occurred in the NWMR (northwestern Mediterranean region) during the autumn of 1982. The selection of these two cases is mainly based on the enormous socioeconomic impact they had, which is why even today they are well remembered by the population. Both events appear, for example, in the list of major flood disasters in Europe between 1950 and 2005 [10] and are still present in the scientific community and the media. The first of these episodes occurred in October and particularly affected the Spanish Levant area. The highest precipitation amounts were observed on days 19, 20 and 21, especially on day 20, with a maximum of 426 mm fallen in Cofrentes (Valencia, Spain). Particularly dramatic was the situation in the vicinity of the Tous dam, since the exceptionally intense precipitation recorded in the river Júcar basin (where the dam is situated) caused its rupture, seriously aggravating flooding downstream. The consequences were catastrophic; there were 40 fatal victims and about 630M\$ (uninflated) in economic-losses [10]. The second event took place only a few days later, between November 6 and 8, with special intensity on the 7th. In this occasion, precipitation affected especially the northeast of Spain (Catalonia), Andorra and the south-east of France, with remarkable amounts such as the 408 mm recorded in Valcebollère (French Pyrenees) and 342 mm in La Molina (Catalan Pyrenees), both in 24 hours. The consequences of the event were also catastrophic; 42 casualties, adding the victims of Spain, Andorra and France [124], and about 300M\$ (uninflated) in damages in Catalonia alone [13].

The chapter is structured as follows: Section 4.2 describes the methodology and the data used. Section 4.3 and 4.4 show the results obtained by applying the WVTs method to the cases of October and November 1982, respectively, and finally, Section 4.5 contains a summary and

conclusions of the work.

## 4.2 Methods

In the present study, we aim at applying the new WVTs moisture tagging capability recently implemented into the Weather Research and Forecasting (WRF) regional meteorological model, the so-called WRF-WVTs tool presented in the previous chapter. This implementation has been thoroughly validated [2], showing that the method presents a high accuracy, and thus it will allow us to quantify the contribution of different moisture sources and to perform a detailed three dimensional separation of water vapour from different origins in the development of EPEs in the Mediterranean.

### 4.2.1 Experimental design

We consider four source regions, three two-dimensional and one three-dimensional. The three 2D source regions cover the western Mediterranean, the central Mediterranean and the North Atlantic evaporative sources respectively, whereas the 3D source region tags moisture advected from the tropical and subtropical Atlantic and from tropical Africa (Fig. 4.1a). The 2D sources target sea evaporation; however, the tropical and subtropical regions are taken as a 3D source in order to include both evaporation and atmospheric water transport from further possibly relevant tropical or subtropical areas outside the model grid, such as the Gulf of Mexico, which is a relevant moisture source for precipitation in the WMR according to different climatic studies [169, 29]. Special care has been taken not to tag humidity from any source twice. For example, moisture evaporated in the North Atlantic is only considered once, even when it reaches the Iberian Peninsula after traversing the 3D subtropical source region. Finally, we note that we do not contemplate all possible moisture sources, such as land evapotranspiration from different continental regions. We assume that in autumn it is very diminished and hence it does not have a potentially important contribution [e.g. 170, 171].

With this sources' selection, we will be able to clarify the origin of moisture on the large scale only. In other words, we can determine whether moisture is of local or remote origin, but we will not be able to ensure, for example, where exactly in the Atlantic or tropics this humidity mostly comes from. We could subdivide the four selected sources into many more and then achieve much more detail, but for each selected moisture source a separate simulation must be carried out, with the corresponding increase in computational cost. For example, for  $1 \times 1$  degree source regions, this means hundreds of simulations just for one case. The selection proposed here is based on the choice of quite extensive sources, which does not mean they are not enlightening: a distinction is made between local (Mediterranean) and remote (Atlantic) humidity; within the remote we distinguish between tropical and non-tropical and within the local between western and central Mediterranean.

Simulations for both events start 10 days before their respective main date (October 20 and November 7), thereby allowing moisture sufficient time to evaporate and travel to the area affected by extreme rainfall (highlighted in red in Fig. 4.1b). Furthermore, this 10-day period roughly coincides with the average residence time of water vapour in the atmosphere [e.g. 172, 173]; thus we can neglect the contribution of the moisture present at initial time in the atmospheric volume of the considered domain. The total time span of the experiments is 12 days.



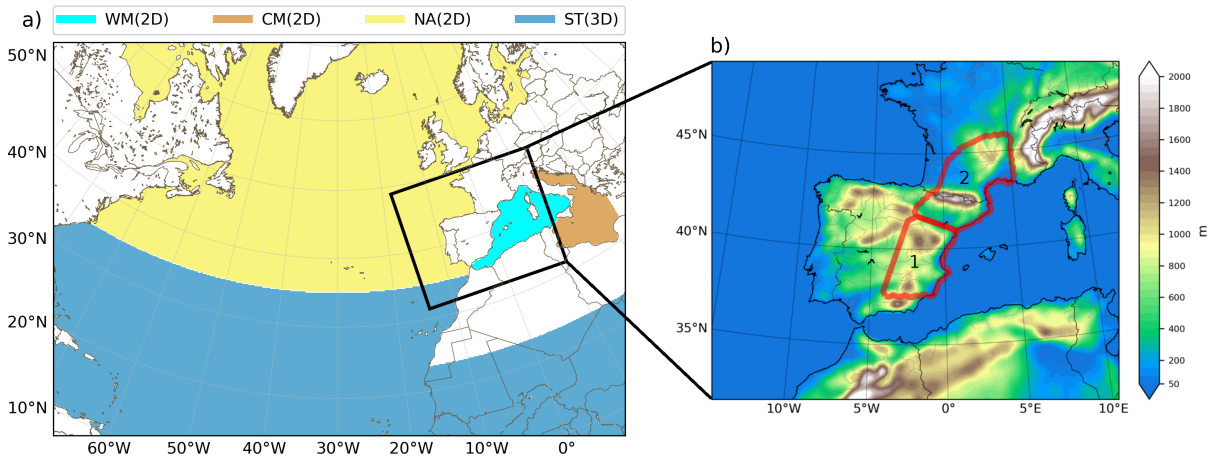


Figure 4.1: (a) Simulation domain and moisture sources considered: western Mediterranean (light blue), central Mediterranean (brown) and North Atlantic (yellow) two-dimensional sources and tropical and subtropical three-dimensional source (dark blue). (b) Domain for precipitation analysis with topography (m) in shades. The areas highlighted in red are the most affected by the October (1) and the November event (2).

## 4.2.2 Model configuration and data used

The simulations for the two 1982 EPEs are performed with the WRF model version 3.8.1 [147] using a single domain of 20km horizontal resolution and 35 vertical levels. Initial and boundary conditions were obtained from ERA-Interim reanalysis [174] with spatial resolution of  $0.7^\circ$  and updated every six hours. In addition to the YSU boundary layer parameterization, WSM6 microphysics scheme and Kain-Fritsch convective parameterization (required when the WRF-WVTs tool in its current version is activated), we have also used the Rapid Radiative Transfer Model [RRTM; 150] and Dudhia [151] schemes for long and shortwave radiation, respectively, and the Noah Land Surface Model [Noah LSM; 149]. Spectral nudging of the synoptic circulation in the grid (about 1000km wavelength and longer) towards reanalysis has been applied to avoid distortions due to the interaction between the model's solution and the lateral boundary conditions [153]. Finally, for model rainfall validation we use the MESCAN [53] precipitation analysis.

## 4.3 The October event

### 4.3.1 Synoptic situation and precipitation

The October 1982 case, also known as the Tous event, was associated with a cold-core COL, which had originated from an Atlantic trough and was centered aloft over Morocco on the 20th, the main day of the episode (Fig. 4.2b). This configuration caused a marked increase in instability and the emergence of dynamic forcings favouring the appearance of upward air motions in the Spanish Levant area, the one most affected by the torrential rains. At lower levels, the cyclone consisted of an extensive low-pressure system with center over Algeria, which organized a relatively warm (Fig. 4.2a) and very humid (Fig. 4.2b) easterly flow almost perpendicular to the coast, increasing the chances of heavy precipitation. In Fig. 4.2b, the

high amount of TPW on the east coast of Spain is particularly noteworthy, with values well above 30 mm. All these elements provided a quasi-ideal scenario for the occurrence of deep moist convection. In fact, during October 20, a mesoscale convective complex [175], the first identified in Europe, developed east-southeast of the Iberian Peninsula, ultimately causing the EPE [although it was finally defined as a mesoscale convective system, MCS, due to its minor dimensions, 45]. For a more in-depth analysis of the factors contributing to this event, please refer to Romero et al. [15].

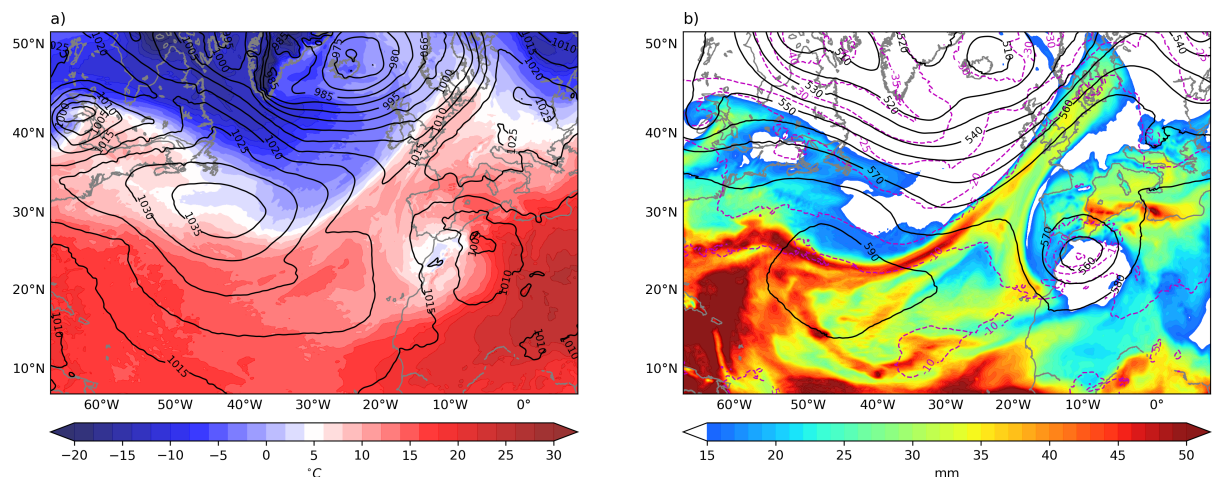


Figure 4.2: Synoptic situation (from WRF simulation) on October 20, 1982, at 12:00 UTC. (a) Mean sea level pressure (contours, hPa) and 850 hPa temperature (shades, C). (b) Geopotential height (solid black contours, dam) and temperature (magenta dashed contours, C) at 500 hPa and total precipitable water (shades, mm).

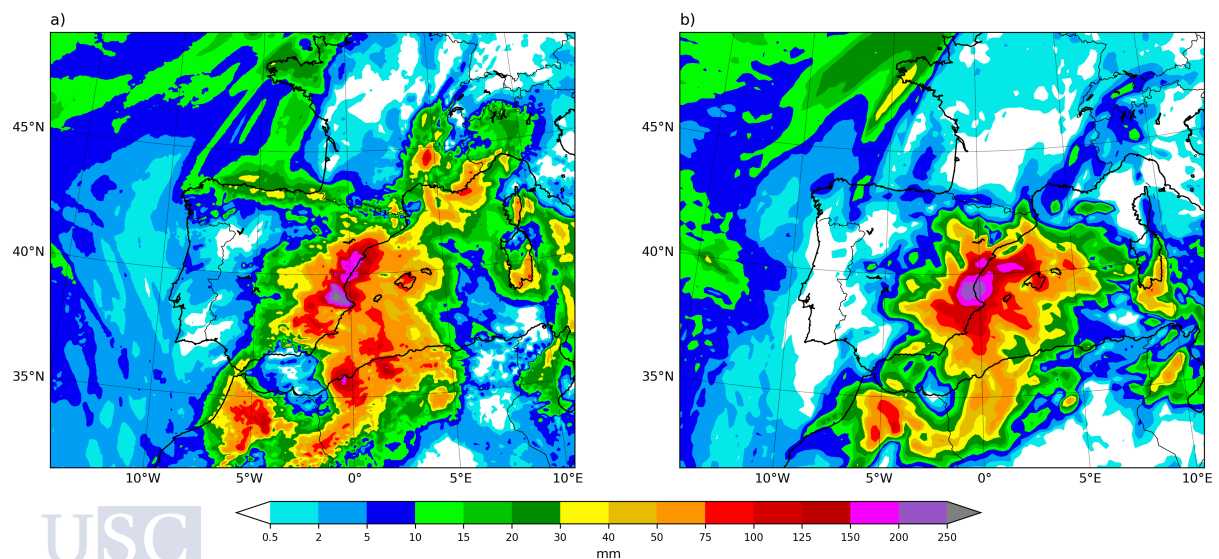


Figure 4.3: (a) Observed (from MESCAN analysis) and (b) simulated total precipitation (mm) from October 19 at 06:00 UTC to October 22 at 06:00 UTC.

Figure 4.3 shows the observational analysis (Fig. 4.3a) and simulated (Fig. 4.3b) precipitation during the days of the event (October 19, 20 and 21). As mentioned earlier, the

most affected region by the EPE was the Spanish Levant area and especially the Valencian Community, with maximum precipitation accumulations above 250 mm towards the interior of this region. Note that the recorded amounts in some stations were actually much higher; however, localized peak values are smoothed out in the analyzed precipitation field, since it has a resolution of 5.5 km. Precipitation was well organized around this maximum, which is consistent with the fact that the rains were produced by an almost stationary MCS. The simulated precipitation shows a very good agreement with the observational analysis, both in amounts and spatial distribution. Therefore, despite some discrepancies, we conclude that the model reproduces the episode realistically.

### 4.3.2 Moisture origin

Figure 4.4 shows at 12:00 UTC on October 20, the TPW originating from the different moisture sources considered during the previous 10.5 days, i.e. from the beginning of the simulation (00:00 UTC, October 10). Moisture from evaporation in the western (Fig. 4.4a) and central Mediterranean (Fig. 4.4b), with total content values in the 5-10 mm range in both cases, remains stagnant in the Mediterranean area, suggesting that throughout the period before the event, the flow was weak in the region as a result of the prevailing anticyclonic situation. The low pressure system situated over North Africa blocks the direct advance of evaporated moisture from the North Atlantic toward the Spanish Levant area (Fig. 4.4c). Notwithstanding, some of this humidity reaches the region by making its way around the cyclone, and the attained values of TPW from this source are still significant, of around 5 mm. The most important contribution from any source corresponds, however, to that of moisture advected from the tropics and subtropics (Fig. 4.4d). Following the circulation around the low in North Africa, a well-defined moisture plume rising across the Sahara reaches the east coast of Spain, yielding values of TPW of around 15 mm; locally even exceeding 25 mm.

Figure 4.5 depicts the source-separated vertical distribution of water vapour 12h before (00:00 UTC, October 20) and 12h after (00:00 UTC, October 21) the time in Fig. 4.4. Both absolute and relative contribution from each source are reflected. The values shown are spatial averages over the area most affected by the event, highlighted in red and labelled as 1 in Fig. 4.1b. At the early stages of the episode (Fig. 4.5a and 4.5c), the atmospheric moisture content is dominated by evaporative input from the western Mediterranean and the North Atlantic, and by advection from the tropics and subtropics, with the role played by moisture from the central Mediterranean being negligible. At the lowest levels of the atmosphere, evaporation from the western Mediterranean and the North Atlantic in conjunction represent more than 60% of the existing total water vapour. Above 800 hPa, however, moisture becomes increasingly of tropical and subtropical origin, and above 500 hPa these remote sources account for more than 50% of total humidity. As the dynamics of the event progresses, one day later (Fig. 4.5b and 4.5d) the vertical distribution of moisture source contribution changes substantially. With the settling in of easterly flow induced by the wide low pressure system over North Africa, moisture content from the North Atlantic becomes almost negligible and it's replaced by central Mediterranean evaporation. In addition, the injection of tropical and subtropical water vapour is reinforced, clearly becoming the most relevant source in this phase of the event; its presence is very significant in the entire atmospheric column, accounting for more than 60% of the total moisture above 800 hPa. At this stage, the large amount of water present in the atmosphere at all levels is striking, with a mixing ratio of about 12 g/kg at 950 hPa.



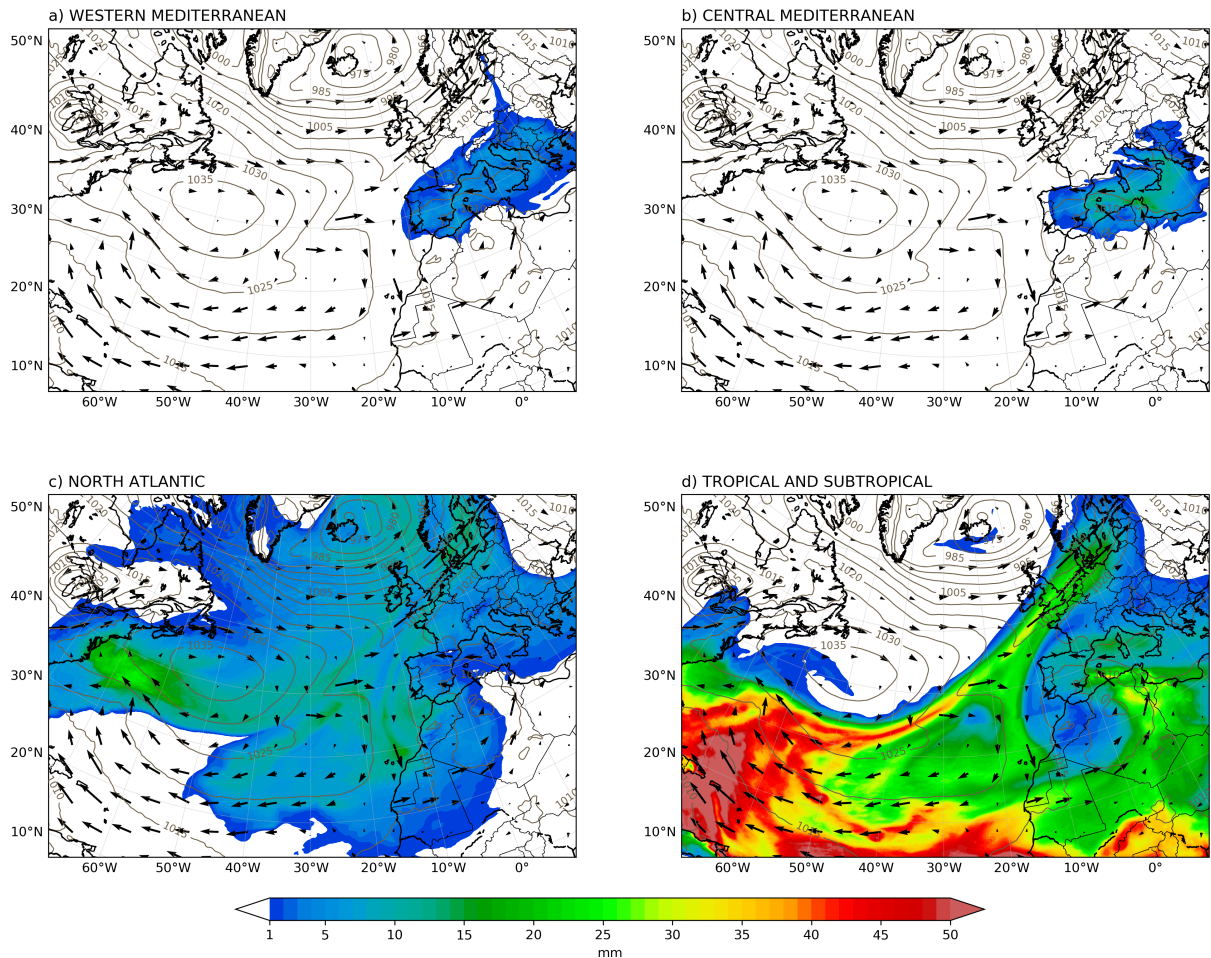


Figure 4.4: Total precipitable water (mm) coming from the western Mediterranean (a), the central Mediterranean (b), the North Atlantic (c) and from the tropical and subtropical Atlantic along with tropical Africa, on October 20 at 12:00 UTC. Contours show mean sea level pressure (hPa) and arrows show the vertically integrated moisture flux ( $\text{kg m}^{-1} \text{s}^{-1}$ ).

Finally, we note that the relative combined contribution of the four sources considered is always higher than 80% throughout the entire column, which agrees with our original hypothesis that other possible moisture sources are of minor importance.

### 4.3.3 Precipitation origin

From the previous analysis, it is apparent that moisture at low levels is dominated by evaporative sources, either local (western Mediterranean) or more distant (first from the North Atlantic, later from the central Mediterranean), while in mid and upper layers it is mostly of remote tropical and subtropical origin, more so as the event develops. Furthermore, the contribution of this advected moisture from lower latitudes increases significantly the water vapour content throughout the column. We examine next how TPW from each origin translates into precipitation, to address the main question that we posed in this study: how much of the accumulated rainfall in the event is coming from the different analyzed sources. Figure 4.6 shows a decomposition of the total precipitation field in Fig. 4.3b according to moisture

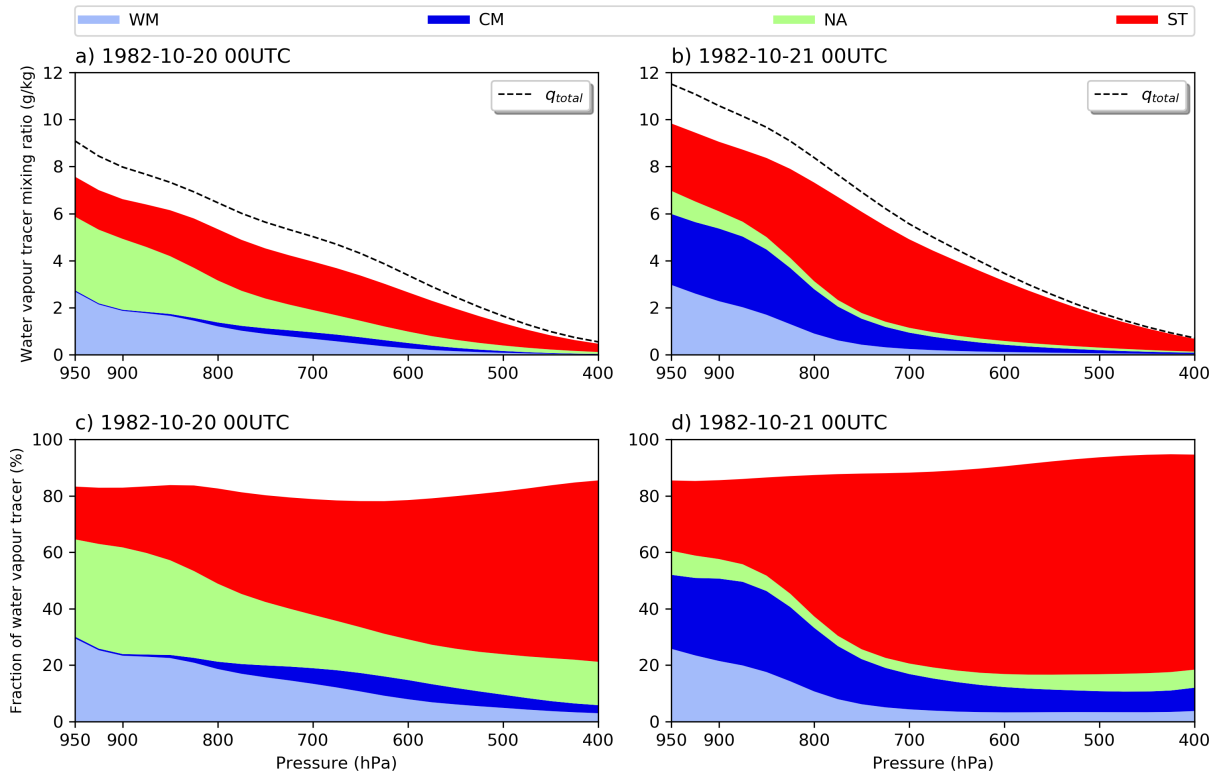


Figure 4.5: Vertical distribution of water vapour coming from the western Mediterranean (light blue), the central Mediterranean (dark blue), the North Atlantic (light green) and from the tropical and subtropical Atlantic along with tropical Africa (red). First-row shows absolute values (g/kg) on October 20 (a) and 21 (b) at 00:00 UTC. Second row depicts relative values (%) on October 20 (c) and 21 (d) at 00:00 UTC. Black dashed lines indicate the total water vapour mixing ratio, from considered and not considered sources (g/kg). Values are area averages over the region highlighted in red and labelled 1 in Fig. 4.1b.

origin. The contribution from the western (Fig. 4.6a) and central (Fig. 4.6b) Mediterranean is approximately equal, with maximum accumulations from October, 19 to 21 exceeding 50 mm in the Spanish Levant area. Here, the amounts coming from North Atlantic evaporation (Fig. 4.6c), albeit significant, barely reach 30 mm. In North Morocco, another of the impacted regions, the contribution of this source is, however, somewhat higher. Rainfall from tropical and subtropical origin (Fig. 4.6d) represents the largest share of the total in virtually the entire area affected by the event, with values well above 50 mm over a wide swath around the location of maximum precipitation in Spain.

The relative contribution of the different sources to total precipitation during the main days of the event are quantified in Table 4.1. Values are calculated over the Spanish Levant area -outlined in red and labelled 1 in Fig. 4.1b- and shown as percentage of total rainfall. Local moisture from evaporation in the western Mediterranean basin accounts for only about 20% of precipitation. If we expand the concept of “local” to include the central Mediterranean, then the contribution from local sources practically doubles, to represent around 40% of the total. In contrast, at least 46% of precipitation originates from water evaporated in remote regions, with tropical and subtropical moisture being the most relevant (31% of the total). The four considered sources account for most of the collected rainfall, around 83%, consistently with the

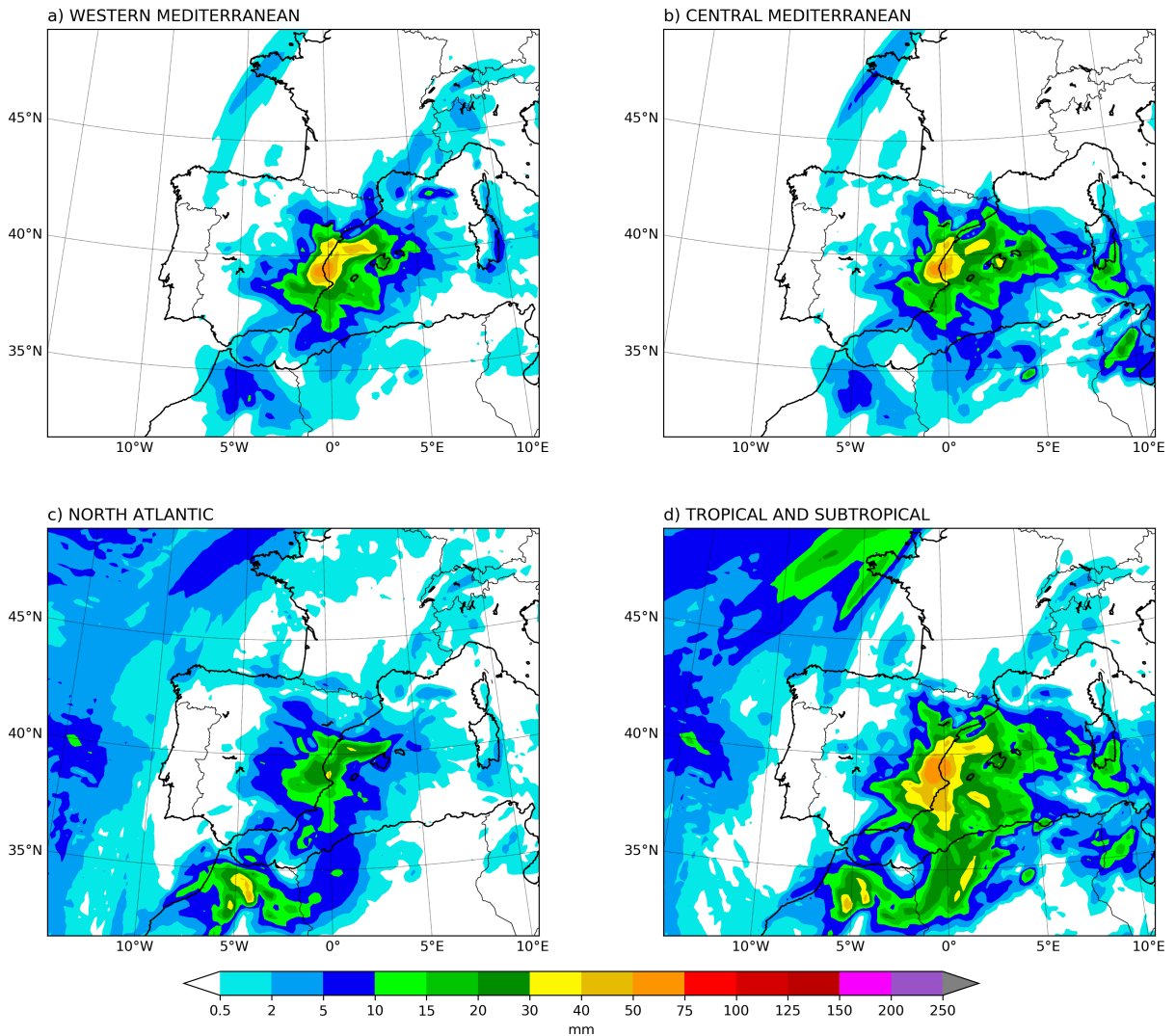


Figure 4.6: Simulated precipitation (mm) coming from the western Mediterranean (a), the central Mediterranean (b), the North Atlantic (c) and the Tropics and Subtropics (d) from October 19 of at 06:00 UTC to October 22 at 06:00 UTC.

values seen in the previous section for water vapour throughout the atmospheric column.

Table 4.1: Relative contribution (%) of the considered moisture sources to the accumulated precipitation from October 19 at 06:00 UTC to October 21 at 06:00 UTC in the most affected area (region 1 in Fig. 4.1b).

Western Mediterranean	Central Mediterranean	North Atlantic	Tropics/Subtropics
19,14	18,28	14,89	31,02

## 4.4 The November event

### 4.4.1 Synoptic situation and precipitation

As the October episode, the case of November had a very high social and economic impact, but the weather conditions leading to it were very different. There was neither COL nor cold air aloft in the most affected regions by extreme precipitation (northeast Spain and southeast France); instead, the EPE was connected with a strong omega block pattern (Fig. 4.7b). At 12:00 UTC November 7, the main day of the event, an extensive upper-level ridge associated with a strong surface anticyclone covered a large part of Europe, while a deep trough was located west of the Iberian Peninsula, thus leaving northeastern Spain and southwestern France in the frontal zone on its leading side. At the surface (Fig. 4.7a), a very deep low-pressure system located off the coast of Galicia organized a very intense, persistent (due to the block pattern) and relatively warm low-level south-southwesterly flow into the most affected regions. Another crucial feature drawing attention in Fig. 4.7b is the very high values of TPW in much of the eastern half of the Iberian Peninsula, seemingly transported to the region by an atmospheric river, which favoured the high accumulations of rainfall. All these elements indicate that dynamic rather than thermal factors were the most relevant in this case. For a more in-depth analysis of the development of this event, please refer to Trapero et al. [124].

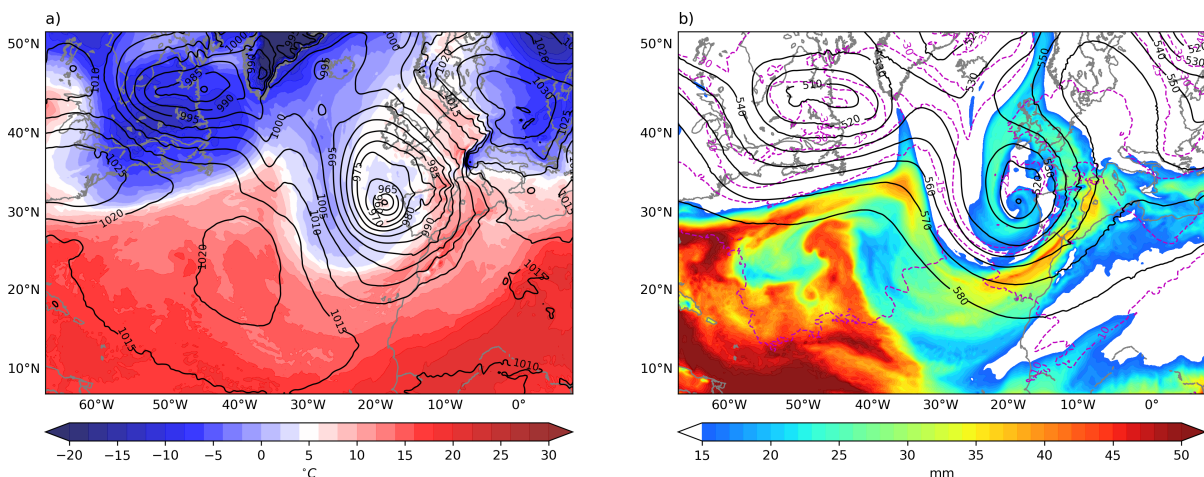


Figure 4.7: Similar to Fig. 4.2 but for November 7, 1982, at 12:00 UTC.

Figure 4.8 shows the observational analysis (Fig. 4.8a) and simulated (Fig. 4.8b) precipitation during the main days of the event (November 6, 7 and 8). The spatial pattern in Fig. 4.8a indicates that orography played a very important role, since the maximum precipitation occurs in mountainous areas. This is especially evident in the Pyrenees and the southern section of the French Massif Central, where the highest rainfall accumulations were recorded. Precipitation peaks in the latter mountain ranges are well above 250 mm, although, as in the October case, there were much higher amounts measured at specific locations (exceeding 400 mm in just 24 h) that are smoothed out in the analysis. In this November event, extreme precipitation affected, nevertheless, a very large region, including the Iberian Peninsula, Morocco and Southern France, and was not so local as in the episode from the previous month. This suggests that the nature of precipitation was very different in both cases; in October, it was associated with deep convection whereas in November, precipitation was



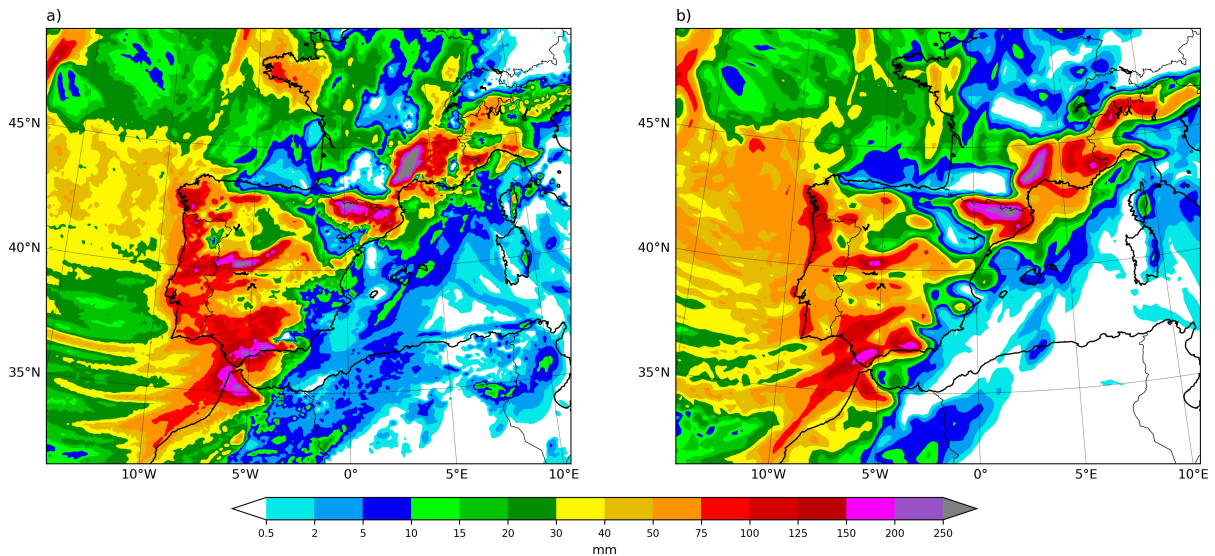


Figure 4.8: Similar to Fig. 4.3 but from November 6 at 06:00 UTC to November 9 at 06:00 UTC.

mainly stratiform, with strong embedded convective cells triggered by the terrain in mountain areas. Therefore, the persistence (forced by the block pattern) and orographic lift enhancement of precipitation, together with a good supply of moisture, were the key factors in this episode. The model simulates realistically these processes and captures the actual spatial distribution and total accumulations of rainfall closely (Fig. 4.8b).

#### 4.4.2 Moisture origin

Figure 4.9 shows at 12:00 UTC, November 7, the TPW generated from each considered origin from the beginning of the simulation, 10.5 days before (October 28, 00:00 UTC). The deep low-pressure system located off the coast of Galicia picks up moisture from all the sources and redistributes it in different ways. TPW from evaporation in the western (Fig. 4.9a) and central Mediterranean (Fig. 4.9b) is advected due northwest, across France and the British Isles and finally transported into the Atlantic following the cyclonic circulation around the low. The Iberian Peninsula lies only marginally within this path, and as a result, the amount of TPW from the western Mediterranean is small there, less than 5 mm in Catalonia, and negligible for moisture from the central Mediterranean. However, in southeast France, the other region most affected by the rains, the contributions from these two sources are substantially more relevant, with values of more than 10 mm of western Mediterranean TPW in the vicinity of the Gulf of Lion. Meanwhile, North Atlantic moisture is transported in large amounts toward the Iberian Peninsula by the intense south-westerly flow associated with the low (Fig. 4.9c), and TPW from this origin attains values of around 15 mm in the western Iberian margin. Some of this Atlantic water vapour extends to the Mediterranean and France with diminished amounts of TPW, below 10 mm. Finally, as in the October case, the most important contribution to TPW corresponds to that of moisture advected from the tropics and subtropics (Fig. 4.9d). A well-defined moisture plume or atmospheric river enters the Mediterranean through the Strait of Gibraltar, stretches along the east coast of Spain and reaches the south of France, leaving values well in excess of 20 mm of TPW in some of these areas.



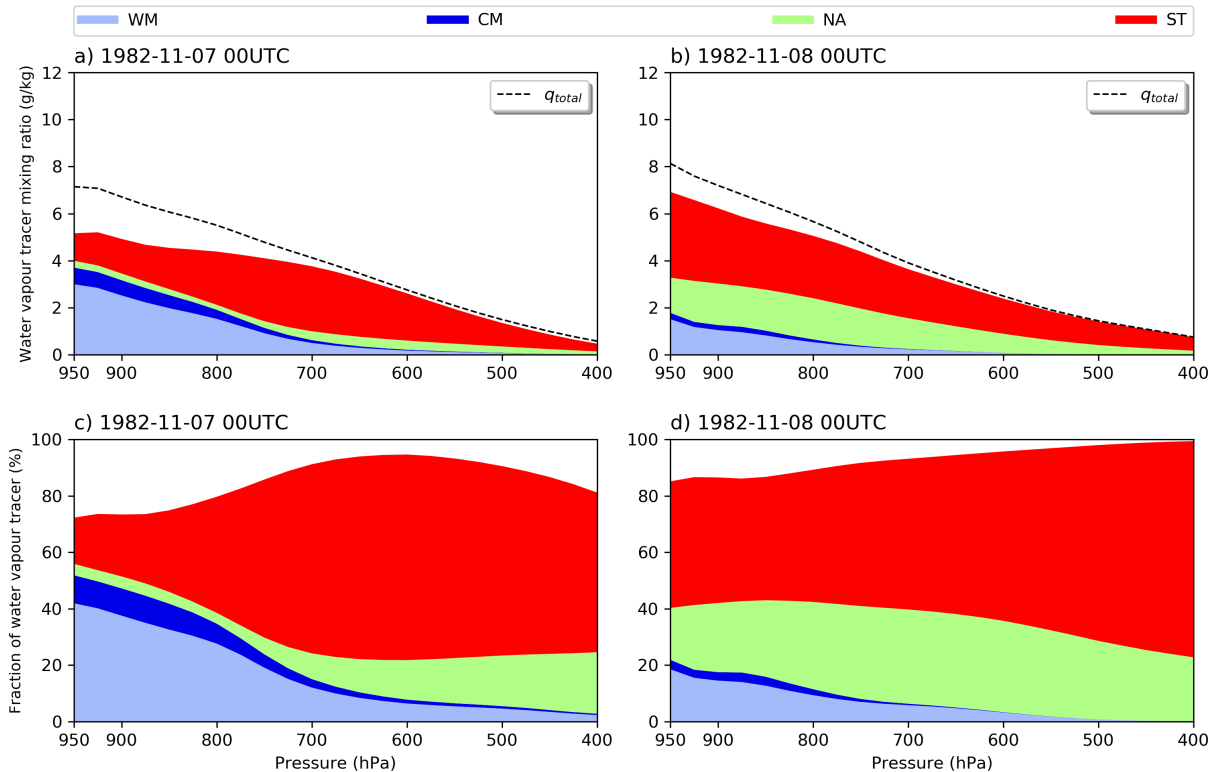


Figure 4.10: Similar to Fig. 4.5 but on November 7 (a, c) and 8 (b, d) at 00:00 UTC. The analysis is now over region 2 in Fig. 4.1b.

### 4.4.3 Precipitation origin

With regards to the origin of precipitation, Fig. 4.11 shows the share corresponding to each considered source. The largest contributions are clearly from North Atlantic (Fig. 4.11c) and tropical and subtropical moisture (Fig. 4.11d). North Atlantic water vapour is found in significant amounts in rainfall in all the affected areas, and it's by far the dominant source in the western half of the Iberian Peninsula, the most exposed to the west-southwesterly flow of the storm off shore. Precipitation of tropical and subtropical origin extends along the path of the atmospheric river discussed in the previous section, in a band stretching from the strait of Gibraltar all the way to the Alps, covering most of the eastern half of the Iberian Peninsula and southeast France. In all these regions, moisture from the North Atlantic is also a significant source, but tropical and subtropical water vapour is clearly the most important contribution. In the north-eastern tip of the Iberian Peninsula and southeast France there is a relevant additional input from western Mediterranean humidity (Fig. 4.11a), and in the French Massif Central, even modest precipitation amounts from central Mediterranean evaporation (Fig. 4.11b). These areas where all major source contributions overlap are precisely the most impacted by the event and where the highest rainfall accumulations were recorded.

Table 4.2 shows the area averaged relative contribution of each source over northeast Spain and southeast France (region number 2, outlined in red in Fig. 4.1b, the same used for the vertical distribution of moisture analysis in Fig. 4.11). In this region, which includes the Pyrenees and the French Massif Central mountains where the most intense downpours occurred, tropical and subtropical sources are clearly dominant, with a contribution surpassing 50%. Western Mediterranean and North Atlantic moisture play an intermediate role, contributing

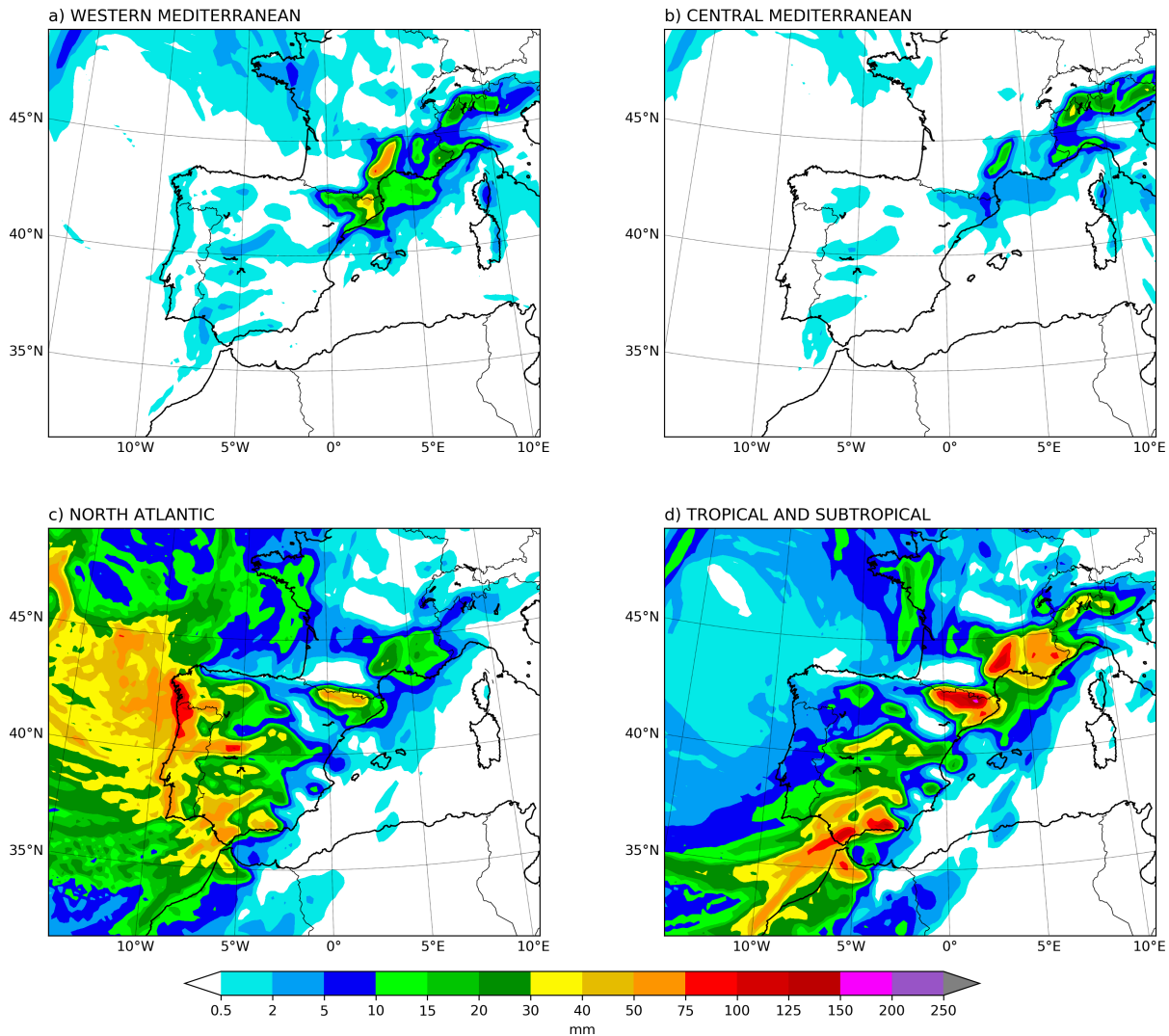


Figure 4.11: Similar to Fig. 4.6 but from 06th of November at 06:00 UTC to 09th of November at 06:00 UTC.

each between 15 and 20%. Of the latter two sources, North Atlantic water vapour is more relevant in the Pyrenees whereas that of the western Mediterranean is so in the Massif Central. The input of the central Mediterranean is on average negligible, of only around 3%. These results indicate that in the most affected areas, the contribution to precipitation from remote sources (about 70%) is much more important than that from local sources (less than 20%). The residual amount (11.8%) is, as in the October event, a sum of small contributions from other various sources. We note, however, that although the share of western Mediterranean moisture is somewhat modest, its relevance is particularly noteworthy; Fig. 4.11 suggests that without a contribution from the Mediterranean, rainfall accumulations in northeast Spain and southeast France would be comparable to those in many other regions of the Iberian Peninsula, and it is likely that the damage caused would have been much less.



Table 4.2: Same as Table 4.1 but from November 6 at 06:00 UTC to November 9 at 06:00 UTC and over region 2 in Fig. 4.1b.

Western Mediterranean	Central Mediterranean	North Atlantic	Tropics/Subtropics
15,60	2,96	18,20	51,39

## 4.5 Summary and conclusions

Torrential rain episodes causing flooding are recurrent features of climate on the shores of the western Mediterranean. The meteorological drivers for such events can be quite different and nevertheless result in similar outcomes, with catastrophic consequences in terms of damages. We investigate here this type of episodes on the basis of a common hypothesis; for the most extreme events occur, one of the necessary ingredients is a large amount of precipitable water, which is to a great extent advected from remote regions.

We selected two infamous western Mediterranean high precipitation events occurred during the same season, autumn of 1982 (October and November). Both evolved from very different synoptic situations. The case of October was more thermally driven, with the presence of cold air aloft associated with an upper level cut-off low, and deep convection developing and organizing in the form of a mesoscale convective system. In contrast, the November case was more dynamically forced, since it unfolded in the prefrontal and frontal zone of a strong Atlantic baroclinic storm. In this event, orography played a very relevant role, by enhancing the ascent producing precipitation and, in some mountain ranges such as the Pyrenees, also by triggering deep convection. The configurations of the selected cases represent two of the most frequently found during these episodes.

To assess the relevance of locally generated and remote precipitable water, we analyzed four potential moisture sources: evaporation in the western or central Mediterranean, evaporation in the North Atlantic and advection from the tropics and subtropics. Mediterranean sources were regarded as local while tropical, subtropical and Atlantic sources were considered as remote sources. Simulations were carried out with the WRF atmospheric model coupled with a moisture tagging technique, the so-called WRF-WVTs tool. Lateral boundary forcing came from ERA-Interim reanalysis and a single domain at 20 km resolution was used for calculations. In addition to estimating the contribution of the different sources to the large rainfall accumulations recorded during the episodes, we analyzed the vertical distribution of moisture transport toward the affected areas, in order to obtain a three dimensional diagnosis of the involvement of water vapour from each source in the dynamics of the events. As a result of our findings, we state the following conclusions.

- In both episodes, the largest moisture contribution to the torrential rains was from tropical and subtropical sources. In the case of November, more than half of the rainfall recorded in the most affected area came from this origin, while in the case of October its predominance was somewhat less pronounced, representing around 31% of the total rainfall.
- In the October event, evaporated moisture in the western and central Mediterranean, i.e. local moisture, played a very important role, with these sources contributing nearly

20% of total precipitation each. Evaporated moisture in the North Atlantic was also a significant contributor, accounting for around 15% of total precipitation, although it was the least important of the four sources.

- In the November event, the North Atlantic and the western Mediterranean acted as secondary sources, while the contribution of the central Mediterranean was almost negligible. Even so, the Mediterranean's contribution is particularly noteworthy: many regions in the Iberian Peninsula received large amounts of rain, coming from Atlantic and tropical and subtropical moisture sources; however, the extra input from the Mediterranean in northeast Spain and southeast France caused the rainfall in these areas to be even higher, so they ultimately were the most damaged areas.
- As for the distinction between remote and local sources, in the October event the contribution of both was similar whereas in the November case the largest share was clearly from remote sources.
- Moisture transport at medium and high levels played a key role in producing the observed large amounts of rainfall. Most water vapour at these layers resulted from long distance advection from the tropics and subtropics, which, as mentioned above, was the main source for the extreme precipitation. There were also high mixing ratios from this remote origin at lower layers, but the maximum values were at medium levels of the atmosphere.
- In the lower layers of the atmosphere, moisture was generally mostly from local evaporative sources in the western and central Mediterranean, while water vapour from evaporation in the North Atlantic was distributed at different levels.
- In both cases, moisture from the tropics and subtropics was transported through very defined moisture plumes or atmospheric rivers.
- The combination of high water vapour content at low levels from local sources and at middle and upper levels from remote sources yielded very large values of total precipitable vapour in the column in both events, but more so in the October case.

Our results suggest that the role played by remote sources is fundamental in producing the extraordinary rain accumulations observed in this type of extreme events and that the contribution of local Mediterranean sources is not sufficient to reach such high values. However, to corroborate this fact, it is necessary to study many other events in order to obtain more robust conclusions. Therefore, the case studies presented here represent only a first step in the application of the water vapour tracer method to Mediterranean precipitation extremes.

# Chapter 5

## Climatology of moisture sources in western Mediterranean extreme precipitation events

\* The results from this chapter will be published soon as D. Insua-Costa<sup>1</sup>, M. Senande-Rivera<sup>1</sup>, G. Miguez-Macho<sup>1</sup>, and C. Llasat<sup>2</sup>, “A global perspective on western Mediterranean precipitation extremes”, Accepted at NPJ Climate and Atmospheric Science, 2021.

<sup>1</sup> CRETUS, Non-linear Physics Group, Universidade de Santiago de Compostela, Galicia, Spain

<sup>2</sup> Departament of Applied Physics, Universitat de Barcelona, Barcelona, Spain

### 5.1 Introduction

In this chapter we extend our analysis to a larger number of EPEs with the aim of definitively clarifying the origin of the humidity fuelling frequent torrential rains in the Mediterranean. As in Chapter 4, we use a moisture tagging tool coupled to an atmospheric model, a technique that has been considered as representative of “ground truth” due to its high accuracy compared with other moisture tracking methods [75, 74]. The results shown here would not have been achieved without the previous work presented in Chapters 2, 3 and 4. Therefore, this chapter brings together all the efforts made to meet the main objectives set out in this thesis.

One of the main novelties of the results presented below is that we simulate a very large number of EPEs (160). In addition, based on our previous experience (Chapter 4), we have designed a new model configuration, with a domain of study which covers almost the entire Northern Hemisphere in order to assess the influence of possible tropical-extratropical interactions and, in general, potential connections with very distant regions. All of which allows us to draw more robust and general conclusions than in previous studies [27, 28, 29, 30, 31, 32, 33, 34, 3], which have generally used qualitative moisture tracking tools and focused on a smaller number of cases and a smaller study region.

Our results could be of particular interest in the context of climate change, as knowledge of the origin of the moisture that feeds EPEs has been identified as crucial for attributing them



to global warming [177, 178]. Specifically, the search for the moisture sources is essential to evaluate whether anomalously high evaporation somewhere, as for example in response to warmer sea surface temperatures, may be enhancing precipitation in them.

The chapter is structured as follows: Section 5.2 describes the methods, where we explain the novelties of the model configuration. Section 5.3 shows the results for the 160 EPEs studied and Section 5.4 contains a summary and conclusions of the work.

## 5.2 Methods

### 5.2.1 Extreme precipitation events studied

The 160 analysed events were extracted from the database of daily EPEs presented in Chapter 3 and published in a previous article [1]. The events were selected according to their magnitude, which means that the 160 studied EPEs are the strongest registered in the Mediterranean areas of Spain, Andorra, France and Italy in the period 1980-2015.

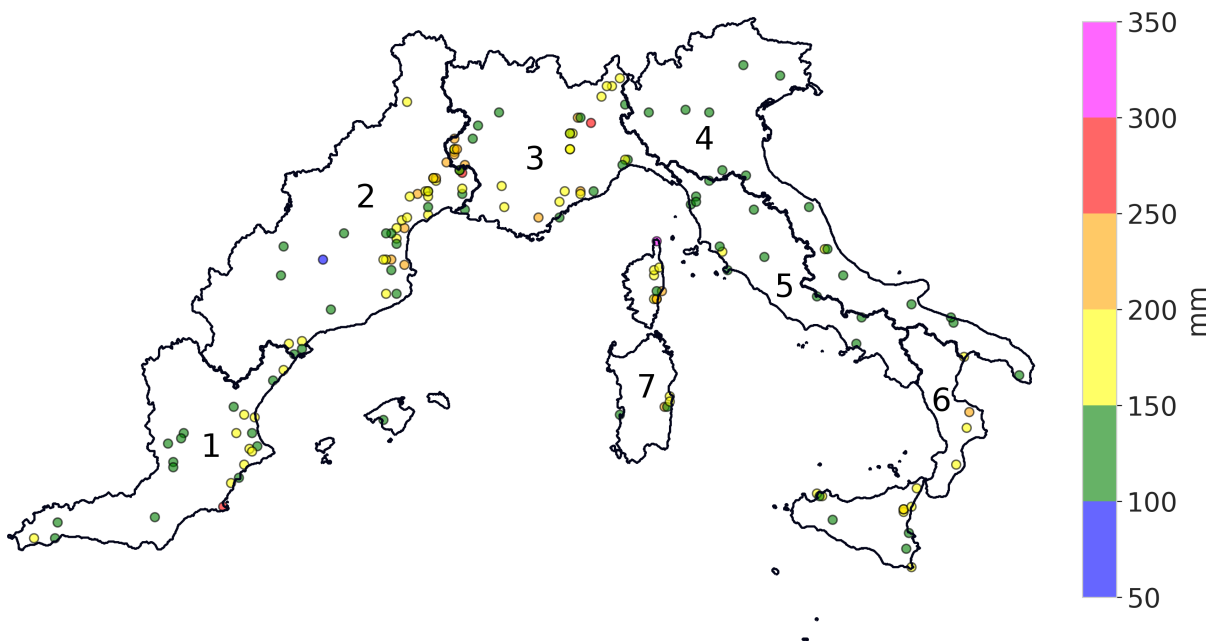


Figure 5.1: Maximum precipitation in the events analysed. The numbers indicate the different subregions into which the study region has been divided.

The study area (Fig. 5.1) encompasses the western Mediterranean European sector and has been divided into 7 subregions, as shown in Section 1.3. Each point in Fig. 5.1 shows the location and value of maximum precipitation in each of the cases studied. Precipitation data are from the MESCAN [53] gridded precipitation dataset.

### 5.2.2 Moisture source configuration

To calculate the precipitation fractions from each analysed source we make use of subdivision of the Mediterranean region shown in Fig. 5.1. For the calculation of the fractions in a given EPE, only those subregions affected by the event were considered, i.e., those where

the established precipitation threshold was exceeded. For example, if an event affects region 1 and 3, the precipitation fractions ( $PF$ ) would be calculated as:

$$PF^k = \frac{\sum_{i,j \in R1} TP_{i,j}^k + \sum_{i,j \in R3} TP_{i,j}^k}{\sum_{i,j \in R1} P_{i,j}^k + \sum_{i,j \in R3} P_{i,j}^k} \quad (5.1)$$

Where  $P_{i,j}$  is the total amount of precipitation accumulated at a given grid point  $(i, j)$ ,  $TP_{i,j}^k$  is precipitation coming from the “ $k$ ” moisture source, and  $i, j \in R1$  refers to the model grid points in region 1 and  $i, j \in R3$  the model grid points in region 3. The precipitable water and water vapour fractions are calculated in the same way as the precipitation fractions.

In Eq. 5.1 “ $k$ ” ranges from 1 to 12, since 12 different sources were analysed, which are shown in Fig. 5.2 along with the semi-hemispheric domain employed by the atmospheric model enabled for moisture tracking. The choice of sources was based primarily on the fact that we were interested in distinguishing between: (1) local and remote, (2) tropical and non-tropical, (3) marine and continental. The sources in the interior of the domain are all of type 2D, i.e., they are used to track the evaporated moisture on them. However, the two sources at the northern and southern end of the domain (AR and SH in Fig. 5.2) are of type 3D. This type of source is used to track all the moisture contained in them at any vertical level. In our case, these two 3D sources were selected to track all moisture entering from the northern and southern edge of the domain, i.e., that coming from the Arctic region or the Southern Hemisphere. Thus, this source configuration takes into account all possible moisture sources.

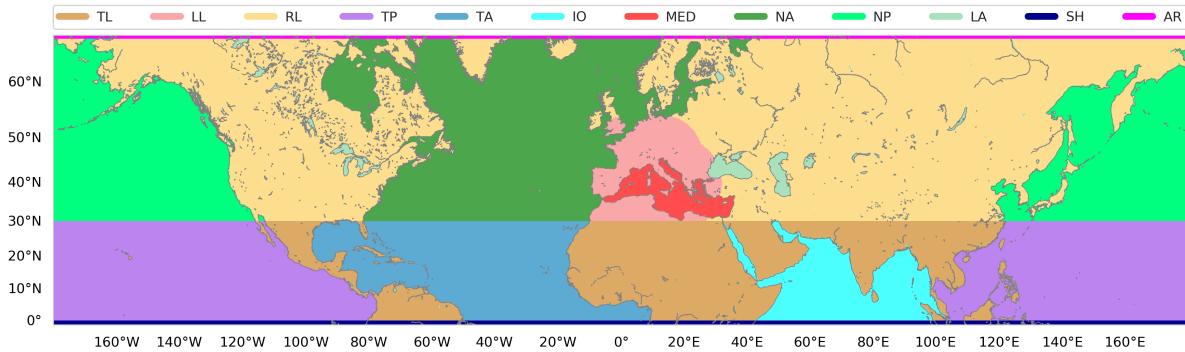


Figure 5.2: Simulation domain and the 12 moisture sources analysed, which are represented with different colours: Tropical Land (TL), Local Land (LL), Remote Land (RL), Tropical Pacific (TP), Tropical Atlantic (TA), Indian Ocean (IO), Mediterranean (MED), North Atlantic (NA), North Pacific (NP), Lakes and Inland Seas (LA), Southern Hemisphere (SH) and Arctic (AR).

### 5.2.3 Simulation set-up

For each of the 160 analysed events, a total of 12 simulations of 31 day duration were performed, one for each studied moisture source. Therefore, the total number of simulations was 1920, approximately equivalent to a period of 160 years, which involved a high computational cost (about 2 million core-hours). As in the previous chapter, we use the WRF-WVTs tool for moisture tracking [2]. The WRF atmospheric model was configured with a horizontal resolution of 20 km and a total of 39 vertical levels. The simulation domain (Fig. 5.2) had 1416 by

362 grid points, in the east-west and north-south directions, respectively. Since the simulation domain forms a longitudinal belt, periodic boundary conditions were used at the east and west boundaries. Initial and boundary conditions for the northern and southern boundaries were taken from ERA5 reanalysis [42] and updated every 6 hours. The simulations were initialized 30 days prior to the extreme precipitation day under consideration in order to allow sufficient time for moisture to evaporate. If the simulations had been started at a time closer to the event, much of the involved moisture would have already been present at initial time and would not have been tagged by the moisture tracking tool. Importantly, a spectral nudging technique [153] was employed to prevent the simulation from deviating substantially from the large-scale reanalysis fields, which allowed the model to provide realistic results even 30 days after the start of the simulation. Finally, the main parameterizations used were: YSU for the boundary layer [140], WSM6 for microphysics [141] and Kain-Fritsch for convection [142]. These parameterizations were selected since they are currently the only ones compatible with the moisture tracking tool. For a validation of the model results, please see Fig. 5.11 in the Appendix to this chapter.

## 5.2.4 ENSO correlations

We performed a correlation analysis between precipitation fractions from the Atlantic Ocean and Pacific Ocean and the El Niño 3.4 index [179]. The objective was to check whether in EPEs occurred during the positive ENSO phase, moisture contributions from the Atlantic or the Pacific are higher. For this purpose, Pearson correlation coefficients, which measure the linear relationship between precipitation fractions and the El Niño 3.4 index, were calculated. The statistical significance of this linear relationship is computed from a two-tailed t-test.

## 5.3 Results

### 5.3.1 Moisture always comes from multiple sources

The precipitation fractions coming from each source are shown in Fig. 5.3, from highest to lowest contribution from left to right. The Mediterranean Sea (red) is the main moisture source with an average input to precipitation of almost 35%. Although variability is high and its maximum contribution is 70%, it is rarely dominant (greater than 50%). The North Atlantic (dark green) is the second most important source, with an average and maximum percentages of 25% and 70%, respectively. Moisture from local recycling, i.e. moisture evapotranspired over land areas near the study region (light red), has an average contribution of 10.2% with higher values in warmer months (see Section 5.3.2), occasionally exceeding 40%. The fourth most important contribution is from a very distant source, the tropical Atlantic, with almost 10% and a maximum above 35%.

Combining the contributions of these four sources, we obtain a precipitation fraction of less than 80%. The remaining 20% share comes from a string of small contributions from different sources, which together play a fundamental role in intensifying rainfall. In fact, although their average individual contributions are small, variability is high and in some cases these generally minor sources play a major role. In Fig. 5.4 we show the precipitation fractions for the 25 most extreme cases, representing the wide variety and great difference in contributions from one event to another. It has been previously pointed out [180] that a wide variety of sources can contribute to Mediterranean precipitation extremes; however, the precise source contribution

## Chapter 5. Climatology of moisture sources in western Mediterranean extreme precipitation events

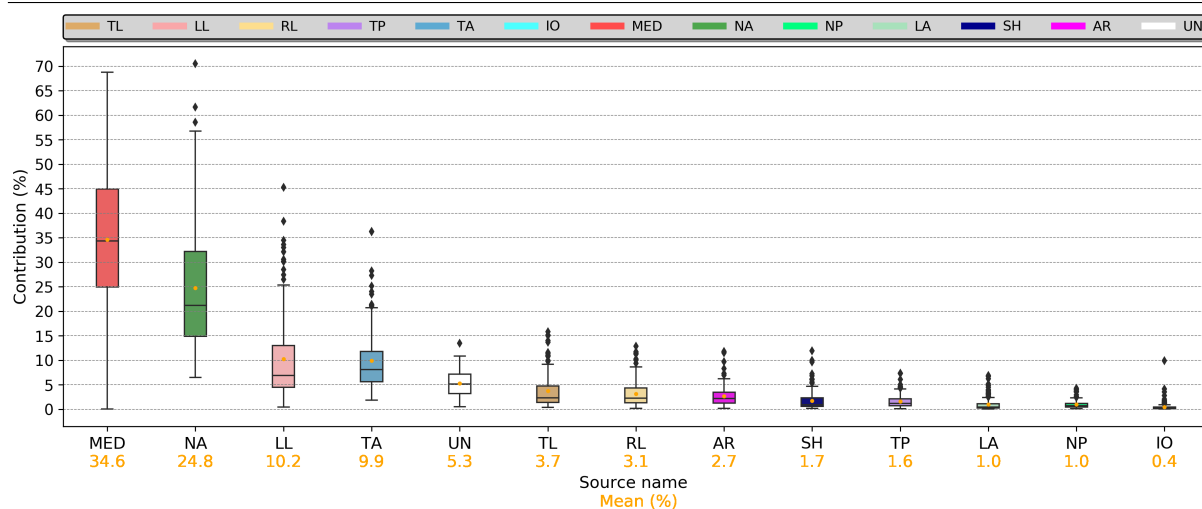


Figure 5.3: Box diagrams for the 160 simulated events according to the moisture source. The abbreviation UN refers to moisture of undefined origin. The orange dot on the diagrams and the orange number on the x-axis show the average contribution of each source for the 160 cases.

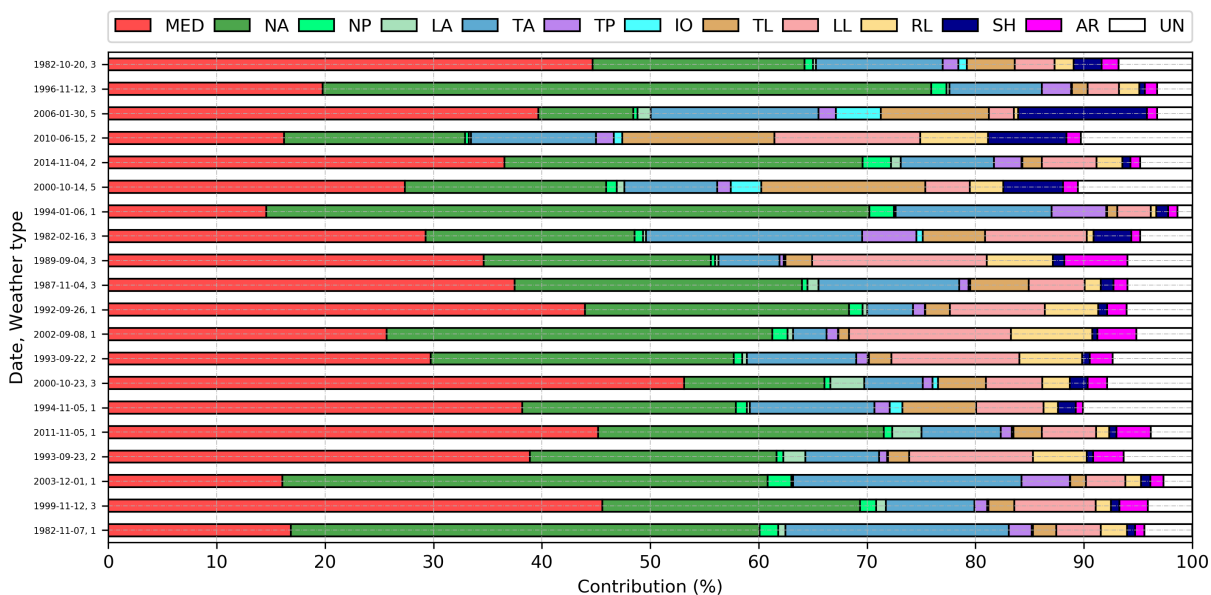


Figure 5.4: Precipitation fractions for the 25 EPEs with the highest magnitude coming from the different sources. The y-axis shows the day on which extreme precipitation occurred, as well as the weather type associated with the event. The magnitude decreases from bottom to top, so the first episode in the ranking is represented by the bar at the bottom of the figure (1982-11-07).

numbers has not been quantified until now. Only a small fraction of the total rainfall could not be assigned to any of the 12 sources (white in Fig. 5.3 and 5.4) because it corresponds to precipitation fed by old moisture, evaporated before the start of the simulations.

### 5.3.2 Intra-annual variability of moisture sources

The contribution of the different moisture sources varies widely throughout the year. Perhaps the clearest example is the evapotranspired humidity over the continents (sources TL, LL and RL in Fig. 5.2), which has an annual average of 17%, but in the warmer months (May, June, July and August) is around 40%, as shown in Fig. 5.5. Therefore, for much of the year, this is the source that contributes the most to extreme rainfall events in the Mediterranean Region. However, during the warm season, EPEs are usually minor cases associated with local afternoon convection. In autumn, when the contrast between Mediterranean Sea surface temperatures and air temperatures is highest, EPEs affect a larger area and are more organised and persistent. This is the reason why most of the studied cases, which correspond to the highest magnitude episodes within the period 1980-2015, are located in fall months. Specifically, of the 160 analysed events, 113 (71%) are concentrated in September, October and November. During these months, contributions from the Mediterranean and the Atlantic are much greater than land evapotranspiration. In September, the land still has a remarkable contribution (about 20%), but as winter approaches, this input decreases to values of 10% or less. The Mediterranean has a contribution generally below 30%, but precisely in the months when most episodes are recorded, its contribution reaches values close to 40% on average. The Atlantic reaches maximum values in the cold months, so that at the beginning of the extreme rainy season (September) its contribution is still below 30%, but at the end of the season (November) it is already the predominant source.

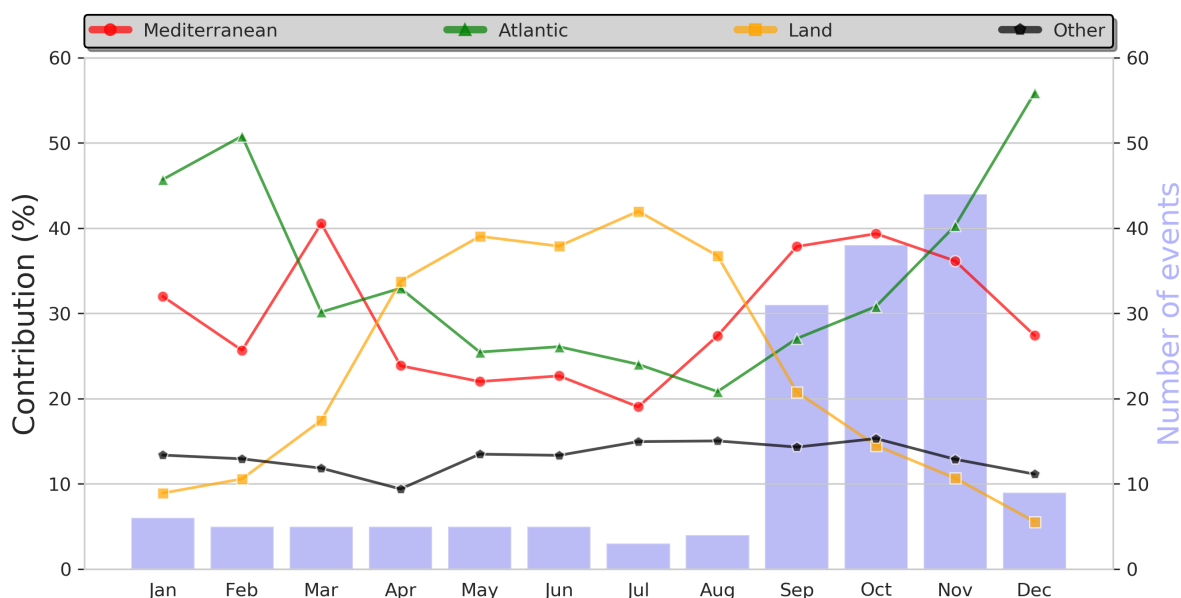


Figure 5.5: Monthly distribution of the 160 analyzed events (bars) and the mean precipitation fractions from the Mediterranean (red), Atlantic (green), land (orange) and other sources (black) for those events.

### 5.3.3 Remote contributions prevail in the most intense cases

We group all sources into two categories: local, which are those closest to the studied region, i.e. the Mediterranean Sea and surrounding continental lands (red and light red in

Fig. 5.2) and remote, encompassing the remaining 10 sources, which are farther away. In addition, we have classified the studied events according to their magnitude (Section 2.3.3). The aim is to clarify whether moisture from sources outside the Mediterranean are mainly responsible for the precipitation recorded in the most extreme cases.

Figure 5.6a shows that for the 160 studied cases, the average contribution of remote sources to precipitation is 10% higher than that of local sources. This difference is somewhat accentuated if we only consider the 25 most extreme cases, which were associated with major floods (Section 2.4.2). In these catastrophic cases, local sources contributed with slightly more than 40% and remote sources almost 60% of the moisture. Considering the main local source and the main remote source (Fig. 5.6b), i.e. the Mediterranean Sea and the Atlantic Ocean (combining NA and TA in Fig. 5.2), we can see that their average contribution for the total number of cases is practically the same (34.6 Mediterranean Sea vs. 34.7 Atlantic). However, in the most extreme cases the contribution of the Atlantic is marginally higher.

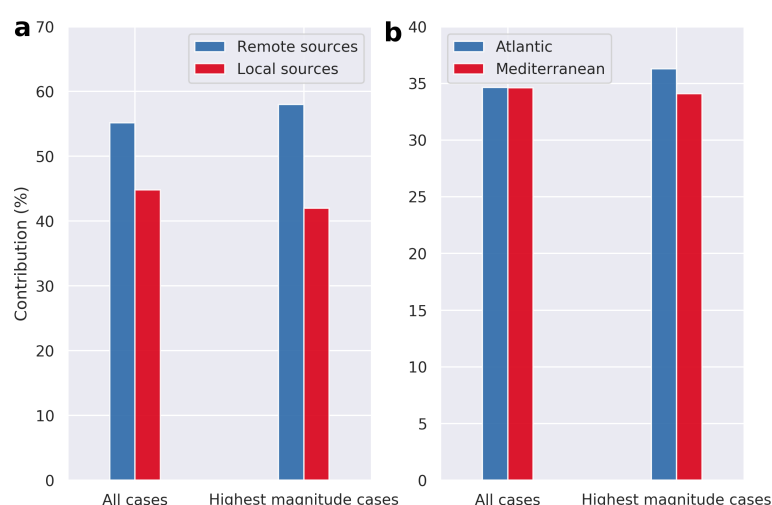


Figure 5.6: (a) Total contribution from remote sources (blue) versus local sources (red) averaged for all cases studied (left) and for the 25 highest magnitude cases (right). (b) Same comparison but for the Atlantic Ocean versus the Mediterranean Sea.

While Atlantic moisture advection maybe especially important for the most extraordinary EPEs in particular areas [32], we would like to emphasize that, commonly, the difference between the most extreme cases and the rest is small. Therefore, it would not be correct to interpret that in general, extraordinary cases are always dominated by remote sources and that weaker events are always dominated by local ones.

### 5.3.4 Moisture sources and weather types

According to the weather type classification of Chapter 2, of the 160 simulated events, 57 are type 1, 31 are type 2, 41 are type 3, and 26 are type 3. In addition, 5 events were classified as undefined weather type, as they presented a low correlation with any of the atmospheric patterns shown in Fig. 2.5. Fig. 5.7 shows the Mediterranean and Atlantic contributions for the cases of each type. Atmospheric configurations 1 and 2 are characterized by a higher moisture contribution from the Atlantic (40%) than from the Mediterranean (30%). Just the opposite is true for types 3 and 4, for which the contribution from the Mediterranean is higher.



Previous studies [30, 181] have suggested that local sources are dominant except in cases produced by purely cyclonic situations, in which the contribution of local and remote sources would be more balanced. They proposed a conceptual model in which contributions from the Mediterranean Sea could be between 40 and 60% depending on the atmospheric pattern driving the event. We find that the Mediterranean contribution is 30-40% (Fig. 5.7b) instead of 40-60%. Adding precipitation recycling over land, which was omitted in these previous studies, we obtain a local contribution of 40-50%, closer to, but still lower than, the proposed by these authors.

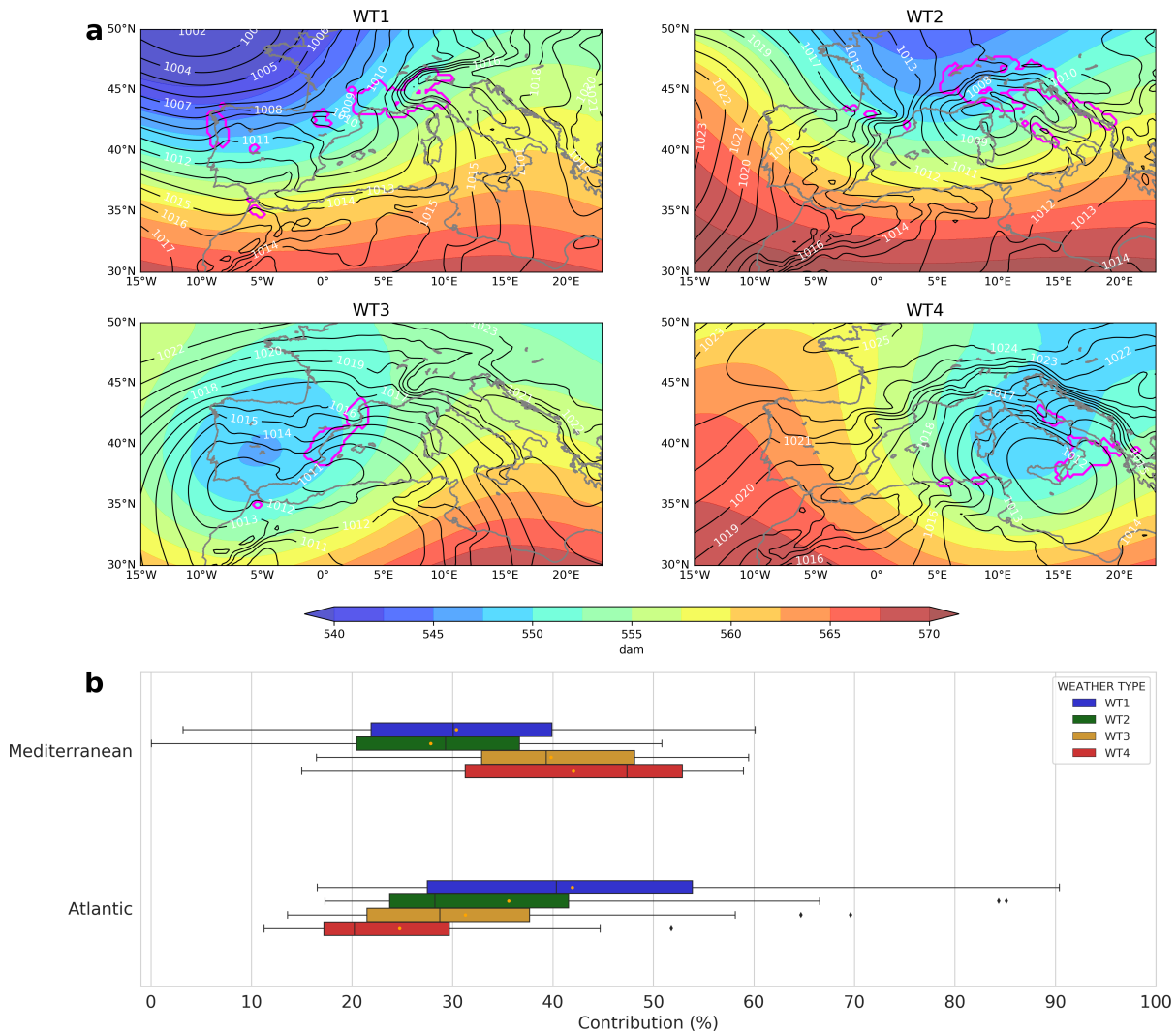


Figure 5.7: (a) Weather types (previously shown in Fig. 2.5). (b) Box diagrams showing the precipitation fractions from the Mediterranean and Atlantic sources for all cases associated with weather type 1 (blue), 2 (green), 3 (orange) and 4 (red).

In summary, our results show that the cases associated with the arrival of Atlantic cyclones from the west, both at low and high levels of the atmosphere, have a greater contribution from this oceanic basin, whereas Mediterranean lows, which usually favour south-easterly winds, have a greater Mediterranean contribution. However, although moisture contributions vary with weather type, neither the Mediterranean nor the Atlantic are predominant (contribution greater than 50%) on average for any of the atmospheric configurations that usually result



in catastrophic precipitation in the western Mediterranean. In particular our estimates of the contribution of the Mediterranean are lower than in previous studies [30, 181], even for the most favourable synoptic patterns.

### 5.3.5 High efficiency of Mediterranean water vapour

In terms of total precipitable water (TPW) contained in the atmospheric column during the events, the contribution of the Mediterranean Sea is lower than in terms of precipitation. Specifically, the fraction of TPW with Mediterranean origin is 27.4% on average, about 7% less than in precipitation (Fig. 5.8a). For the Atlantic Ocean the opposite is true, its contribution is higher in terms of TPW (39.4%) than in terms of precipitation (34.7%). This shows that Mediterranean water vapour is more efficiently rained than water vapour from remote regions.

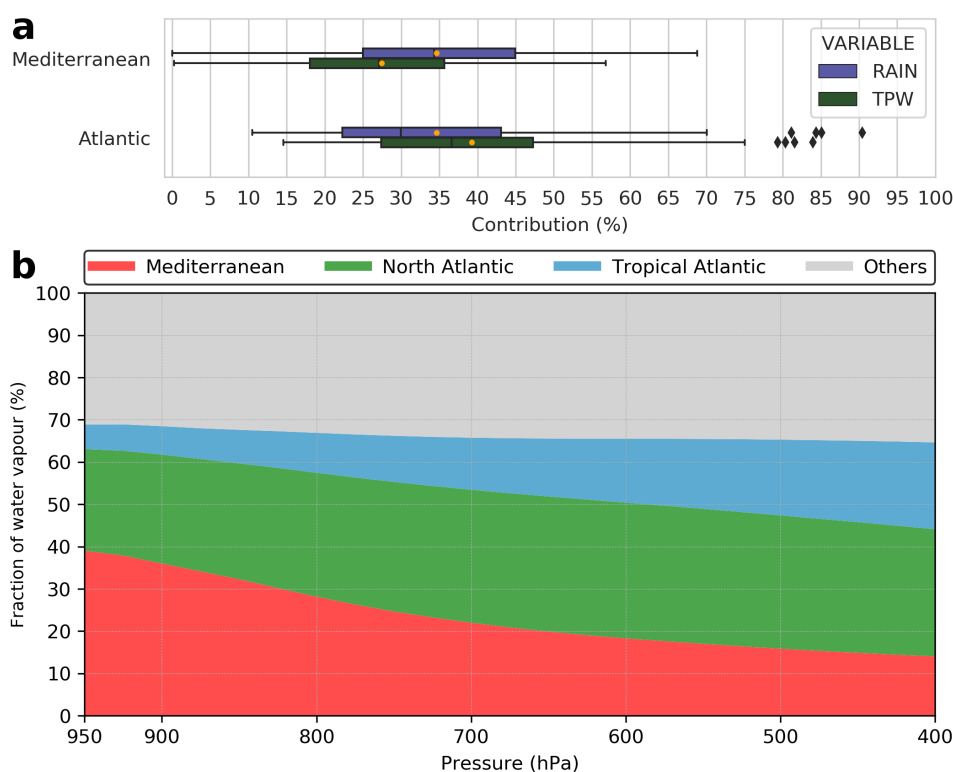


Figure 5.8: (a) Comparison between the Mediterranean and Atlantic contributions to the 160 studied events in terms of rainfall (blue) and total precipitable water (TPW, green). (b) Cumulative plot showing the vertical distribution (in pressure levels) of water vapour fractions from the different sources.

The underlying reason lies in the vertical distribution of humidity from the different sources, which violates the well-mixed assumption. This hypothesis, which is implicitly included in many of the numerical models for the study of moisture origin [63, 64, 76, 72, 38], proposes that water vapour is perfectly mixed vertically, so that the fraction of vapour from any moisture source would be independent of height. Our results demonstrate that this assumption does not hold. Figure 5.8b shows that, for the average of the 160 studied cases, the fraction of water vapour from the Mediterranean is much higher at low levels (30-40%) than at high levels (15-20%). Since high specific humidity values at low levels are essential to establish a highly

potentially unstable environment, we conclude that Mediterranean moisture plays a particularly remarkable role in terms of convective available potential energy. On the contrary, the vapour fraction of Atlantic origin is more important aloft, especially for water vapour coming from the more distant tropical Atlantic. Thus, in the strong convection occurring in these episodes, the total condensate has a higher contribution of low level converging moisture than of entraining water vapour in the updraft at mid and upper levels.

### 5.3.6 Tropical-extratropical interactions

Some authors have proposed that tropical moisture exports [182] could be a precursor of flooding in the Mediterranean Region [33, 34, 183]. The argument is that some extratropical low-pressure systems can descend sufficiently in latitude so as to capture fairly moist air masses from the intertropical convergence zone and advect them into the mid-latitudes via tropical plumes or atmospheric rivers [184, 185, 40], increasing the water vapour content in the atmospheric column in those locations and thus the probability of excessive rainfall. Eastward moving tropical cyclones or their extratropical remnants may also play a key role in some cases, by injecting large amounts of tropical moisture into the Mediterranean basin [27, 186]. However, the extent of the influence of these tropical-extratropical interactions on Mediterranean precipitation extremes remains unclear.

We show that the average percentage of precipitation fed by tropical moisture is 17.3% (summing TA, TP, TL, IO and SH in Fig. 5.3), with maximum values above 40%. Although most of it (9.9%) corresponds to tropical Atlantic moisture, in some cases this input can come from much more distant regions. As an example, Fig. 5.9a shows the precipitable water amount originating in the tropical Pacific region for an extraordinary EPE that affected Catalonia (Spain) in February 1982. More than 5% (see Fig. 5.4) of the total precipitation can be traced to a moisture plume from that remote tropical Pacific provenance that managed to cross the entire Atlantic. In total, the tropical contribution in this case amounted to 34.7%.

Previous studies emphasize the importance of African tropical moisture in some EPEs [28, 30, 34, 181, 183, 184, 185, 40]. We find that, although its contribution can indeed reach significant values in some cases (up to 15%, Fig. 5.3), there could be a misunderstanding in this respect. This is because much of the moisture advected from the interior of the African continent does not actually originate in that area. Figures 5.9a,b and c, which correspond to the catastrophic flooding episode of Var (France) in June 2010, illustrate this fact adequately. More than 30% of the rainfall was fed by an African tropical plume (see Fig. 5.4). However, the moisture evapotranspired over tropical land (Fig. 5.9b) explains only 14% of the total rainfall. This means that African tropical plumes also transport moisture from other sources, such as are in this Var case, moisture originating in the Southern Hemisphere (7.23%, Fig. 5.9c) or in the tropical Atlantic (11.54%, Fig. 5.9d). Southern Hemisphere moisture would come mostly from the tropical South Atlantic, with minor contributions from South America and Southern Africa.

If we add moisture coming from other extremely distant sources (RL, AR and NP in Fig. 5.2) to the tropical moisture, we find that on average 24.1% of the total extreme precipitation in the Mediterranean Region is due to moisture transport on scales of several thousand kilometres. This percentage could potentially reach 30% if we consider that the moisture of undefined origin (5.3%, Fig. 5.3) has a residence time of more than 30 days and, therefore, had probably travelled long distances.

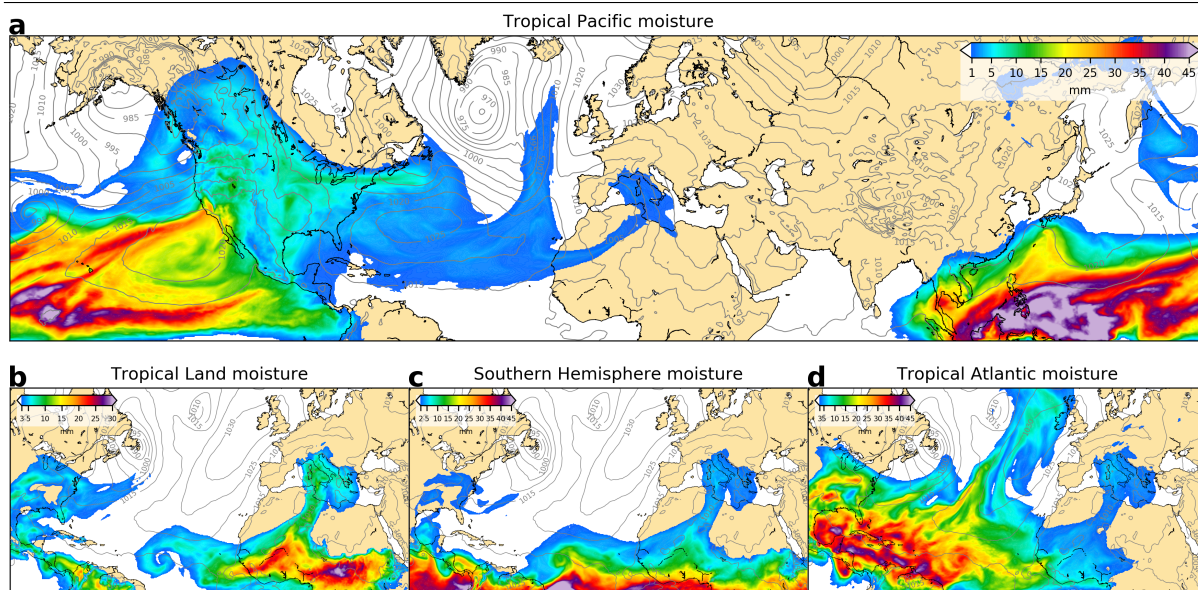


Figure 5.9: Sea level pressure and total precipitable water from evaporation over the tropical Pacific during the February 1982 Catalonia (Spain) extreme precipitation event (a). The same fields but referring to moisture from the tropical land (b), the Southern Hemisphere (c) and the tropical Atlantic (d) during the catastrophic Var (France) flood event in June 2010. Fields are shown at 12 UTC on February 16, 1982 (a) and June 15, 2010 (b,c and d).

### 5.3.7 Correlation between moisture contributions and ENSO

Some authors propose indirect connections between extreme Mediterranean rainfall and climatic anomalies in remote regions, i.e., teleconnections. For example, a positive correlation with El Niño-Southern Oscillation (ENSO) has been claimed [187, 188, 189]. The process that would link both events would be an anomalous atmospheric circulation pattern in the Atlantic Ocean that would appear during El Niño years favouring moisture transport from this basin into the Mediterranean [187, 188].

In order to verify this hypothesis, precipitation fractions from the Atlantic (TA plus NA) and Pacific (TP plus NP) were correlated with the El Niño 3.4 index. The results can be seen in Fig. 5.10 and show that there is no significant correlation ( $p\text{-value} > 0.05$ ) for either the Atlantic or the Pacific. The low correlation between the two variables suggests that EPEs in the western Mediterranean are not favoured by extra moisture input from the Atlantic or Pacific during El Niño years. The highest contributions from these basins appear indistinctly in years with positive, negative or neutral ENSO phase.

Rather, our results suggest a more direct connection between the Mediterranean and different parts of the planet. A connection that is direct in the sense that it simply reflects the extensive interrelations within Earth's general atmospheric circulation, whereby evaporation thousands of kilometres away ends up intensifying an EPE in the Mediterranean without the need for any organized anomalous dynamic pattern linking the two processes. This long-distance moisture supply implies energy redistributions of the same scale, which are very relevant for Earth's climate balance.

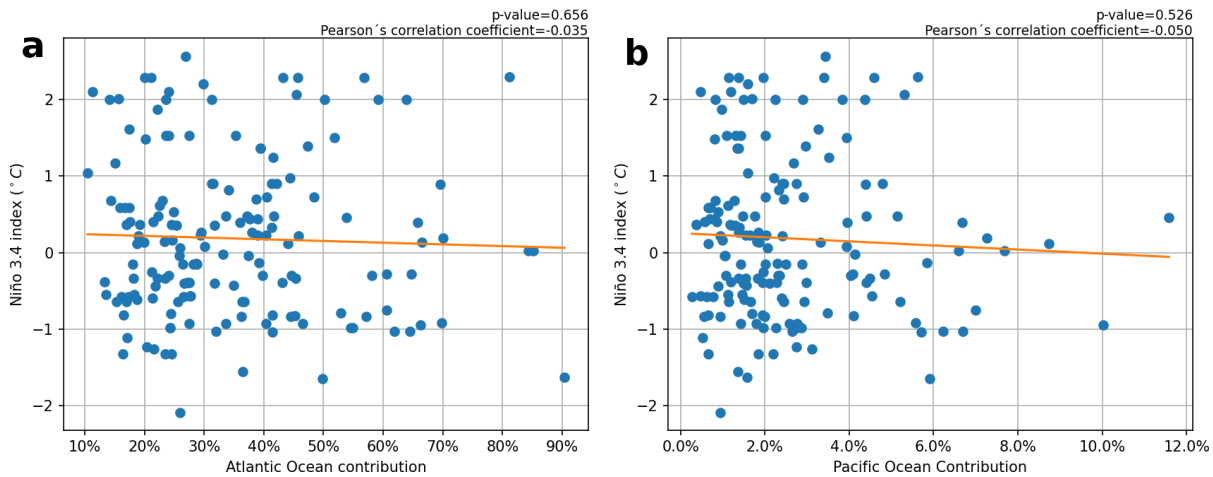


Figure 5.10: Linear relationship between the El Niño 3.4 index and the moisture contributions from the Atlantic (a) and Pacific (b). Each point corresponds to one of the 160 events analysed. The orange line comes from a least-squares linear regression. Correlation coefficients are shown in the upper right corner.

## 5.4 Summary and conclusions

The large precipitation amounts that are usually registered during individual events in the Mediterranean Region require high values of water vapour in the atmospheric column to occur. However, with only the moisture provided by the Mediterranean Sea, such high values would hardly be reached. Even adding local recycling and despite the high precipitation efficiency of the low-level Mediterranean humidity, it would generally not be sufficient to produce catastrophic rainfall amounts; thus, a contribution from remote sources is necessary. This contribution from afar is often, but not always, the main input for these events. Moisture transport from the tropics and, in general, from extremely distant sources, plays in many cases an essential role as precipitation enhancer. Our simulation results suggest that the key contribution of this long distant moisture transport may actually be the norm, not just for the Mediterranean, but elsewhere across the hemisphere as well. Therefore, when studying Mediterranean precipitation extremes, and perhaps extremes in general, in the context of climate change, a global perspective must be taken, considering that alterations in remote regions, for example, of sea surface temperature, can have a direct influence on these potentially catastrophic events.

## APPENDIX

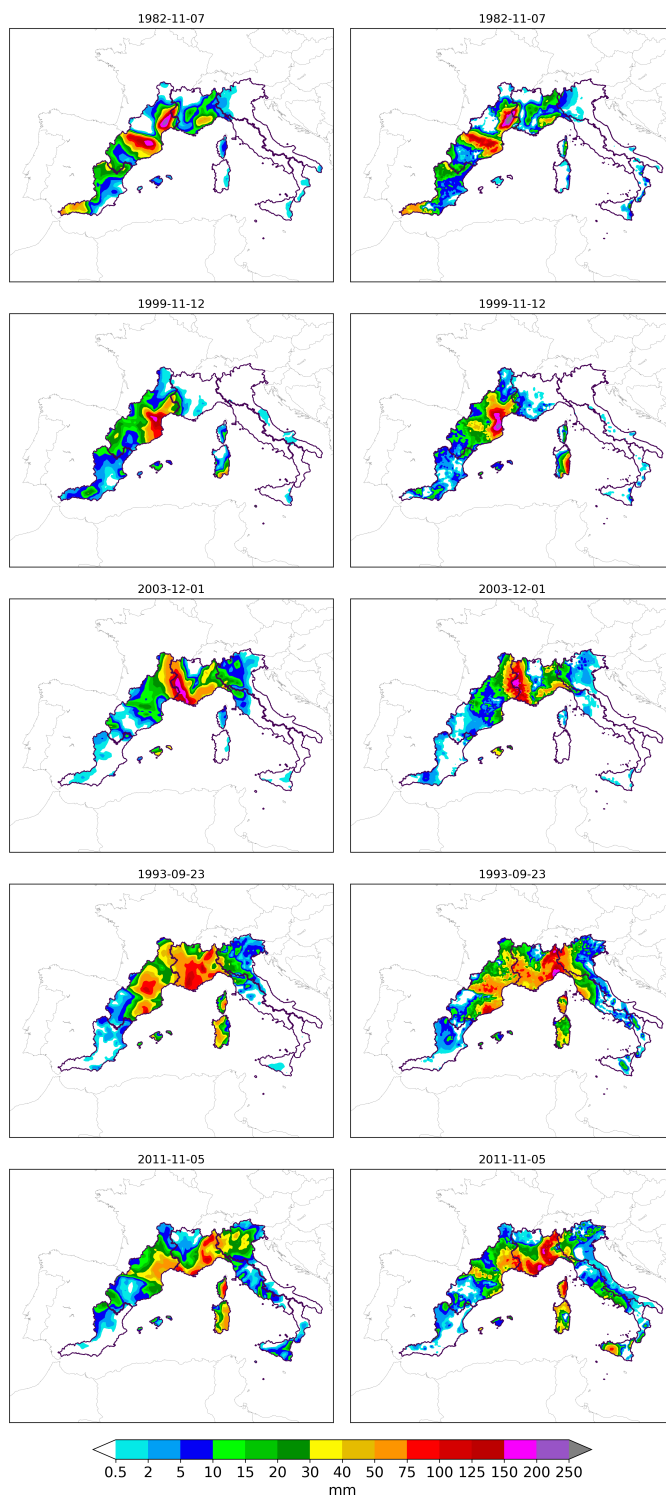


Figure 5.11: Simulated (left column) and observed (right column) precipitation for the 25 most extreme events analysed. Observed precipitation is from the MESCAN [53] precipitation analysis. This figure is continued on the following pages.



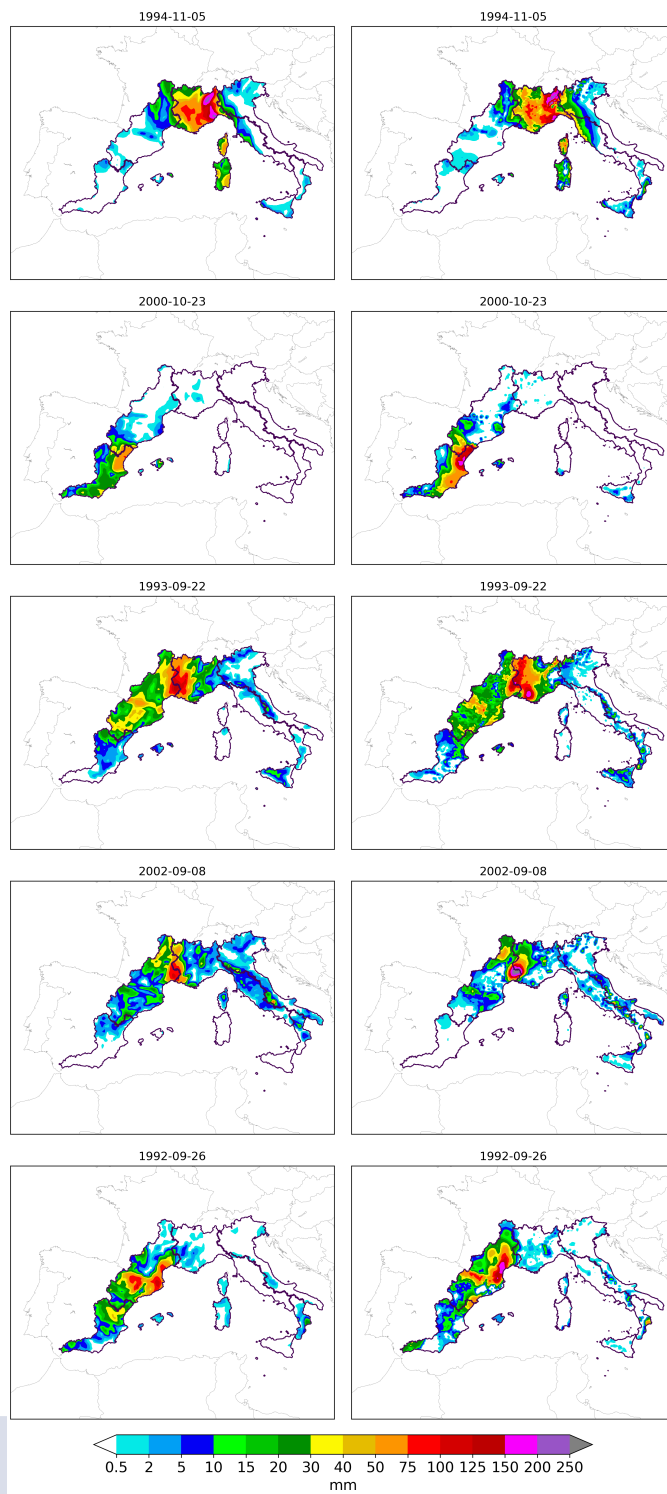


Figure 5.11: Continued.



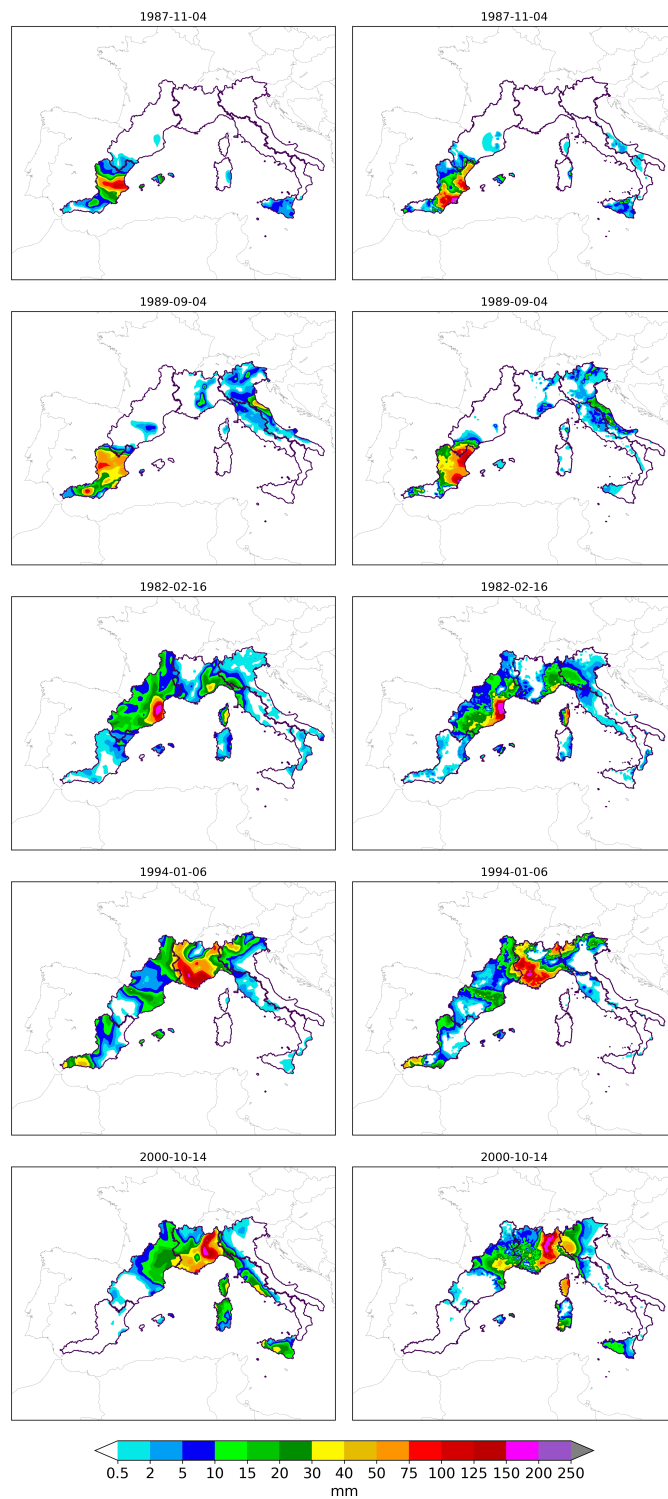


Figure 5.11: Continued.

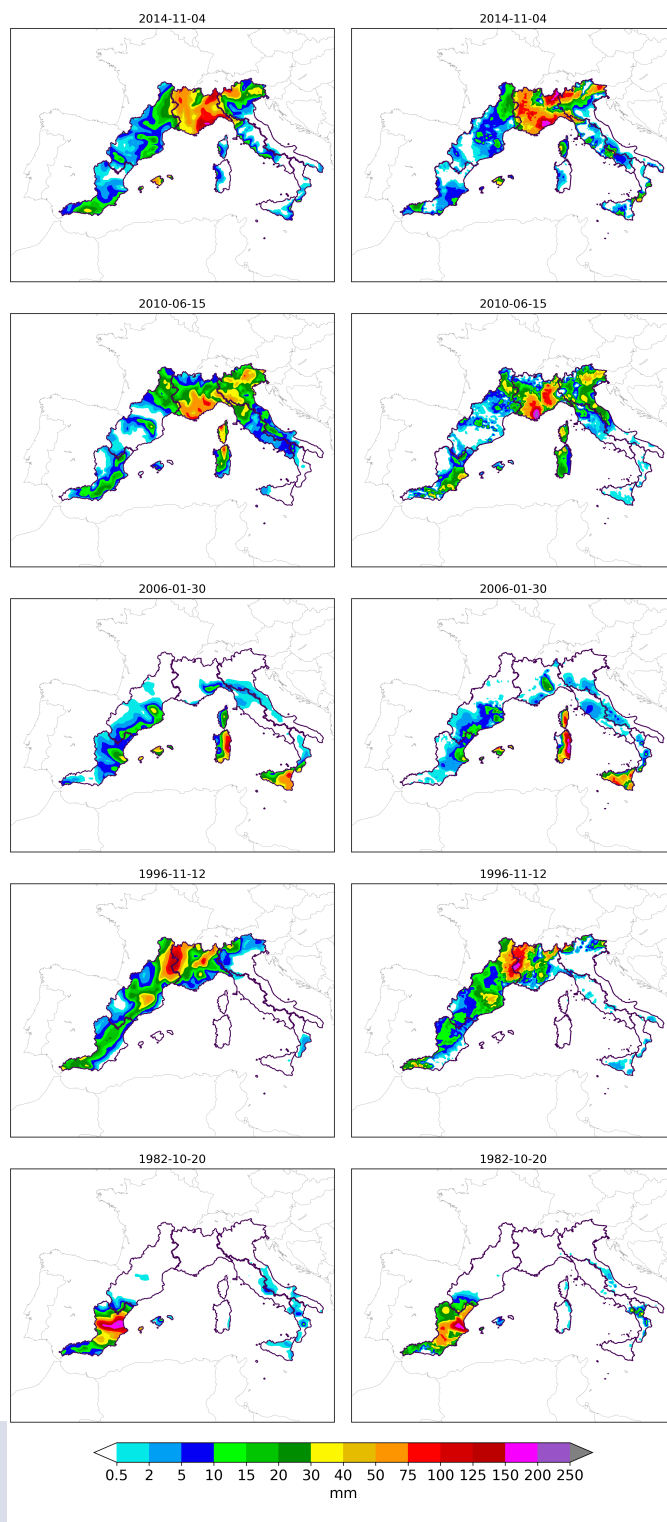


Figure 5.11: Continued.

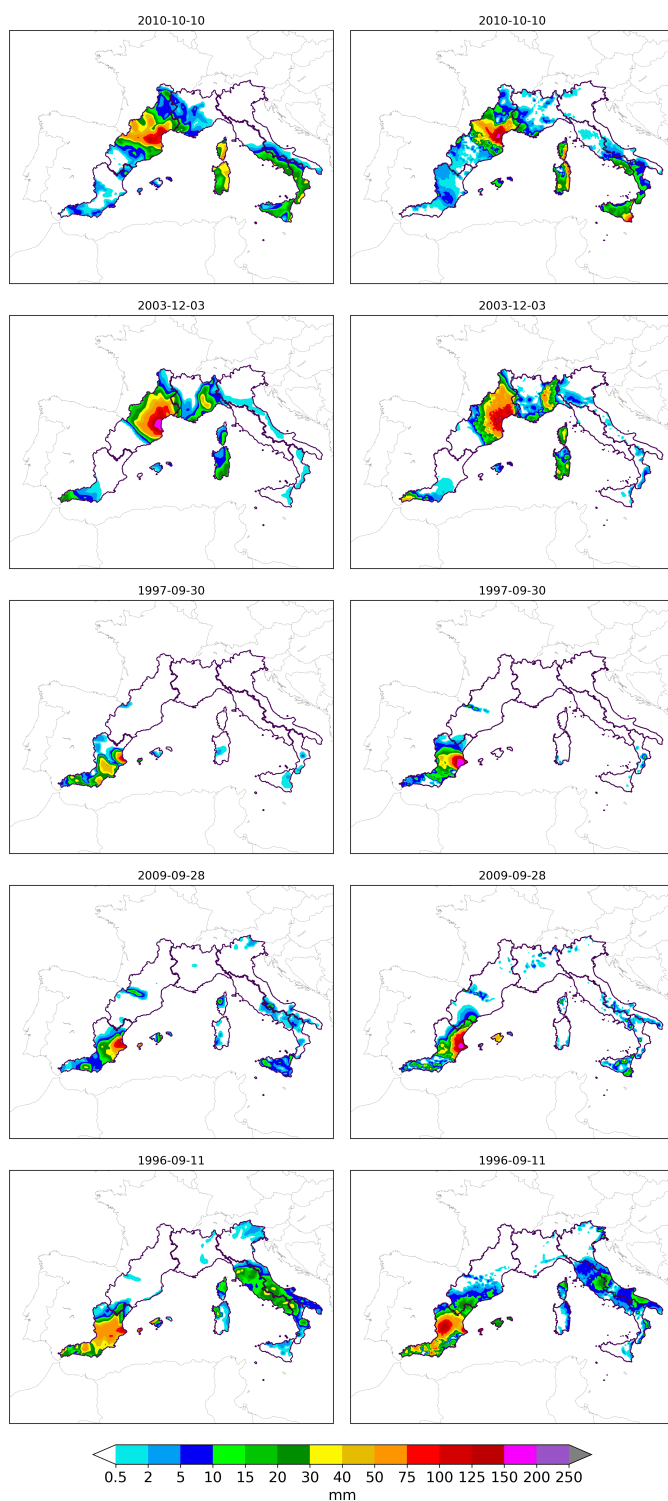


Figure 5.11: Continued.



# Chapter 6

## General Conclusions

This thesis can be subdivided into two parts, one corresponding to the preliminary work (Chapters 2, 3 and 4) and the other in which the main objective is addressed, i.e. to establish a clear model of the sources feeding western Mediterranean precipitation extremes (Chapter 5). The conclusions of the preliminary work (sub-objectives 1-4, Section 1.1.2) are presented in short paragraphs, while those related to the main objective (sub-objectives 5-12, Section 1.1.2) follow a question-and-answer format in order to summarise and avoid repetition of the previous chapters, which already have their own conclusions section.

### Preliminary work

- A total of 1991 daily extreme precipitation events were detected in the period 1980-2015 using an impact-related threshold and high-resolution gridded precipitation data.
- The events were ranked according to their magnitude, which would subsequently allow for the 160 most intense events to be selected for moisture source studies. The analysis of such a large number of cases represents one of the main novelties of this thesis and was a major computational challenge. It was also found that the most extreme events were largely conducive to flooding, underpinning the robustness of the ranking.
- The spatial and temporal distribution of the events was analysed. The results showed that most of the events are concentrated in south or east-facing coastal areas, especially those of the Valencian Community and the Languedoc-Roussillon region. In addition, we showed that more than 75% of the most extreme cases are concentrated in the autumn months (SON).
- Using the principal components analysis method, the events were grouped into weather types. We found that only 4 types can explain most of the episodes (77% variance explained). In particular, 42% of the most extreme cases were associated with a single weather type. This classification would later allow us to analyse the variability in the contribution of the different sources depending on the atmospheric pattern leading to the events.
- A moisture tracking technique, known as water vapour tracers and coupled to the WRF atmospheric model, was fine-tuned. After improvements in the tool code, a validation showed that it was highly accurate, with errors of less than 1%. This high accuracy was a

significant improvement over previous studies. Finally, the tool code was made available to other researchers.

- The tracking technique was first applied to a Great Lake-effect snowstorm, and then tested in the western Mediterranean for the two flood events of autumn 1982. The model was set up so that both local and remote sources could be studied and, based on this experience, the simulation domain was later extended to cover even more distant sources such as the Pacific Ocean. The results reinforced previous studies and our initial hypothesis, since a high contribution from distant sources was found; moisture from tropical and subtropical sources, transported via atmospheric rivers, accounted for 31% of the rainfall in one case and 51% in the other.

## Main objective

- **Is the Mediterranean Sea the main moisture source for extreme precipitation events in the western Mediterranean region?** No. Although its contribution is highly relevant, it is rarely dominant (above 50%). Specifically, its average contribution is 34.6%.
- **How does the contribution of the Atlantic Ocean compare to that of the Mediterranean Sea?** It is practically the same on average. If we add the contributions of the North Atlantic (24.8%) and the tropical Atlantic (9.9%) we reach a percentage very similar to that of the Mediterranean Sea.
- **How important are contributions from tropical and, in general, extremely remote sources?** These act as precipitation enhancers. On average, up to a quarter of the total extreme rainfall in the western Mediterranean comes from extremely distant sources. The main source within this group is the tropical Atlantic (9.9%). Other sources even further afield, such as the tropical continental areas, the southern hemisphere or the tropical Pacific, generally contribute discreet amounts of moisture separately (3.7, 1.7 and 1.6% on average, respectively) but together they can play a prominent role in many cases.
- **Therefore, which sources are more important, local or remote?** If we consider the Mediterranean Sea and nearby land as local, we find that their contribution is lower on average than the summed contribution of the rest of the sources, which are more distant. However, the difference is not very marked on average (44.5% local versus 55.5% remote), so that in some cases the contribution from local sources may be dominant.
- **In the most extreme cases, is there a higher relative contribution of moisture from remote sources?** Yes, but marginally so. Among the 160 simulated cases, we did not find a significant difference between the first and the last ones in terms of magnitude. This means that even in the not so extreme cases remote moisture input is necessary.
- **How is the vertical distribution of moisture from the different sources?** The fraction of moisture originating in the Mediterranean is higher at lower atmospheric levels. For the Atlantic and in general for the remote sources it is just the opposite, they have a higher relative contribution at high levels. This contradicts the well-mixed assumption, underlying many moisture tracking models.



- **How does the contribution of different sources vary according to season?** In summer, the continental contribution is the most important. However, in this season there is a lower occurrence of extreme precipitation events. In autumn, when most events occur, the largest contributions are from the Atlantic Ocean and the Mediterranean Sea. In addition, the Atlantic contribution becomes more important the closer to winter.
- **And according to weather patterns?** In the events caused by Atlantic lows, the Atlantic contribution is higher, while in cases caused by Mediterranean lows, the Mediterranean contribution prevails over that of the Atlantic. However, neither Atlantic nor Mediterranean average contributions are dominant (above 50%) on average for any of these atmospheric situations. In other words, in almost all cases there is an important extra contribution from other sources, which can be very varied.
- **What do these results imply for the field of meteorology in general and climate change in particular?** Our results indicate that if we want to fully understand Mediterranean extreme precipitation events, we cannot study them only from a regional perspective. For example, when attempting to attribute any of these events to climate change, not only local alterations, such as the increase in Mediterranean Sea water temperature, but also possible alterations in remote and very remote sources should be studied.



# List of Figures

1.1	Storage (black numbers) and transport (red numbers) of water within the hydrological cycle (adapted with permission of John Wiley and Sons from ref. [38]). . . . .	37
1.2	Climatology (annual mean) of the 95 <sup>th</sup> percentile of the <i>CAPE</i> over the period 1979-2019. Data are from the ERA5 reanalysis [42] (adapted with permission of Springer Nature from ref. [43]). . . . .	38
1.3	Region of study. Each colour represents a different sub-region. . . . .	40
1.4	Annual mean precipitation for the climatological period 1980-2015 (a) and topography (b) of the western Mediterranean region. Data are from the MESCAN analysis [53]. . . . .	40
1.5	Monthly distribution of precipitation for the seven sub-regions and for the entire region (TOTAL). The red line indicates the average daily precipitation on wet days. Data are from the MESCAN analysis [53] and monthly averages are calculated in the period 1980-2015. . . . .	42
1.6	Monthly mean of sea surface temperature (blue), 2 meters air temperature (green) and total precipitable water (black) over the western Mediterranean basin. The red shading marks the sea-air temperature difference. Data are from the ERA5 reanalysis [42] and monthly averages are calculated in the period 1980-2015. . . . .	43
1.7	Continental precipitation recycling estimated from an offline Eulerian model. It is estimated that, on average, 40% of precipitation on land comes from terrestrial evapotranspiration (adapted with permission of John Wiley and Sons from ref. [72]). . . . .	44
1.8	Schematic representation of the difference between Lagrangian and Eulerian moisture tracking models. The Eulerian approach is grid-based while the Lagrangian is trajectory-based (adapted with permission of Copernicus Publications from ref. [82]). . . . .	45
1.9	Schematic representation of the space discretisation used by the finite difference method (adapted with permission of John Wiley and Sons from ref. [87]). . . . .	46
2.1	Annual mean precipitation on land from MESCAN (a) and from E-OBS (b) for the climatological period 1980-2015. . . . .	50
2.2	Threshold (mm) used to detect potentially catastrophic daily rainfall. Grey indicates 60 mm. . . . .	52
2.3	Spatial distribution of extreme precipitation in the western Mediterranean region: total number of potentially catastrophic rain days from 1980 to 2015. Grey indicates 0 to 3 days. . . . .	55

2.4	Relationship between the magnitude of events and flood occurrence. Each magnitude bin is made of 25 events. The magnitude of the bins decreases in the x-axis from left to right, so that bin 1 is composed of the 25 most extreme cases. The fraction of EPEs with floods indicates (in percent) how many of the events in each bin caused severe flooding. . . . .	56
2.5	Mean sea level pressure (black contours, hPa), geopotential height (colours, dam) and daily precipitation (magenta contour, amounts above 10 mm) of the four most frequent atmospheric patterns associated with extreme precipitation in the western Mediterranean region, referred to as weather type 1 (a), 2 (b), 3 (c) and 4 (d). . . . .	58
2.6	Fraction of events (in %) associated with weather type 1 (blue), 2 (green), 3 (yellow) and 4 (red), for total episodes (a) and for the top 100 cases in the magnitude ranking (b). Gray indicates the fraction of undefined (U) events, not associated with any of the four types considered. . . . .	59
2.7	Temporal distribution of potentially catastrophic rainfall in the western Mediterranean region, for total episodes (a) and for the 100 most extreme cases (b). Bars indicate the percentage of events (on average) that occur each month. Gray indicates the fraction of undefined (U) events, not associated with any of the four types considered. . . . .	60
2.8	Mean sea level pressure (contours, hPa) and 500hPa geopotential height (colours, dam) for the example episodes of weather type 1 (a), 2 (b), 3 (c) and 4 (d). The fields are shown at 12:00 UTC on the day of the events. . . . .	62
2.9	Accumulated precipitation during the example episodes of Fig. 2.8. . . . .	62
2.10	Total number of hazardous rain days from 1980 to 2008 according to MESCAN (a) and SPREAD combined with APGD (b). . . . .	65
3.1	Sketch representing the fundamentals of the moisture tracers method, including the tagging of 3D and 2D moisture sources. . . . .	70
3.2	Simulation domains for the validation (D1) and example application experiments (D2). . . . .	73
3.3	Moisture sources considered for validation calculations: two-dimensional (a) and three-dimensional (b). . . . .	74
3.4	Total monthly accumulated tracer precipitation ( <i>mm</i> ): from lake evaporation (a), sea evaporation (b), land evapotranspiration (c), lateral boundary advection (d), initial moisture (e) and sum of all contributions (f). . . . .	75
3.5	Total monthly accumulated model precipitation ( <i>mm</i> ) (a), tracer precipitation absolute error ( <i>mm</i> ) (b) and tracer precipitation relative error (%) in areas where precipitation exceeds 1 mm (c). . . . .	76
3.6	Mean error (blue) and standard desviation (red) ( <i>mm</i> ) for 3h accumulated tracer rain (a), tracer snow (c) and tracer graupel (e). Relative contribution of each moisture source [lake evaporation (LK, purple), sea evaporation (S, light blue), land evapotranspiration (LN, dark blue), lateral boundary advection (B, green), initial moisture (I, red)] to 3h accumulated rain (b), snow (d) and graupel (f). . . . .	78
3.7	Same as Fig. 3.6 but for total precipitable water (TPW) ( <i>mm</i> ). . . . .	79
3.8	Relative error for mean domain tracer total precipitable water (TPW, red), 3h accumulated tracer rain (blue), tracer snow (green), and tracer graupel (purple). . . . .	79

3.9	Synoptic situation on 18 November 2014 at 12:00 UTC. Mean sea level pressure (contours, <i>hPa</i> ) and 850hPa temperature (shades, $^{\circ}C$ ) (a). Geopotential height (contours, <i>m</i> ) and 500 hPa temperature (shades, $^{\circ}C$ ) (b). . . . .	81
3.10	Topography of the nested domain ( <i>m</i> ) (a) and lake surface temperature of the Great Lakes ( $^{\circ}C$ ) (b) on 18 November 2014 at 12:00 UTC. . . . .	82
3.11	Total precipitable water ( <i>mm</i> ) originating from lake evaporation on 17 (a), 18 (c), 19 (e) and 20 (g) November 2014 at 12:00 UTC and their percentage contribution to total precipitable water for the same times (b, d, f, h). Wind barbs show 10m winds and contours 850hPa temperature ( $^{\circ}C$ ). . . . .	83
3.12	Observed (a) and simulated (b) accumulated snow water equivalent ( <i>mm</i> ) from 17 November at 06:00 UTC to 21 November at 06:00 UTC. . . . .	84
3.13	Simulated accumulated tracer snow water equivalent (i.e., coming from the lakes' evaporation) ( <i>mm</i> ) (a) and its percentage contribution to total simulated accumulated snow water equivalent (b) from 17 November at 06:00 UTC to 21 November at 06:00 UTC. . . . .	84
4.1	(a) Simulation domain and moisture sources considered: western Mediterranean (light blue), central Mediterranean (brown) and North Atlantic (yellow) two-dimensional sources and tropical and subtropical three-dimensional source (dark blue). (b) Domain for precipitation analysis with topography ( <i>m</i> ) in shades. The areas highlighted in red are the most affected by the October (1) and the November event (2). . . . .	90
4.2	Synoptic situation (from WRF simulation) on October 20, 1982, at 12:00 UTC. (a) Mean sea level pressure (contours, <i>hPa</i> ) and 850 hPa temperature (shades, $^{\circ}C$ ). (b) Geopotential height (solid black contours, <i>dam</i> ) and temperature (magenta dashed contours, $^{\circ}C$ ) at 500 hPa and total precipitable water (shades, <i>mm</i> ). . . . .	91
4.3	(a) Observed (from MESCAN analysis) and (b) simulated total precipitation ( <i>mm</i> ) from October 19 at 06:00 UTC to October 22 at 06:00 UTC. . . . .	91
4.4	Total precipitable water ( <i>mm</i> ) coming from the western Mediterranean (a), the central Mediterranean (b), the North Atlantic (c) and from the tropical and subtropical Atlantic along with tropical Africa, on October 20 at 12:00 UTC. Contours show mean sea level pressure ( <i>hPa</i> ) and arrows show the vertically integrated moisture flux ( $kg\ m^{-1}\ s^{-1}$ ). . . . .	93
4.5	Vertical distribution of water vapour coming from the western Mediterranean (light blue), the central Mediterranean (dark blue), the North Atlantic (light green) and from the tropical and subtropical Atlantic along with tropical Africa (red). First-row shows absolute values ( <i>g/kg</i> ) on October 20 (a) and 21 (b) at 00:00 UTC. Second row depicts relative values (%) on October 20 (c) and 21 (d) at 00:00 UTC. Black dashed lines indicate the total water vapour mixing ratio, from considered and not considered sources ( <i>g/kg</i> ). Values are area averages over the region highlighted in red and labelled 1 in Fig. 4.1b. . . . .	94
4.6	Simulated precipitation ( <i>mm</i> ) coming from the western Mediterranean (a), the central Mediterranean (b), the North Atlantic (c) and the Tropics and Subtropics (d) from October 19 of at 06:00 UTC to October 22 at 06:00 UTC. . . . .	95
4.7	Similar to Fig. 4.2 but for November 7, 1982, at 12:00 UTC. . . . .	96

4.8	Similar to Fig. 4.3 but from November 6 at 06:00 UTC to November 9 at 06:00 UTC. . . . .	97
4.9	Similar to Fig. 4.4 but for November 7 at 12:00 UTC. . . . .	98
4.10	Similar to Fig. 4.5 but on November 7 (a, c) and 8 (b, d) at 00:00 UTC. The analysis is now over region 2 in Fig. 4.1b. . . . .	99
4.11	Similar to Fig. 4.6 but from 06th of November at 06:00 UTC to 09th of November at 06:00 UTC. . . . .	100
5.1	Maximum precipitation in the events analysed. The numbers indicate the different subregions into which the study region has been divided. . . . .	104
5.2	Simulation domain and the 12 moisture sources analysed, which are represented with different colours: Tropical Land (TL), Local Land (LL), Remote Land (RL), Tropical Pacific (TP), Tropical Atlantic (TA), Indian Ocean (IO), Mediterranean (MED), North Atlantic (NA), North Pacific (NP), Lakes and Inland Seas (LA), Southern Hemisphere (SH) and Arctic (AR). . . . .	105
5.3	Box diagrams for the 160 simulated events according to the moisture source. The abbreviation UN refers to moisture of undefined origin. The orange dot on the diagrams and the orange number on the x-axis show the average contribution of each source for the 160 cases. . . . .	107
5.4	Precipitation fractions for the 25 EPEs with the highest magnitude coming from the different sources. The y-axis shows the day on which extreme precipitation occurred, as well as the weather type associated with the event. The magnitude decreases from bottom to top, so the first episode in the ranking is represented by the bar at the bottom of the figure (1982-11-07). . . . .	107
5.5	Monthly distribution of the 160 analyzed events (bars) and the mean precipitation fractions from the Mediterranean (red), Atlantic (green), land (orange) and other sources (black) for those events. . . . .	108
5.6	(a) Total contribution from remote sources (blue) versus local sources (red) averaged for all cases studied (left) and for the 25 highest magnitude cases (right). (b) Same comparison but for the Atlantic Ocean versus the Mediterranean Sea. . . . .	109
5.7	(a) Weather types (previously shown in Fig. 2.5). (b) Box diagrams showing the precipitation fractions from the Mediterranean and Atlantic sources for all cases associated with weather type 1 (blue), 2 (green), 3 (orange) and 4 (red). . . . .	110
5.8	(a) Comparison between the Mediterranean and Atlantic contributions to the 160 studied events in terms of rainfall (blue) and total precipitable water (TPW, green). (b) Cumulative plot showing the vertical distribution (in pressure levels) of water vapour fractions from the different sources. . . . .	111
5.9	Sea level pressure and total precipitable water from evaporation over the tropical Pacific during the February 1982 Catalonia (Spain) extreme precipitation event (a). The same fields but referring to moisture from the tropical land (b), the Southern Hemisphere (c) and the tropical Atlantic (d) during the catastrophic Var (France) flood event in June 2010. Fields are shown at 12 UTC on February 16, 1982 (a) and June 15, 2010 (b,c and d). . . . .	113



---

5.10	Linear relationship between the El Niño 3.4 index and the moisture contributions from the Atlantic (a) and Pacific (b). Each point corresponds to one of the 160 events analysed. The orange line comes from a least-squares linear regression. Correlation coefficients are shown in the upper right corner. .	114
5.11	Simulated (left column) and observed (right column) precipitation for the 25 most extreme events analysed. Observed precipitation is from the MESCAN [53] precipitation analysis. This figure is continued on the following pages. . .	115
5.11	Continued. . . . .	116
5.11	Continued. . . . .	117
5.11	Continued. . . . .	118
5.11	Continued. . . . .	119



# List of Tables

1.1	Information from the seven regions considered in the study. For each region (rows) we show in columns (from left to right): name of the different sub-regions (NUTS) encompassed, total area (in thousand of $km^2$ ) and the main orientation of the coastline. . . . .	41
2.1	The first 25 episodes in the EPEs database, i.e., the 25 episodes with the highest magnitude (those in the first bin of Fig. 2.4). For each episode (rows) we show in columns (from left to right): the position in the ranking, dates, the affected regions, the associated weather type and whether or not there was flooding, according to FLOODHYMEX and EM-DAT data. . . . .	61
3.1	The different WVTs implementations (including the present): reference, name of the models in which the WVTs tool has been implemented and scale of these models. . . . .	68
4.1	Relative contribution (%) of the considered moisture sources to the accumulated precipitation from October 19 at 06:00 UTC to October 21 at 06:00 UTC in the most affected area (region 1 in Fig. 4.1b). . . . .	95
4.2	Same as Table 4.1 but from November 6 at 06:00 UTC to November 9 at 06:00 UTC and over region 2 in Fig. 4.1b. . . . .	101



# List of publications

- (I) D. Insua-Costa, M. Lemus-Cánovas, G. Miguez-Macho, and M. C. Llasat, “Climatology and ranking of hazardous precipitation events in the western Mediterranean area”, *Atmospheric Research*, vol. 255, p. 105521, 2021. DOI: <https://doi.org/10.1016/j.atmosres.2021.105521>.

## **Author contribution**

DIC designed the experiment, performed the simulations and the data analysis, created the figures and wrote the first manuscript draft.

## **Quality indexes**

Impact factor: 5.369

CiteScore: 8.6

Quartile: Q1 (16/94 in METEOROLOGY & ATMOSPHERIC SCIENCES)

- (II) D. Insua-Costa and G. Miguez-Macho, “A new moisture tagging capability in the Weather Research and Forecasting model: Formulation, validation and application to the 2014 Great Lake-effect snowstorm”, *Earth System Dynamics*, vol. 9, no. 1, pp. 167–185, 2018. DOI: <https://doi.org/10.5194/esd-9-167-2018>.

## **Author contribution**

DIC designed the experiment, performed the simulations and the data analysis, created the figures and wrote the first manuscript draft.

## **Quality indexes**

Impact factor: 5.540

CiteScore: 7.6

Quartile: Q1 (20/200 in GEOSCIENCES, MULTIDISCIPLINARY)

- (III) D. Insua-Costa, G. Miguez-Macho, and C. Llasat, “Local and remote moisture sources for extreme precipitation: A study of the two catastrophic 1982 western Mediterranean episodes”, *Hydrology and Earth System Sciences*, vol. 23, no. 9, pp. 3885–3900, 2019. DOI: <https://doi.org/10.5194/hess-23-3885-2019>.

## **Author contribution**

DIC designed the experiment, performed the simulations and the data analysis, created the figures and wrote the first manuscript draft.

**Quality indexes**

Impact factor: 5.748

CiteScore: 9.3

Quartile: Q1 (17/200 in GEOSCIENCES, MULTIDISCIPLINARY), Q1 (7/98 in WATER RESOURCES)

- (IV) D. Insua-Costa, M. Senande-Rivera, G. Miguez-Macho, and C. Llasat, “A global perspective on western Mediterranean precipitation extremes”, Accepted at NPJ Climate and Atmospheric Science, 2021.

**Author contribution**

DIC designed the experiment, performed the simulations and the data analysis, created the figures and wrote the first manuscript draft.

**Quality indexes**

Impact factor: 8.624

CiteScore: 8.8

Quartile: Q1 (5/94 in in METEOROLOGY & ATMOSPHERIC SCIENCES)





# Appendix: Copyright Permissions

Figure. 1.1

The screenshot shows the CCC RightsLink interface. At the top, there are navigation links for "My Orders", "My Library", and "My Profile". A welcome message for "damian.insua@usc.es" is displayed, along with links for "Log out", "Help", and "FAQ". Below this, the breadcrumb "My Orders > Orders > All Orders" is shown. The main heading is "License Details". A paragraph states: "This Agreement between Damián Insua Costa ('You') and John Wiley and Sons ('John Wiley and Sons') consists of your license details and the terms and conditions provided by John Wiley and Sons and Copyright Clearance Center." There are "Print" and "Copy" buttons. A table lists license details:

License Number	5226500769941
License date	Jan 12, 2022
Licensed Content Publisher	John Wiley and Sons
Licensed Content Publication	Reviews of Geophysics
Licensed Content Title	Oceanic and terrestrial sources of continental precipitation
Licensed Content Author	Raquel Nieto, Ana María Durán-Quesada, Anita Drummond, et al
Licensed Content Date	Nov 8, 2012
Licensed Content Volume	50
Licensed Content Issue	4
Licensed Content Pages	41
Type of Use	Dissertation/Thesis
Requestor type	University/Academic
Format	Electronic
Portion	Figure/table
Number of figures/tables	1
Will you be translating?	No
Title	A CLIMATOLOGY OF WESTERN MEDITERRANEAN PRECIPITATION EXTREMES FOCUSING ON THE STUDY OF MOISTURE ORIGIN
Institution name	University of Santiago de Compostela
Expected presentation date	Feb 2022
Portions	Figure 1
Requestor Location	Damián Insua Costa Rua Xose Maria Suarez Nunez s/n Campus Vida  Santiago de Compostela, 15782 Spain Attn: University of Santiago de Compostela
Publisher Tax ID	EU826007151
Total	<b>0.00 EUR</b>

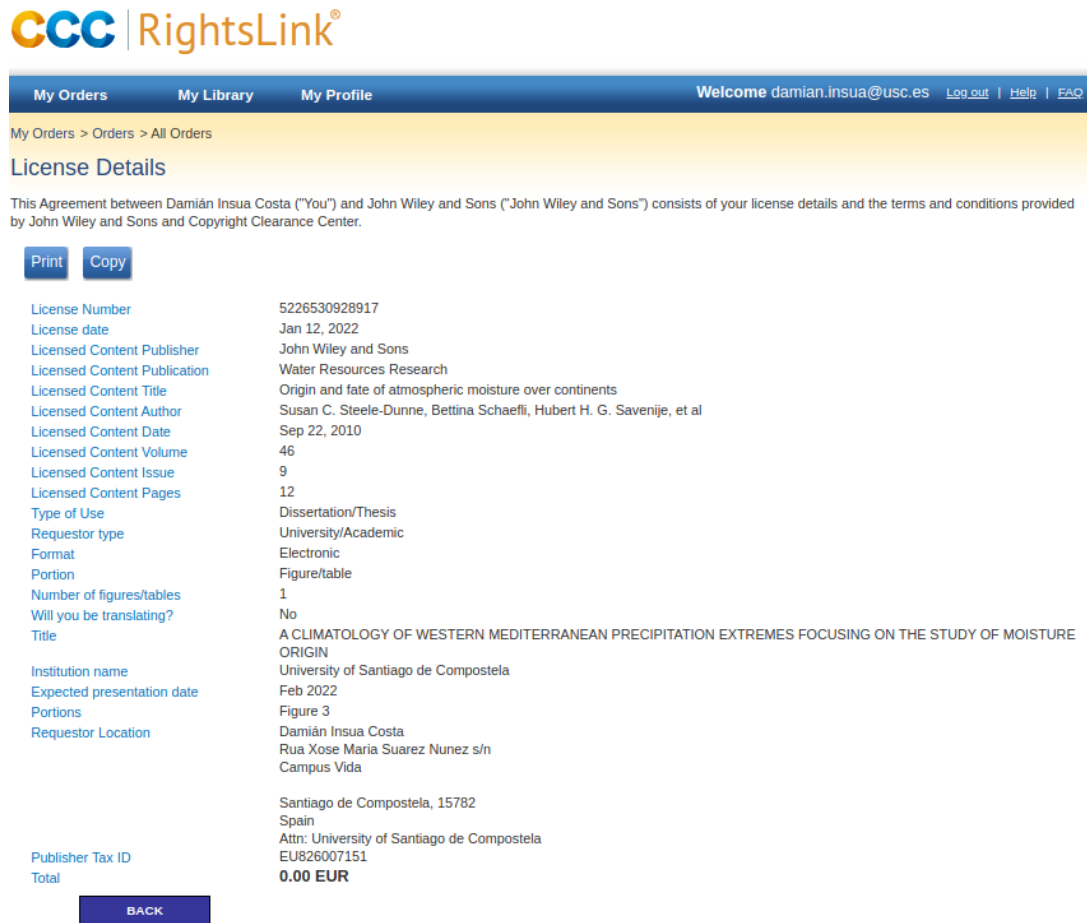
A "BACK" button is located at the bottom of the license details section.

Figure. 1.2

The screenshot shows the CCC RightsLink interface for a Springer Nature article. At the top, there are navigation links for "My Orders", "My Library", and "My Profile". A welcome message for "damian.insua@usc.es" is displayed, along with links for "Log out", "Help", and "FAQ". Below this, the breadcrumb "My Orders > Orders > All Orders" is shown. The main heading is "License Details". A paragraph states: "This Agreement between Damián Insua Costa ('You') and John Wiley and Sons ('John Wiley and Sons') consists of your license details and the terms and conditions provided by John Wiley and Sons and Copyright Clearance Center." There are "Print" and "Copy" buttons. A table lists license details:

License Number	5226500769941
License date	Jan 12, 2022
Licensed Content Publisher	John Wiley and Sons
Licensed Content Publication	Reviews of Geophysics
Licensed Content Title	Oceanic and terrestrial sources of continental precipitation
Licensed Content Author	Raquel Nieto, Ana María Durán-Quesada, Anita Drummond, et al
Licensed Content Date	Nov 8, 2012
Licensed Content Volume	50
Licensed Content Issue	4
Licensed Content Pages	41
Type of Use	Dissertation/Thesis
Requestor type	University/Academic
Format	Electronic
Portion	Figure/table
Number of figures/tables	1
Will you be translating?	No
Title	A CLIMATOLOGY OF WESTERN MEDITERRANEAN PRECIPITATION EXTREMES FOCUSING ON THE STUDY OF MOISTURE ORIGIN
Institution name	University of Santiago de Compostela
Expected presentation date	Feb 2022
Portions	Figure 1
Requestor Location	Damián Insua Costa Rua Xose Maria Suarez Nunez s/n Campus Vida  Santiago de Compostela, 15782 Spain Attn: University of Santiago de Compostela
Publisher Tax ID	EU826007151
Total	<b>0.00 EUR</b>

A "BACK" button is located at the bottom of the license details section.

**Figure. 1.7**


**CCC | RightsLink®**

My Orders   My Library   My Profile   Welcome damian.insua@usc.es   Log out | Help | FAQ

My Orders > Orders > All Orders

### License Details

This Agreement between Damián Insua Costa ("You") and John Wiley and Sons ("John Wiley and Sons") consists of your license details and the terms and conditions provided by John Wiley and Sons and Copyright Clearance Center.

[Print](#)   [Copy](#)

License Number	5226530928917
License date	Jan 12, 2022
Licensed Content Publisher	John Wiley and Sons
Licensed Content Publication	Water Resources Research
Licensed Content Title	Origin and fate of atmospheric moisture over continents
Licensed Content Author	Susan C. Steele-Dunne, Bettina Schaeffli, Hubert H. G. Savenije, et al
Licensed Content Date	Sep 22, 2010
Licensed Content Volume	46
Licensed Content Issue	9
Licensed Content Pages	12
Type of Use	Dissertation/Thesis
Requestor type	University/Academic
Format	Electronic
Portion	Figure/table
Number of figures/tables	1
Will you be translating?	No
Title	A CLIMATOLOGY OF WESTERN MEDITERRANEAN PRECIPITATION EXTREMES FOCUSING ON THE STUDY OF MOISTURE ORIGIN
Institution name	University of Santiago de Compostela
Expected presentation date	Feb 2022
Portions	Figure 3
Requestor Location	Damián Insua Costa Rua Xose Maria Suarez Nunez s/n Campus Vida  Santiago de Compostela, 15782 Spain Attn: University of Santiago de Compostela EU826007151
Publisher Tax ID	
Total	<b>0.00 EUR</b>

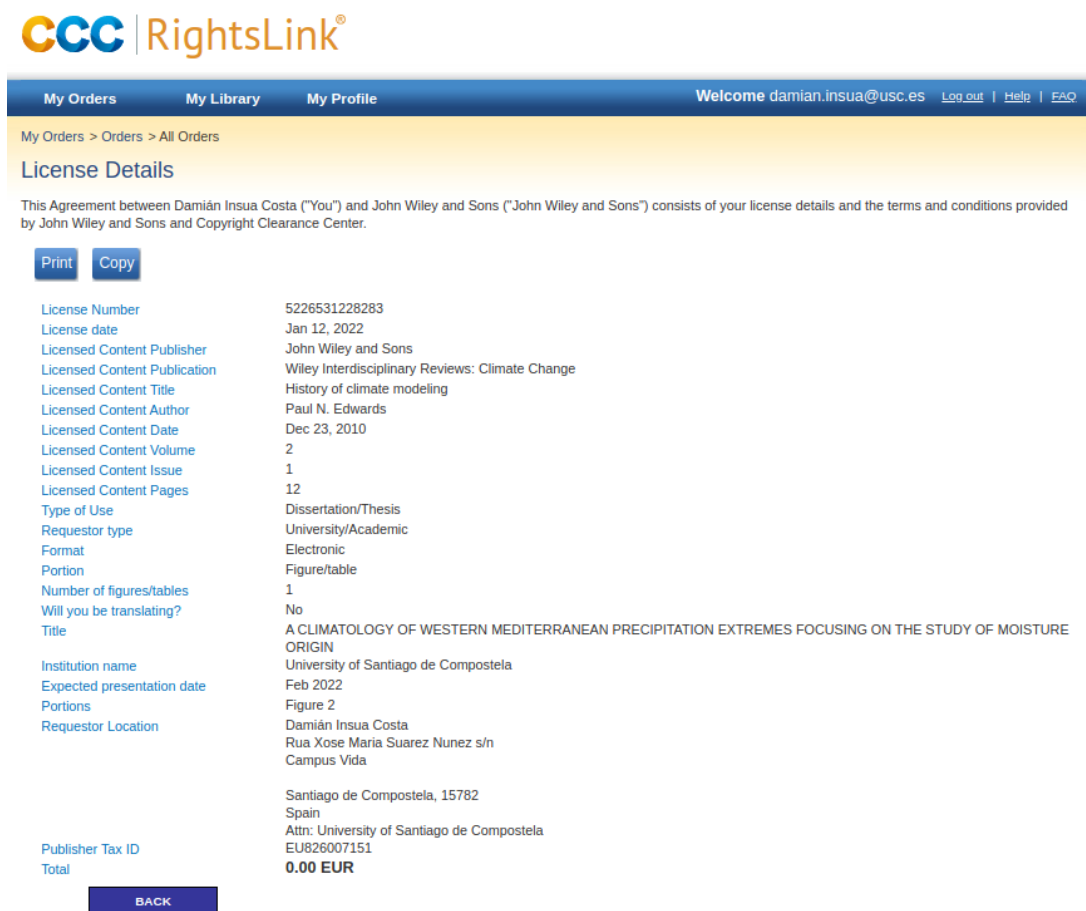
[BACK](#)

**Figure. 1.8**

This figure is published in an article by Copernicus Publications. All articles from this publisher are licenced under the Creative Commons Attribution 4.0 licence (<https://creativecommons.org/licenses/by/4.0/>) and therefore permission is not required. For further information, please refer to [https://www.hydrology-and-earth-system-sciences.net/policies/licence\\_and\\_copyright.html](https://www.hydrology-and-earth-system-sciences.net/policies/licence_and_copyright.html).



Figure. 1.9



**CCC | RightsLink®**

My Orders   My Library   My Profile   Welcome damian.insua@usc.es   Log out | Help | FAQ

My Orders > Orders > All Orders

### License Details

This Agreement between Damián Insua Costa ("You") and John Wiley and Sons ("John Wiley and Sons") consists of your license details and the terms and conditions provided by John Wiley and Sons and Copyright Clearance Center.

[Print](#)   [Copy](#)

License Number	5226531228283
License date	Jan 12, 2022
Licensed Content Publisher	John Wiley and Sons
Licensed Content Publication	Wiley Interdisciplinary Reviews: Climate Change
Licensed Content Title	History of climate modeling
Licensed Content Author	Paul N. Edwards
Licensed Content Date	Dec 23, 2010
Licensed Content Volume	2
Licensed Content Issue	1
Licensed Content Pages	12
Type of Use	Dissertation/Thesis
Requestor type	University/Academic
Format	Electronic
Portion	Figure/table
Number of figures/tables	1
Will you be translating?	No
Title	A CLIMATOLOGY OF WESTERN MEDITERRANEAN PRECIPITATION EXTREMES FOCUSING ON THE STUDY OF MOISTURE ORIGIN
Institution name	University of Santiago de Compostela
Expected presentation date	Feb 2022
Portions	Figure 2
Requestor Location	Damián Insua Costa Rua Xose Maria Suarez Nunez s/n Campus Vida  Santiago de Compostela, 15782 Spain Attn: University of Santiago de Compostela EU826007151
Publisher Tax ID	
Total	<b>0.00 EUR</b>

[BACK](#)

**Article 1.** D. Insua-Costa, M. Lemus-Cánovas, G. Miguez-Macho, and M. C. Llasat, “Climatology and ranking of hazardous precipitation events in the western Mediterranean area”, *Atmospheric Research*, vol. 255, p. 105521, 2021. DOI: <https://doi.org/10.1016/j.atmosres.2021.105521>.



Publisher: Elsevier  
Copyright © 1969, Elsevier

**Creative Commons**  
This is an open access article distributed under the terms of the [Creative Commons CC-BY](https://creativecommons.org/licenses/by/4.0/) license, which permits unrestricted use, distribution, and reproduction in any medium, provided the original work is properly cited.  
You are not required to obtain permission to reuse this article.  
To request permission for a type of use not listed, please contact [Elsevier](https://www.elsevier.com/permissions) Global Rights Department.  
Are you the [author](#) of this Elsevier journal article?

**Article 2.** D. Insua-Costa and G. Miguez-Macho, “A new moisture tagging capability in the Weather Research and Forecasting model: Formulation, validation and application to the 2014 Great Lake-effect snowstorm”, *Earth System Dynamics*, vol. 9, no. 1, pp. 167–185, 2018. DOI: <https://doi.org/10.5194/esd-9-167-2018>.

This article was published by Copernicus Publications. All articles from this publisher are licenced under the Creative Commons Attribution 4.0 licence (<https://creativecommons.org/licenses/by/4.0/>) and therefore permission is not required. For further information, please refer to [https://www.earth-system-dynamics.net/policies/licence\\_and\\_copyright.html](https://www.earth-system-dynamics.net/policies/licence_and_copyright.html).

**Article 3.** D. Insua-Costa, G. Miguez-Macho, and C. Llasat, “Local and remote moisture sources for extreme precipitation: A study of the two catastrophic 1982 western Mediterranean episodes”, *Hydrology and Earth System Sciences*, vol. 23, no. 9, pp. 3885–3900, 2019. DOI: <https://doi.org/10.5194/hess-23-3885-2019>.

This article was published by Copernicus Publications. All articles from this publisher are licenced under the Creative Commons Attribution 4.0 licence (<https://creativecommons.org/licenses/by/4.0/>) and therefore permission is not required. For further information, please refer to [https://www.hydrology-and-earth-system-sciences.net/policies/licence\\_and\\_copyright.html](https://www.hydrology-and-earth-system-sciences.net/policies/licence_and_copyright.html).

**Article 4.** D. Insua-Costa, M. Senande-Rivera, G. Miguez-Macho, and C. Llasat, “A global perspective on western Mediterranean precipitation extremes”, Accepted at *NPJ Climate and Atmospheric Science*, 2021.

This article, when published, will also be licenced under the Creative Commons Attribution 4.0 licence (<https://creativecommons.org/licenses/by/4.0/>), as are all articles in the journal *NPJ Climate and Atmospheric Science*. No permission is therefore required. For further information, please refer to <https://www.nature.com/npjclimatsci/open-access>.

# Bibliography

- [1] D. Insua-Costa, M. Lemus-Cánovas, G. Miguez-Macho, and M. C. Llasat, “Climatology and ranking of hazardous precipitation events in the western Mediterranean area,” *Atmospheric Research*, vol. 255, p. 105521, 2021.
- [2] D. Insua-Costa and G. Miguez-Macho, “A new moisture tagging capability in the Weather Research and Forecasting model: Formulation, validation and application to the 2014 Great Lake-effect snowstorm,” *Earth System Dynamics*, vol. 9, no. 1, pp. 167–185, 2018.
- [3] D. Insua-Costa, G. Miguez-Macho, and C. Llasat, “Local and remote moisture sources for extreme precipitation: A study of the two catastrophic 1982 western Mediterranean episodes,” *Hydrology and Earth System Sciences*, vol. 23, no. 9, pp. 3885–3900, 2019.
- [4] D. R. Easterling, G. A. Meehl, C. Parmesan, S. A. Changnon, T. R. Karl, and L. O. Mearns, “Climate extremes: Observations, modeling, and impacts,” *Science*, vol. 289, no. 5487, pp. 2068–2074, 2000.
- [5] P. Adhikari, Y. Hong, K. R. Douglas, D. B. Kirschbaum, J. Gourley, R. Adler, and G. R. Brakenridge, “A digitized global flood inventory (1998-2008): Compilation and preliminary results,” *Natural Hazards*, vol. 55, no. 2, pp. 405–422, 2010.
- [6] R. P. Allan and B. J. Soden, “Atmospheric warming and the amplification of precipitation extremes,” *Science*, vol. 321, no. 5895, pp. 1481–1484, 2008.
- [7] S. K. Min, X. Zhang, F. W. Zwiers, and G. C. Hegerl, “Human contribution to more-intense precipitation extremes,” *Nature*, vol. 470, no. 7334, pp. 378–381, 2011.
- [8] M. G. Donat, A. L. Lowry, L. V. Alexander, P. A. O’Gorman, and N. Maher, “More extreme precipitation in the world’s dry and wet regions,” *Nature Climate Change*, vol. 7, no. 2, pp. 154–158, 2017.
- [9] C. Ramis, V. Homar, A. Amengual, R. Romero, and S. Alonso, “Daily precipitation records over mainland Spain and the Balearic Islands,” *Natural Hazards and Earth System Sciences*, vol. 13, no. 10, pp. 2483–2491, 2013.
- [10] J. I. Barredo, “Major flood disasters in Europe: 1950-2005,” *Natural Hazards*, vol. 42, no. 1, pp. 125–148, 2007.
- [11] M. C. Llasat, M. Barriendos, A. Barrera, and T. Rigo, “Floods in Catalonia (NE Spain) since the 14th century. Climatological and meteorological aspects from historical

- documentary sources and old instrumental records,” *Journal of Hydrology*, vol. 313, no. 1-2, pp. 32–47, 2005.
- [12] M. C. Llasat, M. Llasat-Botija, M. A. Prat, F. Porcú, C. Price, A. Mugnai, K. Lagouvardos, V. Kotroni, D. Katsanos, S. Michaelides, Y. Yair, K. Savvidou, and K. Nicolaidis, “High-impact floods and flash floods in Mediterranean countries: The FLASH preliminary database,” *Advances in Geosciences*, vol. 23, pp. 47–55, 2010.
- [13] M. C. Llasat, M. Llasat-Botija, O. Petrucci, A. A. Pasqua, J. Rosselló, F. Vinet, and L. Boissier, “Towards a database on societal impact of Mediterranean floods within the framework of the HYMEX project,” *Natural Hazards and Earth System Science*, vol. 13, no. 5, pp. 1337–1350, 2013.
- [14] Gaume, E., Borga, M., Llasat, M. C., Maouche, S., Lang, M., , and M. Diakakis, “Mediterranean extreme floods and flash floods,” in *The Mediterranean Region under Climate Change, A Scientific Update*, I. Editions, Ed., Marseille, 2016, ch. 3, pp. 133–144.
- [15] R. Romero, C. A. Doswell, C. Ramis, R. Romero, C. A. D. III, and C. Ramis, “Mesoscale Numerical Study of Two Cases of Long-Lived Quasi-Stationary Convective Systems over Eastern Spain,” *Monthly Weather Review*, vol. 128, no. 11, pp. 3731–3751, 2000.
- [16] A. Buzzi, N. Tartaglione, and P. Malguzzi, “Numerical Simulations of the 1994 Piedmont Flood: Role of Orography and Moist Processes,” *Monthly Weather Review*, vol. 126, no. 9, pp. 2369–2383, 1998.
- [17] P. Alpert, T. Ben-Gai, A. Baharad, Y. Benjamini, D. Yekutieli, M. Colacino, L. Diodato, C. Ramis, V. Homar, R. Romero, S. Michaelides, and A. Manes, “The paradoxical increase of Mediterranean extreme daily rainfall in spite of decrease in total values,” *Geophysical Research Letters*, vol. 29, no. 11, pp. 31–1–31–4, 2002.
- [18] M. Diakakis, “An inventory of flood events in Athens, Greece, during the last 130 years. Seasonality and spatial distribution,” *Journal of Flood Risk Management*, vol. 7, no. 4, pp. 332–343, 2014.
- [19] M. C. Llasat, R. Marcos, M. Turco, J. Gilabert, and M. Llasat-Botija, “Trends in flash flood events versus convective precipitation in the Mediterranean region: The case of Catalonia,” *Journal of Hydrology*, vol. 541, pp. 24–37, 2016.
- [20] E. Sánchez, C. Gallardo, M. A. Gaertner, A. Arribas, and M. Castro, “Future climate extreme events in the Mediterranean simulated by a regional climate model: A first approach,” *Global and Planetary Change*, vol. 44, no. 1-4, pp. 163–180, 2004.
- [21] X. Gao, J. S. Pal, and F. Giorgi, “Projected changes in mean and extreme precipitation over the Mediterranean region from a high resolution double nested RCM simulation,” *Geophysical Research Letters*, vol. 33, no. 3, 2006.
- [22] K. Goubanova and L. Li, “Extremes in temperature and precipitation around the Mediterranean basin in an ensemble of future climate scenario simulations,” *Global and Planetary Change*, vol. 57, no. 1-2, pp. 27–42, 2007.

- [23] Y. Trambly and S. Somot, “Future evolution of extreme precipitation in the Mediterranean,” *Climatic Change*, vol. 151, no. 2, pp. 289–302, 2018.
- [24] P. Drobinski, V. Ducrocq, P. Alpert, E. Anagnostou, K. Béranger, M. Borga, I. Braud, A. Chanzy, S. Davolio, G. Delrieu, C. Estournel, N. Filali Boubrahmi, J. Font, V. Grubišić, S. Gualdi, V. Homar, B. Ivančan-Picek, C. Kottmeier, V. Kotroni, K. Lagouvardos, P. Lionello, M. C. Llasat, W. Ludwig, C. Lutoff, A. Mariotti, E. Richard, R. Romero, R. Rotunno, O. Roussot, I. Ruin, S. Somot, I. Taupier-Letage, J. Tintor, R. Uijlenhoet, and H. Wernli, “HYMEX: A 10-year multidisciplinary program on the mediterranean water cycle,” *Bulletin of the American Meteorological Society*, vol. 95, no. 7, pp. 1063–1082, 2014.
- [25] V. Ducrocq, I. Braud, S. Davolio, R. Ferretti, C. Flamant, A. Jansa, N. Kalthoff, E. Richard, I. Taupier-Letage, P. A. Ayrat, S. Belamari, A. Berne, M. Borga, B. Boudevillain, O. Bock, J. L. Boichard, M. N. Bouin, O. Bousquet, C. Bouvier, J. Chiggiato, D. Cimini, U. Corsmeier, L. Coppola, P. Cocquerez, E. Defer, J. Delanoë, P. Di Girolamo, A. Doerenbecher, P. Drobinski, Y. Dufournet, N. Fourrié, J. J. Gourley, L. Labatut, D. Lambert, J. Le Coz, F. S. Marzano, G. Molinié, A. Montani, G. Nord, M. Nuret, K. Ramage, W. Rison, O. Roussot, F. Said, A. Schwarzenboeck, P. Testor, J. Van Baelen, B. Vincendon, M. Aran, and J. Tamayo, “HyMeX-SOP1: The field campaign dedicated to heavy precipitation and flash flooding in the northwestern mediterranean,” *Bulletin of the American Meteorological Society*, vol. 95, no. 7, pp. 1083–1100, 2014.
- [26] M. C. Llasat, “Episodios de lluvias copiosas en Catalunya: génesis, evolución y factores coadyuvantes,” Ph.D. dissertation, 1987.
- [27] O. Reale, L. Feudale, and B. Turato, “Evaporative moisture sources during a sequence of floods in the Mediterranean region,” *Geophysical Research Letters*, vol. 28, no. 10, pp. 2085–2088, 2001.
- [28] B. Turato, O. Reale, and F. Siccardi, “Water Vapor Sources of the October 2000 Piedmont Flood,” *Journal of Hydrometeorology*, vol. 5, no. 4, pp. 693–712, 2004.
- [29] R. Nieto, L. Gimeno, A. Drumond, and E. Hernandez, “A Lagrangian identification of the main moisture sources and sinks affecting the Mediterranean area,” *WSEAS Transactions on Environment and Development*, vol. 6, no. 5, pp. 365–374, 2010.
- [30] F. Duffourg and V. Ducrocq, “Origin of the moisture feeding the heavy precipitating systems over southeastern France,” *Natural Hazards and Earth System Science*, vol. 11, no. 4, pp. 1163–1178, 2011.
- [31] A. Winschall, S. Pfahl, H. Sodemann, and H. Wernli, “Impact of North Atlantic evaporation hot spots on southern Alpine heavy precipitation events,” *Quarterly Journal of the Royal Meteorological Society*, vol. 138, no. 666, pp. 1245–1258, 2012.
- [32] J. G. Pinto, S. Ulbrich, A. Parodi, R. Rudari, G. Boni, and U. Ulbrich, “Identification and ranking of extraordinary rainfall events over Northwest Italy: The role of Atlantic moisture,” *Journal of Geophysical Research Atmospheres*, vol. 118, no. 5, pp. 2085–2097, 2013.



- [33] A. Winschall, S. Pfahl, H. Sodemann, and H. Wernli, “Comparison of Eulerian and Lagrangian moisture source diagnostics - The flood event in eastern Europe in May 2010,” *Atmospheric Chemistry and Physics*, vol. 14, no. 13, pp. 6605–6619, 2014.
- [34] S. O. Krichak, J. Barkan, J. S. Breitgand, S. Gualdi, and S. B. Feldstein, “The role of the export of tropical moisture into midlatitudes for extreme precipitation events in the Mediterranean region,” *Theoretical and Applied Climatology*, vol. 121, no. 3-4, pp. 499–515, 2015.
- [35] M. Reale and P. Lionello, “Synoptic climatology of winter intense precipitation events along the Mediterranean coasts,” *Natural Hazards and Earth System Sciences*, vol. 13, no. 7, pp. 1707–1722, 2013.
- [36] A. Jansa, P. Alpert, P. Arbogast, A. Buzzi, B. Ivancan-Picek, V. Kotroni, M. C. Llasat, C. Ramis, E. Richard, R. Romero, and A. Speranza, “MEDEX: A general overview,” *Natural Hazards and Earth System Sciences*, vol. 14, no. 8, pp. 1965–1984, 2014.
- [37] C. A. Doswell, H. E. Brooks, and R. A. Maddox, “Flash flood forecasting: An ingredients-based methodology,” *Weather and Forecasting*, vol. 11, no. 4, pp. 560–581, 1996.
- [38] L. Gimeno, A. Stohl, R. M. Trigo, F. Dominguez, K. Yoshimura, L. Yu, A. Drumond, A. M. Durn-Quesada, and R. Nieto, “Oceanic and terrestrial sources of continental precipitation,” *Reviews of Geophysics*, vol. 50, no. 4, pp. 1–41, 2012.
- [39] L. Gimeno, R. Nieto, M. Vázquez, and D. A. Lavers, “Atmospheric rivers: A mini-review,” *Frontiers in Earth Science*, vol. 2, no. March, 2014.
- [40] R. Lorente-Plazas, J. P. Montavez, A. M. Ramos, S. Jerez, R. M. Trigo, and P. Jimenez-Guerrero, “Unusual Atmospheric-River-Like Structures Coming From Africa Induce Extreme Precipitation Over the Western Mediterranean Sea,” *Journal of Geophysical Research: Atmospheres*, vol. 125, no. 2, 2020.
- [41] J. Marshall and R. A. Plumb, *Atmosphere, Ocean, and Climate Dynamics*, 2008.
- [42] H. Hersbach, B. Bell, P. Berrisford, S. Hirahara, A. Horányi, J. Muñoz-Sabater, J. Nicolas, C. Peubey, R. Radu, D. Schepers, A. Simmons, C. Soci, S. Abdalla, X. Abellan, G. Balsamo, P. Bechtold, G. Biavati, J. Bidlot, M. Bonavita, G. De Chiara, P. Dahlgren, D. Dee, M. Diamantakis, R. Dragani, J. Flemming, R. Forbes, M. Fuentes, A. Geer, L. Haimberger, S. Healy, R. J. Hogan, E. Hólm, M. Janisková, S. Keeley, P. Laloyaux, P. Lopez, C. Lupu, G. Radnoti, P. de Rosnay, I. Rozum, F. Vamborg, S. Villaume, and J. N. Thépaut, “The ERA5 global reanalysis,” *Quarterly Journal of the Royal Meteorological Society*, vol. 146, no. 730, pp. 1999–2049, 2020.
- [43] M. Taszarek, J. T. Allen, M. Marchio, and H. E. Brooks, “Global climatology and trends in convective environments from ERA5 and rawinsonde data,” *npj Climate and Atmospheric Science*, vol. 4, no. 1, 2021.
- [44] J. M. Wallace and P. V. Hobbs, *Atmospheric Science: An Introductory Survey: Second Edition*, 2006.

- [45] A. Rivera and R. Riosalido, "Mediterranean convective systems as viewed by Meteosat. A case study," in *Proc. 6th Meteosat Scientific Users Meeting, Amsterdam*, 1986, pp. 101–104.
- [46] J. M. López, "A Mediterranean derecho: Catalonia (Spain), 17th August 2003," *Atmospheric Research*, vol. 83, no. 2-4 SPEC. ISS., pp. 272–283, 2007.
- [47] J. Bech, N. Pineda, T. Rigo, M. Aran, J. Amaro, M. Gayà, J. Arús, J. Montanyà, and O. van der Velde, "A Mediterranean nocturnal heavy rainfall and tornadic event. Part I: Overview, damage survey and radar analysis," *Atmospheric Research*, vol. 100, no. 4, pp. 621–637, 2011.
- [48] T. Rigo, M. Berenguer, and M. d. C. Llasat, "An improved analysis of mesoscale convective systems in the western Mediterranean using weather radar," *Atmospheric Research*, vol. 227, pp. 147–156, 2019.
- [49] M. M. Miglietta, J. Mazon, and R. Rotunno, "Numerical simulations of a tornadic supercell over the mediterranean," *Weather and Forecasting*, vol. 32, no. 3, pp. 1209–1226, 2017.
- [50] J. B. Cohuet, R. Romero, V. Homar, V. Ducrocq, and C. Ramis, "Initiation of a severe thunderstorm over the Mediterranean Sea," *Atmospheric Research*, vol. 100, no. 4, pp. 603–620, 2011.
- [51] J. Mateo, D. Ballart, C. Brucet, M. Aran, and J. Bech, "A study of a heavy rainfall event and a tornado outbreak during the passage of a squall line over Catalonia," *Atmospheric Research*, vol. 93, no. 1-3, pp. 131–146, 2009.
- [52] J. R. Holton and G. J. Hakim, *An introduction to dynamic meteorology: Fifth edition*, 2012, vol. 9780123848.
- [53] C. Soci, E. Bazile, F. O. Besson, and T. Landelius, "High-resolution precipitation re-analysis system for climatological purposes," *Tellus, Series A: Dynamic Meteorology and Oceanography*, vol. 68, no. 1, 2016.
- [54] R. Rotunno and R. Ferretti, "Orographic effects on rainfall in MAP cases IOP 2b and IOP 8," *Quarterly Journal of the Royal Meteorological Society*, vol. 129, no. 588 PART B, 2003.
- [55] M. C. Llasat, "High magnitude storms and floods," *The Physical Geography of the Mediterranean*, edited by: Woodward, JC, Oxford University Press, Oxford, pp. 513–540, 2009.
- [56] A. Rios-Entenza, "Impact of land-atmosphere fluxes on the spring precipitation regime of the Iberian Peninsula," Ph.D. dissertation, 2014.
- [57] R. Nieto, L. Gimeno, L. de la Torre, P. Ribera, D. Gallego, R. García-Herrera, J. A. García, M. Nuñez, A. Redaño, and J. Lorente, "Climatological features of cutoff low systems in the Northern Hemisphere," *Journal of Climate*, vol. 18, no. 16, pp. 3085–3103, 2005.

- [58] R. Nieto, M. Sprenger, H. Wernli, R. M. Trigo, and L. Gimeno, “Identification and climatology of cut-off lows near the tropopause,” *Annals of the New York Academy of Sciences*, vol. 1146, pp. 256–290, 2008.
- [59] A. Jansa, A. Genoves, M. A. Picornell, J. Campins, R. Riosalido, and O. Carretero, “Western Mediterranean cyclones and heavy rain. Part 2: Statistical approach,” *Meteorological Applications*, vol. 8, pp. 43–56, 2001.
- [60] J. Campins, A. Genovés, M. A. Picornell, and A. Jansà, “Climatology of Mediterranean cyclones using the ERA-40 dataset,” *International Journal of Climatology*, vol. 31, no. 11, pp. 1596–1614, 2011.
- [61] U. Dayan, K. Nissen, and U. Ulbrich, “Review Article: Atmospheric conditions inducing extreme precipitation over the eastern and western Mediterranean,” *Natural Hazards and Earth System Sciences*, vol. 15, no. 11, pp. 2525–2544, 2015.
- [62] J. P. Peixoto and A. H. Oort, *Physics of climate*. New York: American Institute of Physics, 1992.
- [63] K. L. Brubaker, D. Entekhabi, and P. S. Eagleson, “Estimation of continental precipitation recycling,” *Journal of Climate*, vol. 6, no. 6, pp. 1077–1089, 1993.
- [64] E. A. B. Eltahir and R. L. Bras, “Precipitation recycling,” *Reviews of geophysics*, vol. 34, no. 3, pp. 367–378, 1996.
- [65] K. E. Trenberth, “Atmospheric moisture recycling: Role of advection and local evaporation,” *Journal of Climate*, vol. 12, no. 5 II, pp. 1368–1381, 1999.
- [66] A. Rios-Entenza and G. Miguez-Macho, “Moisture recycling and the maximum of precipitation in spring in the Iberian Peninsula,” *Climate Dynamics*, vol. 42, no. 11-12, pp. 3207–3231, 2014.
- [67] M. I. Budyko, “Climate and Life, 508 pp.” Academic Press, New York, 1974.
- [68] F. Dominguez, P. Kumar, X. Z. Liang, and M. Ting, “Impact of atmospheric moisture storage on precipitation recycling,” *Journal of Climate*, vol. 19, no. 8, pp. 1513–1530, 2006.
- [69] G. I. Burde, C. Gandush, and Y. Bayarjargal, “Bulk recycling models with incomplete vertical mixing. Part II: Precipitation recycling in the Amazon basin,” *Journal of Climate*, vol. 19, no. 8, pp. 1473–1489, 2006.
- [70] M. G. Bosilovich, “On the vertical distribution of local and remote sources of water for precipitation,” *Meteorology and Atmospheric Physics*, vol. 80, no. 1-4, pp. 31–41, 2002.
- [71] K. Yoshimura, T. Oki, N. Ohte, and S. Kanae, “Colored Moisture Analysis Estimates of Variations in 1998 Asian Monsoon Water Sources,” *Journal of the Meteorological Society of Japan*, vol. 82, no. 5, pp. 1315–1329, 2004.
- [72] R. J. Van Der Ent, H. H. G. Savenije, B. Schaefli, and S. C. Steele-Dunne, “Origin and fate of atmospheric moisture over continents,” *Water Resources Research*, vol. 46, no. 9, pp. 1–12, 2010.

- [73] H. F. Goessling and C. H. Reick, “What do moisture recycling estimates tell us? Exploring the extreme case of non-evaporating continents,” *Hydrology and Earth System Sciences*, vol. 15, no. 10, pp. 3217–3235, 2011.
- [74] —, “On the ”well-mixed” assumption and numerical 2-D tracing of atmospheric moisture,” *Atmospheric Chemistry and Physics*, vol. 13, no. 11, pp. 5567–5585, 2013.
- [75] R. J. Van Der Ent, O. A. Tuinenburg, H. R. Knoche, H. Kunstmann, and H. H. Savenije, “Should we use a simple or complex model for moisture recycling and atmospheric moisture tracking?” *Hydrology and Earth System Sciences*, vol. 17, no. 12, pp. 4869–4884, 2013.
- [76] P. A. Dirmeyer and K. L. Brubaker, “Contrasting evaporative moisture sources during the drought of 1988 and the flood of 1993,” *Journal of Geophysical Research Atmospheres*, vol. 104, no. D16, pp. 19 383–19 397, 1999.
- [77] A. Stohl and P. James, “A Lagrangian Analysis of the Atmospheric Branch of the Global Water Cycle. Part I: Method Description, Validation, and Demonstration for the August 2002 Flooding in Central Europe,” *Journal of Hydrometeorology*, vol. 5, pp. 656–678, 2004.
- [78] —, “A Lagrangian Analysis of the Atmospheric Branch of the Global Water Cycle. Part II: Moisture Transports between Earth’s Ocean Basins and River Catchments,” *Journal of Hydrometeorology*, vol. 6, no. 6, pp. 961–984, 2005.
- [79] L. Gimeno, A. Drumond, R. Nieto, R. M. Trigo, and A. Stohl, “On the origin of continental precipitation,” *Geophysical Research Letters*, vol. 37, no. 13, pp. 1–7, 2010.
- [80] P. James, A. Stohl, N. Spichtinger, S. Eckhardt, and C. Forster, “Climatological aspects of the extreme European rainfall of August 2002 and a trajectory method for estimating the associated evaporative source regions,” *Natural Hazards and Earth System Science*, vol. 4, no. 5/6, pp. 733–746, 2004.
- [81] A. Stohl, C. Forster, and H. Sodemann, “Remote sources of water vapor forming precipitation on the Norwegian west coast at 60°N - A tale of hurricanes and an atmospheric river,” *Journal of Geophysical Research Atmospheres*, vol. 113, no. 5, pp. 1–13, 2008.
- [82] O. A. Tuinenburg and A. Staal, “Tracking the global flows of atmospheric moisture and associated uncertainties,” *Hydrology and Earth System Sciences*, vol. 24, no. 5, pp. 2419–2435, 2020.
- [83] C. Abbe, “The physical basis of long-range weather forecasts,” *Monthly Weather Review*, vol. 29, no. 12, pp. 551–561, 1901.
- [84] V. Bjerknes, “Das Problem der Wettervorhersage betrachtet vom Standpunkt der Mechanik und Physik,” *Meteorol. Z.*, vol. 21, pp. 1–7, 1904.
- [85] L. F. Richardson, “Weather prediction by numerical process Cambridge University Press,” *Monthly Weather Review*, vol. 1922, no. February, p. 219, 1922.

- [86] P. Bauer, A. Thorpe, and G. Brunet, “The quiet revolution of numerical weather prediction,” *Nature*, vol. 525, no. 7567, pp. 47–55, 2015.
- [87] P. N. Edwards, “History of climate modeling,” *Wiley Interdisciplinary Reviews: Climate Change*, vol. 2, no. 1, pp. 128–139, 2011.
- [88] H. E. Brooks and D. J. Stensrud, “Climatology of heavy rain events in the United States from hourly precipitation observations,” *Monthly Weather Review*, vol. 128, no. 4, pp. 1194–1201, 2000.
- [89] R. Romero, J. Guijarro, C. Ramis, and S. Alonso, “A 30-year (1964–1993) daily rainfall data base for the Spanish Mediterranean regions: first exploratory study,” *International Journal of Climatology*, vol. 18, no. 5, pp. 541–560, 1998.
- [90] A. M. Ramos, R. M. Trigo, and M. L. Liberato, “A ranking of high-resolution daily precipitation extreme events for the Iberian Peninsula,” *Atmospheric Science Letters*, vol. 15, no. 4, pp. 328–334, 2014.
- [91] M. Belo-Pereira, E. Dutra, and P. Viterbo, “Evaluation of global precipitation data sets over the Iberian Peninsula,” *Journal of Geophysical Research Atmospheres*, vol. 116, no. 20, 2011.
- [92] S. Herrera, J. M. Gutiérrez, R. Ancell, M. R. Pons, M. D. Frías, and J. Fernández, “Development and analysis of a 50-year high-resolution daily gridded precipitation dataset over Spain (Spain02),” *International Journal of Climatology*, vol. 32, no. 1, pp. 74–85, 2012.
- [93] M. Brunetti, M. Maugeri, T. Nanni, and A. Navarra, “Droughts and extreme events in regional daily Italian precipitation series,” *International Journal of Climatology*, vol. 22, no. 5, pp. 543–558, 2002.
- [94] D. Ricard, V. Ducrocq, and L. Auger, “A climatology of the mesoscale environment associated with heavily precipitating events over a northwestern Mediterranean area,” *Journal of Applied Meteorology and Climatology*, vol. 51, no. 3, pp. 468–488, 2012.
- [95] L. E. McPhillips, H. Chang, M. V. Chester, Y. Depietri, E. Friedman, N. B. Grimm, J. S. Kominoski, T. McPhearson, P. Méndez-Lázaro, E. J. Rosi, and J. Shafiei Shiva, “Defining Extreme Events: A Cross-Disciplinary Review,” *Earth’s Future*, vol. 6, no. 3, pp. 441–455, 2018.
- [96] S. I. Seneviratne, N. Nicholls, D. Easterling, C. M. Goodess, S. Kanae, J. Kossin, Y. Luo, J. Marengo, K. Mc Innes, M. Rahimi, M. Reichstein, A. Sorteberg, C. Vera, X. Zhang, M. Rusticucci, V. Semenov, L. V. Alexander, S. Allen, G. Benito, T. Cavazos, J. Clague, D. Conway, P. M. Della-Marta, M. Gerber, S. Gong, B. N. Goswami, M. Hemer, C. Huggel, B. Van den Hurk, V. V. Kharin, A. Kitoh, A. M. Klein Tank, G. Li, S. Mason, W. Mc Guire, G. J. Van Oldenborgh, B. Orłowsky, S. Smith, W. Thiaw, A. Velegarakis, P. Yiou, T. Zhang, T. Zhou, and F. W. Zwiers, *Changes in climate extremes and their impacts on the natural physical environment*, 2012, vol. 9781107025.

- [97] W. Liu, J. Wu, R. Tang, M. Ye, and J. Yang, “Daily precipitation threshold for rainstorm and flood disaster in the mainland of China: An economic loss perspective,” *Sustainability (Switzerland)*, vol. 12, no. 1, 2020.
- [98] R. Romero, G. Sumner, C. Ramis, and A. Genovés, “A classification of the atmospheric circulation patterns producing significant daily rainfall in the Spanish Mediterranean area,” *International Journal of Climatology*, vol. 19, no. 7, pp. 765–785, 1999.
- [99] A. Lana, J. Campins, A. Genovés, and A. Jansà, “Atmospheric patterns for heavy rain events in the Balearic Islands,” *Advances in Geosciences*, vol. 12, pp. 27–32, 2007.
- [100] S. Federico, E. Avolio, L. Pasqualoni, and C. Bellecci, “Atmospheric patterns for heavy rain events in Calabria,” *Natural Hazards and Earth System Science*, vol. 8, no. 5, pp. 1173–1186, 2008.
- [101] E. E. Houssos, C. J. Lolis, and A. Bartzokas, “Atmospheric circulation patterns associated with extreme precipitation amounts in Greece,” *Advances in Geosciences*, vol. 17, pp. 5–11, 2008.
- [102] C. Martínez, J. Campins, A. Jansà, and A. Genovés, “Heavy rain events in the Western Mediterranean: an atmospheric pattern classification,” *Advances in Science and Research*, vol. 2, no. 1, pp. 61–64, 2008.
- [103] J. Gilabert and M. C. Llasat, “Circulation weather types associated with extreme flood events in Northwestern Mediterranean,” *International Journal of Climatology*, vol. 38, no. 4, pp. 1864–1876, 2018.
- [104] L. Häggmark, K. I. Ivarsson, S. Gollvik, and P. O. Olofsson, “Mesan, an operational mesoscale analysis system,” *Tellus, Series A: Dynamic Meteorology and Oceanography*, vol. 52, no. 1, pp. 2–20, 2000.
- [105] F. Taillefer, “CANARI Technical Documentation based on ARPEGE cycle CY25T1 (AL25T1 for ALADIN),” Toulouse, France, 2002.
- [106] R. Serrano-Notivol, S. Beguería, M. Á. Saz, L. A. Longares, and M. De Luis, “SPREAD: A high-resolution daily gridded precipitation dataset for Spain - An extreme events frequency and intensity overview,” *Earth System Science Data*, vol. 9, no. 2, pp. 721–738, 2017.
- [107] F. A. Isotta, C. Frei, V. Weingartner, M. Perčec Tadić, P. Lassègues, B. Rudolf, V. Pavan, C. Cacciamani, G. Antolini, S. M. Ratto, M. Munari, S. Micheletti, V. Bonati, C. Lussana, C. Ronchi, E. Panettieri, G. Marigo, and G. Vertačnik, “The climate of daily precipitation in the Alps: Development and analysis of a high-resolution grid dataset from pan-Alpine rain-gauge data,” *International Journal of Climatology*, vol. 34, no. 5, pp. 1657–1675, 2014.
- [108] R. C. Cornes, G. van der Schrier, E. J. van den Besselaar, and P. D. Jones, “An Ensemble Version of the E-OBS Temperature and Precipitation Data Sets,” *Journal of Geophysical Research: Atmospheres*, vol. 123, no. 17, pp. 9391–9409, 2018.



- [109] M. C. Llasat, M. Llasat-Botija, O. Petrucci, A. A. Pasqua, J. Rossello, F. Vinet, and L. Boissier, “Floods in the north-western Mediterranean region: Presentation of the HYMEX database and comparison with pre-existing global databases,” *Houille Blanche*, no. 1, pp. 5–9, 2013.
- [110] M. Barriendos, D. Coeur, M. Lang, M. C. Llasat, R. Naulet, F. Lemaitre, and A. Barrera, “Stationarity analysis of historical flood series in France and Spain (14th–20th centuries),” *Natural Hazards and Earth System Science*, vol. 3, no. 6, pp. 583–592, 2003.
- [111] C. Schär, N. Ban, E. M. Fischer, J. Rajczak, J. Schmidli, C. Frei, F. Giorgi, T. R. Karl, E. J. Kendon, A. M. Tank, P. A. O’Gorman, J. Sillmann, X. Zhang, and F. W. Zwiers, “Percentile indices for assessing changes in heavy precipitation events,” *Climatic Change*, vol. 137, no. 1-2, pp. 201–216, 2016.
- [112] P. Esteban, P. D. Jones, J. Martín-Vide, and M. Mases, “Atmospheric circulation patterns related to heavy snowfall days in Andorra, Pyrenees,” *International Journal of Climatology*, vol. 25, no. 3, pp. 319–329, 2005.
- [113] A. Philipp, C. Beck, R. Huth, and J. Jacobeit, “Development and comparison of circulation type classifications using the COST 733 dataset and software,” *International Journal of Climatology*, vol. 36, no. 7, pp. 2673–2691, 2016.
- [114] M. Lemus-Canovas, M. Ninyerola, J. A. Lopez-Bustins, S. Manguan, and C. Garcia-Sellés, “A mixed application of an objective synoptic classification and spatial regression models for deriving winter precipitation regimes in the Eastern Pyrenees,” *International Journal of Climatology*, vol. 39, no. 4, pp. 2244–2259, 2019.
- [115] M. Lemus-Canovas, J. A. Lopez-Bustins, L. Trapero, and J. Martin-Vide, “Combining circulation weather types and daily precipitation modelling to derive climatic precipitation regions in the Pyrenees,” *Atmospheric Research*, vol. 220, pp. 181–193, 2019.
- [116] R. B. Cattell, “The scree test for the number of factors,” *Multivariate Behavioral Research*, vol. 1, no. 2, pp. 245–276, 1966.
- [117] M. B. Richman, “Rotation of principal components,” *Journal of Climatology*, vol. 6, no. 3, pp. 293–335, 1986.
- [118] M. Lemus-Canovas, J. A. Lopez-Bustins, J. Martin-Vide, and D. Royé, “synoptReg: An R package for computing a synoptic climate classification and a spatial regionalization of environmental data,” *Environmental Modelling and Software*, vol. 118, pp. 114–119, 2019.
- [119] J. Martín-Vide and J. A. Lopez-Bustins, “The Western Mediterranean Oscillation and rainfall in the Iberian Peninsula,” *International Journal of Climatology*, vol. 26, no. 11, pp. 1455–1475, 2006.
- [120] J. A. Lopez-Bustins and M. Lemus-Canovas, “The influence of the Western Mediterranean Oscillation upon the spatio-temporal variability of precipitation over Catalonia (northeastern of the Iberian Peninsula),” *Atmospheric Research*, vol. 236, 2020.



- [121] J. Martin-Vide, A. Sanchez-Lorenzo, J. A. Lopez-Bustins, M. J. Cordobilla, A. Garcia-Manuel, and J. M. Raso, "Torrential rainfall in northeast of the Iberian Peninsula: synoptic patterns and WeMO influence," *Advances in Science and Research*, vol. 2, no. 1, pp. 99–105, 2008.
- [122] M. Milelli, M. C. Llasat, and V. Ducrocq, "The cases of June 2000, November 2002 and September 2002 as examples of mediterranean floods," *Natural Hazards and Earth System Science*, vol. 6, no. 2, pp. 271–284, 2006.
- [123] E. Fiori, A. Comellas, L. Molini, N. Reborá, F. Siccardi, D. J. Gochis, S. Tanelli, and A. Parodi, "Analysis and hindcast simulations of an extreme rainfall event in the Mediterranean area: The Genoa 2011 case," *Atmospheric Research*, vol. 138, pp. 13–29, 2014.
- [124] L. Trapero, J. Bech, F. Duffourg, P. Esteban, and J. Lorente, "Mesoscale numerical analysis of the historical November 1982 heavy precipitation event over Andorra (Eastern Pyrenees)," *Natural Hazards and Earth System Sciences*, vol. 13, no. 11, pp. 2969–2990, 2013.
- [125] I. Font, *Climatología de España y Portugal [in Spanish]*. Madrid: Instituto Nacional de Meteorología, 1983.
- [126] R. Koster, J. Jouzel, R. Suozzo, G. Russell, D. Rind, and P. Eaglesonl, "the NASA/GISS GCM. Water evaporating from various," *Water*, vol. 13, no. 1, pp. 121–124, 1986.
- [127] S. Joussaume, R. Sadourny, and C. Vignal, "Origin of precipitating water in a numerical simulation of the July climate," *Ocean-Air Interact*, vol. 1, pp. 43–56, 1986.
- [128] A. Numaguti, "Origin and recycling processes of precipitating water over the Eurasian continent: Experiments using an atmospheric general circulation model," *Journal of Geophysical Research: Atmospheres*, vol. 104, no. D2, pp. 1957–1972, 1999.
- [129] M. Werner, M. Heimann, and G. Hoffmann, "Isotopic composition and origin of polar precipitation in present and glacial climate simulations," *Tellus, Series B: Chemical and Physical Meteorology*, vol. 53, no. 1, pp. 53–71, 2001.
- [130] M. G. Bosilovich and S. D. Schubert, "Water Vapor Tracers as Diagnostics of the Regional Hydrologic Cycle," *Journal of Hydrometeorology*, vol. 3, no. 2, pp. 149–165, 2002.
- [131] D. Noone and I. Simmonds, "Annular variations in moisture transport mechanisms and the abundance of  $\delta^{18}\text{O}$  in Antarctic snow," *Journal of Geophysical Research Atmospheres*, vol. 107, no. 24, pp. 1–11, 2002.
- [132] M. G. Bosilovich, Y. C. Sud, S. D. Schubert, and G. K. Walker, "Numerical simulation of the large-scale North American monsoon water sources," *Journal of Geophysical Research: Atmospheres*, vol. 108, no. 16, 2003.
- [133] H. A. Singh, C. M. Bitz, J. Nusbaumer, and D. C. Noone, "A mathematical framework for analysis of water tracers: Part 1: Development of theory and application to the

- preindustrial mean state,” *Journal of Advances in Modeling Earth Systems*, vol. 8, no. 2, pp. 991–1013, 2016.
- [134] H. Sodemann, H. Wernli, and C. Schwierz, “Sources of water vapour contributing to the Elbe flood in August 2002 - A tagging study in a mesoscale model,” *Quarterly Journal of the Royal Meteorological Society*, vol. 135, no. 638, pp. 205–223, 2009.
- [135] H. R. Knoche and H. Kunstmann, “Tracking atmospheric water pathways by direct evaporation tagging: A case study for West Africa,” *Journal of Geophysical Research Atmospheres*, vol. 118, no. 22, pp. 12 345–12 358, 2013.
- [136] G. Miguez-Macho, A. Rios-Entenza, and F. Dominguez, “The impact of soil moisture and evapotranspiration fluxes on the spring water cycle in the Iberian Peninsula: A study with moisture tracers in WRF,” in *AGU Fall Meeting Abstracts*, 2013.
- [137] J. Arnault, R. Knoche, J. Wei, and H. Kunstmann, “Evaporation tagging and atmospheric water budget analysis with WRF: A regional precipitation recycling study for West Africa,” *Water Resources Research*, vol. 52, no. 3, pp. 1544–1567, 2016.
- [138] F. Dominguez, G. Miguez-Macho, and H. Hu, “WRF with Water Vapor Tracers: A Study of Moisture Sources for the North American Monsoon,” *Journal of Hydrometeorology*, vol. 17, no. 7, pp. 1915–1927, 2016.
- [139] J. Eiras-Barca, F. Dominguez, H. Hu, A. D. Garaboa-Paz, and G. Miguez-Macho, “Evaluation of the Moisture Sources in two Extreme Landfalling Atmospheric River Events using an Eulerian WRF-Tracers tool,” *Earth System Dynamics Discussions*, vol. 2017, pp. 1–21, 2017.
- [140] S. Y. Hong, Y. Noh, and J. Dudhia, “A New Vertical Diffusion Package with an Explicit Treatment of Entrainment Processes,” *Monthly Weather Review*, vol. 134, no. 9, pp. 2318–2341, 2006.
- [141] S. Y. Hong and J. Lim, “The WRF single-moment 6-class microphysics scheme (WSM6),” *Journal of the Korean Meteorological Society*, vol. 42, no. 2, pp. 129–151, 2006.
- [142] J. S. Kain, “The Kain–Fritsch Convective Parameterization: An Update,” *Journal of Applied Meteorology*, vol. 43, no. 1, pp. 170–181, 2004.
- [143] H.-M. Henry Juang and S.-Y. Hong, “Forward Semi-Lagrangian Advection with Mass Conservation and Positive Definiteness for Falling Hydrometeors,” *Monthly Weather Review*, vol. 138, no. 5, pp. 1778–1791, 2010.
- [144] P. Bechtold, E. Bazile, F. Guichard, P. Mascart, and E. Richard, “A mass-flux convection scheme for regional and global models,” *Quarterly Journal of the Royal Meteorological Society*, vol. 127, no. 573, pp. 869–886, 2001.
- [145] J. S. Kain and J. M. Fritsch, “A One-Dimensional Entraining/Detraining Plume Model and Its Application in Convective Parameterization,” *Journal of the Atmospheric Sciences*, vol. 47, no. 23, pp. 2784–2802, 1990.

- [146] J. S. Kain, M. E. Baldwin, and S. J. Weiss, "Parameterized Updraft Mass Flux as a Predictor of Convective Intensity," *Weather and Forecasting*, vol. 18, no. 1, pp. 106–116, 2003.
- [147] W. Skamarock, J. Klemp, J. Dudhi, D. Gill, D. Barker, M. Duda, X.-Y. Huang, W. Wang, and J. Powers, "A Description of the Advanced Research WRF Version 3," *Technical Report*, no. June, p. 113, 2008.
- [148] U. D. o. C. National Centers for Environmental Prediction, National Weather Service, NOAA, "NCEP FNL Operational Model Global Tropospheric Analyses, continuing from July 1999," Boulder CO, 2000.
- [149] F. Chen and J. Dudhia, "Coupling an Advanced Land Surface–Hydrology Model with the Penn State–NCAR MM5 Modeling System. Part II: Preliminary Model Validation," *Monthly Weather Review*, vol. 129, no. 4, pp. 587–604, 2001.
- [150] E. J. Mlawer, S. J. Taubman, P. D. Brown, M. J. Iacono, and S. A. Clough, "Radiative transfer for inhomogeneous atmospheres: RRTM, a validated correlated-k model for the longwave," *Journal of Geophysical Research: Atmospheres*, vol. 102, no. D14, pp. 16 663–16 682, 1997.
- [151] J. Dudhia, "Numerical Study of Convection Observed during the Winter Monsoon Experiment Using a Mesoscale Two-Dimensional Model," *Journal of the Atmospheric Sciences*, vol. 46, no. 20, pp. 3077–3107, 1989.
- [152] X. D. Liu, "Weighted essentially non-oscillatory schemes," *Journal of Computational Physics*, vol. 115, no. 1, pp. 200–212, 1994.
- [153] G. Miguez-Macho, G. L. Stenchikov, and A. Robock, "Spectral nudging to eliminate the effects of domain position and geometry in regional climate model simulations," *Journal of Geophysical Research: Atmospheres*, vol. 109, no. 13, pp. 1–15, 2004.
- [154] H. Sodemann and A. Stohl, "Moisture Origin and Meridional Transport in Atmospheric Rivers and Their Association with Multiple Cyclones\*," *Monthly Weather Review*, vol. 141, no. 8, pp. 2850–2868, 2013.
- [155] B. L. Wiggin, "Great snows of the Great Lakes," *Weatherwise*, vol. 3, no. 6, pp. 123–126, 1950.
- [156] V. Eichenlaub, "Lake effect snowfall to the lee of the Great Lakes: its role in Michigan," *Bulletin American Meteorological Society*, vol. 51, no. 5, pp. 403–412, 1970.
- [157] M. R. Hjelmfelt and R. B. Roscoe, "Numerical simulation of the airflow over Lake Michigan for a major lake-effect snow event," *Monthly Weather Review*, vol. 111, pp. 205–219, 1983.
- [158] T. A. Niziol, W. R. Snyder, and J. S. Waldstreicher, "Winter Weather Forecasting throughout the Eastern United States. Part IV: Lake Effect Snow," *Weather and Forecasting*, vol. 10, no. 1, pp. 61–77, 1995.

- [159] D. M. Wright, D. J. Posselt, and A. L. Steiner, “Sensitivity of Lake-Effect Snowfall to Lake Ice Cover and Temperature in the Great Lakes Region,” *Monthly Weather Review*, vol. 141, no. 2, pp. 670–689, 2013.
- [160] D. H. Lenschow, “Two examples of planetary boundary layer modification over the Great Lakes,” *Journal of the Atmospheric Sciences*, vol. 30, no. 4, pp. 568–581, 1973.
- [161] S. S. Chang and R. R. Braham, “Observational study of a convective internal boundary layer over Lake Michigan,” *Journal of the Atmospheric Sciences*, vol. 48, no. 20, pp. 2265–2279, 1991.
- [162] S. A. Changnon, “How a Severe Winter Impacts on Individuals,” *Bulletin of the American Meteorological Society*, vol. 60, no. 2, pp. 110–114, 1979.
- [163] V. L. Eichenlaub, *Weather and Climate of the Great Lakes Region*. Indiana: University of Notre Dame Press, 1978.
- [164] T. W. Schmidlin, “Impacts of severe winter weather during December 1989 in the Lake Erie snowbelt,” *Journal of Climate*, vol. 6, no. 4, pp. 759–767, 1993.
- [165] J. R. Gat, C. J. Bowser, and C. Kendall, “The contribution of evaporation from the Great Lakes to the continental atmosphere: estimate based on stable isotope data,” *Geophysical Research Letters*, vol. 21, no. 7, pp. 557–560, 1994.
- [166] M. V. Machavaram and R. Krishnamurthy, “Earth surface evaporative process: A case study from the Great Lakes region of the United States based on deuterium excess in precipitation,” *Geochimica et Cosmochimica Acta*, vol. 59, no. 20, pp. 4279–4283, 1995.
- [167] U. D. o. C. National Weather Service, NOAA, “Lake Effect Summary: November 17-19, 2014,” 2014.
- [168] T. Carroll, D. Cline, C. Olheiser, A. Rost, A. Nilsson, G. Fall, C. Bovitz, and L. Li, “NOAA’s National Snow Analyses,” *Proceedings of the 74th Annual Meeting of the Western Snow Conference*, pp. 1–14, 2006.
- [169] L. Gimeno, R. Nieto, R. M. Trigo, S. M. Vicente-Serrano, and J. I. López-Moreno, “Where Does the Iberian Peninsula Moisture Come From? An Answer Based on a Lagrangian Approach,” *Journal of Hydrometeorology*, vol. 11, no. 2, pp. 421–436, 2009.
- [170] H. Sodemann and E. Zubler, “Seasonal and inter-annual variability of the moisture sources for alpine precipitation during 1995-2002,” *International Journal of Climatology*, vol. 30, no. 7, pp. 947–961, 2010.
- [171] A. Drumond, R. Nieto, E. Hernandez, and L. Gimeno, “A Lagrangian analysis of the variation in moisture sources related to drier and wetter conditions in regions around the Mediterranean Basin,” *Natural Hazards and Earth System Sciences*, vol. 11, no. 8, pp. 2307–2320, 2011.
- [172] K. E. Trenberth, “Atmospheric moisture residence times and cycling: Implications for rainfall rates and climate change,” *Climatic Change*, vol. 39, no. 4, pp. 667–694, 1998.

- [173] R. J. Van Der Ent and O. A. Tuinenburg, "The residence time of water in the atmosphere revisited," *Hydrology and Earth System Sciences*, vol. 21, no. 2, pp. 779–790, 2017.
- [174] D. P. Dee, S. M. Uppala, A. J. Simmons, P. Berrisford, P. Poli, S. Kobayashi, U. Andrae, M. A. Balmaseda, G. Balsamo, P. Bauer, P. Bechtold, A. C. Beljaars, L. van de Berg, J. Bidlot, N. Bormann, C. Delsol, R. Dragani, M. Fuentes, A. J. Geer, L. Haimberger, S. B. Healy, H. Hersbach, E. V. Hólm, L. Isaksen, P. Kållberg, M. Köhler, M. Matricardi, A. P. McNally, B. M. Monge-Sanz, J. J. Morcrette, B. K. Park, C. Peubey, P. de Rosnay, C. Tavolato, J. N. Thépaut, and F. Vitart, "The ERA-Interim reanalysis: Configuration and performance of the data assimilation system," *Quarterly Journal of the Royal Meteorological Society*, vol. 137, no. 656, pp. 553–597, 2011.
- [175] R. A. Maddox, "Mesoscale Convective Complexes," *Bulletin of the American Meteorological Society*, vol. 61, no. 11, pp. 1374–1387, 1980.
- [176] M. C. Llasat, *Gota fría*, 1991, vol. 165.
- [177] K. E. Trenberth and J. T. Fasullo, "Climate extremes and climate change: The Russian heat wave and other climate extremes of 2010," *Journal of Geophysical Research Atmospheres*, vol. 117, no. 17, 2012.
- [178] K. E. Trenberth, J. T. Fasullo, and T. G. Shepherd, "Attribution of climate extreme events," *Nature Climate Change*, vol. 5, no. 8, pp. 725–730, 2015.
- [179] N. A. Rayner, D. E. Parker, E. B. Horton, C. K. Folland, L. V. Alexander, D. P. Rowell, E. C. Kent, and A. Kaplan, "Global analyses of sea surface temperature, sea ice, and night marine air temperature since the late nineteenth century," *Journal of Geophysical Research: Atmospheres*, vol. 108, no. 14, 2003.
- [180] A. Winschall, H. Sodemann, S. Pfahl, and H. Wernli, "How important is intensified evaporation for Mediterranean precipitation extremes?" *Journal of Geophysical Research*, vol. 119, no. 9, pp. 5240–5256, 2014.
- [181] F. Duffourg and V. Ducrocq, "Assessment of the water supply to Mediterranean heavy precipitation: A method based on finely designed water budgets," *Atmospheric Science Letters*, vol. 14, no. 3, pp. 133–138, 2013.
- [182] P. Knippertz and H. Wernli, "A lagrangian climatology of tropical moisture exports to the northern hemispheric extratropics," *Journal of Climate*, vol. 23, no. 4, pp. 987–1003, 2010.
- [183] M. L. C. Wu, O. Reale, and S. D. Schubert, "A characterization of African easterly waves on 2.5-6-day and 6-9-day time scales," *Journal of Climate*, vol. 26, no. 18, pp. 6750–6774, 2013.
- [184] B. Ziv, "A subtropical rainstorm associated with a tropical plume over Africa and the Middle-East," *Theoretical and Applied Climatology*, vol. 69, no. 1-2, pp. 91–102, 2001.
- [185] S. Rubin, B. Ziv, and N. Paldor, "Tropical plumes over eastern North Africa as a source of rain in the Middle East," *Monthly Weather Review*, vol. 135, no. 12, pp. 4135–4148, 2007.

- [186] J. G. Pinto, M. Kława, U. Ulbrich, R. Rudari, and P. Speth, “Extreme precipitation events over northwest Italy and their relationship with tropical-extratropical interactions over the Atlantic,” in *In: Proceedings of third EGS Plinius conference on Mediterranean storms*, Baja Sardinia, 2001, pp. 321–332.
- [187] A. Mariotti, N. Zeng, and K. M. Lau, “Euro-Mediterranean rainfall and ENSO-a seasonally varying relationship,” *Geophysical Research Letters*, vol. 29, no. 12, pp. 59–1–59–4, 2002.
- [188] J. Shaman and E. Tziperman, “An atmospheric teleconnection linking ENSO and Southwestern European precipitation,” *Journal of Climate*, vol. 24, no. 1, pp. 124–139, 2011.
- [189] S. O. Krichak, J. S. Breitgand, S. Gualdi, and S. B. Feldstein, “Teleconnection-extreme precipitation relationships over the Mediterranean region,” *Theoretical and Applied Climatology*, vol. 117, no. 3-4, pp. 679–692, 2014.







The present thesis aims to definitively clarify the origin of the moisture feeding torrential rains in the western Mediterranean region. To this end, we simulate more than one hundred events, thus improving previous knowledge on this subject, generally based on specific case studies. The main conclusion from this thesis is that the contribution of the Mediterranean Sea as moisture source is, on average, lower than often assumed, around 35%. We find that remote sources, in some cases as distant as the tropical Pacific or the southern hemisphere, play a crucial role in these events. In fact, the contribution from remote sources is on average 10% higher than that from local sources. Therefore, to fully understand such catastrophic events, we must study them from a more global rather than regional approach.